EVALUATION OF DYNAMIC RESPONSE OF SOILS SUBJECTED TO REGULAR AND IRREGULAR EXCITATIONS USING CYCLIC TRIAXIAL TESTS

A Thesis

Submitted in Partial Fulfilment of the Requirements

for the Degree of

DOCTOR OF PHILOSOPHY

by

SHIV SHANKAR KUMAR

Department of Civil Engineering
Indian Institute of Technology Guwahati
Guwahati – 781039

March 2018

I dedicate this dissertation to

my mother

"Late Usha Devi"

STATEMENT

I do hereby declare that the matter embodied in this thesis is the result of investigations carried out by me in the Department of Civil Engineering, Indian Institute of Technology Guwahati, Guwahati, Assam, India.

In keeping with the general practice of reporting scientific observations, due acknowledgements have been made wherever the work described is based on findings of other investigators.

Place: IIT Guwahati

Date: March 22, 2018 Shiv Shankar Kumar

CERTIFICATE

This is to certify that the thesis entitled "**Evaluation of Dynamic Response of Soils Subjected to Regular and Irregular Excitations using Cyclic Triaxial Tests**", submitted by **Shiv Shankar Kumar** (Roll No. 126104027), to the Indian Institute of Technology Guwahati, for the award of degree of Doctor of Philosophy in Civil Engineering, is a record of bonafide research work carried out by him under our supervision and guidance. The thesis work, in our opinion, has reached the requisite standard fulfilling the requirement for the degree of Doctor of Philosophy.

The results contained in this thesis have not been submitted in part or full to any other University or Institute for award of any degree or diploma.

Dr. A. Murali Krishna
Associate Professor
Department of Civil Engineering
Indian Institute of Technology Guwahati
Guwahati-781039, India

Dr. Arindam Dey
Assistant Professor
Department of Civil Engineering
Indian Institute of Technology Guwahati
Guwahati-781039, India

ACKNOWLEDGEMENT

I take the opportunity and immense pleasure to convey my wholehearted gratitude to all the generous people to whom I have been associated at IIT Guwahati. The work reported in this thesis was carried out under the esteemed supervision and guidance of ***Dr. A. Murali Krishna*** *and* ***Dr. Arindam Dey****. My special thanks to* ***Dr. A. Murali Krishna*** *for his constant guidance and supervision during my M. Tech research and, introducing me in the field of research. I remain deeply grateful to both of them not only for their guidance and constant encouragement throughout the course, but also for their invaluable advice and encouragement that enriched my doctoral study.*

I would like to thank my Doctoral Committee members, Dr. Sreedeep S., Dr. Sandip Das and Dr. Hemant B. Kaushik, for sparing their valuable time in reviewing my work. I extend my sincere thanks to the other faculty members of the Geotechnical Engineering Division of IIT Guwahati for their cooperation, whenever required. I would like to thank Head of the Department, Dr. S. Dutta, and the former Heads of the Department, Dr. S. K. Deb and Dr. A. K. Sarma, for the facilities provided for conducting the research. I express my heartfelt gratitude and thanks to Dr. Utpal Kumar Barua, Kamrup Polytechnic, for providing the borelog data of the Guwahati city, and PESMOS, Department of Earthquake Engineering, IIT Roorkee, from where I used earthquake data for the ground response analysis. I gratefully acknowledge the unstinted help provided by Mr. Hari Ram Upadhyaya, Mr. Madhav and Mr. Upen Gohain, during different phases of my research work. Furthermore, I would like to thank the office staff of Civil Engineering Department, for their support in administrative works.

I convey my special thanks to my friends: Mr. Pawan K. Sah, Mr. Harinarayan, Mr. Chiranjib P. Sarma, Mr. Doordarshi Chaterjee, Mr. Pradeep K. Dammala, Mr. Rana Acharyya, Mr. Suchit K. Patel, Mr. Chandrabhanu, Mr. Arya Anuj, Mr. Bikash K. Sah, Mr.

Prashant K. Jha, Mr. Sanandam B., Mr. Vinay K. Gadi, Mr. Krishanu Mukherjee, Mr. Sudheer K. Yamsani, Mr. Janarul Saikh, Mr. Dipjyoti Baglari, Mr. Tanmoy Deb, Ms. Jumrik Taipodia, Ms. Yagom Gapak, Ms. Madhulata Boga, Ms. Chinumani, Mr. Sathwik Kashyap, Mr. Sai Sandeep, Mr. Prasath SB, Mr. K. Naveen Reddy and many others, who made my time enjoyable during my research at IIT Guwahati.

My special thanks to Dr. Awdhesh K. Choudhary, Dr. Arghadeep Biswas, Dr. Arup Bhattacharjee, Dr. Sodom Bali Reddy, Dr. Abhijit Deka and Dr. V. Srikanth for their valuable suggestions, moral support and encouraging interactions which helped me improve my skills.

Lastly, but most importantly, I want to acknowledge the greatest supports, love and encouragements received from my parents, my wife (Komal) and my loving son, Karthikeyan, without whom it would never be possible.

Shiv Shankar Kumar

ABSTRACT

With increasing urbanization, demand of seismic resistant geotechnical structures is turning out to be a challenging task for geotechnical engineers. Most of the damages during the seismic incidences are greatly influenced by the response of soil deposits, which are further governed by the dynamic properties of the soils and the pore-pressure variations. Moreover, the irregular nature of earthquakes impart the influence of excitation frequencies, rate of loading, number of loading cycles and peak amplitudes of excitations, on the dynamic response of the soil. Evaluation of dynamic response (dynamic properties and liquefaction evaluation) of different soils, subjected to regular and irregular seismic loadings, have been reported in several literatures. It is imperative and necessary that the regional soils are intricately characterized of their own dynamic responses for more prudent analyses.

Assam, located in the North-eastern region of India, is one of the most seismically active regions in the world and has experienced several devastating earthquakes of different magnitudes in the past. Moreover, the soil substrata, in most of this region, consist of significant quantities of saturated silty sand, making it more susceptible to liquefaction in case of a major earthquake. Owing to the frequent occurrence of low and moderate magnitude earthquakes, with the possibility of occurrence of high magnitude motions due to the seismic gap, it becomes immensely important to investigate the dynamic response of the locally available soils in Assam region. In view of the above, the present study is focussed to investigate the dynamic behaviour of cohesionless soil (Brahmaputra Sand, BS) and cohesive soil (Red Soil, RS) available in the Guwahati region, Assam.

The objective of the present study was achieved by conducting static and cyclic triaxial tests on BS and RS at different investigating parameters and testing conditions. Static triaxial tests were carried out on BS (at dry and saturated state) and RS to investigate the monotonic

behaviour of soils at different relative density (D_r), confining stress (σ'_c) and displacement rate. To evaluate the dynamic properties of the soils, strain- and stress- controlled cyclic triaxial tests, with regular excitations, were conducted at different shear strain (γ), D_r and σ'_c. Further, the liquefaction potential and liquefaction parameters of saturated BS soil were determined through stress-controlled cyclic triaxial tests conducted with regular excitations and a comparison of the same obtained through strain-controlled tests was established. The response of BS soil was also examined using irregular (earthquake) excitations. In order to describe the strain-dependent dynamic responses, both external LVDTs and on-sample transducers have been used, the latter being effective in highlighting the local strains developed in a soil specimen upon the application of global strain. The results of the investigations, i.e. the strain dependent dynamic properties of BS and RS, were further used in conducting the ground response analysis (GRA) of Guwahati city to manifest the importance and necessity of application of the experimentally determined dynamic response of the locally prevailing soils in contrast to the utilization of existing standard dynamic models.

The outcomes are sequentially presented in regard to the monotonic shear tests, estimation of dynamic soil properties, liquefaction potential evaluation and ground response analysis. The tests results obtained from monotonic shear tests are presented in terms of stress-strain response and stress path plots of both the soils, which are observed to be significantly affected by saturation, confining stress, relative density and displacement rate. The friction angle of saturated BS, tested at consolidated undrained condition, was found to be approximately 2˚-3˚ lesser than that of dry BS. The application of on-sample LVDTs was found to be effective in delineating the local-strain response of the soil specimen and could efficiently portray the variations in the shear modulus obtained from global and local strain approaches. BS soil exhibited stiffer response upon using the local strains for the computation of strain-dependent shear modulus from monotonic tests.

Both strain-controlled and stress-controlled tests on BS and RS revealed that the hysteresis loops obtained at high cyclic strain amplitudes (γ) or higher number of cycles (N) exhibited noticeable asymmetric nature. A modified methodology for asymmetric hysteresis loops has been proposed for the evaluation of dynamic properties. Application of on-sample LVDTs during the cyclic tests aided in the determination of the shear modulus and damping ratio over a wide strain range, encompassing both low (~3×10^{-3} %) as well as high strains (~5 %). Based on the strain- and stress-controlled regular excitations, the liquefaction potential of BS has been evaluated, which manifested the initiation of liquefaction at γ = 0.75% (average value), for all magnitudes of relative densities (D_r = 30-90%) and effective confining pressure (σ'_c = 50-150 kPa). Based on the stress-controlled irregular excitation, the BS specimens are observed to liquefy under the following optimum conditions: peak ground acceleration (PGA) $\geq$ 0.36g, cyclic stress ratio (CSR) $\geq$ 0.3 and γ_{max} > 0.5% for D_r = 30-90% and σ'_c = 50-150 kPa. Therefore, the limiting value of γ = 0.5% can be suitably adopted for the liquefaction potential evaluation studies for loose BS soil of North-eastern region of India.

One-dimensional equivalent linear GRA were carried out for Guwahati city using the commercial software, DEEPSOIL. The experimentally evaluated dynamic soil properties and existing standard dynamic property models available in literature were used in GRA. Considering different earthquake records having varying strong motion parameters, the results of GRA were presented in terms of peak ground acceleration (PGA), Fourier amplification ratio (FAR) and peak spectral acceleration (PSA). The differences in the outcomes highlighted the importance and necessity of considering the experimentally evaluated dynamic soil properties of the regional soils to obtain precise site-specific GRA outcomes.

Overall, the thesis presents the dynamic properties of regional soils obtained using cyclic triaxial tests. The findings of the research can be successfully used in several practical applications related to earthquake geotechnical engineering, and thus serves the profession.

TABLE OF CONTENTS

Abstract ……..……..……..……i

Table of Contents…….…….……....v

List of Figures ..…….…….……..ix

List of Tables …….…….…….……..xix

Chapter 1 Introduction **1**

1.1 General 1

1.2 Aim of the Study 3

1.3 Organization of thesis 4

Chapter 2 Literature Review **5**

2.1 Introduction 5

2.2 Monotonic response of soils 5

2.3 Cyclic response of soils 11

2.3.1 Studies based on the regular (sinusoidal) loading 11

2.3.2 Studies based on the irregular (earthquake) loading 28

2.4 Local strain measurements in static and cyclic laoding 38

2.5 Application of dynamic properties of soils 43

2.6 Critical appraisal of literature review 46

2.7 Objectives and scope of the study 47

2.8 Summary 48

Chapter 3 Materials and Methodology **49**

3.1 Introduction 49

3.2 Material descriptions 49

3.2.1 Cohesionless soil 50

3.2.2 Cohesive soil 50

3.3 Testing apparatus and components 53
3.3.1 Triaxial frame 53
3.3.2 Triaxial cell 54
3.3.3 Dynamic actuator 55
3.3.4 Submersible load cell 56
3.3.5 Air water cylinder 56
3.3.6 Automatic volume change device 58
3.3.7 Pressure transducers 58
3.3.8 Dry air receiver unit 59
3.3.9 Compact dynamic controller 59
3.4 Testing methodology 61
3.4.1 Sample preparation 61
3.4.2 Saturation 64
3.4.3 Triaxial shear tests 67
3.4.4 Measurement of local strains 74
3.5 Summary 78
Chapter 4 Monotonic Shear Tests 79
4.1 Introduction 79
4.2 Testing program 79
4.3 Tests on dry cohesionless soil 80
4.4 Tests on saturated cohesionless soil 82
4.4.1 Effect of confining pressure 85
4.4.2 Effect of relative density 88
4.4.3 Effect of loading rate 91
4.4.4 Local strain measurements 95
4.5 Comparative behaviour of dry and saturated cohesionless soil 103
4.6 Tests on Cohesive soil 106

4.7 Summary 108

Chapter 5 Cyclic Shear Tests: Dynamic Properties 109

5.1 Introduction 109

5.2 Testing program 109

5.3 Tests on saturated cohesionless soil 111

5.3.1 Strain-controlled cyclic loading 111

5.3.2 Dynamic properties of saturated cohesionless soil using on-sample LVDTs 131

5.3.3 Stress-controlled cyclic loading 136

5.3.4 Comparison of strain-controlled and stress-controlled tests results 143

5.4 Tests on dry cohesionless soil 145

5.5 Comparison of strain-controlled tests results of dry and saturated cohesionless soil 149

5.6 Tests on cohesive soil 157

5.7 Summary 161

Chapter 6 Cyclic Shear Tests: Liquefaction Evaluation 163

6.1 Introduction 163

6.2 Testing program 163

6.3 Strain-controlled tests with regular excitations 163

6.4 Stress-controlled tests with regular excitations 170

6.5 Stress-controlled tests with irregular excitations 184

6.6 Summary 195

Chapter 7 Ground Response Analysis 197

7.1 Introduction 197

7.2 Study region 197

7.3 Site characterization 198

7.3.1 Dynamic properties of soils 200

7.4 GRA Methodology 202

7.4.1 Fundamentals of EQL method 203

7.5 Strong ground motions 204

7.6 Results and discussions 205

7.6.1 Influence of specific strong motion on GRA of Guwahati city 206

7.6.2 Influence of various strong motions on GRA of Guwahati city 214

7.7 Summary 229

Chapter 8 Concluding Remarks 231

8.1 Summary of the thesis 231

8.2 Conclusions 231

8.3 Limitations of the study 234

8.4 Scope of the future research 235

References 237

List of Publications 257

LIST OF FIGURES

Fig. 1.1 Different modes of seismic damages (a) ground failure (b) liquefaction (c) foundation failure (d) landslide (www.google.co.in) 3

Fig. 2.1 Typical plot of the effect of sample preparation method in triaxial testing at different testing conditions (Miura and Toki, 1982) 7

Fig. 2.2 Comparison of drained and undrained testing conditions on dense sand (redrawn after Seed and Lee, 1966) 8

Fig. 2.3 Typical plot of effect of confining pressure on (a) stress-strain response (b) stress path for sand (Ishihara, 1993) 8

Fig. 2.4 Typical plots representing the effect of saturation on undrained behavior of sand (Della et al., 2011) 9

Fig. 2.5 Typical plots of (a) stress-strain response (b) excess PWP, with strain at different loading rates on saturated sand under undrained condition (Watanabe and Kusakabe, 2013) 10

Fig. 2.6 Undrained behaviour of sand: (a) Deviator stress versus axial strain (b) PWP versus axial strain (c) Mean effective (p') stress versus deviator stress (σ_d) (Arab et al., 2016) 11

Fig. 2.7 Cyclic stress ratio versus number of cycles for different sample preparation techniques (redrawn after Mulilis et al., 1977) 12

Fig. 2.8 Effect of specimen size on cyclic stresses causing initial liquefaction of Monterey Zero sand (redrawn after Wong et al., 1975) 12

Fig. 2.9 Comparison of shear modulus of undisturbed and disturbed dense sand samples (Katayama et al., 1986) 13

Fig. 2.10 Comparison of damping ratio of undisturbed and disturbed dense sand samples (Katayama et al., 1986) 14

Fig. 2.11 Shear modulus versus shear strain for σ'_c = 98 kN/m^2 with different void ratios (Kokusho, 1980) 15

Fig. 2.12 Variation of shear modulus ratio with γ for dense sand subjected to different σ'_c (Kokusho, 1980) 15

Fig. 2.13 Variation of damping ratio with γ for dense sand subjected to different σ'_c (Kokusho, 1980) 16

Fig. 2.14 Cyclic stress ratio at f = 10 Hz for initial liquefaction versus initial σ'_c (redrawn after Mulilis, 1975) 17

Fig. 2.15 Effect of loading waveform on number of cycles required for initial liquefaction of moist tamped specimens (adapted from Mulilis et al., 1978) 17

Fig. 2.16 Variation of shear modulus of Ottawa sand with loading frequency (after Lin et al., 1996) 19

Fig. 2.17 Variation of damping ratio of Ottawa sand with loading frequency (after Lin et al., 1996) 19

Fig. 2.18 Variation of modulus ratio with shear strain at different loading frequencies (Govindaraju, 2005) 20

Fig. 2.19 Variation of damping ratio with shear strain at different loading frequencies (Govindaraju, 2005) 20

Fig. 2.20 Relationship between G/G_{max} and *PI* for normally-consolidated and over-consolidated soils (Vucetic and Dobry, 1991) 22

Fig. 2.21 Relationship between damping ratio and *PI* for normally-consolidated and over-consolidated soils (Vucetic and Dobry, 1991) 22

Fig. 2.22 CSR versus *N* for reconstituted saturated samples at different *PI* values and 5% DA axial strain (redrawn after Prakash and Puri, 1982) 23

Fig. 2.23 CSR versus *N* for low plasticity silts (Prakash and Sandoval, 1982) 23

Fig. 2.24 Cyclic stress ratio with the number of cycles during one-way and two-way cyclic loading (Yasuhara et al., 1992). 24

Fig. 2.25 Typical results of cyclic simple shear strain controlled tests with definitions of volumetric cyclic threshold strain for settlement (after Hsu and Vucetic, 2004, 2006) 25

Fig. 2.26 Change of pore pressure for different stress ratios (Yildirim and Ersan, 2007) 26

Fig. 2.27 Variation of cumulative γ with *N* for (a) f = 1 Hz (b) f = 0.1 Hz (c) f = 0.01 Hz, respectively (Li et al., 2011) 27

Fig. 2.28 Variation of accumulative PWP with *N* for (a) f = 1 Hz (b) f = 0.1 Hz (c) f = 0.01 Hz, respectively (Li et al., 2011) 27

Fig. 2.29 Laboratory simulation of liquefaction occurrence during Niigata earthquake (Ishihara and Yasuda, 1972) 28

Fig. 2.30 Typical cyclic triaxial test results from irregular excitation (Sawada et al., 2006) .. 29

Fig. 2.31 Typical cyclic response of soil under irregular seismic excitations (Sassa and Yamazaki, 2017) 29

Fig. 2.32 (a) On-sample LVDTs attached to the bitumen macadam specimen (b) Schematic diagram of the arrangement of on-sample LVDTs (Brown and Snaith, 1974) 38

Fig. 2.33 Different types of local strain measurement appurtenances: (a) Electrolevel gage (Symes and Burland, 1984) (b) LVDT (Cuccovillo and Coop, 1997) (c) Cantilever LVDT (Yimsiri et al., 2005) (d) Local strain gauge (Clayton and Khatrush, 1986) (e) Elastomer gage (Safaqah and Riemer, 2007) 40

Fig. 2.34 Modulus reduction curve based on the on-sample LVDTs (Gookin et al., 1996) 42

Fig. 2.35 Typical stress-strain response based on the on-sample LVDTs (Yimsiri et al., 2005) 42

Fig. 2.36 Typical representation of modulus reduction and damping ratio curves used for GRA 45

Fig. 3.1 Particle size distribution of BS and RS 51

Fig. 3.2 FESEM image of (a) BS (b) RS 52

Fig. 3.3 Compaction curve of RS 52

Fig. 3.4 Cyclic triaxial pressure system with connections and components 53

Fig. 3.5 Triaxial frame with actuator and base pedestal 54

Fig. 3.6 Triaxial cell and its components 55

Fig. 3.7 Dynamic actuator and its components 56

Fig. 3.8 Submersible load cell attached with triaxial cell 57

Fig. 3.9 Air Water Cylinder (AWC) unit 57

Fig. 3.10 Automatic Volume Change (AVC) unit 58

Fig. 3.11 Pressure transducers 59

Fig. 3.12 Dry air receiver unit 60

Fig. 3.13 (a) Compact Dynamic Controller (CDC) unit (b) Data logger unit 60

Fig. 3.14 Schematic diagram of a cyclic triaxial test setup 61

Fig. 3.15 (a) Split mould used for the preparation of sand specimen (b) Sand pouring into the mould (c) Prepared BS specimen 62

Fig. 3.16 (a) Mould for the preparation of RS specimen (b) Mould ready to be filled with water-mixed soil from one end, while the other end is fixed with the collar (c) Prepared RS specimen 64

Fig. 3.17 Consolidation schematic of test specimen (after Head, 1992) 67

Fig. 3.18 (a) Typical loading pattern (input) and (b) Deviatoric stress variation (output) for a strain-controlled cyclic test 70

Fig. 3.19 (a) Typical loading pattern (input) and (b) Deviatoric stress variation (output) for a stress-controlled cyclic test 71

Fig. 3.20 (a) Acceleration time histories (b) Frequency domain representation (c) Typical irregular stress time histories of input motions 73

Fig. 3.21 (a) Soil specimen with on-sample LVDTs (b) Schematic diagram for the assemblage and fixities used in local strain measurement 76

Fig. 3.22 Calibration curve of on-sample LVDTs 77

Fig. 4.1 Stress-strain variation for DBS subjected to different σ'_c 81

Fig. 4.2 Stress path plot for DBS subjected to different σ'_c 81

Fig. 4.3 Variation of excess PWP for DBS subjected to different σ'_c 82

Fig. 4.4 Variation of secant modulus at different σ'_c for DBS subjected to different σ'_c 82

Fig. 4.5 Stress-strain variation for SBS subjected to different σ'_c 83

Fig. 4.6 Stress path plot for SBS subjected to different σ'_c 84

Fig. 4.7 Variation of excess PWP for SBS subjected to different σ'_c 84

Fig. 4.8 Variation of secant modulus for SBS subjected to different σ'_c 85

Fig. 4.9 Stress-strain response for SBS at D_r = 30% 86

Fig. 4.10 Change in excess PWP for SBS at D_r = 30% 87

Fig. 4.11 Total and effective stress path for SBS at D_r = 30% 88

Fig. 4.12 Variation of Skempton's A-parameter for SBS at D_r = 30% 88

Fig. 4.13 Stress-strain response for SBS at different D_r 89

Fig. 4.14 Stress path plot for SBS at different D_r 90

Fig. 4.15 Variation in excess PWP for SBS at different D_r 90

Fig. 4.16 Variation in Skempton's A-parameter for SBS at different D_r 91

Fig. 4.17 Shear stiffness for SBS at different D_r 91

Fig. 4.18 Stress-strain response for SBS at different loading rates and D_r 92

Fig. 4.19 Variations in maximum deviator stress for SBS at different loading rates 93

Fig. 4.20 Variation of secant modulus for SBS at D_r = 30% at different loading rates 94

Fig. 4.21 Comparative variation of secant modulus of SBS at D_r = 30% and 90% for different loading rates 94

Fig. 4.22 Variation in excess PWP in SBS at different loading rates and D_r 95

Fig. 4.23 Variation in stress path of SBS at different loading rates and D_r 95

Fig. 4.24 Response of on-sample LVDTs at (*a*) D_r = 30% (*b*) D_r = 90%; Response of global and local LVDTs at (*c*) D_r = 30% (*d*) D_r = 90%; Stress-strain response (*e*) D_r = 30% (*f*) D_r = 90%; (*g*) Secant modulus based on global and local axial strain at D_r = 90% (h) Poisson's ratio at different D_r and σ'_c 98

Fig. 4.25 Effect of rubber band attachment on stress-strain response of SBS at different σ'_c 101

Fig. 4.26 Effect of rubber band attachment on stress-strain response of SBS at different D_r 101

Fig. 4.27 Variation of stress-strain of SBS with global and local strains 102

Fig. 4.28 Variation of secant modulus of SBS with global and local strains 103

Fig. 4.29 Comparative stress-strain variation of SBS and DBS 104

Fig. 4.30 Comparative stress paths plot for SBS and DBS 105

Fig. 4.31 Comparative variation of excess PWP of DBS and SBS 105

Fig. 4.32 Comparative variation of secant modulus of SBS and DBS 106

Fig. 4.33 Typical stress-strain response of RS specimen 107

Fig. 4.34 Typical variation in excess PWP of RS specimen 107

Fig. 4.35 Typical stress path plots for RS specimen 108

Fig. 5.1 Typical test results at ε = 0.20%, f = 1 Hz, σ'_c = 100 kPa and D_r = 30% (a) Axial strain vs N (b) Deviator stress vs N (c) PWP ratio vs N (d) Stress path plot (e) Hysteresis loops 112

Fig. 5.2 (a-h) Typical shear stress-shear strain plots at different γ for initial two cycles at D_r = 30%, σ'_c = 100 kPa and f = 1 Hz 114

Fig. 5.3 A typical symmetrical hysteresis loop (redrawn after Kramer, 1996) 115

Fig. 5.4 A typical asymmetrical hysteresis loop 115

Fig. 5.5 Variation of shear modulus with N at different shear strains 116

Fig. 5.6 Variation of shear modulus with shear strain based on ASHL 117

Fig. 5.7 Comparative variation of shear modulus with shear strain based on SHL and ASHL 117

Fig. 5.8 Variation of G/G_{max} with γ at different σ'_c and D_r 119

Fig. 5.9 Comparison of G/G_{max} for different soils 120

Fig. 5.10 Particle size distribution of different soils 120

Fig. 5.11 (a-f) Variation of $D^{\#}$ and D with N for γ = 0.045-0.75% 122

Fig. 5.12 Variation of D with γ at different σ'_c 123

Fig. 5.13 Variation of $D^{\#}$ with γ at different σ'_c 123

Fig. 5.14 Variation of D with γ at different D_r 124

Fig. 5.15 Variation of $D^{\#}$ with γ at different D_r 125

Fig. 5.16 Comparison of D and $D^{\#}$ of SBS 126

Fig. 5.17 Comparison of damping ratio of different soils from available data in literature .. 127

Fig. 5.18 Effect of loading frequency on shear modulus 128

Fig. 5.19 Effect of loading frequency on damping ratio 128

Fig. 5.20 Variation of excess PWP ratio with number of loading cycles at different loading frequencies 129

Fig. 5.21 Variation of excess PWP ratio with loading frequency for N = 1 130

Fig. 5.22 Variation of shear modulus with shear strain for f = 0.5–4.0 Hz and σ'_c = 50–150 kPa 130

Fig. 5.23 Variation of damping ratio with shear strain for f = 0.5–4.0 Hz and σ'_c = 50–150 kPa 131

Fig. 5.24 Strain time histories from external and on-sample LVDTs at peak axial strains (a) 0.03% (b) 0.2% (c) 0.66% 132

Fig. 5.25 Stress-strain plots based on external and on-sample LVDTs at D_r = 90%, σ'_c = 100 kPa and f = 1 Hz 133

Fig. 5.26 Comparative plot of shear modulus of SBS based on the external and on-sample LVDTs 134

Fig. 5.27 Comparative modulus reduction of SBS based on external and on-sample LVDTs 135

Fig. 5.28 (a-d) Typical test results obtained from stress-controlled cyclic triaxial test of SBS 137

Fig. 5.29 Variation of shear modulus of SBS with shear strain from stress-controlled loading 137

Fig. 5.30 Variation of damping ratio of SBS with shear strain from stress-controlled loading 139

Fig. 5.31 Hysteresis loop at N = 1 for different *CSR* 139

Fig. 5.32 Hysteresis loop at N = 23 for different *CSR* 140

Fig. 5.33 Variation of shear strain with number of cycles for different CSR 140

Fig. 5.34 Variation of excess PWP ratio with number of cycles for different CSR 141

Fig. 5.35 Variation of excess PWP ratio with shear strain for different CSR 141

Fig. 5.36 Variations of shear modulus and damping ratio with loading frequency for N = 1 142

Fig. 5.37 Variations of r_u and shear strain with loading frequency for N = 1 143

Fig. 5.38 Variations of r_u with number of loading cycles at different loading frequencies ... 143

Fig. 5.39 Variation of shear modulus obtained from strain- and stress-controlled excitations 145

Fig. 5.40 Variation of damping ratio obtained from strain- and stress-controlled excitations 145

Fig. 5.41 (a-d) Typical test results of DBS at ε = 0.20%, f = 1 Hz and σ'_c = 100 kPa 146

Fig. 5.42 (a-j) Typical shear stress-shear strain plot for SBS at different γ for initial two cycles at D_r = 60%, σ'_c = 100 kPa and f = 1 Hz 147

Fig. 5.43 Variation of shear modulus of DBS with shear strain at different σ'_c from strain-controlled tests 148

Fig. 5.44 Variation of damping ratio of DBS with shear strain at different σ'_c from strain-controlled tests 149

Fig. 5.45 Typical comparative hysteresis loops for SBS and DBS at two consecutive loading cycles (N = 1 to 2) 150

Fig. 5.46 Comparative variation of shear modulus for SBS and DBS with number of cycles from strain-controlled tests 151

Fig. 5.47 Comparative variation of damping ratio for SBS and DBS with number of cycles from strain-controlled tests 152

Fig. 5.48 Comparative variation of shear modulus for DBS and SBS with shear strain at different σ'_c from strain-controlled tests 153

Fig. 5.49 Comparative variation of modulus reduction for DBS and SBS with shear strain at different σ'_c from strain-controlled tests 154

Fig. 5.50 Variation of damping ratio of SBS with shear strain at different σ'_c from strain-controlled tests 154

Fig. 5.51 Comparative variations in damping ratio for DBS and SBS from strain-controlled tests 155

Fig. 5.52 Comparative modulus reduction curves obtained from present investigation and existing literatures 156

Fig. 5.53 Comparative damping ratio curves obtained from present investigation and existing literatures 156

Fig. 5.54 Stress-controlled stage cyclic loading applied on RS specimen 158

Fig. 5.55 A typical representation of the variations of G, D and r_u obtained from stage cyclic loading of RS specimen 158

Fig. 5.56 Hysteresis loop obtained at different loading cycles in stress-controlled loading of RS specimen 159

Fig. 5.57 Variation of shear modulus of RS obtained from stress-controlled tests 160

Fig. 5.58 Variation of G/G_{max} and damping ratio of RS obtained from stress-controlled tests 160

Fig. 6.1 Variation of r_u with N from a cyclic strain controlled test of SBS 164

Fig. 6.2 Variation of maximum r_u with N at different γ 165

Fig. 6.3 Variation of maximum r_u with N at different σ'_c and γ 166

Fig. 6.4 Variation of maximum r_u with N at different D_r and γ 167

Fig. 6.5 Variation of shear stress and CSR with N at different (a) γ (b) σ'_c (c) D_r 168

Fig. 6.6 Stress path plot from stress-controlled tests of SBS at various CSR 172

Fig. 6.7 Variation in r_u with number of cycles at different *CSR* obtained from stress-controlled test 172

Fig. 6.8 Variations in γ with number of cycles at different *CSR* obtained from stress-controlled test 173

Fig. 6.9 Variation of CSR with number of loading cycles obtained from stress-controlled test 173

Fig. 6.10 Variation of r_u with N at different σ'_c and *CSR* for D_r = 30% 174

Fig. 6.11 Variation of γ with N at different σ'_c and *CSR* for D_r = 30% 176

Fig. 6.12 Variation of r_u with N at different σ'_c and *CSR* at D_r = 60% 176

Fig. 6.13 Variation of γ with N at different σ'_c and *CSR* at D_r = 60% 177

Fig. 6.14 Variation of r_u with N at different D_r and CSR at σ'_c = 50 kPa 179

Fig. 6.15 Variation of γ with N at different D_r and *CSR* at σ'_c = 50 kPa 179

Fig. 6.16 Variation of r_u with N for simultaneous increase of D_r and σ'_c 181

Fig. 6.17 Variation of γ with N for simultaneous increase of D_r and σ'_c 182

Fig. 6.18 Variation of CSR with N_L 182

Fig. 6.19 Pore pressure models (relationship between r_u and N/N_L) proposed from present study in comparison to the existing literature 183

Fig. 6.20 Relationship between r_u and γ based on the stress-controlled approach obtained from the present study and that reported by Cetin and Bilge (2012) 184

Fig. 6.21 Accumulation of shear strain and excess PWP ratio in SBS specimens at σ'_c = 100 kPa for different D_r and subjected to (a) Bhuj (b) Tezpur (c) Kobe strong motions 186

Fig. 6.22 Accumulation of shear strain and excess PWP ratio in SBS specimens at D_r = 30% and different σ'_c for (a) Bhuj (b) Tezpur (c) Kobe strong motions 190

Fig. 6.23 Accumulation of shear strain and excess PWP ratio in SBS specimens subjected to Bhuj motion of PGA 0.103g for simultaneous variation in D_r and σ'_c 192

Fig. 6.24 Accumulation of shear strain and excess PWP ratio in SBS samples prepared at D_r = 60% and σ'_c = 100 kPa, and subjected to scaled earthquake motions of PGA 0.103g and 0.36g 193

Fig. 7.1 (a) Seismicity of India and study region (IS 1893: 2002) (b) Seismic fault details nearby the study region (Raghukanth and Dash, 2010) 198

Fig. 7.2 Location of boreholes used for GRA of Guwahati city 199

Fig. 7.3 Typical borehole profile at sites (a) BRGN (b) STGN (c) ALKSX (d) SUND 200

Fig. 7.4 Soil models for locally available soils used for GRA of Guwahati city 202

Fig. 7.5 Acceleration time histories of input motions used for GRA study 205

Fig. 7.6 Variation in PHA along the depth at BRGN, STGN, ALKSX and SUND sites subjected to Bhuj motion 207

Fig. 7.7 Variations in strain at (a) BRGN and SUND (b) STGN and ALKSX sites subjected to Bhuj motion 208

Fig. 7.8 Variations in amplification ratio at BRGN, STGN, ALKSX and SUND sites subjected to Bhuj motion 208

Fig. 7.9 Variations in PSA at BRGN, STGN, ALKSX and SUND sites subjected to Bhuj motion 209

Fig. 7.10 Variations in PGA at surface level due to Bhuj motion based on (a) experimental data (b) VD-SI data 210

Fig. 7.11 Variations in peak FAR at surface level due to Bhuj motion based on (a) experimental data (b) VD-SI data 212

Fig. 7.12 Variations in PSA at surface level due to Bhuj motion based on (a) experimental data (b) VD-SI data 213

Fig. 7.13 Variations in PHA with depth at BRGN due to Bhuj, Tezpur and Kobe motions . 214

Fig. 7.14 Variations in strain with depth at BRGN using (a) Bhuj and Tezpur motions (b) Kobe motion 215

Fig. 7.15 Variations in amplification ratio at surface level for BRGN due to Bhuj, Tezpur and Kobe motions 216

Fig. 7.16 Variations in SA at surface level for BRGN due to Bhuj, Tezpur and Kobe motions 216

Fig. 7.17 PGA based on Bhuj motion using (a) experimental data (b) VD-SI data 218

Fig. 7.18 PGA based on Tezpur motion using (a) experimental data (b) VD-SI data 219

Fig. 7.19 PGA based on Kobe motion using (a) experimental data (b) VD-SI data..... 220

Fig. 7.20 FAR based on Bhuj motion using (a) experimental soil data (b) VD-SI data..... 221

Fig. 7.21 FAR based on Tezpur motion using (a) experimental soil data (b) VD-SI data 222

Fig. 7.22 FAR based on Kobe motion using (a) experimental data (b) VD-SI data..... 223

Fig. 7.23 PSA based on Bhuj motion using (a) experimental data (b) VD-SI data 225

Fig. 7.24 PSA based on Tezpur motion using (a) experimental data (b) VD-SI data..... 226

Fig. 7.25 PSA based on Kobe motion using (a) experimental data (b) VD-SI data 227

LIST OF TABLES

Table 2.1 Typical frequency range for cyclic triaxial test 18

Table 2.2 Summary of literature review on the variation of shear modulus and damping ratio with different parameters 30

Table 2.3 Summary of literature review on the variation of liquefaction potential with different parameters 34

Table 2.4 Various instrumentations for local strain measurement in triaxial tests 39

Table 2.5 Material curves used in GRA 44

Table 3.1 Physical properties of Brahmaputra Sand (BS) 50

Table 3.2 Physical properties of Red Soil (RS) 51

Table 3.3 Time taken to saturate sand specimen 63

Table 3.4 Testing program for monotonic tests 68

Table 3.5 Investigation parameters of the strain-controlled CT tests 70

Table 3.6 Investigation parameters used in stress-controlled CT tests 71

Table 3.7 Investigating parameters of the irregular seismic excitations 74

Table 5.1 Investigation parameters of the strain-controlled CT tests 110

Table 5.2 Investigation parameters used in stress-controlled CT tests 110

Table 5.3 Estimated G_{max} for BS 118

Table 5.4 Estimated G_{max} values for BS 134

Table 6.1 Parameters of the strain controlled cyclic triaxial tests 170

Table 6.2 Summary of results regarding the number of cycles and shear strain generated at the onset of liquefaction for SBS subjected to regular excitation and at different σ'_c . 178

Table 6.3 Summary of results regarding the number of cycles and shear strain generated at the onset of liquefaction for SBS subjected to regular excitation and prepared at different D_r 180

Table 6.4 Summary of investigations on BS specimens prepared at different D_r and subjected to various strong motions 188

Table 6.5 Summary of investigations on BS specimen subjected to different σ'_c and strong motions 191

Table 6.6 Summary of results subjected to scaled ground motions with same PGA 194

Table 6.7 Ground motion parameters of scaled PGA of 0.103g and 0.36g 194

Table 7.1 Strong motion parameters for different earthquakes used for the analysis..... 205

Table 7.2 Comparison of percentage difference in PGA, PSA and FAR obtained using VD-SI and Experimental data for GRA of Guwahati city using Bhuj motion 214

Table 7.3 Comparison of percentage difference in PGA, PSA and FAR obtained using VD-SI and Experimental data for GRA Guwahati city using Bhuj, Tezpur and Kobe motions 228

NOTATIONS AND ABBREVIATIONS

Δu	Pore pressure increment
$\Delta\sigma_c$	Cell pressure increment
A_c	Area of specimen after consolidation
B-value	Skempton's B-parameter
$CSR_{desired}$	Desired cyclic stress ratio ($\pm\sigma_d/2\sigma'_c$)
CSR_{max}	Maximum value of CSR in irregular laoding
D	Damping ratio based on SHL
$D^{\#}$	Damping ratio based on ASHL
D_r	Relative density
e	Void ratio
f	Loading frequency
G *and* G_a	Shear modulus based on SHL and ASHL, respectively
G/G_{max}	Normalized shear modulus
G_{max}	Maximum shear modulus
M_w	Magnitude of earthquake
N	Number of cycles
N_L	Number of cycle to liquefaction
p'	Mean effective stress
P_c	Estimated cyclic load to be applied on the specimen
r_u	Excess PWP ratio
$r_{u,max}$	Maximum value of excess PWP ratio
u_e	Excess PWP
w	Water content, used to prepare cohesive soil specimen
γ	Shear strain amplitude
γ_{max}	Maximum shear strain
γ_t	Threshold shear strain
σ_v	Total overburden vertical stress
σ'_c	Effective confining stress
σ_d	Deviatoric stress
$\sigma_{d,\,max}$	Maximum or peak deviatoric stress
τ	Shear stress

τ_{max}	Maximum shear stress
ϕ	Internal frictional angle of soil
AWC	Air water cylinder
ASHL	Asymmetrical hysteresis loop
AVC	Automatic volume change
BP	Back pressure
BS	Brahmaputra sand i.e. Cohesionless soil
CP	Cell pressure
CDC	Compact dynamic controller
CSR	Cyclic stress ratio
CT	Cyclic traixal
DA	Double amplitude
DBS	Dry Brahmaputra sand
FAR	Fourier amplitude acceleration
GRA	Ground Response Analysis
LVDT	Linear Variable Differential Transducer
LL	Liquid limit
MDD	Maximum dry density
OMC	Optimum moisture content
OCR	Overconsolidation ratio
PSD	Particle size distribution
PGA or PHA	Peak ground/horizontal acceleration
PSA	Peak spectral acceleration
PL	Plastic limit
PI	Plasticity index
SP	Poorly graded sand
PWP	Pore-water pressure
RS	Red soil i.e. Cohesive soil
SBS	Saturated Brahmaputra sand
SI	Seed and Idriss (1970)
SHL	Symmetrical hysteresis loop
VD	Vucetic and Dobry (1991)

Chapter 1 INTRODUCTION

1.1 GENERAL

With increasing urbanization, demand of seismic resistant geotechnical structures such as buildings, bridges and embankments has become a prominent and challenging task for geotechnical engineers. Most of the damages (Fig. 1.1), during the past earthquake incidences, are greatly influenced by the response of soil deposits. Since, earthquake is one of the most devastating natural phenomena on the earth, geotechnical ground response analysis is an important step to foresee the potential consequence of strong earthquakes. In this regard, as well as in other engineering problems, the properties of soils in terms of secant modulus or elastic modulus, dynamic shear modulus, damping ratio and pore pressures variations etc. are required. Dynamic response of soil and soil-supported structures depends on the soil stratification, stiffness of the soil, and the amplitude and frequency contents of the earthquake motions (Kramer, 1996).

The behaviour of soils during earthquakes is quite complex due to the irregular nature of loading and having a wide range of frequency content. The dynamic responses of soils are portrayed through the dynamic soil properties and the liquefaction parameters. Dynamic soil properties namely shear modulus and damping ratio and, liquefaction potential parameters namely cyclic stress ratio (CSR) and excess pore water pressure ratio (r_u) are the primary investigating parameters for various dynamic studies related to the ground response analysis as well as for design or requalification of earthquake resistant structures.

In order to assess the damages to structures subjected to earthquakes or cyclic loads and establishing the avenues for the damage mitigation, various idealized models, analytical and numerical techniques are in practice (Okur and Ansal, 2007; Maheshwari et al., 2012). All the models and techniques require the dynamic soil properties in terms of modulus reduction curve,

damping ratio curve and fitting constants of pore water pressure model as input parameters, which can be evaluated using variety of field and laboratory experimentations. Various instruments such as cyclic triaxial apparatus, simple shear apparatus, resonant column apparatus and bender elements are available to evaluate the dynamic properties and liquefaction potential parameters of soils for different range of strains and stresses (Kramer, 1996). Each of the appurtenances and the corresponding methodologies applied have their own inherent advantages and disadvantages. Therefore, the selection of test method should be based on the conditions of the site and problem of concern (Jafarzadeh and Sadeghi, 2012). For the evaluation of dynamic response of soils (estimation of dynamic properties and liquefaction potential parameters), past studies have considered both regular and/or irregular loadings. Additionally, both global and local strain measurements have been taken into for the analyses and estimation of average and on-sample strains, to study their effect on the overall and local response of the samples over a wide range of strains.

Although, several literatures are available on the assessment of dynamic properties of soils from different parts of the world, it is extremely necessary to find the same for local regional soils for prudent applications. Since the soils of different regions differ in their composition, estimation of specific dynamic properties and determination of their associated responses are essential and very crucial.

Assam, the North-eastern region of India, is one of the most seismically active regions in the world (IS: 1893-2002), and has experienced several devastating earthquakes of different moment magnitudes in the past, ranging from M_w5 to M_w8.7 (Raghukanth, 2008). Extensive liquefaction, approximately in 126 acres area, during 1950 Assam earthquake, was also reported (Raghukanth, 2008; Poddar, 1953). Due to frequent occurrence of low and moderate magnitude earthquakes, and possible high magnitude earthquakes are expected to occur in the region owing to the seismic gap, it is extremely important to understand the response of the soils under

dynamic conditions to ascertain the possible damages and get equipped with proper mitigation measures.

Fig. 1.1 Different modes of seismic damages (a) ground failure and (b) liquefaction during 2010 Christchurch earthquake, (c) foundation failure during 1964 Niigata earthquake (d) landslide in Brazil druing 2011 disaster

1.2 AIM OF THE STUDY

The aim of the present study is to investigate the dynamic behaviour and dynamic properties of local soils (cohesionless and cohesive soils) collected from Guwahati region, Assam. Since Assam and entire Northeast region are highly seismically active, the obtained results would be helpful for the seismic studies of this region.

The broad objective of the study is to investigate the response of local soils using regular (sinusoidal) and irregular (earthquake) motions, in terms of strain dependent dynamic properties i.e. shear modulus and damping ratios and liquefaction parameters, through cyclic

triaxial (CT) tests. Further, the results of this investigation will be used in ground response analysis to ascertain the behaviour of the region under strong motions.

1.3 ORGANIZATION OF THESIS

The investigations and outcomes of the present study have been reported sequentially in this thesis through several chapters which are organized as follows:

Chapter 1 briefly discusses the significance of the research, broad objective of the study and organization of the thesis.

Chapter 2 presents a review of literature relevant to the present research work. The chapter concludes with critical appraisal of the literature and detailed scope of the work.

Chapter 3 describes the materials used in the study and their basic characterizations. The chapter also describes the cyclic triaxial testing equipment used in the study, the corresponding testing programs and their accompanying details.

Chapter 4 presents results of the monotonic compression shear tests conducted on cohesionless and cohesive soils along with the interpretation of the outcomes.

Chapter 5 presents the detailed dynamic response of local soils, in terms of dynamic properties i.e. shear modulus and damping ratio, of RS and BS soils under strain and stress-controlled cyclic loading conditions.

Chapter 6 presents the liquefaction evaluation of BS at different loading conditions such as regular and irregular seismic excitations using cyclic triaxial tests.

Chapter 7 presents the ground response analysis of Guwahati city using evaluated and existing material models incorporating the dynamic properties.

Chapter 8 presents the summary of the work, conclusions from the present thesis work, and future scope of the work.

Chapter 2 LITERATURE REVIEW

2.1 INTRODUCTION

Targeting the broad objective of this study, this chapter presents detailed review of literatures on the responses of soils under monotonic and cyclic loading. Further, discussions have been categorised based on the literature on cyclic loading considering the two prevalent loading patterns: (1) regular (sinusoidal) and (2) irregular (transient) excitations. Since, cyclic triaxial tests commonly used to evaluate the response of soils at high shear strains, the on-sample transducers was used to measure the intermediate/local strains and, accordingly literatures in this regard have been discussed in this chapter. Literatures pertaining to the importance and application of the dynamic soil properties in ground response analysis have also been reviewed and presented. Finally, the critical appraisal of the literature reviewed and a detailed objective of the present study have concluded the chapter.

2.2 MONOTONIC RESPONSE OF SOILS

The responses of stress-strain behaviour of different soils under static loading may be different due to the structural orientation or arrangement of soil particles. Several literatures are available on the behaviour of soils under uniaxial loading at different testing conditions.

Miura and Toki (1982) have experimentally investigated the response of sand under different sample preparation techniques such as moist sample preparation, dry tapping and wet tapping as shown in Fig. 2.1. It was highlighted that the adoption of different sample preparation methodologies affects the behaviour and shear strength of soil. Similar observations have also been reported by several researchers, when the soil specimens were prepared by dry or wet pluviation, slurry deposition or water sedimentation and vibrations or moist-tamping method (Ladd, 1978; Chaney and Mulilis, 1978; Vaid and Negussey, 1988; Ishihara, 1993; Amini and

Qi, 2000; Vaid and Sivathayalan, 2000; Amini and Chakravrty, 2003; Juneja and Raghunandan, 2010; Della et al., 2011).

The test methodologies such as compression or extension shear of a saturated triaxial specimen at drained or undrained conditions affects the strength of soil. Seed and Lee (1966) have conducted the triaxial shearing at both drained and undrained conditions of the sand. Typical the stress-strain responses reported, are presented in Fig. 2.2. It has been observed that the shearing under undrained condition reflects higher stress-strain response in comparison to the drained condition, because both soil particles and water are assumed to be incompressible and load taken by soil-water medium is higher at undrained shearing condition than the drained shearing.

Ishihara (1993) carried out the triaxial tests on saturated sand at different effective confining pressures and the responses are presented in Fig. 2.3. Fig. 2.3a represents that the strength (resistance to deform and failure) the soil sample increases with the increase of confining pressures. During undrained triaxial tests, the initially effective stress decreases due to the increase of pore water pressure (PWP), reflecting contractive behaviour of sand, and reaches the minimum deviator stress as shown in Fig. 2.3b. The state of minimum deviator stress is called as state of phase transformation, at which soil changes the phase from contractive to dilative (Ishihara, 1993). The contractive behaviour and excess PWP development were more prominent at high confining pressure. Tests on the saturated sand under undrained monotonic loading also revealed the possibility of static liquefaction (Castro, 1975; Kramer and Seed, 1988; Dash and Sitharam, 2011).

Della et al. (2011) carried out undrained triaxial compression tests at different degrees of saturation, represented by varying Skempton's B-parameter (ranging between 32 and 90%), the results of which are presented in Fig. 2.4. It can be seen that the increase in the degree of saturation leads to a reduction in the resistance of the deviatoric stress (Fig. 2.4a) and an

increase in the pore-water pressure (Fig. 2.4b). The stress path plot in Fig. 2.4c also signifies the role of the degree of saturation in the reduction of the effective mean stress and the maximum deviatoric stress. Della et al. (2011) also indicated that the increase in degree of saturation (higher value of Skempton's pore pressure coefficient 'B') reduces the soil dilatancy and amplifies the contractive phase. Based on undrained triaxial compression shear tests, Sarma et al. (2016) have also reported that with increase of degree of saturation, initial stiffness and resistance (peak deviator stress) of the soil decreases. Literatures also revealed that the increase in degree of saturation leads to a decreases in the liquefaction resistance of soil (Martin et al., 1978; Yoshimi et al., 1989; Ishihara et al., 2001, 2004; Yang and Elgamal, 2002; Yang et al., 2004; Bouferra et al., 2007; Arab et al., 2016).

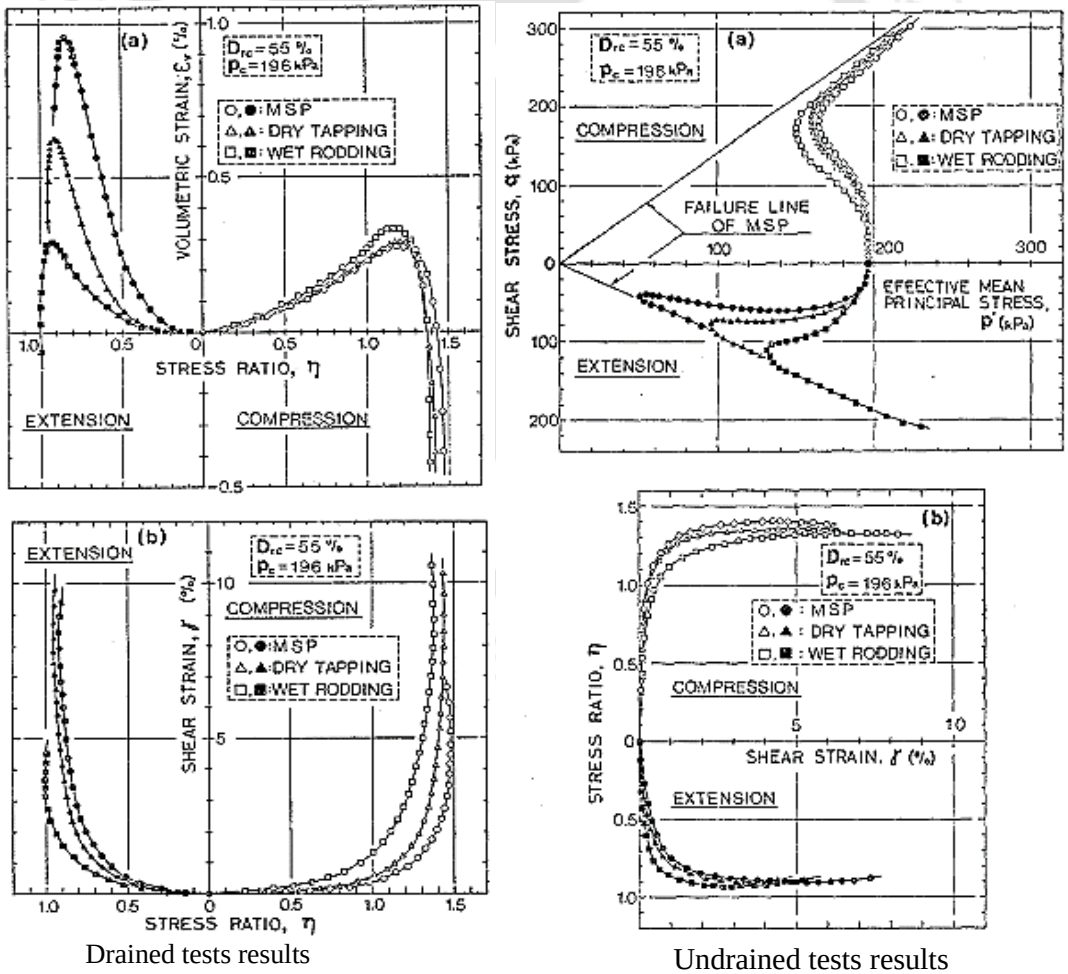

Drained tests results

Undrained tests results

Fig. 2.1 Typical plot of the effect of sample preparation method in triaxial testing at different testing conditions (Miura and Toki, 1982)

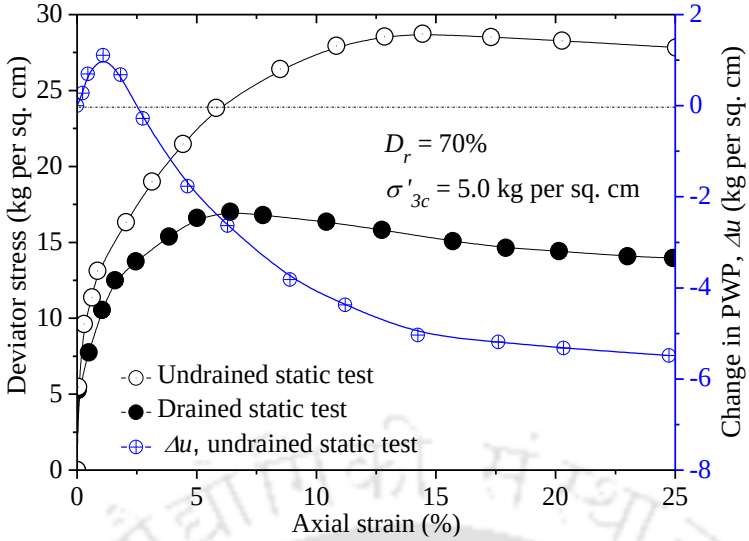

Fig. 2.2 Comparison of drained and undrained testing conditions on dense sand (redrawn after Seed and Lee, 1966)

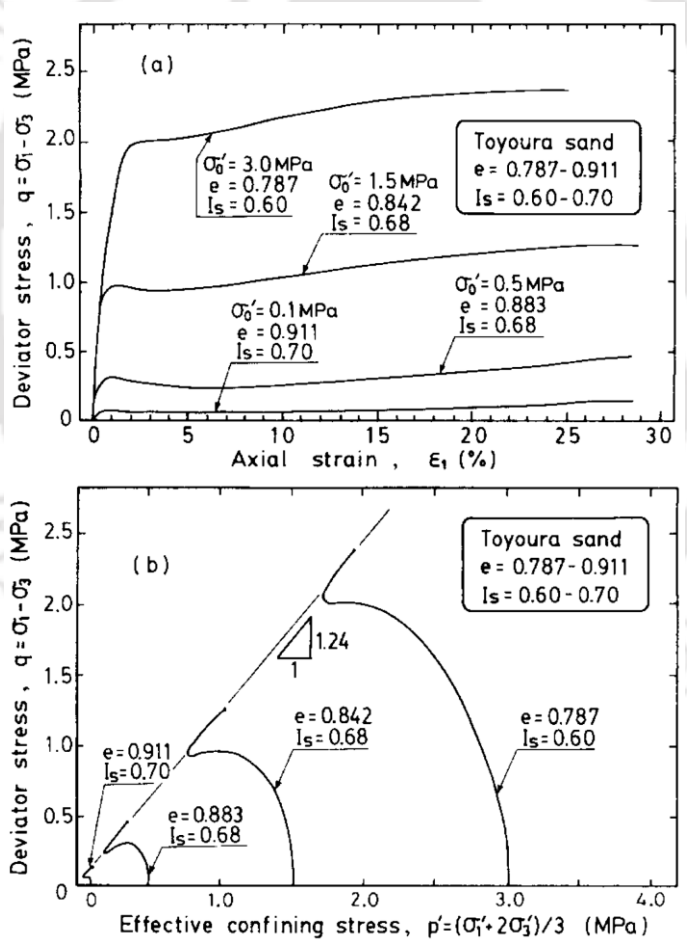

Fig. 2.3 Typical plot of effect of confining pressure on (a) stress-strain response (b) stress path for sand (Ishihara, 1993)

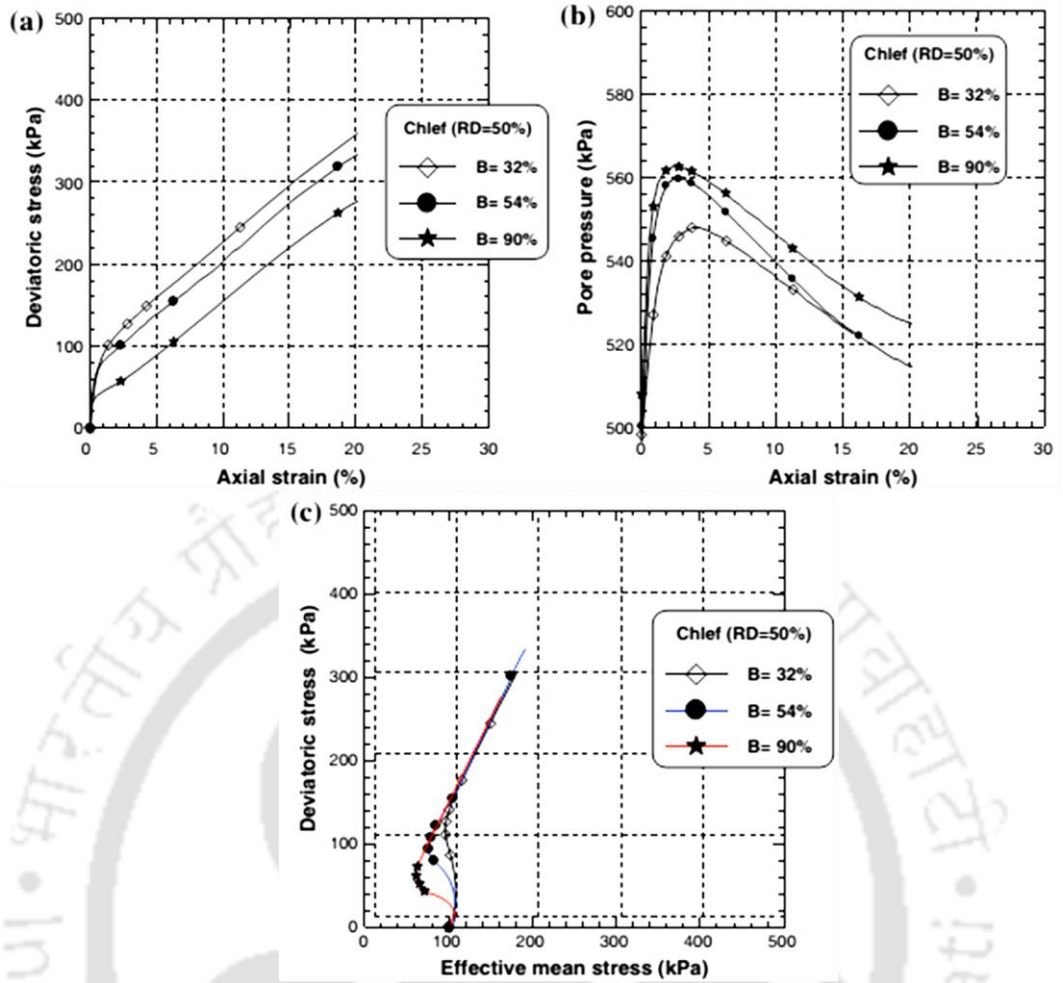

Fig. 2.4 Typical plots representing the effect of saturation on undrained behavior of sand (Della et al., 2011)

Yamamuro et al. (2011) have investigated the effect of strain rates on sandy soil specimens. It was reported that with the increase in strain rates the elasto-plastic stiffness of sand increased significantly. It was also reported that with increasing strain rates the failure shear strength of sand increased moderately whereas, the axial strain at peak stress decreased significantly and the volumetric strains became more dilatant. Several other researchers have also reported the effects of strain rate on the soil behaviour for various practical purposes, such as design of pile foundation and stability of an earth fill dam during earthquakes, but no conclusive consensus were reported because of contradicting conclusions (Casagrande and Shannon, 1948; Whitman and Healy, 1962; Lee et al., 1969; Ito and Fujimoto, 1981; Yamamuro and Lade, 1993; Tatsuoka et al., 2008; Omidvar et al., 2012; Watanabe and Kusakabe, 2013;

Svoboda, 2013). Watanabe and Kusakabe (2013) reported the behaviour of undrained tests on saturated sand, in terms of the variations in deviator stress and excess pore water pressure with axial strain, at different loading rates as shown in Fig. 2.5. It was confirmed from Fig. 2.5a that the sand exhibits stiffer response and higher shear strength when it is subjected to faster strain rate. The peak strength, defined at the maximum deviator stress, also increases with the increase of strain rate. Fig. 2.5b presents the variations in excess pore water pressure with strain rate. It is seen that the rate of generation and redistribution of excess pore water pressure is reduced with the increase in strain rate was higher.

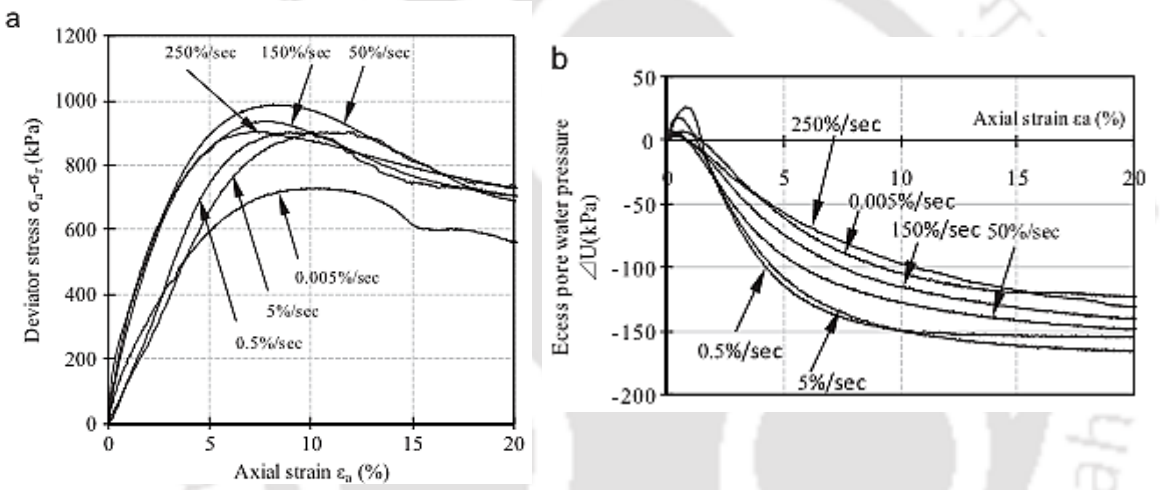

Fig. 2.5 Typical plots of (a) stress-strain response (b) excess PWP, with strain at different loading rates on saturated sand under undrained condition (Watanabe and Kusakabe, 2013)

Arab et al. (2016) carried out undrained tests on sandy specimens at different initial relative densities (D_r) and the results are presented in Fig. 2.6. Fig. 2.6 (a) presents the deviator stress versus axial strain, Fig. 2.6 (b) presents the pore pressure versus axial strain and, Fig. 2.6 (c) presents the mean effective stress (p') versus deviator stress (σ_d). It was obserevd that the specimens reconstituted at D_r = 64 % and 78 % shows higher resistance to deform than the specimen prepared at D_r = 8%. It was also obserevd that loose sand (D_r = 8 %) shows a phase of contractancy (Fig. 2.6c), due to the generation of the high pore water pressure (Fig. 2.6b), followed by a phase of dilatancy characterizing the decrease of the pore water pressure (Fig.

2.6c). Similar observations were also been reported by Ishihara (1993) and De and Basudhar (2008).

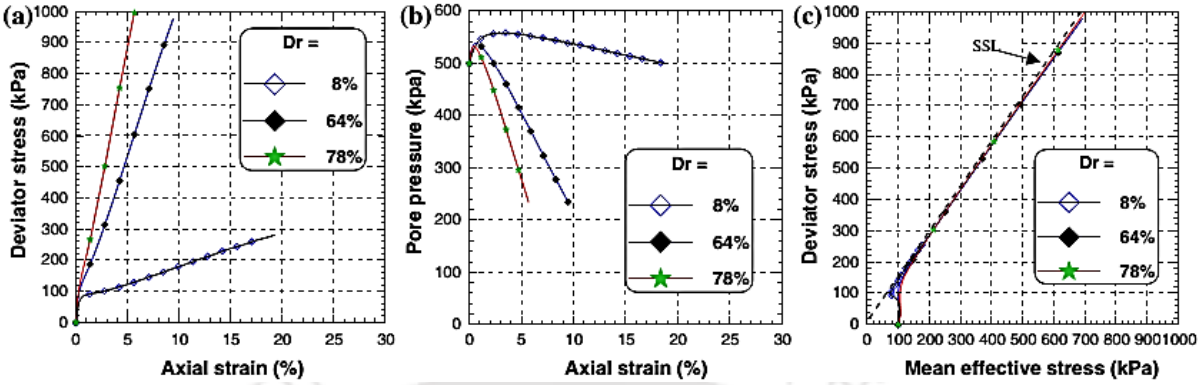

Fig. 2.6 Undrained behaviour of sand: (a) Deviator stress versus axial strain (b) PWP versus axial strain (c) Mean effective (p') stress versus deviator stress (σ_d) (Arab et al., 2016)

2.3 CYCLIC RESPONSE OF SOILS

2.3.1 Studies based on the regular (sinusoidal) loading

Several researchers have worked on the evaluation of dynamic properties and response of soils at different test conditions and experimentation techniques. Different methodologies for sample preparation such as air-pluviation, wet-tamping, moist-vibration, trimming, spooning and raining technique, dry deposition and water-sedimentation are common in practice. Mulilis et al. (1977) have reported that the air-pluviation technique and moist-vibration technique provides loose and dense soil specimens, respectively. It was also reported that the strength of soil obtained by moist taming is generally 58% higher than that obtained by dry tamping (pluviated air), shown in Fig. 2.7. The strength of soil is not only affected by methods of sample preparation, but also by testing methodology (Ishihara et al., 1978; Silver et al., 1980; Tatsuoka et al., 1982). Considering 70 mm and 300 mm diameter specimens with similar height-to-diameter ratios, Wong et al. (1975) compared the effects of size on cyclic strength of Monterey sand samples, and reported that the specimen of 300 mm diameter was approximately 10% weaker in strength than the specimen of diameter 70 mm, in terms of the cyclic deviator stress to initiate liquefaction (Fig. 2.8). Cyclic strength of the undisturbed specimen was

approximately 15% greater than that of the reconstituted specimens (Ishihara et al., 1978a). Silver and Ishihara (1977) have also reported that the strength ratio of undisturbed and reconstituted samples ranged between 1.14–1.22.

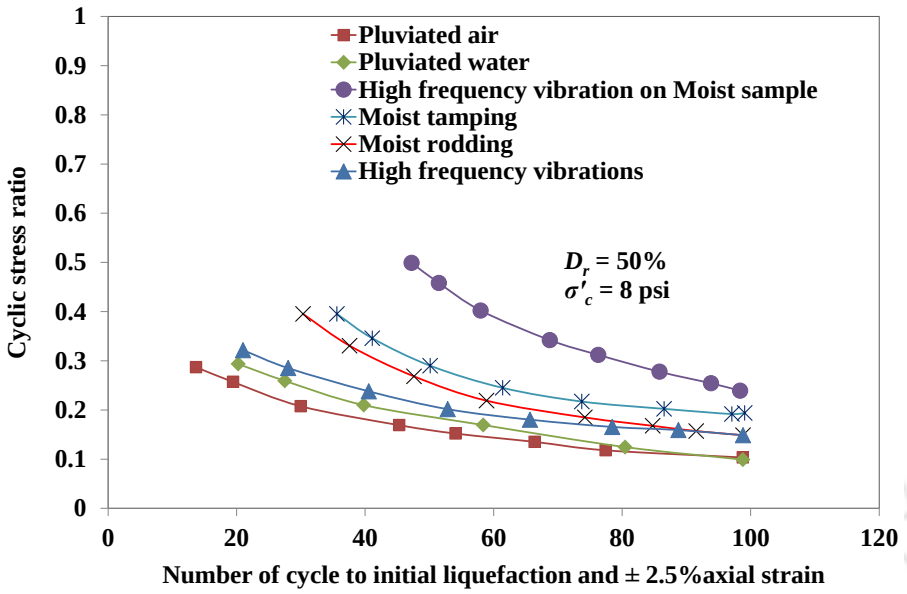

Fig. 2.7 Cyclic stress ratio versus number of cycles for different sample preparation techniques (redrawn after Mulilis et al., 1977)

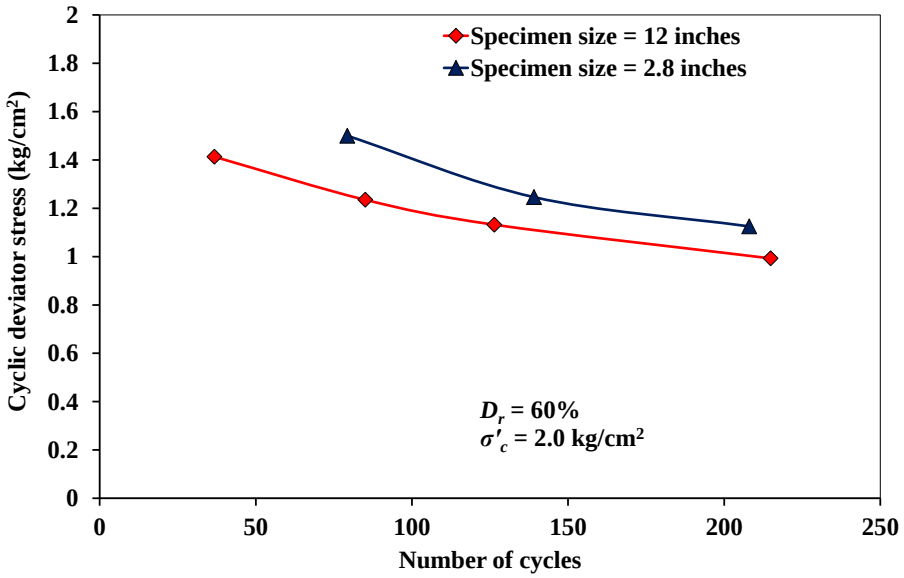

Fig. 2.8 Effect of specimen size on cyclic stresses causing initial liquefaction of Monterey Zero sand (redrawn after Wong et al., 1975)

Katayama et al. (1986) have reported that, for Fujisawa sand, the undisturbed sample reflects almost double the shear modulus than that of the disturbed sample as depicted in Fig. 2.9. However, damping ratios for the disturbed and undisturbed samples were not significantly different, as shown in Fig. 2.10. The shear modulus obtained from stress-controlled cyclic triaxial tests were slightly higher than strain-controlled cyclic triaxial tests at a given shear strain level, due to the influence of the method of sample preparation (Govindaraju, 2005). Townsend (1978) reviewed the effect of testing procedure and material characteristics on the cyclic strength of cohesionless soils. It was found that the specimen preparation methods (intact and reconstituted specimens), confining stress, relative density, loading waveform, particle size (D_{50}) and gradation, and overconsolidation ratio (OCR) have significant effect on the cyclic strength. However, other factors such as freezing intact specimens, loading frequency and specimen size having minor effects on the cyclic strength. Walberg (1977) examined the freezing effects on cyclic strength of undisturbed reconstituted sand specimens and reported that the freezing has practically no effect on cyclic strength.

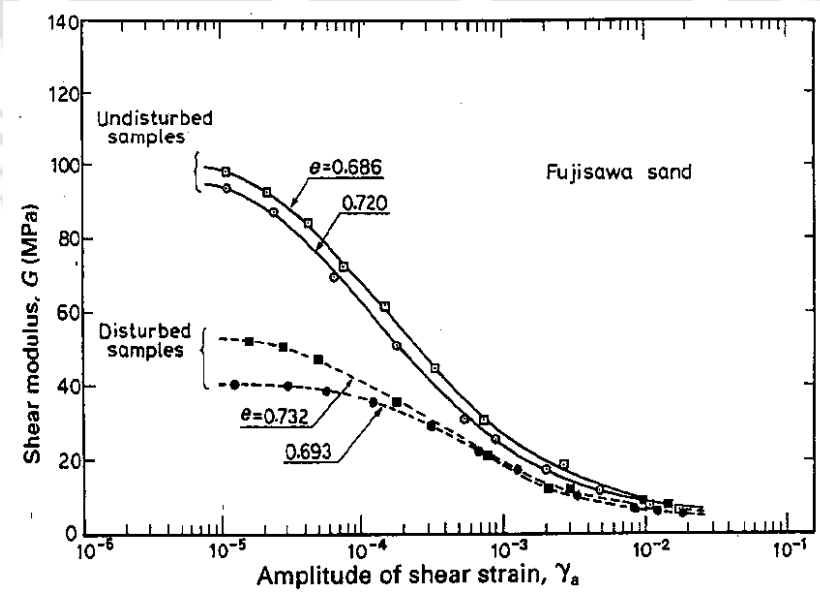

Fig. 2.9 Comparison of shear modulus of undisturbed and disturbed dense sand samples (Katayama et al., 1986)

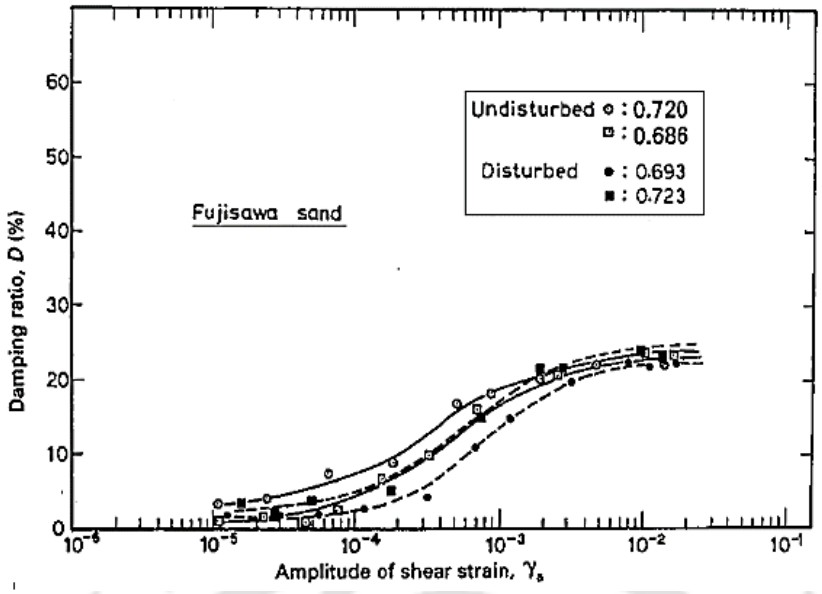

Fig. 2.10 Comparison of damping ratio of undisturbed and disturbed dense sand samples (Katayama et al., 1986)

Kokusho (1980) performed a series of cyclic triaxial tests on isotropically consolidated saturated Toyoura sand (initial void ratios: 0.64-0.80) subjected to different effective confining stress (19.6 kPa-294 kPa) and frequency (0.02 Hz-0.1 Hz). It was reported that the shear modulus and damping ratio are significantly affected by initial void ratio shown in Fig. 2.11. It was also reported that with the increase in confining pressure, shear modulus increases and damping ratios decreases, shown in Fig. 2.12 and Fig. 2.13, respectively. Similar observations related to the effect of confining pressure and void ratio (relative density) on strain-dependent dynamic properties have been reported by several researchers (Tatsuoka et al., 1978; Iwasaki and Tatsuoka, 1977; Iwasaki et al., 1978; Kokusho, 1980; Lin et al., 1996; Vucetic et al., 1998; Feng and Sutter, 2000; Sitharam et al., 2004a,b; Mohtar et al., 2013). Further, researchers have reported that the number of cycles, required causing initial liquefaction and failure, increases with increase in confining pressure (Ishihara et al., 1978b; Silver et al., 1980; Hosri, 1984; Choudhary et al., 2010). Sitharam et al. (2012) have reported that the progressive degradation of stiffness and accumulation of strain during strain-controlled and stress-controlled tests, respectively, causes liquefaction due to increase in excess PWP resulting in the softening of the

sand specimen. It was also reported that, in comparison to the strain-controlled cyclic tests, the use of stress-controlled cyclic tests is less reliable for the determination of shear modulus and damping ratio because of the development of different strain amplitudes in compression and extension phases.

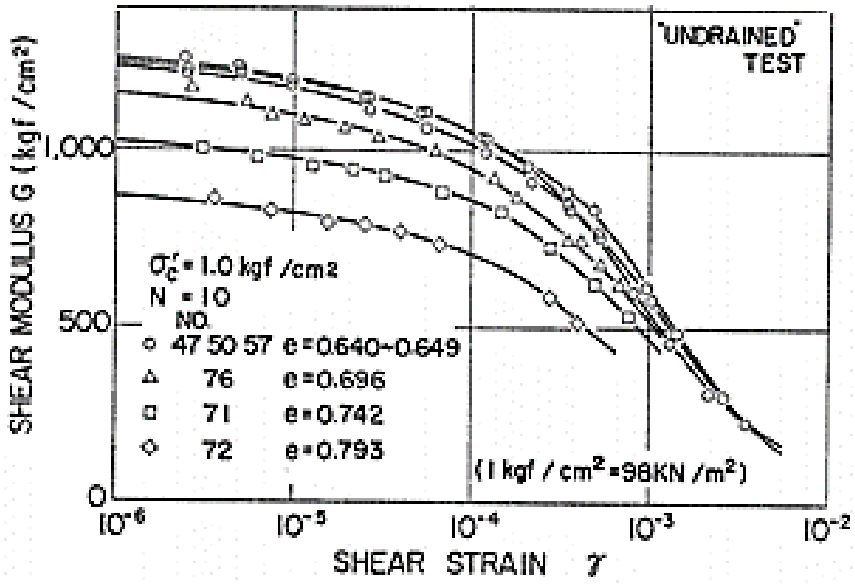

Fig. 2.11 Shear modulus versus shear strain for σ'_c = 98 kN/m^2 with different void ratios (Kokusho, 1980)

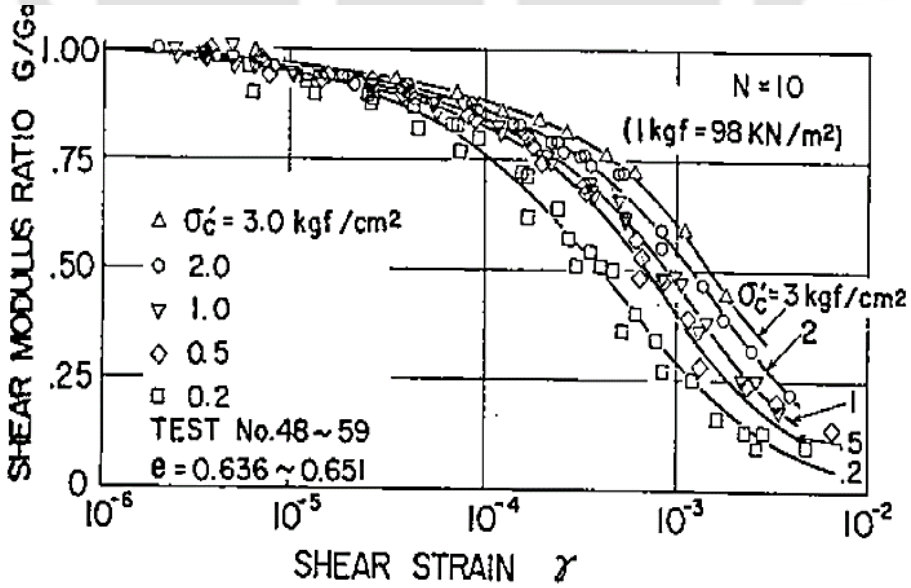

Fig. 2.12 Variation of shear modulus ratio with γ for dense sand subjected to different σ'_c (Kokusho, 1980)

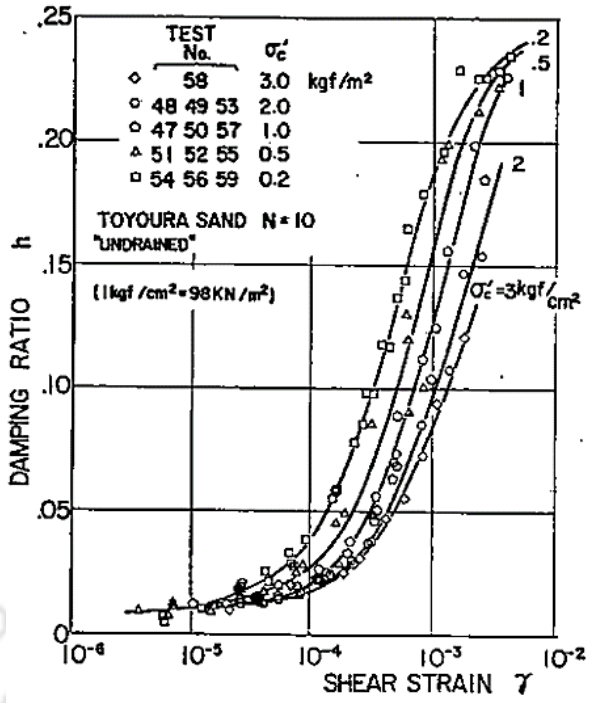

Fig. 2.13 Variation of damping ratio with γ for dense sand subjected to different σ'_c (Kokusho, 1980)

Mulilis (1975) reported that the liquefaction behaviour is influenced by the methods of sample preparation and effective confining pressure, as shown in Fig. 2.14. However, Talaganov (1996) reported that the effects of both relative density and confining pressure on liquefaction potential of sand are not significant. Experimental investigations (Laboratory and centrifuge test) and numerical modelling also revealed that the liquefaction potential increases with depth depending upon peak ground acceleration and soil conditions (Seed and Idriss, 1971; Elgamal et al., 1996; Byrne et al., 2004; Sreng et al., 2015; Qu et al., 2016). Tumi (1983) and Govindaraju (2005) have reported that the liquefaction resistance is decreased with the increase of confining pressure based on the stress-controlled tests, while the same is found to increase on the adoption of strain-controlled approach. Thus, it can be stated that the liquefaction resistance of sandy soil is significantly affected by testing conditions. During cyclic loading, it is common practice of applying sinusoidal loading waveform by converting earthquake motion to the equivalent number of harmonic loading cycles. Several researchers have reported the dynamic properties of soil and the cyclic strength based on the use of other waveforms, namely

rectangular and triangular waveforms. Seed and Chan (1964) and Thiers (1965) have investigated and reported that the triangular loading waveform resulted in 5–20% higher strength than the rectangular loading. Mulilis et al. (1978) reported that application of sinusoidal waveform resulted in approximately 30% higher cyclic strength than both rectangular and triangular waveforms as represented in Fig. 2.15.

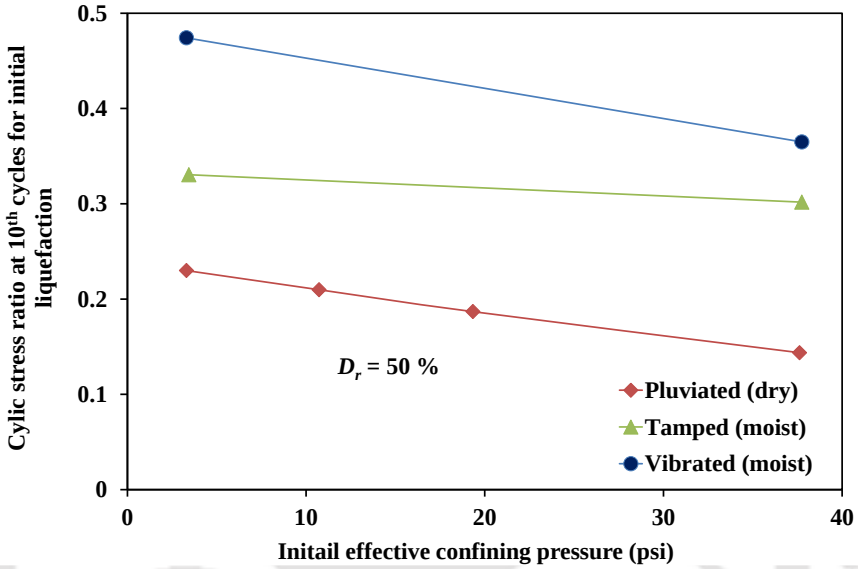

Fig. 2.14 Cyclic stress ratio at f = 10 Hz for initial liquefaction versus initial σ'_c (redrawn after Mulilis, 1975)

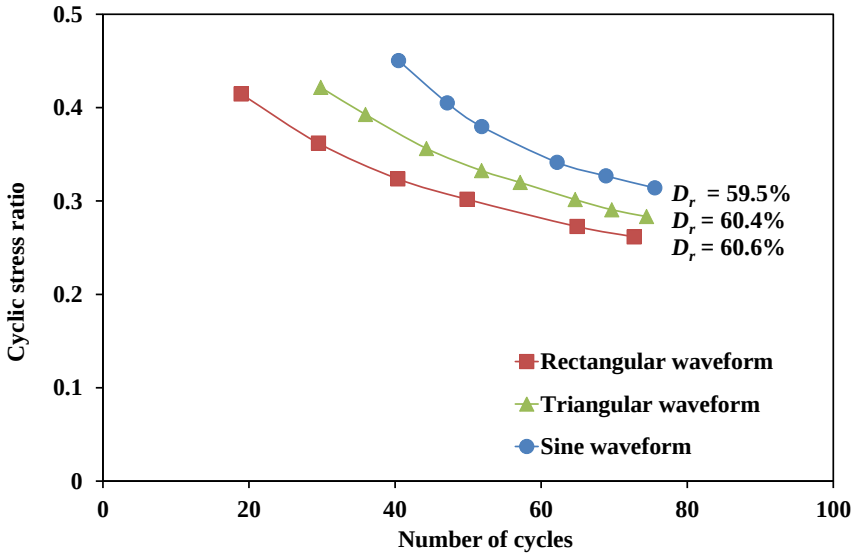

Fig. 2.15 Effect of loading waveform on number of cycles required for initial liquefaction of moist tamped specimens (adapted from Mulilis et al., 1978)

Since, the earthquake contains wide range of frequency, several researchers have studied the response of soil at different loading frequency. Table 2.1 enlists the frequency ranges of uniform sinusoidal loadings mostly used in a cyclic triaxial test to approximate different dynamic loadings (*www.gdsinstruments.com*).

Table 2.1 Typical frequency range for cyclic triaxial test

Loading type	Typical test frequency
Wave action	0.1 Hz
Wind action	0.1 - 1 Hz
Earthquake	1 Hz
Rail transit	> 1 Hz
Vibrating machinery	≤ 20 Hz

Bhattacharya (2007) has reported that the predominant frequency range of earthquakes are 0.5-10 Hz. Lee and Fitton (1969) reported that the lower loading frequency produced slightly lower strength. However, Wong et al., (1975) and Wang (1972) reported that the lower loading frequency gives slightly higher strength, which is in contrast to the above-mentioned finding. Based on the both resonant column and cyclic torsional shear tests, Lin et al. (1988, 1996) observed that the shear modulus was not significantly affected by the excitation frequency, while damping ratio was significantly influenced (Fig. 2.16 and Fig. 2.17). Based cyclic triaxial tests, similar observations have been reported by Govindaraju (2005), presented in Fig. 2.18 and Fig. 2.19. Govindaraju (2005) has also studied the effect of loading frequency on excess PWP generation with number of loading cycles, through strain-controlled tests (γ = 0.4%), and reported that the excess PWP generation at any given cycle is not much pronounced in the frequency range 0.2 - 3.0 Hz. Dash and Sitharam (2009, 2011) have reported that the rate of excess PWP generation increases with the increase in frequency and magnitude of loading. Choudhary et al. (2010) have performed stress-controlled undrained cyclic triaxial tests, to

evaluate liquefaction resistance of Solani sand, and reported that at higher frequency of excitation, the chances of liquefaction increases.

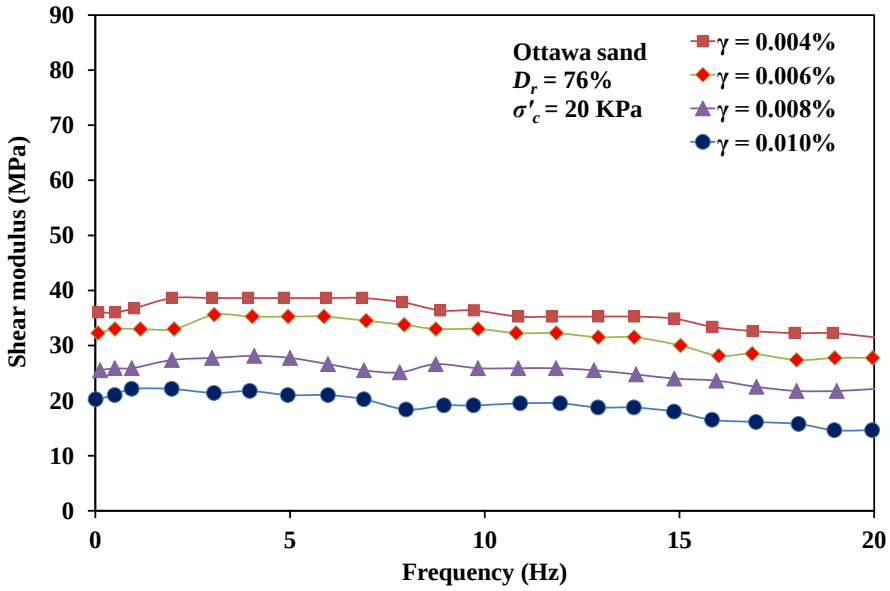

Fig. 2.16 Variation of shear modulus of Ottawa sand with loading frequency (after Lin et al., 1996)

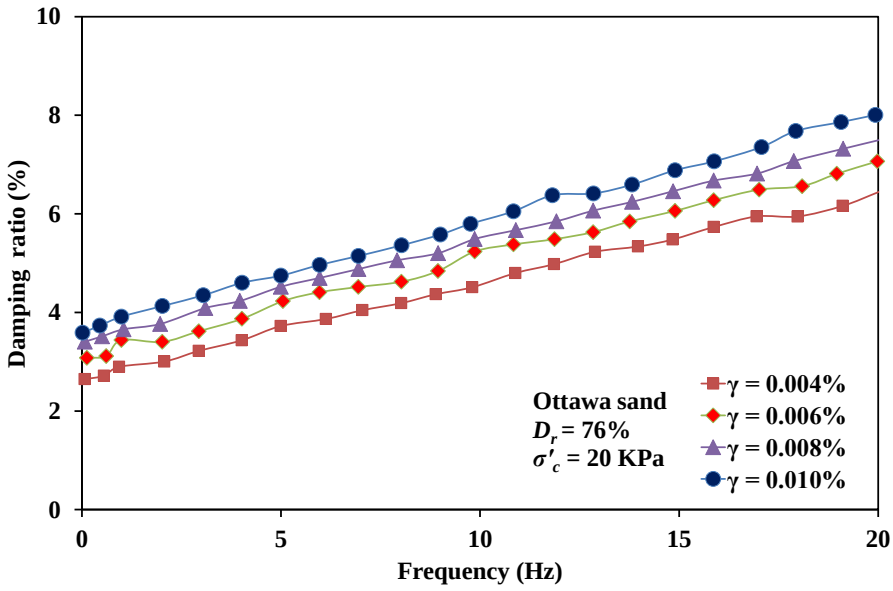

Fig. 2.17 Variation of damping ratio of Ottawa sand with loading frequency (after Lin et al., 1996)

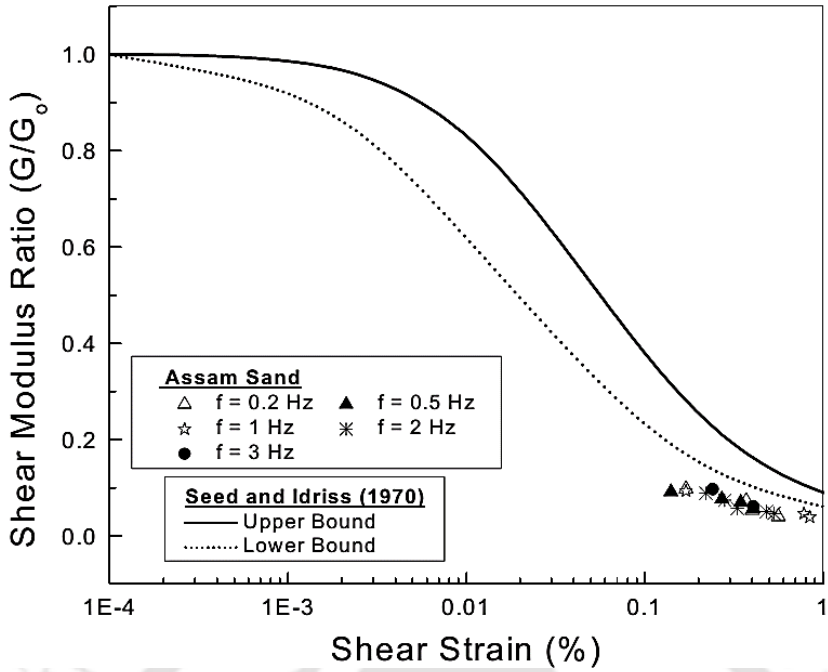

Fig. 2.18 Variation of modulus ratio with shear strain at different loading frequencies (Govindaraju, 2005)

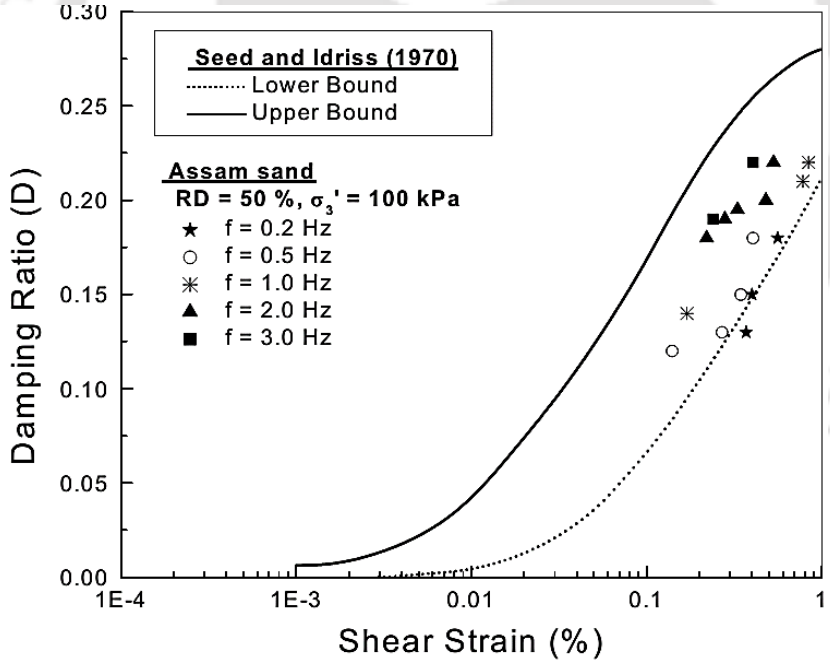

Fig. 2.19 Variation of damping ratio with shear strain at different loading frequencies (Govindaraju, 2005)

Wong et al. (1975) have conducted stress-controlled cyclic triaxial tests, on reconstituted specimens of Monterey zero sand at D_r = 60%, to study the effect of frequency for providing the relationship between cyclic deviator stress and the number of cycles required to cause initial

liquefaction. Two frequencies, 1 cycle/min (0.017 Hz) and 20 cycles/min (0.33 Hz), were used for the tests and it was reported that the effect of frequency on the liquefaction of saturated sand is negligibe. Wang and Kavazanjian (1989) carried out stress-controlled cyclic triaxial tests on Monterey zero sand at D_r = 54% and, loading frequencies of 0.25 Hz and 1.0 Hz. It was concluded that the liquefaction potential of sand is not dependent on the loading frequency. Yilmaz et al. (2004) have performed cyclic triaxial tests on silt-clay mixtures subjected to cyclic axial load at frequencies 0.5 Hz and 1.0 Hz to reflect the proper response of viscosity. Teachavorasinskun et al. (2002) have performed cyclic triaxial tests on clay soil at load frequency of 0.1 and 1.0 Hz. It was reported that the shear modulus was not significantly affected by loading frequency whereas, the damping ratio slightly decreased as the load frequency increased. Similar observations have also been reported by Ravishankar et al. (2005) and Maheshwari et al. (2012a). Lombardi et al. (2014) have used frequency of 0.1 Hz for loading cycle with the assumption of minimal effect of viscosity on cyclic behaviour of soils. Chattaraj and Sengupta (2016a) have evaluated the strain dependent dynamic properties of soil along with the liquefaction potential of sandy soil, considering the frequency of 1 Hz, for the assessments of geotechnical problems involving dynamic loading.

Vucetic and Dobry (1991) have studied the influence of the plasticity index (*PI*) on the cyclic stress-strain parameters over normally consolidated and over-consolidated (OCR = 1–15) clay (Fig. 2.20 and Fig. 2.21). It was reported that, compared to the soils with lower *PI*, soils with higher PI tend to have a more linear cyclic stress-strain response at smaller strains and degrades less at larger shear strain (γ).

Prakash and Puri (1982) and Puri (1984) have conducted an experimental investigation on the cyclic strength of undisturbed and reconstituted samples of a loessial soil at different plasticity index values. It has been seen that the cyclic stress ratio causing the 5% double amplitude axial strain condition increased with an increase in the plasticity index (Fig. 2.22).

However, Prakash and Sandoval (1992) performed stress-controlled cyclic triaxial tests to investigate the effect plasticity index on the liquefaction potential of silty soils of low plasticity and, reported that the cyclic stress ratio causing liquefaction at a given number of cycles decreases with the increase in plasticity index (Fig. 2.23).

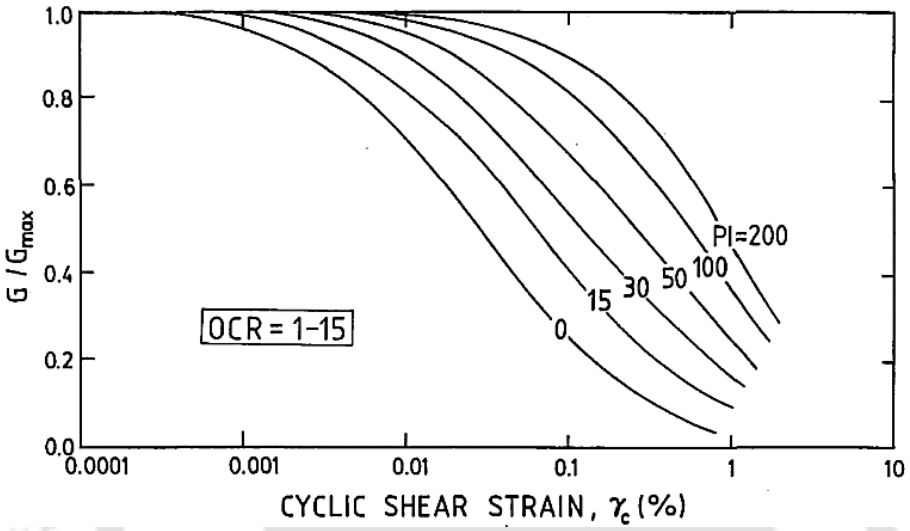

Fig. 2.20 Relationship between G/G_{max} and *PI* for normally-consolidated and over-consolidated soils (Vucetic and Dobry, 1991)

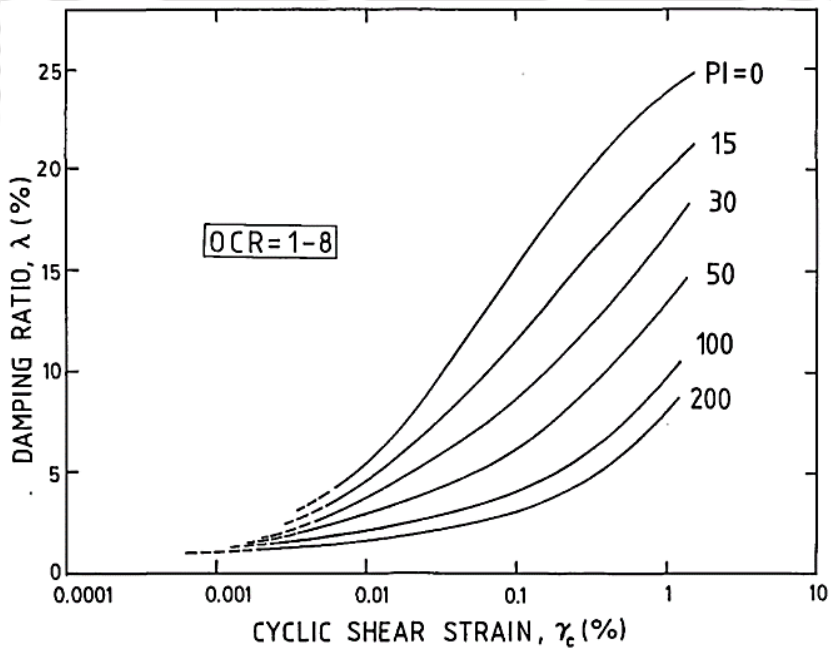

Fig. 2.21 Relationship between damping ratio and *PI* for normally-consolidated and over-consolidated soils (Vucetic and Dobry, 1991)

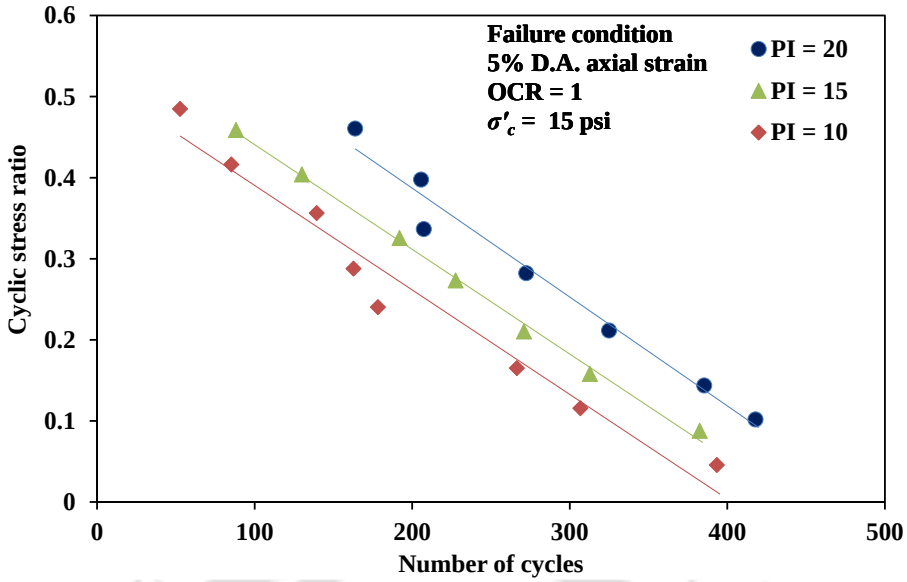

Fig. 2.22 CSR versus *N* for reconstituted saturated samples at different *PI* values and 5% DA axial strain (redrawn after Prakash and Puri, 1982)

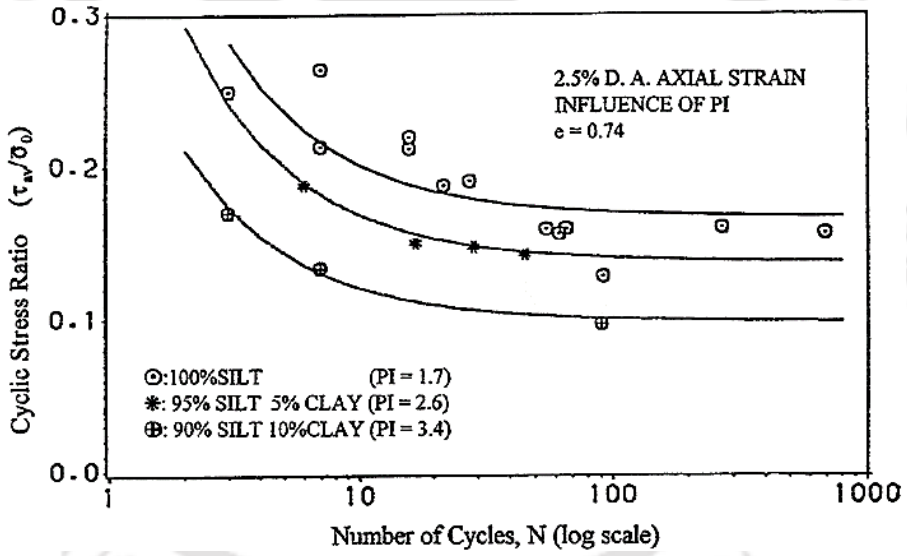

Fig. 2.23 CSR versus *N* for low plasticity silts (Prakash and Sandoval, 1982)

Yasuhara et al. (1992) performed cyclic triaxial tests in order to investigate the behavior of clay specimens during undrained cyclic loading. The soil tested was Ariake clay, a highly plastic marine clay (*Gs* = 2.58- 2.65, *LL* = 115=123% and *PI* = 72-69). Cyclic loading was applied on the isotropically consolidated specimens under stress-controlled conditions at frequencies of 0.1, 1.0 and 3.0 Hz. One-way and two-way loading patterns were used. Excess pore pressure and residual shear strain both developed more rapidly under two-way cyclic loading than under one-way loading. Therefore, cyclic strength of clay samples under two-way

loading was found to be slightly smaller than that under one-way loading (Fig. 2.24).

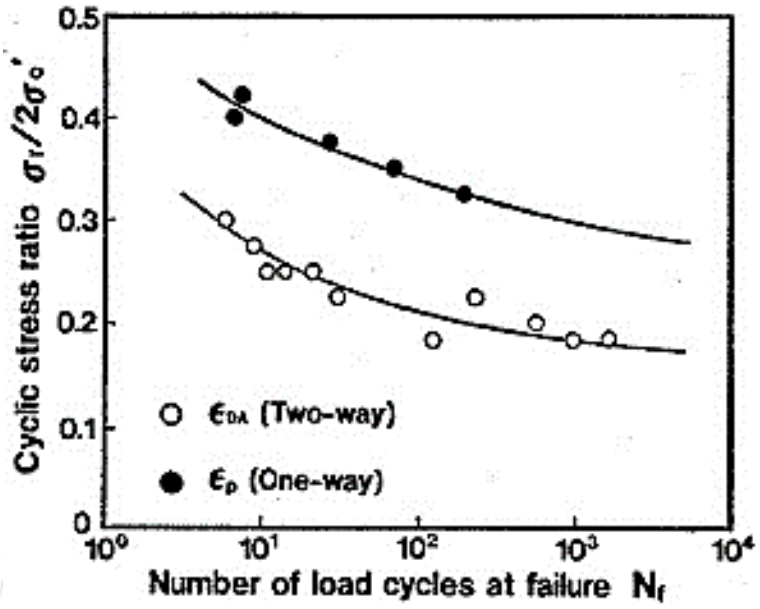

Fig. 2.24 Cyclic stress ratio with the number of cycles during one-way and two-way cyclic loading (Yasuhara et al., 1992).

Hsu and Vucetic (2004, 2006) performed strain-controlled simple shear tests on sand and clay soil (PI range: 0–34) specimens to evaluate the volumetric threshold shear strain for cyclic settlement and cyclic PWP generation. (Fig. 2.25). It was reported that when cyclic shear strain amplitude (γ) was less than the volumetric threshold shear strain for cyclic settlement (γ_t), specimens were not experienced a permanent change in volume or settlement even after a large number of cycles. However, at $\gamma_c > \gamma_t$, large settlement due to residual pore pressure changes occured with the number of cycles. It has also been reported that γ_t in cohesive soil (generally increases with the *PI*) is larger than that in the cohesionless soil. Ladd et al. (1989) have been reported that below threshold cyclic shear strain ($\gamma_t = 1.1\times10^{-2}$), there is no sliding at the contacts between sand particles, due to which no excess pore water pressure build-up is recognized, and influence of relative density is also minimal.

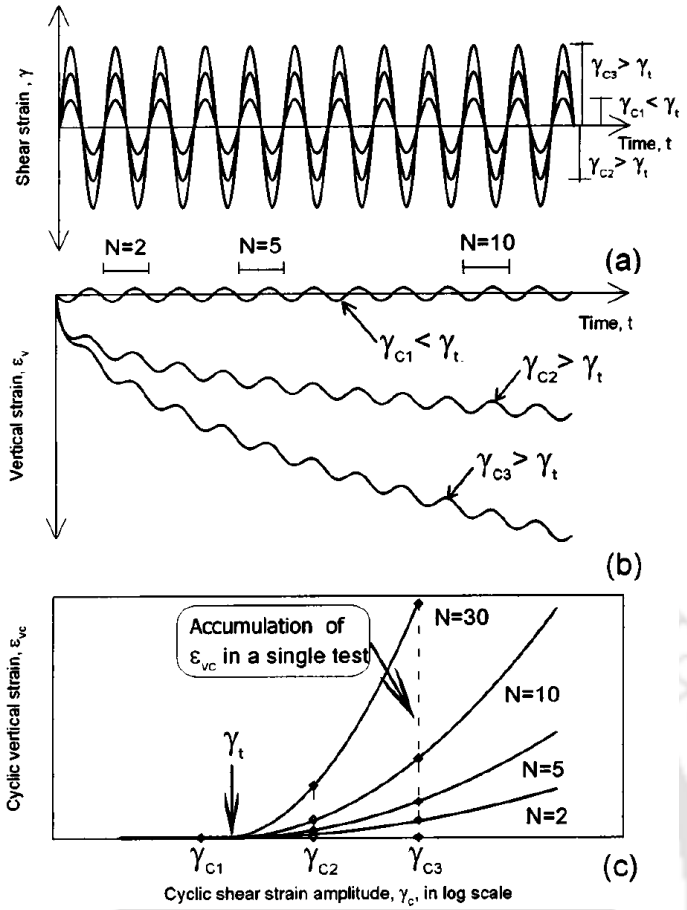

Fig. 2.25 Typical results of cyclic simple shear strain controlled tests with definitions of volumetric cyclic threshold strain for settlement (after Hsu and Vucetic, 2004, 2006)

Yildirim and Ersan (2007) investigated the consolidation settlements of soft clay caused by cyclic loading, using a simple shear device, and also administrated the associated factors such as the number of cycles and stress level. Normally consolidated samples were subjected to five consecutive series of cyclic loading and each series consisted of 50 cycles. Between each cyclic loading series drainage was allowed for 60 minutes. Cyclic tests were performed under stress-controlled conditions at f = 0.1 Hz. Two-way sinusoidal wave loading with different stress levels and number of cycles were employed. It was reported that with the increase in cyclic stress ratio, the pore water pressures increases, as shown in Fig. 2.26. Fig. 2.26 indicates that relatively high PWP at the first loading stage were observed during undrained cyclic loading. However, due to drainage after each cyclic loading stage, which leads to lowering void ratios, excess PWP generation gradually decreased for the consecutive loading stages.

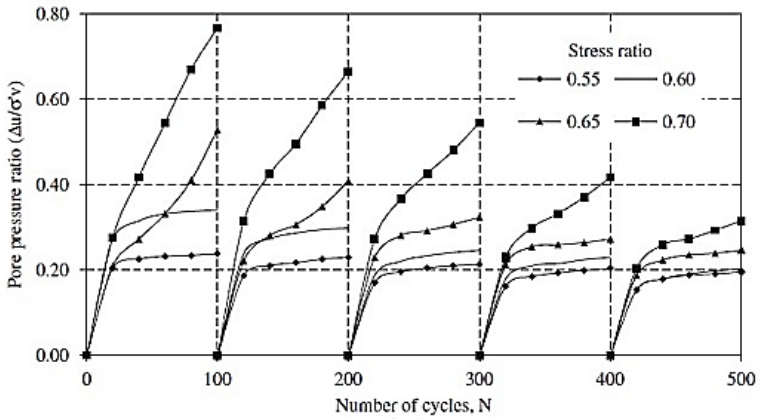

Fig. 2.26 Change of pore pressure for different stress ratios (Yildirim and Ersan, 2007)

Tang et al. (2011) performed cyclic triaxial tests on Mucky clay (Shanghai) to analyse the variation of pore water pressure as well as cyclic creep with increasing the cyclic stress ratio (*CSR*) and number of load cycles. The index properties of clay were: water content = 50.2%, *PL* = 23.2%, and *PI* = 20.2. Samples were consolidated anisotropically, with K_o = 0.7. Axial sinusoidal cyclic loading was applied on the samples with frequencies of 0.5 and 2.5 Hz. Cyclic triaxial tests were conducted continuously on the sample under step loading, in which the initial cyclic stress amplitude was 10 kPa, the periodical amplitude increment was 5 kPa, and each stage consisted of 2000 loading cycles. Li et al. (2011) performed undrained cyclic triaxial tests on soft clays, of marine origin, from Wenzhou city, China. The in-situ clay is normally consolidated with the following index properties: water content = 67.5%, *LL* = 63.4%, and *PI* =35.8. Samples were consolidated under K_o conditions, with an average value of K_o = 0.55. A cyclic sinusoidal wave loading was applied in the vertical direction, while the cell pressure was kept constant. Only one-way cyclic loading was used in experimental program. To study the effect of loading frequency on cyclic behaviour, various test series were performed at frequency of 1.0 Hz, 0.1 Hz and 0.01 Hz. As shown in Fig. 2.27, when the frequency decreases from 1 Hz to 0.01 Hz, the number of cycles required to reach failure decreased drastically. Fig. 2.28 shows the accumulative pore pressure corresponding to Fig. 2.27. Summary of the literatures on the dynamic properties and liquefaction potential of soil are presented in Table 2.2 and Table 2.3,

respectively, which reflect the different investigating parameters and testing conditions.

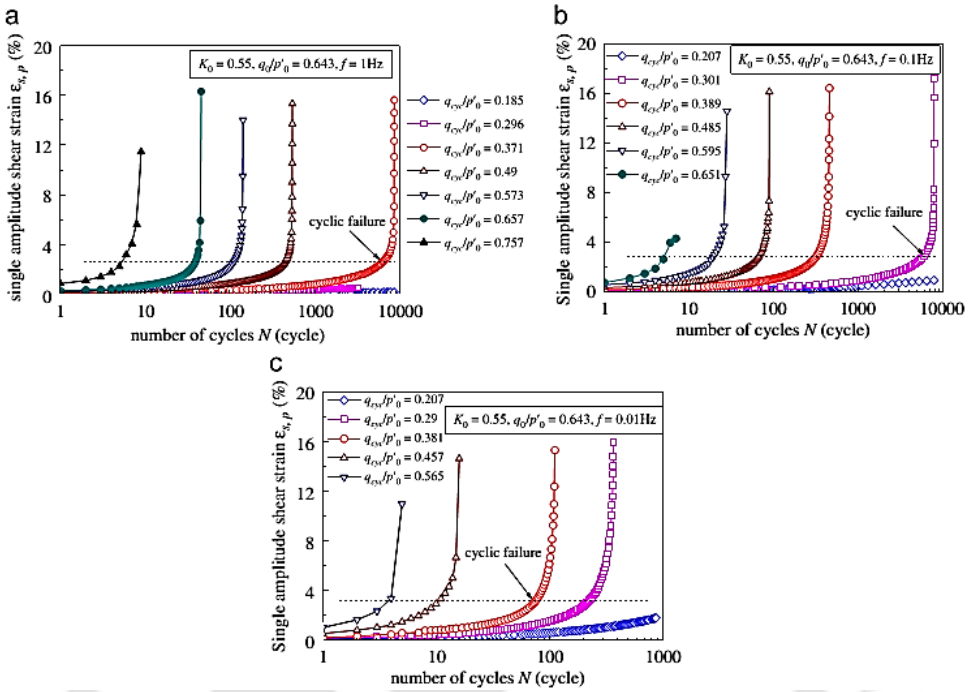

Fig. 2.27 Variation of cumulative γ with N for (a) f = 1 Hz (b) f = 0.1 Hz (c) f = 0.01 Hz, respectively (Li et al., 2011)

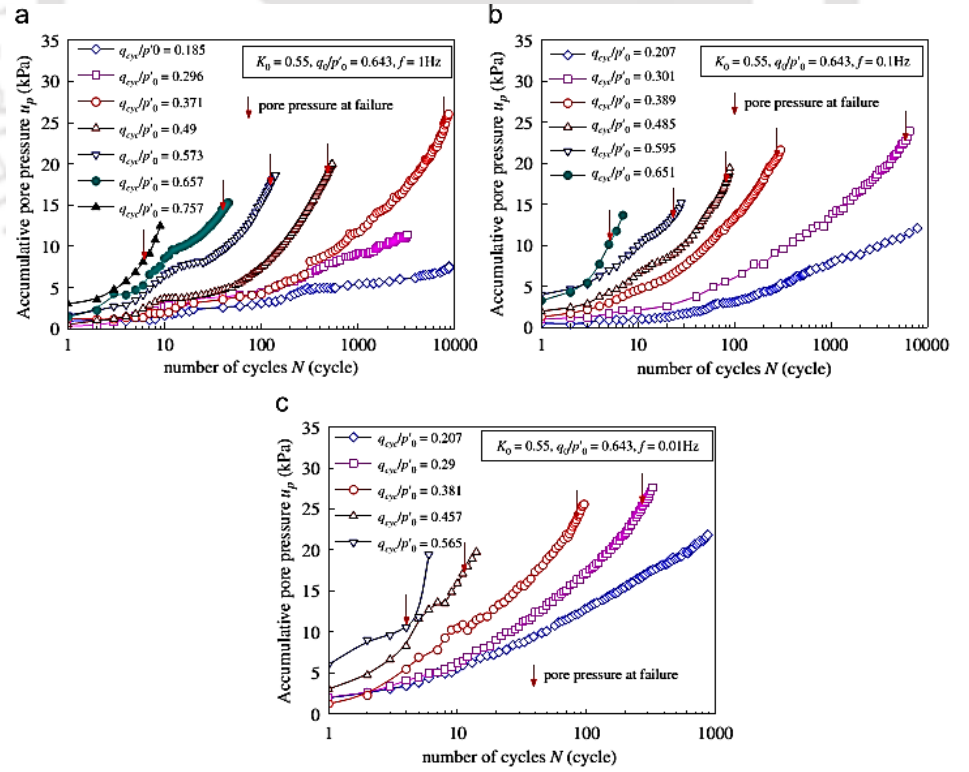

Fig. 2.28 Variation of accumulative PWP with N for (a) f = 1 Hz (b) f = 0.1 Hz (c) f = 0.01 Hz, respectively (Li et al., 2011)

2.3.2 Studies based on the irregular (earthquake) loading

The behaviour of soil during irregular (earthquake) excitation is largely different in comparison to the regular harmonic excitations. Therefore, it is essential to study the behaviour of soils under irregular excitations. Ishihara and Yasuda (1972, 1973, 1975) investigated the dynamic response of saturated sand in terms of liquefaction behaviour using irregular (Fig. 2.29) and regular excitations. It was reported that 47-65% of the maximum shear stress of the irregular stress history can be considered for 20 regular loading cycles in liquefaction analysis. Whereas, Seed and Idriss (1971) have reported that the appropriate number of regular stress cycles depends on the magnitude of earthquake and duration of ground shaking. Tsukamoto et al. (2004) have used irregular time histories on the silty sand specimens in large triaxial test apparatus and, established a relation between the factor of safety against liquefaction and the induced maximum shear strain. Sawada et al. (2006) carried out triaxial tests on unsaturated sandy soils subjected to irregular seismic excitations and, measured the shear strains and volume changes during and after the dynamic irregular excitation (Fig. 2.30). Sassa and Yamazaki (2017) have also used irregular seismic excitations in triaxial tests and, proposed a new simplified liquefaction prediction and assessment method using the irregular waveforms of different seismic strong motions (Fig. 2.31).

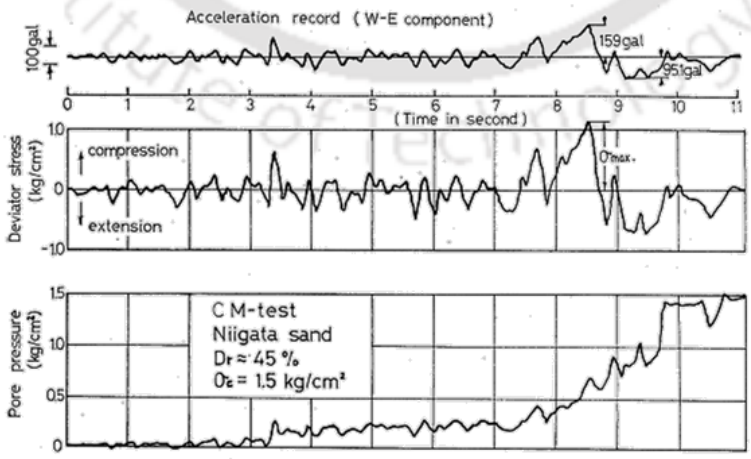

Fig. 2.29 Laboratory simulation of liquefaction occurrence during Niigata earthquake (Ishihara and Yasuda, 1972)

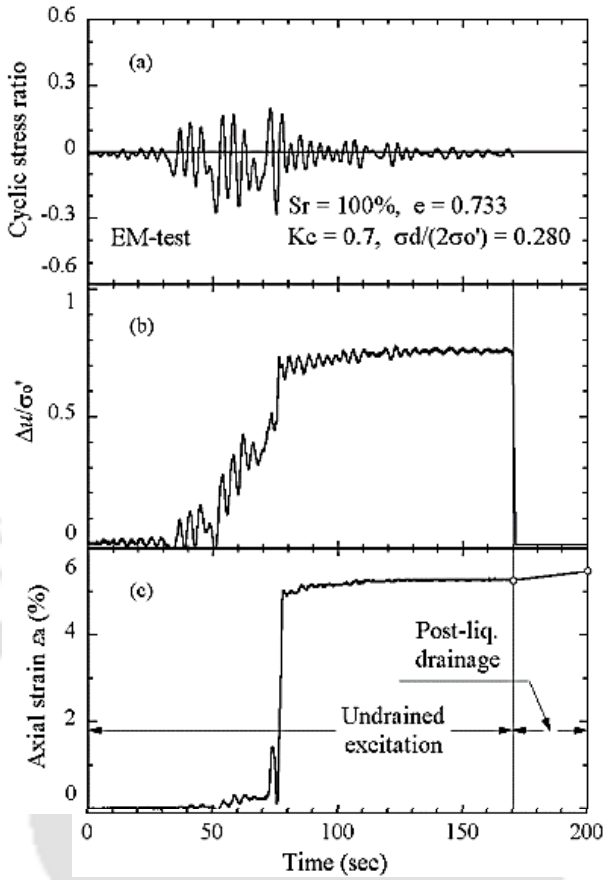

Fig. 2.30 Typical cyclic triaxial test results from irregular excitation (Sawada et al., 2006)

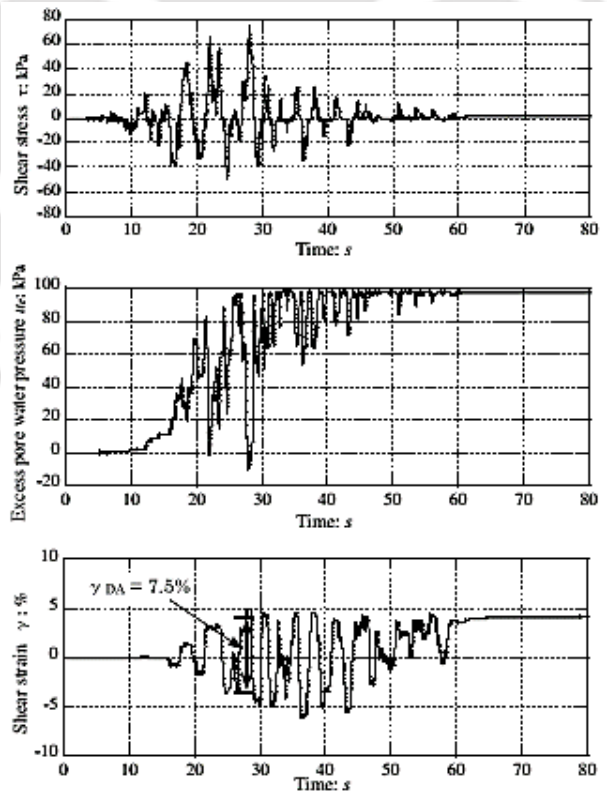

Fig. 2.31 Typical cyclic response of soil under irregular seismic excitations (Sassa and Yamazaki, 2017)

Table 2.2 Summary of literature review on the variation of shear modulus and damping ratio with different parameters

Reference	Sample detail			Test Apparatus	Test method/conditions	Parameters varied
	Soil type	Preparation method	Saturation procedure			Stress applied/Strain level/Frequency/Loading cycles
Khosla and Singh (1978)	Sand (air-dried)	Constant height of fall	-	Geoner triaxial cell	Stress-controlled	f = 2.5 Hz – 25 Hz, $N = 10^7$, D_r = 80%, e = 0.520 – 0.700
Lee (1979)	Clay	Trimmed specimens	Back pressure	Cyclic triaxial and cyclic simple shear test	-	f = 1 Hz
Kokusho (1980)	Sand	Handy vibrator	Back pressure	Cyclic triaxial test	Stress-controlled	γ range = 10^{-6} – 10^{-3}%, f = 0.02 Hz - 0.1 Hz, σ'_c = 19.6 294 kN/m^2, N = 1 – 10, e = 0.64 – 0.80
Kokusho et al. (1982)	Soft clay	Thin walled tube	-	Cyclic triaxial test	-	γ range = 10^{-5} – 10^{-2}, N = 13, e = 0.930 – 3.864, f = 0.05 Hz, OCR = 1 – 15, σ'_c = 16 – 500 kN/m^2
Seed et al. (1986)	Well graded soils	-	-	Cyclic triaxial test	-	γ = ±0.0003%, σ'_c = 2000 – 3000 psf, e = 0.166 – 0.923, D_r = 60 – 100%
Iwasaki and Tatsuoka (1977)	Sands and sand with fine content	Tapping method	-	Resonant column test	Isotropic and anisotropic consolidation	$\gamma = 10^{-6}$ – 10^{-4}%, σ'_c = 0.20 – 6.0 kg/cm^2, e = 0.48 – 1.43
Iwasaki et al. (1978)	Sand	Spooning, Tapping and Raining method	-	Resonant column and Torsional shear test	Isotropic consolidation	$\gamma = 10^{-6}$ – 10^{-2}%, σ'_c = 0.25 – 2.0 kg/cm^2, e = 0.56 – 1.42
Saxena et al. (1987)	Cement sand	Vibration or pluviation technique	-	Resonant column test	-	$\gamma = 10^{-4}$–10^{-2}%, e = 0.618–0.7775, σ'_c = 49 – 588 kN/m^2, D_r = 43, 60 and 80%, Cement content = 0–8%

Andersen and Lauritzsen (1988)	Clay	Undisturbed sample	-	Cyclic triaxial and Direct shear test	Stress-controlled	f = 0.1 Hz, OCR = 1 – 40, N = 1 – 10000, γ = 4.5%/hr for DSS
Tatsuoka et al. (1978)	Sand	Spooning and Raining method	-	Resonant column and Torsional shear test	--	$\gamma = 10^{-6} – 10^{-2}$%, f = 0.1 Hz, e = 0.56 – 1.42, σ'_c = 0.20 – 6.0 kg/cm^2, Fine contents = 0 – 8.8%
Ansal and Erken (1989)	Clay	Remoulded sample	-	Cyclic simple shear test	Stress-controlled	CSR = 1.10 – 0.62, f = 0.1 Hz – 1.0 Hz, N = 1 – 1000
Qian et al. (1991)	Sand	Compaction technique	-	Resonant column test	-	$\gamma = 10^{-6} – 10^{-5}$%, f = 90 Hz – 400 Hz, e = 0.42 – 1.21, σ'_c = 12 – 198 kN/m^2
Vucetic and Dobry (1991)	Clay	-	-	Based on experimental data	-	γ range = 0.01% - 1.0%, OCR = 1 – 15, PI = 0 – 200, N = 1 – 1000
Kagawa (1992)	Clay	-	-	Resonant column and Cyclic simple shear test	Strain-controlled	$\gamma = 10^{-4} – 10^{-1}$% and > 10^{-1}% f = 0.1 Hz – 1.0 Hz, PI = 30 – 60%, e = 0.70 – 2.31, σ'_c = 0.29 – 10 ksf
Pitilakis et al. (1992)	Clay, silty clay and silty sand	Undisturbed and Intact specimen	Saturated	Resonant column and Cyclic triaxial test	-	PI = 5 – 35%, e = 0.43 – 1.63 $\gamma = 10^{-6} – 10^{-1}$%, σ'_c = 20 – 140 kPa
Zavoral and Campanella (1994)	Clay	Trimmed specimen	Saturated	Resonant column and Torsional shear test	-	γ = 0.001% - 1.0%, f = 0.1 Hz – 30 Hz, σ'_c = 69 – 486 kPa
Lin et al. (1996)	Dry sand	Pluviation technique	No saturation	Resonant column or torsional shear test	-	$\gamma = 3 \times 10^{-5}$% - 0.01 %, f = 0.1 Hz – 100 Hz, e = 0.47–0.96, D_r = 51–90%, σ'_c = 20–60 kPa

Lanzo et al. (1997)	Sand and Clay	Trimmed specimen for clay	No saturation for sand and clays fully saturated	Direct simple shear	Strain-controlled	γ = 0.0006% – 0.02%, f = 0.01 Hz – 0.1 Hz, PI = 0 – 75%, σ'_c = 30 – 300 kPa, Silt contents = 0 – 30%, e = 0.54 – 1.72, OCR = 1 – 9.46
Guha et al. (1997)	Clay	Disturbed sample	Back pressure	Resonant column and Cyclic triaxial test	Strain-controlled	γ = 10^{-5}% - 5%, f = 60 Hz – 150 Hz PI = 9 – 42, OCR = 1 – 4, e = 0.47 – 1.10
Vucetic et al. (1998)	Sand and Clay	Constant volume equivalent undrained DSS procedure	No saturation for sand while clay at saturated state	Cyclic simple shear test	Strain-controlled	γ = 0.001% – 0.04%, f = 0.01 – 0.1 Hz PI = 0 – 75 , e = 0.54 – 1.72, OCR = 1 – 9.46, σ'_c = 30 – 300 kPa
Feng and Sutter (2000)	Rubber/sand mixtures	Under-compaction and hand-spooning	No saturation	Torsional resonant column test	-	γ = 0.0001% – 0.1%, % rubber = 0 – 100, e = 0.35 – 0.57, σ'_c = 69 – 483 kPa
Lin et al. (2000)	Gravelly cobble deposits	Equal-weight replacement method	CO_2	Cyclic triaxial and Resonant column test	-	γ = 0.0001% - 1.0%, σ'_c = 58 – 342 kN/m^2, Particle sizes (D_{max}) = 1.27, 2.54, and 5.08 cm
Unnikrishnan et al. (2002)	Clay and sand mixed with geotextile and geo-grid	-	No saturation	Cyclic loading test	Stress-controlled (one-way)	f = 1 Hz, σ'_c = 62, 110 and 158 kPa
Teachavorasinskun et al. (2002)	Clay	Trimmed specimen	Saturated	Cyclic triaxial test	Stress-controlled	γ = 0.01% - 10% f = 0.1Hz – 1.0 Hz, σ'_c = 50 and 100 kPa
Inci et al. (2003)	Clay	Standard or modified Proctor	Saturated	Ultrasonic pulse transmission method	-	PI = 7 – 55%

Sitharam et al. (2004) and GovindaRaju (2005)	Sand	Pouring and dry deposition method	Back pressure	Cyclic triaxial test	Stress- and strain-controlled	CSR = 0.03 – 0.14, γ = 0.13% - 0.77%, f = 0.2 Hz - 3 Hz σ'_c = 25 – 200 kPa, Dr = 9 – 80%
Xenaki and Athanasopoulos (2008)	sandy–silty clay and sand–gravel soils	Using standard proctor test	Back pressure	Torsional resonant column and Cyclic triaxial test	Stress-controlled	$\gamma = 10^{-6}$% - 0.02%, f = 0.1 Hz – 0.5 Hz, D_{50} = 0.012 mm, PI = 17, e = 0.20 – 0.44, Dr = 16 – 90%, σ'_c = 15 – 900 kPa, N = 8 – 290, CSR = 0.13 – 0.45
Stamatopolous (2010)	Sand and silt	Remolded	CO_2	Cyclic triaxial test	Stress-controlled	Fine content = 0 - 25% D_r = 10 – 95%, σ'_c = 50 – 250 kPa e = 0.35 – 0.80
Kirar et al. (2012)	Reinforced and unreinforced sand	Constant height fall with water sedimentation	Back pressure	Cyclic triaxial tests	Strain-controlled	γ = 0.0375%, 0.15%, 1.125%, f = 1 Hz, σ'_c = 50 and 100 kPa, e = 0.54 – 0.85, Dr = 35% Fibre content = 0.25% - 0.75%
Kirar and Maheshwari (2013)	Sand and fines	Constant height fall with water sedimentation method	Back pressure	Cyclic triaxial test	Strain-controlled	γ = 1.125 %, f = 1 Hz Silt content = 0 – 20%, D_r = 35% and 50%, PI = 6%, e = 0.54 – 0.85, D_{50} = 0.21 mm, σ'_c = 50 kPa
Chaney (2013)	Saturated sediment soil	Split mold and trimmed	-	Resonant column test	-	γ = 0.0001% - 0.01%, e = 1.05 – 2.67, PI = 35 – 50%, σ'_c = 69 – 276 kPa Silt = 40–60 %, Clay = 40–50 %
Mohtar et al. (2013)	Sand with plastic fines	Dry pluviation technique	CO_2	Resonant column and Cyclic triaxial test	Stress-controlled	For RC: $\gamma = 10^{-4}$% – 10^{-2}%; For CT: $\gamma > 10^{-2}$%, f = 1 – 120 Hz Bentonite content = 0 – 5% σ'_c = 50 – 193 kPa, D_{50} = 0.40 mm, D_r = 35 – 40%, e = 0.48 – 0.78, N = 1000 – 3000

Table 2.3 Summary of literature review on the variation of liquefaction potential with different parameters

Reference	Sample detail			Test Apparatus	Test method	Parameters varied
	Soil type	Preparation method	Saturation procedure			Stress applied/Rel. density/strain level/No. of cycle/Frequency
Seed and Lee (1966)	Sand	-	Back pressure	Cyclic triaxial test	Stress-controlled	D_r = 38% and 78%, σ'_c = 98 and 196 kN/m^2, σ_d = 38 and 69 kN/m^2, f = 2 cps
Lee and Seed (1967)	Sand	-	Back pressure	Cyclic triaxial test	Stress-controlled	e = 0.61, 0.71, 0.78 and 0.87 Dr = 38%, 78% and 100% σ'_c = 100, 500 and 1000 kN/m^2
Peacock and Seed (1968)	Sand	-	Back pressure	Cyclic simple shear test and cyclic triaxial test	Stress-controlled	e_{max} = 0.83, e_{min} = 0.53 f = 1 Hz - 2 Hz, D_r = 50%, 80% and 90%
Silver et al. (1980)	Sand	Wet tamping and air pluviation	Back pressure	Cyclic triaxial and Cyclic simple shear test	Stress-controlled	D_r = 45% – 80%, σ'_c = 100 kN/m^2 CSR = 0.124, DA axial strain = 10% and 15%
Tatsuoka et al. (1981)	Sand	Intact sandy specimens obtained by sand sampling method	CO2	Cyclic triaxial test	Stress-controlled	σ'_c = 28 – 235 kN/m^2, D_{50} = 0.12 – 0.39 mm, f = 0.5 Hz, Dr = 50%, Fine content = 1 – 32%, DA axial strain = 5%
Tatsuoka et al. (1982)	Sand	Air-pluviation, wet-tamping and wet-vibration	CO_2	Torsional simple shear test	Stress-controlled	CSR = 0.147 – 0.832, D_r = 35% - 95%, DA axial strains = 3%, 7.5% and 15%
Puri (1984) and Prakash and Puri (1982)	Loessial soil	Undisturbed and reconstituted samples	-	Dynamic triaxial test	Stress-controlled	PI = 9 -14, Clay content = 2.0 – 7.2%, % finer than 0.075 mm = 93.0 – 98.0%, DA axial strains = 5%, 10% and 20%, D_{50} = 0.06 mm

Sandoval (1989) and Prakash and Sandoval (1992)	Silty soil	Reconstituted samples	-	Cyclic triaxial test	Stress-controlled	D_{50} = 0.022 mm, PI = 1.7 – 3.4 DA axial strain = 20 %, D_r = 95.4 – 99.8 pcf
Ishibashi et al. (1985)	Sand	Dry tamping method	CO_2	Cyclic torsional simple shear test	Stress-controlled	D_{50} = 0.36 mm, D_r = 40 – 80% e_{min} = 0.50 and e_{max} = 0.76, γ = 0.044 – 0.338%, N = 1 – 40
Vaid and Chern (1983) and Vaid and Finn (1979)	Sand	-	-	Cyclic triaxial and Cyclic simple shear	Stress-controlled	Loose, medium-loose and dense soil
Garga and McKay (1984)	Tailing sand	Reconstituted and thin walled tube sample	-	Cyclic triaxial test	-Isotropic and anisotropic consolidation	DA axial strain = 5% and 2.5%, D_r = 50%
Kramer and Seed (1988)	Sand	Tamping method	-	Cyclic loading test	Load-controlled	D_r = 32%. 37%, 44% and 47% DA axial strain = 10%, D_{50} = 0.12 – 0.20, σ'_c = 1, 2 and 5 ksc
Alarcon-Guzman et al. (1988)	Sand	Reconstituted sample by air pluviation	CO_2	Cyclic torsional shear test	Stress-controlled	D_r = 43 – 46% σ'_c = 0.3 – 10 kg/cm^2
Azzouz et al. (1989)	Clay	Block sample, reconsolidated in the DSS device	-	Direct simple shear test	Stress-controlled	Stress ratio range = 0.05 – 0.85, N = 14 – 10000
Clough et al. (1989)	Cemented sand and artificially sand	Air pluviation	Saturated	Cyclic triaxial test	Stress-controlled	D_r = 55%, CSR = 0.2-0.8
Troncoso (1990)	Sands with silt contents	-	-	Cyclic triaxial test	Stress-controlled	-
Grozic et al. (1999)	Gassy sand	Moist temping method	CO_2	Monotonic triaxial test	Strain-controlled	Strain rate = 0.15 mm/mm

Polito and Martin (2001)	Sand with non-plastic silt	Moist temping	-	Cyclic triaxial test	Stress-controlled	-
Carraro et al. (2003)	Sand with silt	Reconstituted sample	Back pressure	Cyclic triaxial test	-	DA axial strain = 5%, 15% f = 1 Hz
Yasuhara et al. (2003)	Keuper Marl silt	Reconstituted sample	Back pressure	Cyclic triaxial test	Stress- and strain-controlled	OCR range = 1–10 f = 0.1 Hz
Hsu and Vucetic (2004, 2006)	Sand and clay	Trimmed intact soil specimen and laboratory prepared (by compaction) specimen	-	Direct simple shear test	Strain-controlled	γ_t = 0.01 – 0.09%
Zhou and Chen (2007)	Sand	Saturated tamping method	Back pressure	Cyclic triaxial test	Stress-controlled	D_r = 45, 60%, and 75%, 5% DA axial strain, f = 0.1Hz – 1 Hz
Boulanger and Idriss (2006, 2007)	Silts and clays	-	-	Cyclic loading field test	-	-
Ghionna and Porcino (2006)	Sand and gravel	Air pluviation and water sedimentation	CO_2	Cyclic triaxial test	Stress-controlled	Isotropically (K_c = 1) and anisotropically (K_c = 0.59); f = 0.2 Hz
Hazirbaba and Rathje (2009)	Sand and silty sand	-	Back pressure	Cyclic direct shear test	Strain-controlled	γ levels = 0.03%, 0.1% and 0.3% Three different conditions: (a) constant relative density (b) constant sand skeleton void ratio (c) constant overall void ratio
Dash and Sitharam (2011)	Sand – silt mixture	Tamping	CO_2	Cyclic triaxial test	Stress-controlled	CRR = 0.08 – 0.22, D_r = 24% - 73% f = 0.1 Hz

Dash and Sitharam (2009)	Sand – silt mixture	Dry deposition method	CO_2	Cyclic triaxial test	Stress-controlled	CRR = 0.056 – 0.409, D_r = 24% - 73%, f = 0.1 – 0.5 Hz
Ishihara et al. (1978)	Sand with fines 0 - 100%	Thin-wall tube samplers	CO_2	Cyclic triaxial test	Stress-controlled	OCR = 1.0 - 2.0 2.5% DA axial strain
Ladd et al. (1989)	Sand	Moist temping	CO_2	Cyclic triaxial test	Strain-controlled	OCR = 1, 2, 4 and 8 f = 1 Hz
Park and Kim (2013)	Sand with fines contents	Prepared by compaction process	Back pressure	Cyclic triaxial test	Stress-controlled	e = 0.74 – 0.97, PI = 8 – 377, D_r = 43% – 84%, N = 1 – 264, f = 0.1 Hz
Hosri et al. (1984)	Sand and silty clay	Undisturbed trimmed specimens	Back pressure	Cyclic triaxial test	Stress-controlled	CSR = 0.25 – 0.35 N for (u=σ'_3) = 6 – 265 and for 5% DA = 3 – 275, f = 0.2 Hz
Erten and Maher (1994)	Sand and silt (non-plastic and low plastic)	Tamping in split mould with tamping rod	Back pressure	Cyclic triaxial test	Strain-controlled	γ range = 0.015% - 1.5% f = One cycle per minute
Choudhary et al. (2010)	Sand	Water sedimentation	Back pressure	Cyclic triaxial test	Stress-controlled	D_r = 35%, 45% and 55% f = 0.5 Hz, 1.0 Hz and 1.5 Hz
Muley et al. (2012)	Sand with silt content (0% - 20%)	Water sedimentation	Back pressure	Cyclic triaxial test	Strain-controlled	D_r = 35% & 50% f = 1 Hz
Raghunandan and Juneja (2010)	Sand and clay	Dry tamping	CO_2	Cyclic triaxial test	Strain-controlled	CSR = 0.15, γ = 0.4% f = 1Hz
Hanumantharao and Ramana (2010)	Sand-silt mixture	Under compaction moist tamping	Back pressure	Cyclic triaxial test	Stress-controlled	D_r = 30 to 70%, σ'_c = 106 kPa f = 0.5, 1 and 2 Hz, CSR = 0.109-0.30
Amini and Chakravrty (2003)	Sand-gravel composite	Air pluviation and wet pluviation	Back pressure	Cyclic triaxial test	Stress-controlled	σ'_c = 50 – 250 kPa D_r = 46 to 54%

2.4 LOCAL STRAIN MEASUREMENTS IN STATIC AND CYCLIC LAODING

Different techniques and instrumentations for the measurement of local displacement and strains, during a triaxial test, have been reported in the literature as shown in Fig. 2.32 and Fig. 2.33. Special mention can be made of the electrolytic liquid levels as horizontal inclinometers for measuring axial strain (Burland and Symes, 1982), proximity transducers for measuring radial strain (Symes and Burland, 1984), electro-level gauge for measurement of mean local axial strains in a very low-strain level of 0.001% (Jardine et al., 1984, 1985), Hall effect transducer (Clayton and Khatrush, 1986) and submersible proximity sensor (El-Hosri et al., 1981; Hird and Yung, 1989) to measure local strains. Table 2.4 lists the applications of the various sensors in regard to the local strain measurements in triaxial testing of soils.

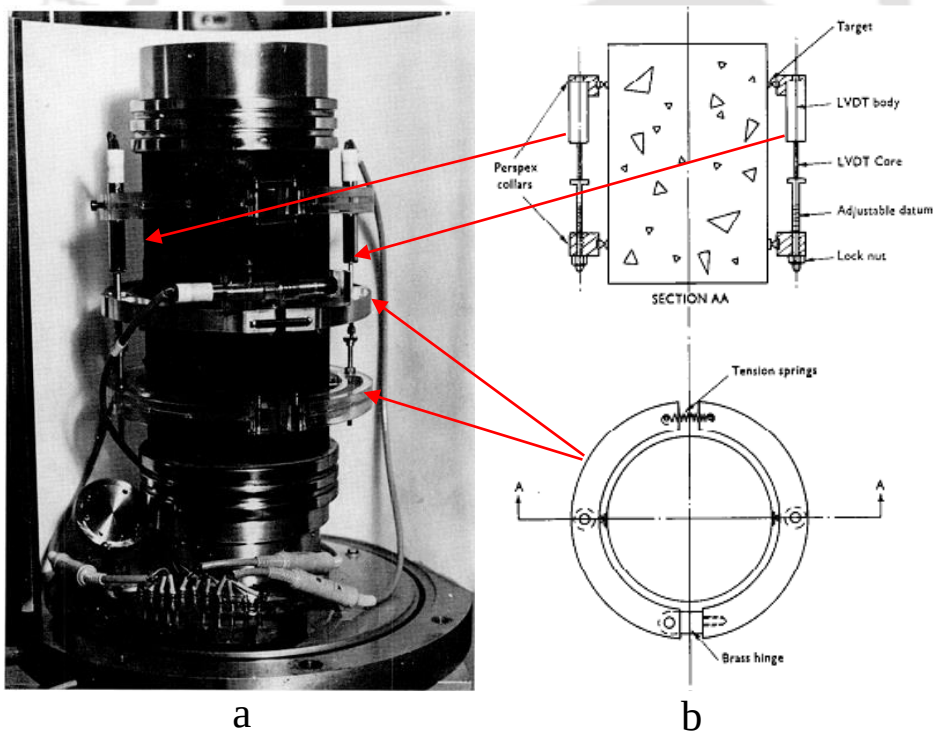

Fig. 2.32 (a) On-sample LVDTs attached to the bitumen macadam specimen (b) Schematic diagram of the arrangement of on-sample LVDTs (Brown and Snaith, 1974)

Burland and Symes (1982) have used Electroleytic levels to measure local torsional strains in the hollow cylinder apparatus. Goto et al. (1991) have used local deformation

transducers (LDT) to estimate the stiffness of soils in triaxial testing. The measuring capacity of LDT in triaxial tests were carried out with gravel, cemented-sand, soft rock and it was reported that the LDT measure strain levels ranging from 10^{-4} % to 1 %, subjected to both monotonic and cyclic loading.

Table 2.4 Various instrumentations for local strain measurement in triaxial tests

Instrumentation	Measurement	References
Electrolytic liquid level	Axial strain	Burland and Symes (1982)
Proximity transducer	Axial and radial strains	Symes and Burland (1984), Cole (1978), Khan and Hoag (1979), Brown et al. (1980), Dupas et al. (1988), Hird and Yung (1989), O'Kelly and Naughton (2008)
Electrolevel gauge	Axial strains in the order of 10^{-3} %	Jardine et al. (1984, 1985)
Hall effect gage sensor	Axial and radial strain in the order of $2x10^{-3}$ %	Clayton and Khatrush (1986), Clayton et al. (1989)
Submersible proximity sensor	Axial strains in the order of 10^{-4} %	El-Hosri et al. (1981)
Inclinometer levels	Axial deformation of triaxial test specimens	Cooke and Price (1974)
Local Deformation Transducers (LDT)	Strain level ranging from 10^{-4} % to 1 %, for both monotonic and cyclic triaxial testing of soils	Goto et al. (1991), Tatsuoka et al. (1990), Dasari et al. (1995), Hoque et al. (1997), Bésuelle and Desrues (2001), Yimsiri et al. (2005)
On-sample LVDTs	Axial and radial strains in the order of 10^{-3}-10^{-4}%	Brown and Snaith (1974), Gookin et al. (1996)
Elastomer gauge	Strains ranging from 0.0005 % to over 10 %, for both monotonic and cyclic triaxial testing of soils	Safaqah and Riemer (2007)
Small Deformation Transducer (SDT)	Fiber Bragg grating sensors to measure local small deformations in a triaxial test specimen	Xu (2017)

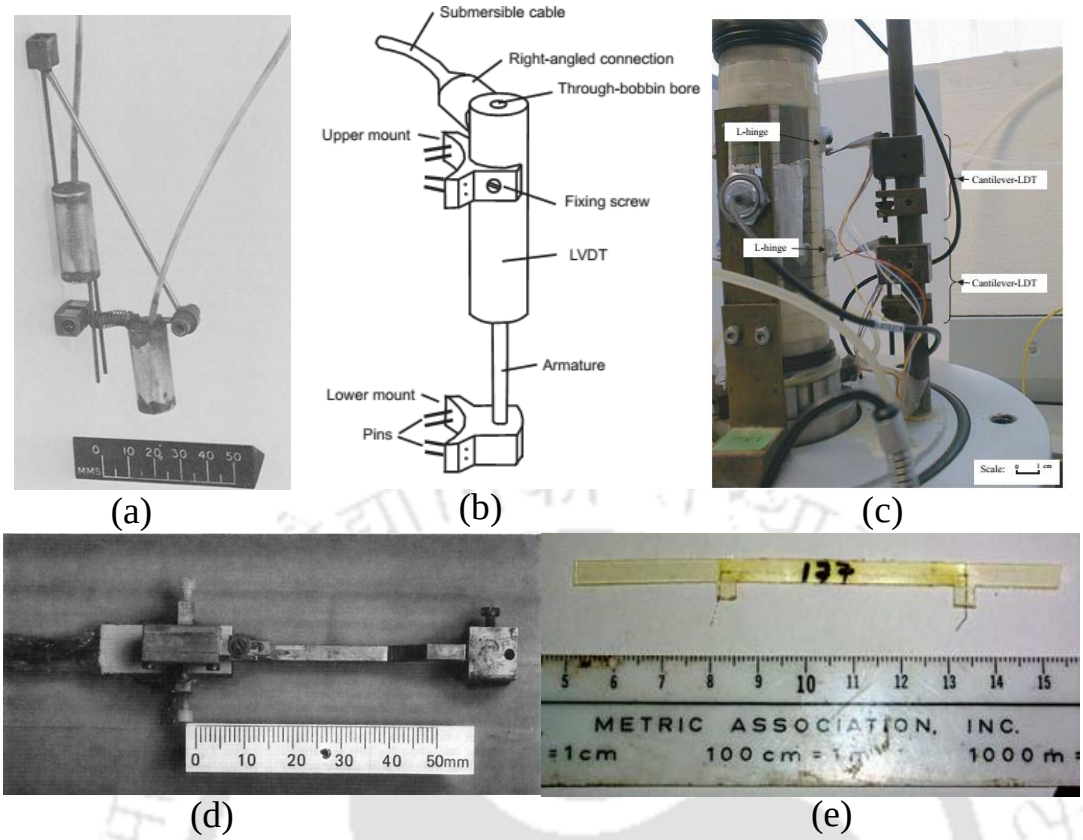

Fig. 2.33 Different types of local strain measurement appurtenances: (a) Electrolevel gage (Symes and Burland, 1984) (b) LVDT (Cuccovillo and Coop, 1997) (c) Cantilever LVDT (Yimsiri et al., 2005) (d) Local strain gauge (Clayton and Khatrush, 1986) (e) Elastomer gage (Safaqah and Riemer, 2007)

Scholey et al. (1995) and Yimsiri and Soga (2002) have made a comprehensive review of above mentioned instrumentations, identifying their advantages, disadvantages, mode of operation, capabilities, limitations, and reported that the LVDTs were negligibly affected by electrical noise and drift. Gookin et al. (1996) have used bender element, proximity transducers and LVDT to measure the small and local strains. It was reported that the bender element provide information on soil properties in the nearly linear elastic (less than 10^{-4} %) range, whereas, the proximity transducers provide the information at small strain range (10^{-2} % - 10^{-3} %), while the LVDT provides the soil properties at strain ranges greater than 10^{-3} % (Fig. 2.34). It was also reported that the external deformation measurements (i.e. external LVDTs) are not satisfactory for estimating small strain properties but accurately measures the large strain properties. LVDTs have also been used during triaxial testing on clay and uncemented sand to

measure the local axial strains and estimation of the undrained shear stiffness at very small axial strain (in order of 0.0001%) (Cuccovillo and Coop, 1997; Santagata et al., 2005). The on-sample LVDTs measured the strain approximately to the level of 1.5×10^{-4}%, when it was used on the dense bitumen macadam specimen (Brown and Snaith, 1974). A cantilever-type local deformation transducer (cantilever-LDT) was also used to measure the local axial strain in triaxial testing on London clay (Yimsiri et al. 2005). Safaqah and Riemer (2007) have used elastomer gage in monotonic and cyclic shear tests on sandy specimen to measures the local strains, and, reported that it can measure wide range of strains from at least 0.0005 % to over 10 %.

Yimsiri et al. (2005) have reported typical output based on the on-sample LVDTs obtained from the monotonic test on London clay specimens (Fig. 2.35). Fig. 2.35a shows the pattern where the obtained results are considered to be reliable. The stress-strain and secant stiffness degradation curves from both sides show similar trend, even though there can be some differences in the actual magnitude due to experimental uncertainty and specimen variability. Fig. 2.35b shows the pattern where the obtained results are considered to be less reliable.

O'Kelly and Naughton (2008) have used proximity transducers and external LVDT to measure local strains (radial as well as axial strains) and global response, respectively of a saturated sandy specimen in a hollow cylinder apparatus. It was reported that the external LVDT measurements reflect significant errors, particularly in the case of the outer wall displacement, due to (a) apparatus compliance (b) specimen end restraint and bedding effects (c) inaccuracies in measuring the volume change of the specimen and its inner bore cavity and (d) the fact that the wall displacements were calculated as mean values over the full specimen volume. Xu (2017) has used a small deformation transducer (SDT) based on fiber Bragg grating sensors to measure local small deformations. It was reported that the SDT measures the local deformations of soil specimens with high accuracy.

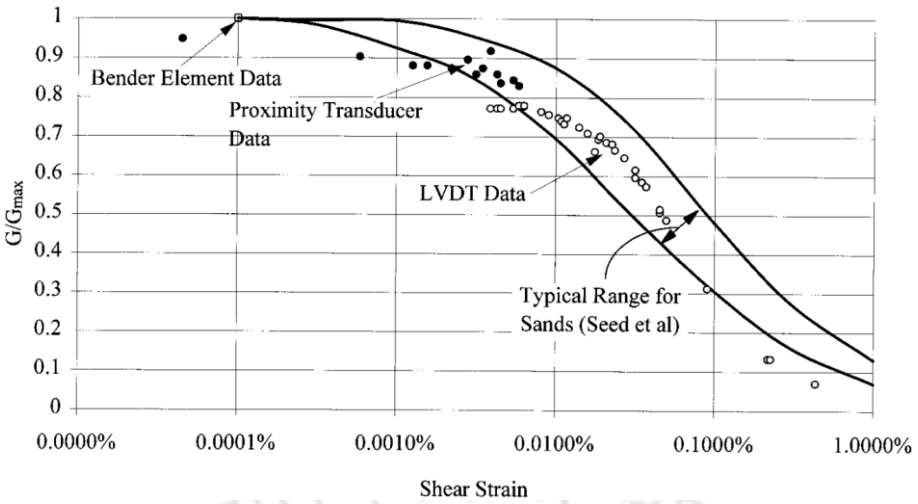

Fig. 2.34 Modulus reduction curve based on the on-sample LVDTs (Gookin et al., 1996)

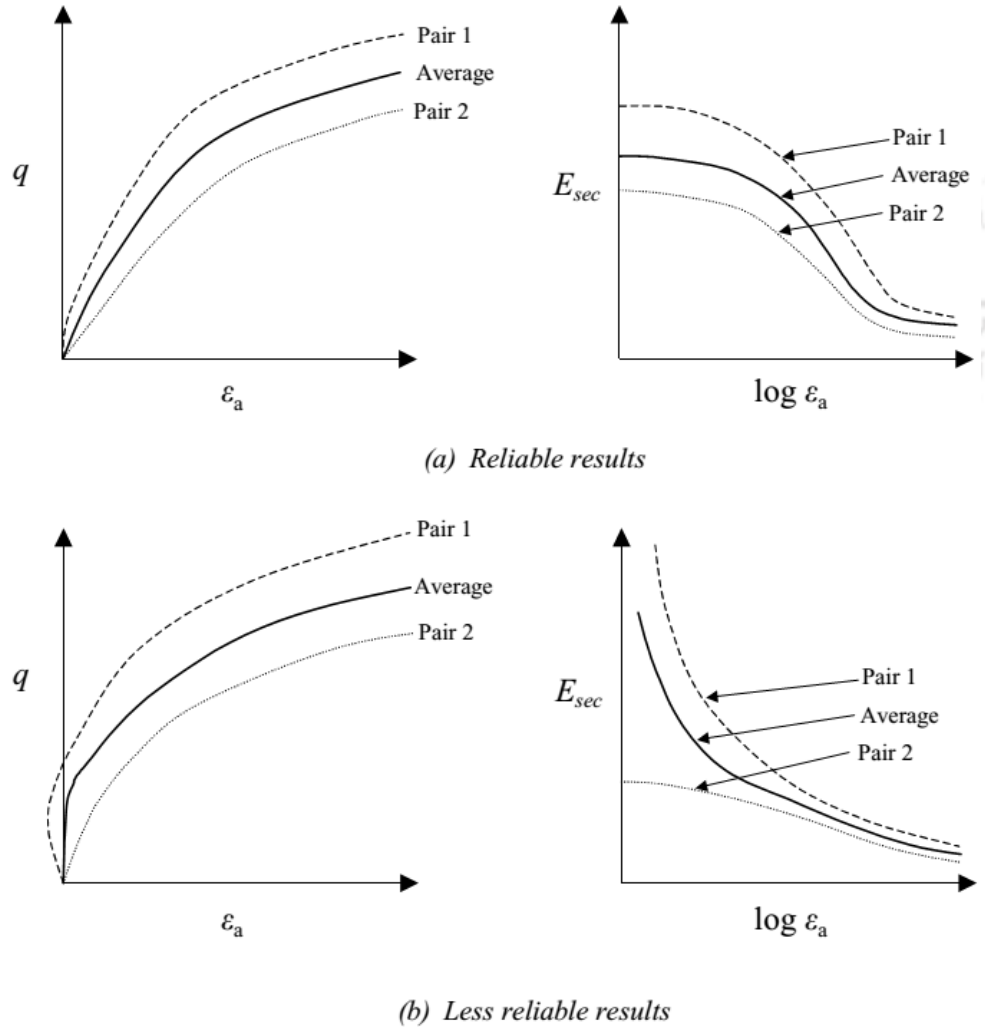

Fig. 2.35 Typical stress-strain response based on the on-sample LVDTs (Yimsiri et al., 2005)

2.5 APPLICATION OF DYNAMIC PROPERTIES OF SOILS

Dynamic soil properties such as modulus reduction curve and damping ratio curve are one of the essential input parameter in the ground response analysis (GRA). GRA is one of the important step in seismic hazards analyses to see potential damages on the ground due to earthquake before the arrival of strong or severe earthquake motions, and provide design ground motion parameters for the design of earthquake resistant structures. GRA generally conducted by equivalent linear and non-linear approach. Several researchers have performed GRA for Indian cities using DEEPSOIL (Hashash et al., 2016) and SHAKE2000 (Ordonez, 2000) methodologies enlisted in Table 2.5. According to Table 2.5, researchers have used already existing material model from the database of DEEPSOIL and SHAKE2000 in GRA for the ease of analysis. The database of DEEPSOIL and SHAKE2000 material model does not incorporate the Indian soil model. Since, soil of each region/continent are different in their particle size characterizations, the use of existing material model for the GRA of Indian cities can mislead from the precise GRA. Therefore, the evaluation of dynamic soil characterizations of each regions especially seismically active region are significantly important for the precise estimation of ground motion parameters. DEEPSOIL methodology facilitates both equivalent linear and non-linear, whereas SHAKE2000 facilitates only equivalent linear approach to perform one-dimensional GRA. Both the methodologies (equivalent linear and non-linear) are used in the site response analysis to find the response of local soil and strong motion during earthquake by solving the dynamic equation of the motion. Equivalent linear method solve the equation of the motion in frequency domain, whereas non-linear method solve in time domain. Equivalent linear analysis is widely used in engineering practice due to its simplicity, however, it does not account for the change in soil properties throughout the duration of the ground motion. Non-linear analysis uses step-by-step integration process and more accurately simulate the actual non-linear behaviour of soils. In both approach (equivalent linear and non-linear) as

well as in both the methodologies (DEEPSOIL and SHAKE2000), each soil layers are defined by dynamic soil properties. These dynamic soil properties such as modulus reduction curves and damping ratio curves are chosen based on the material type such as clay, soil, gravel and rock fill. A typical representation of the modulus reduction curves and damping ratio curves presented in Fig. 2.36, are used in GRA.

Table 2.5 Material curves used in GRA

Researchers	Material curves	Methodology
Ranjan (2005)	Seed and Idriss (1970) for sand, Vucetic and Dobry (1991) for clay, Seed et al. (1986) for gravel, Gazetas (1992) for rock fill	SHAKE2000
Boominathan et al. (2008)	Sun et al. (1988) for clay, Seed and Idriss (1970) for sand, Schnabel (1973) for rock	SHAKE91
Anbazhagan et al. (2010)	Seed and Idriss (1970) for sand, Vucetic and Dobry (1991) for clay	SHAKE2000
Govindaraju and Bhattacharya (2011)	Seed and Idriss (1970) for sand, Vucetic and Dobry (1991) for clay	SHAKE2000
Phanikanth et al. (2011)	Seed and Idriss (1970) for sand, Vucetic and Dobry (1991) for clay	DEEPSOIL
Shukla and Choudhury (2012)	Seed and Idriss (1970) for sand, Vucetic and Dobry (1991) for clay	SHAKE2000
Kumar (2012)	Seed and Idriss (1970) for sand, Vucetic and Dobry (1991) for clay	DEEPSOIL & SHAKE2000
Kumar and Krishna (2012) Kumar and Krishna (2013) Kumar et al. (2014a,b)	Seed and Idriss (1970) for sand, Vucetic and Dobry (1991) for clay	DEEPSOIL
Naik and Choudhury (2013)	Seed and Idriss (1970) for sand, Vucetic and Dobry (1991) for clay	DEEPSOIL
Basu et al. (2017)	Ishibashi and Zhang (1993) for both clay and sand	DEEPSOIL

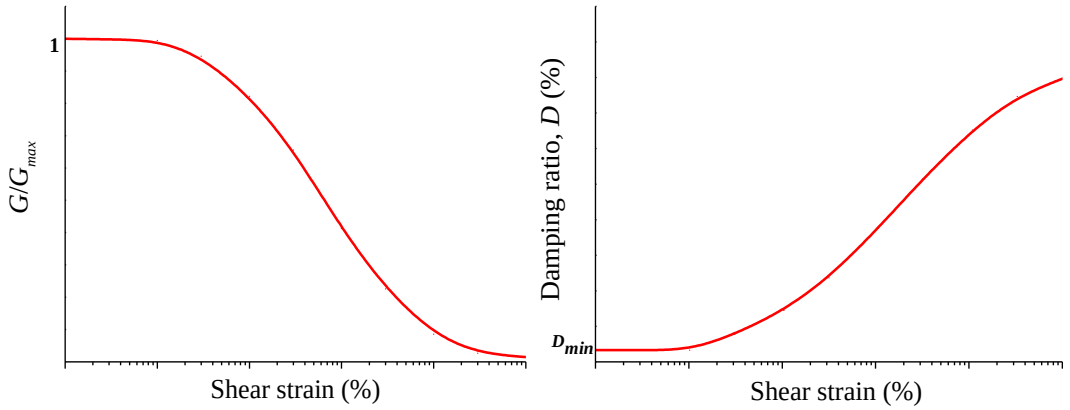

Fig. 2.36 Typical representation of modulus reduction and damping ratio curves used for GRA

Ranjan (2005) has carried out seismic GRA for Dehradun city and reported that the spectral acceleration varies in the range of 0.06g–0.37g at frequency range 1–10 Hz. Govindaraju and Bhattacharya (2011) have carried out site-specific earthquake response study for hazard assessment in Kolkata city. It was reported that the amplification of ground motion was in the range of 4.46–4.82 with the fundamental period ranging from 0.81s to 1.17s and the maximum spectral accelerations at the surface were in the range of 0.78g–0.95g. Phanikanth et al. (2011) have performed one-dimensional equivalent linear GRA for Mumbai city using input motion peak ground acceleration (PGA) range 0.102g–0.834g, and reported the PGA amplification was in the range of 2.50–3.45. Shukla and Choudhury (2012) have carried out one-dimensional GRA for Gujarat and reported that the ground amplification factor was in the range of 1.3–2.0 for the frequency range 1.0–2.7 Hz. One-dimensional equivalent linear GRA have also been performed for Guwahati city using input motion PGA range 0.102g–0.345g and observed the amplification factor was in the range of 1.49–4.29 (Kumar and Krishna, 2013). It has also been reported that the PGA at surface level get amplified from 0.24g–0.43g for an estimated ground motion of an earthquake, M_w = 8.1, at Guwahati city (Raghukanth et al., 2008). Naik and Choudhury (2013) have performed site-specific seismic GRA for Panjim City (Goa) and amplification factor of earthquake motions were reported in the range of 1.56–2.36. Basu et al. (2017) have performed one-dimensional effective stress non-Masing nonlinear GRA

of Guwahati region, using dynamic soil properties (modulus reduction and damping curve) obtained from the empirical relation proposed by Ishibashi and Zhang (1993). The aforementioned GRA studies were performed with the existing soils model such as Seed and Idriss (1970) for sandy soil, and Vucetic and Dobry (1991) for clayey soil or Ishibashi and Zhang (1993) for sandy and clayey soil. In the absence of proper site-specific soil model, the use of existing soil model might lead to the inaccurate estimation of the ground motion parameters involved in earthquake resistant design. Shukla and Choudhury (2012) have also recommended the use of actual dynamic soil properties for more precise GRA results.

2.6 CRITICAL APPRAISAL OF LITERATURE REVIEW

Based on the literature survey, it can be stated that the dynamic soil properties are the best representation of the variations in the properties of soils with shear strain during earthquakes. Therefore, for the evaluation of dynamic properties and liquefaction behaviour of soils, different laboratory instrumentations such as resonant column, dynamic simple shear, cyclic triaxial and shake table tests have been used by researchers. The effects of testing procedures and material characteristics on the dynamic properties and cyclic strength of different soils were reviewed. It can be stated that these properties are significantly affected by many factors such as methods of sample preparation in laboratory (whether intact and reconstituted samples), relative density, confining pressure, cyclic strain amplitudes, cyclic stress ratio, number of loading cycles, methods of loading, overconsolidation ratio, loading frequency, soil plasticity, percentage of fines and soil type. Several studies are available worldwide on the evaluation of dynamic properties (modulus reduction and damping ratio curve) and liquefaction behaviour of soils however; no literatures and studies are available on the dynamic characterization of soils of Assam and entire North-eastern region. Since, the entire North-eastern region comes under the highly seismically active region in the world, the dynamic characterization of soils of this region are very essential to design earthquake resistant structures.

The evaluated material models such as modulus reduction curve and damping ratio curve are key parameter in GRA. Since, soil of each region/continent are different in their particle size characterizations, the evaluation of dynamic soil characterizations of each regions especially seismically active region are significantly important for the precise estimation of ground motion parameters. In the absence of proper site-specific soil model, the use of existing soil model might lead to the inaccurate estimation of the ground motion parameters involved in earthquake resistant design.

2.7 OBJECTIVES AND SCOPE OF THE STUDY

During literature survey, it was observed that the literatures and studies on the dynamic response of soils of the Assam region are relatively scanty. Since, Assam and entire North-eastern region comes under the seismic zone v (IS 1893:2002), the main objective of the present study is to evaluate the material model such as modulus reduction curve and damping ratio curve of the soils presents in this region. Since, the strength of saturated soils are significantly affected by the variations in pore water pressure during dynamic loading, therefore, the other objective is to estimate liquefaction potential of Assam soils. Strain dependent dynamic soil properties are one of the most important input parameters in the seismic ground response studies. Therefore, GRA is an important step to evaluate the design ground motion parameters for the design of earthquake resistant structures in this region. To achieve these objectives, the detailed scope of the present study are:

1. A series of cyclic triaxial tests on cohesionless and cohesive soil were conducted at different investigating parameters such as confining stress, relative density and shear strain to evaluate the strain dependent dynamic soil properties of Assam region. In addition to the evaluation of wide range (low to high strain range) of dynamic soil properties, low strain dynamic soil properties were evaluated using on-sample LVDT. The evaluated dynamic soil properties will be used further for GRA.

2. Further, cyclic triaxial tests were conducted to evaluate the liquefaction behaviour of Assam soil at different testing conditions such as confining stress, relative density, testing methodology, and stress amplitude on cohesionless soil subjected to the irregular seismic excitations (i.e. real earthquake motion) and regular (sinusoidal) excitations.

3. One-dimensional equivalent linear GRA will be carried out for Guwahati city to utilize the estimated dynamic soil properties for application purposes and to precise measurement of seismic design parameters. To see the importance of regional dynamic soil properties in site-specific GRA, the obtained results will be compared with the results estimated from the existing material models.

2.8 SUMMARY

This chapter presented the brief literature review in context to the present study. Discussions on selected studies on the evaluation of dynamic properties and liquefaction evaluation of soils are presented. The measurement of local strains using on-sample transducers have also been discussed. Critical appraisal of the literature reviewed was presented highlighting the importance of dynamic properties and liquefaction study of soil and, need for the study. The chapter is concluded with objective and detailed scope of the present study.

Chapter 3 MATERIALS AND METHODOLOGY

3.1 INTRODUCTION

In almost all geotechnical structures, the supporting foundation soil mass undergo several instances of static and dynamic loadings during their performance period, which may be due to self-weight, construction load, seismic activity, moving vehicles or vibrating machineries. The responses of soils due to the dynamic loading (example, seismic activity or machine vibration) is relatively more complex than that of static loading (example, self-weight and construction load). The responses of the soils widely differ based on their compositions, index properties (such as relative density and consistency), different types and rates of loading. Soils available in Assam region are categorically grey sand, red loam, alluvial and lateritic soil. Assam region is prone to the earthquakes and have experienced several seismic shocks of moderate to severe intensities in the past. Hence, it is immensely important that the typical soils found in the region are investigated of their static and dynamic responses, which form an integral part of geotechnical earthquake engineering applications such as ground response analysis, seismic design and requalification. The present study focuses on the static and dynamic responses of two types of soils, cohesionless Brahmaputra Sand (BS) and cohesive Red soil (RS). Static and cyclic triaxial shear tests have been used to evaluate the behaviour of soils at different shear strain amplitudes. The details of the test materials and their characterization are presented in this chapter. The test methodologies and testing apparatus to achieve this objective have also been described in detail.

3.2 MATERIAL DESCRIPTIONS

Two types of soils: cohesionless Brahmaputra sand and cohesive Red soil were selected for the present study to evaluate their static strength, cyclic strength and strain-dependent dynamic properties. The details of the materials are presented in the following sections.

3.2.1 Cohesionless soil

In the present study, cohesionless soil namely Brahmaputra Sand (BS), collected from Guwahati region (Assam, India), has been used to evaluate its static and dynamic response. Fig. 3.1 depicts the particle size of BS (IS: 2720, Part-IV), containing nearly 5% fine content. The particle size distribution (PSD) is, encompassed within the zone of severely liquefiable soil (Tsuchida, 1970; Ishihara et al., 1980; Xenaki and Athanasopoulos, 2003). Field Emission Scanning Electron Microscope (FESEM) image of the BS, provided in Fig. 3.2(a), exhibits that the particles are sub-angular in shape. Index properties such as specific gravity and, minimum and maximum dry unit weight of BS were determined as per relevant standards (IS: 2720 Part-III; IS: 2720 Part-XIV; ASTM D4253, 4254) and are listed in Table 3.1. As per the Unified Soil Classification System (ASTM D2487), the soil is classified as poorly graded sand (SP).

Table 3.1 Physical properties of Brahmaputra Sand (BS)

Physical properties	Values
Mean grain size, D_{50} (mm)	0.21
Min. dry unit weight (kN/m^3)	13.85
Max. dry unit weight (kN/m^3)	16.84
Specific gravity (G_s)	2.7
Uniformity coefficient (C_u)	1.47
Coefficient of curvature (C_c)	1.09
Classification symbol	SP

3.2.2 Cohesive soil

A locally available cohesive soil, Red soil (RS), was used for this study. The specific gravity (G_s) of the soil particles was found to be 2.65 (according to ASTM D0854). Wet sieve (ASTM D6913) and hydrometer analysis (ASTM D7928) were performed to determine particle size distribution of RS which is presented in Fig. 3.1. Fig. 3.2b presents FESEM image of RS. The

values of liquid limit, plastic limits and plasticity index were determined as 41.5%, 22.6% and 18.9%, respectively (ASTM D4318). The compaction curve of cohesive soil is determined from the standard proctor compaction test (ASTM D698), and is plotted in Fig. 3.3. The maximum dry unit weight and optimum moisture content (OMC) of the soil were found to be 17.5 kN/m^3 and 19.3%, respectively. As per Unified Soil Classification System (ASTM D2487), the soil is classified as low plastic cohesive soil consisting of 21.23% clay, 48.50% silt (0.002 mm–0.075 mm), and 30.27% fine sand (0.075 mm–4.75 mm). The summary of the physical properties of the RS are presented in Table 3.2.

Table 3.2 Physical properties of Red Soil (RS)

Physical properties	values
Specific gravity (G_s)	2.65
Liquid limit (%)	41.50
Plastic limit (%)	22.60
Plasticity index (%)	18.9
Optimum moisture content (%)	19.3
Maximum dry density (g/cc)	1.75

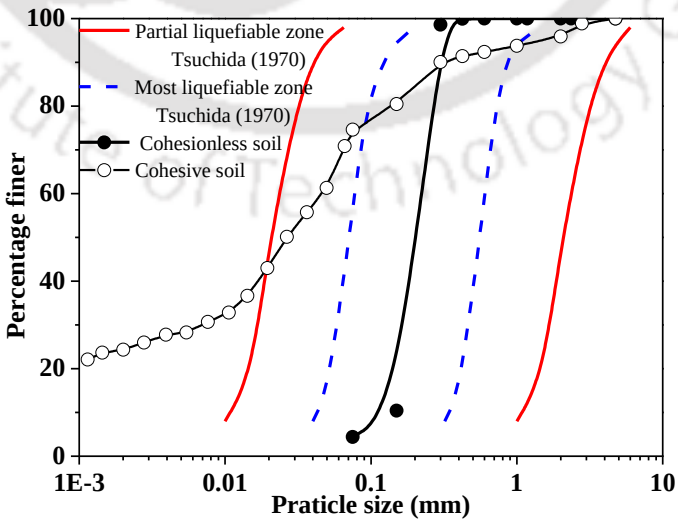

Fig. 3.1 Particle size distribution of BS and RS

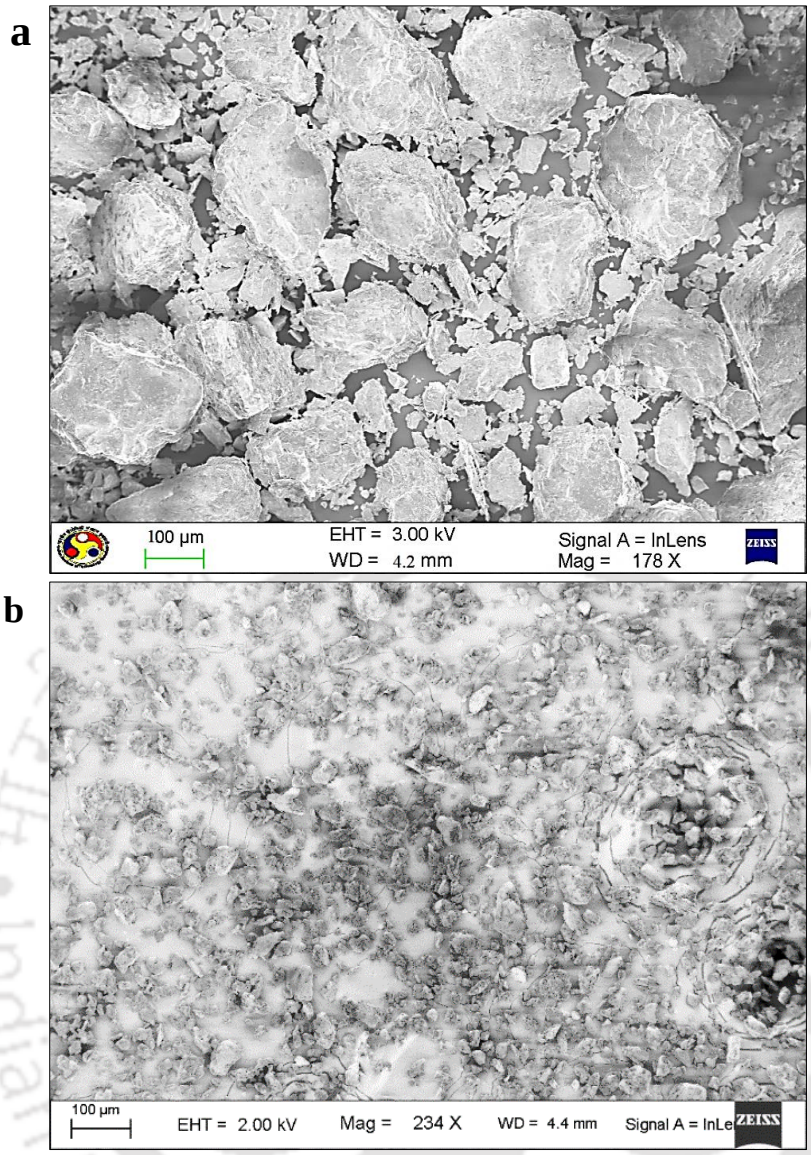

Fig. 3.2 FESEM image of (a) BS (b) RS

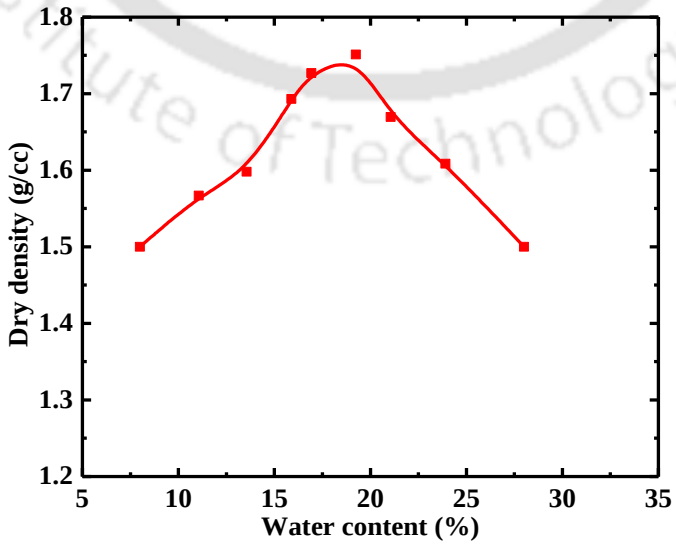

Fig. 3.3 Compaction curve of RS

3.3 TESTING APPARATUS AND COMPONENTS

An automated pneumatic controlled cyclic triaxial testing apparatus (make: Wyekham Farrance), shown in Fig. 3.4, facilitating both monotonic as well as cyclic tests, was used to perform the experimental investigations at different testing conditions. This apparatus comprises of many hardware components and instrumentations, namely the Tritech loading frame, pneumatic actuator, triaxial cell, submersible load cell, Linear Variable Displacement Transducers (LVDTs), pressure transducers, Automatic Volume Change (AVC) device, Compact Dynamic Controller (CDC) unit, dry air receiver unit, data logger and software (DYNATRIAX). The descriptions and working procedure of different components are presented in following sections.

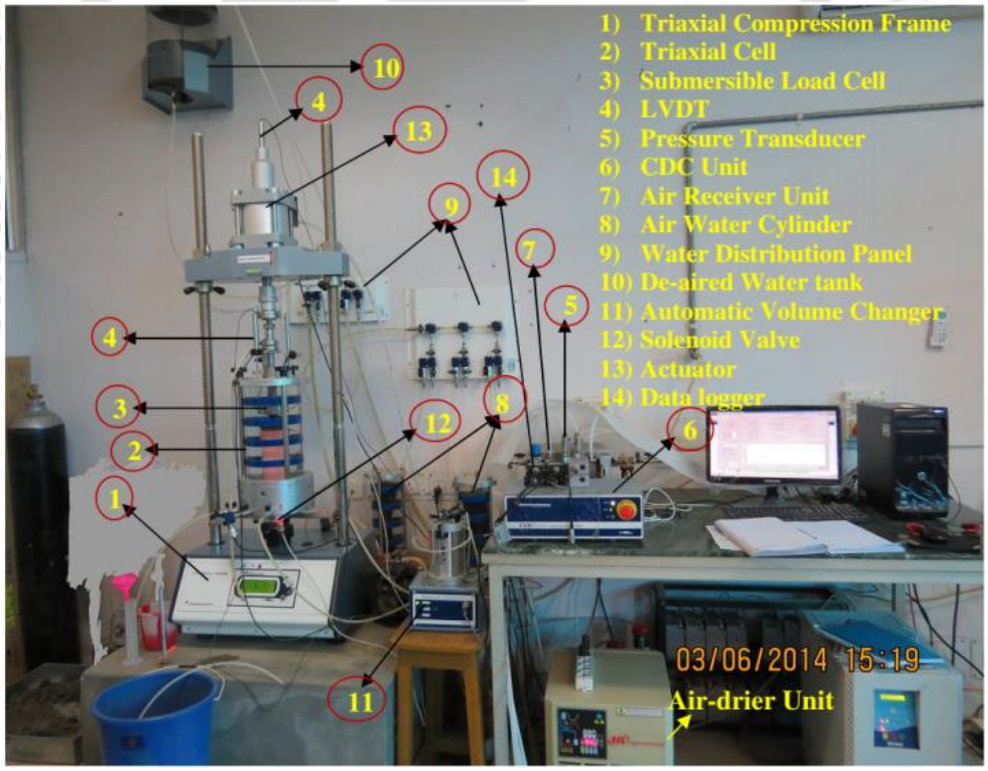

Fig. 3.4 Cyclic triaxial pressure system with connections and components

3.3.1 Triaxial frame

The Tritech triaxial frame of 100 kN capacity, presented in Fig. 3.5, consists of a pneumatic dynamic actuator and base pedestal to mount the triaxial cell. The base pedestal can

accommodate different sizes of soil specimens having diameter 38 mm, 50 mm and 70 mm, with sample heights of 76 mm, 100 mm and 140 mm, respectively. The loading frame is a system to apply the load on the mounted soil specimens, wherein different types of monotonic and cyclic load can be applied as a strain-controlled or a stress-controlled mechanism. Different types of cyclic/dynamic loading (harmonic, triangular, sinusoidal, haversine, and any user-defined random seismic motions) with different rates of deformation (10^{-5} to 10 mm/min) can be applied.

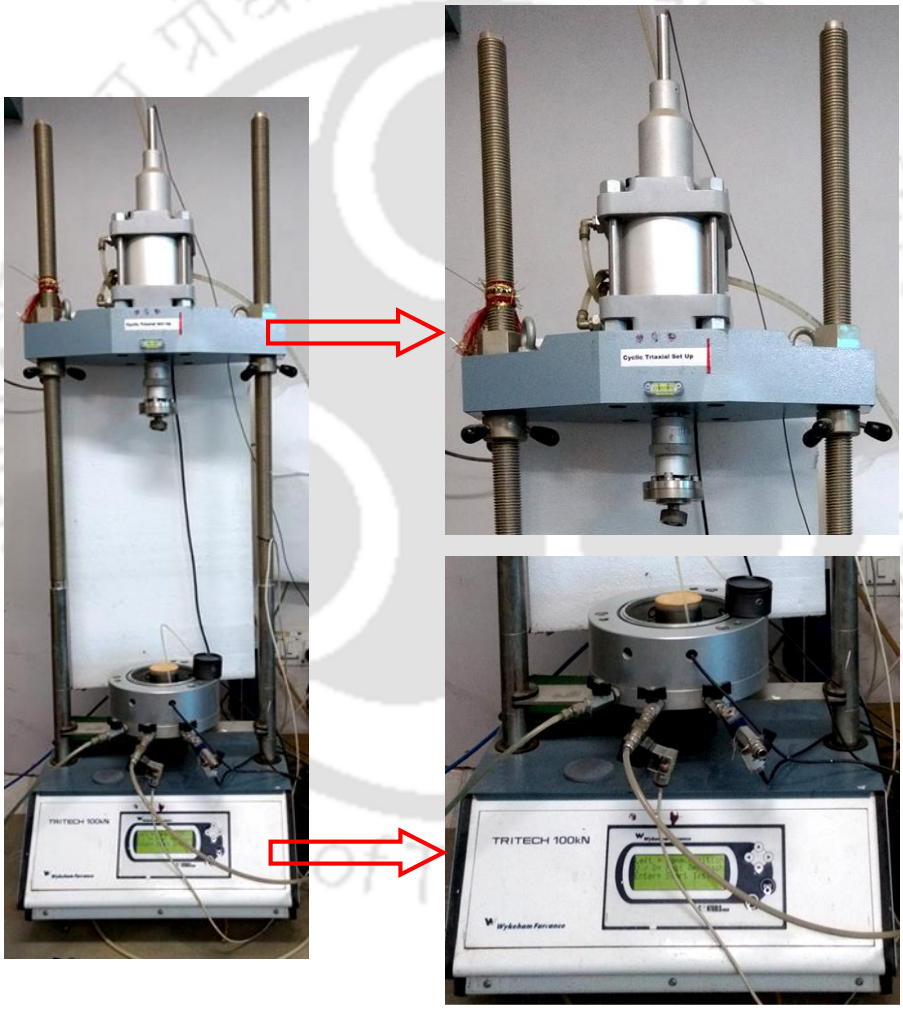

Fig. 3.5 Triaxial frame with actuator and base pedestal

3.3.2 Triaxial cell

The triaxial cell is a confining pressure chamber inside which the soil specimens are mounted for test, made up of a transparent acrylic glass cylinder attached with a submersible load cell

with a confining pressure capacity of 2000 kPa (Fig. 3.6). At the top of triaxial cell, an air bleed valve is provided to apply vacuum or suction in order to maintain a proper connection between the load cell and the top cap. The submersible load cell is connected with top plate of triaxial cell through a ram called load-cell ram, and measures the load applied to the specimen. The load-cell ram moves up and down through a seal during monotonic or cyclic loading. Seal is an element in the triaxial cell, which is used to prevent water leakage and also exerts negligible friction on the loading piston when an external load is employed.

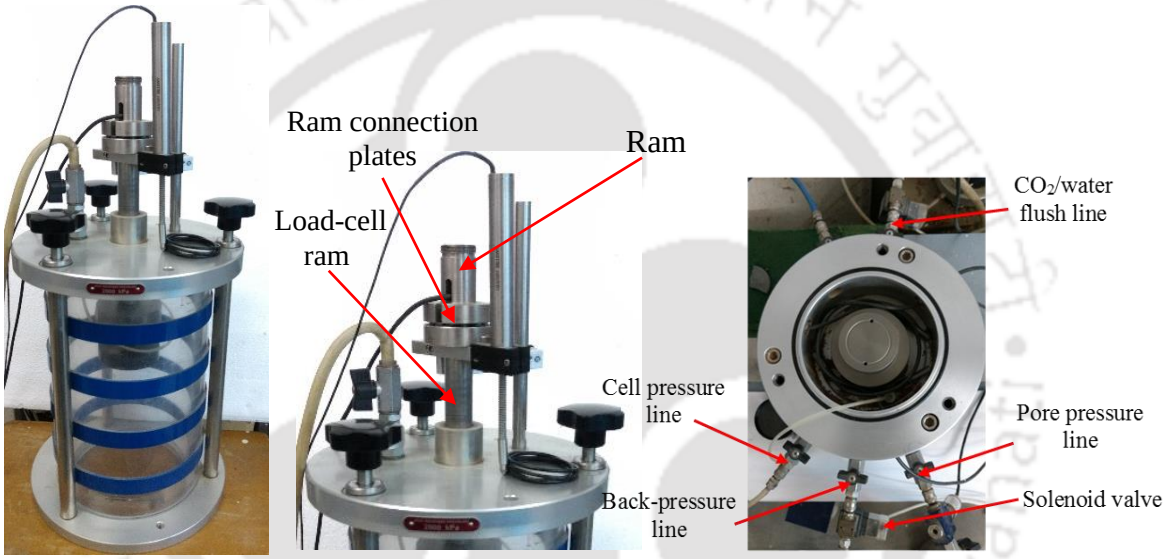

Fig. 3.6 Triaxial cell and its components

3.3.3 Dynamic actuator

Fig. 3.7 shows the dynamic actuator, having a displacement capacity 30 mm and operational frequency range of 0.01-10 Hz, mounted on the top of the triaxial loading frame. For monotonic compression shear tests, the actuator remains locked to its position, while the displacement is applied to the specimen by the rise of the base pedestal. For cyclic shear tests, the actuator moves to and fro about its mean position to generate the alternating loading and unloading mechanisms. To apply the load on the specimen, the actuator piston is connected to the ram (Fig. 3.6) by ram locking collar. Piston locking collar is provided to lock the down movement

of actuator piston while performing monotonic compression shear. During cyclic loading, the actuator position is maintained at the middle of operating displacement capacity (±15 mm), so that it can subject the specimens to both loading and unloading in either of the load or displacement controlled modes. The actuator is controlled by CDC unit and DYNATRIAX software.

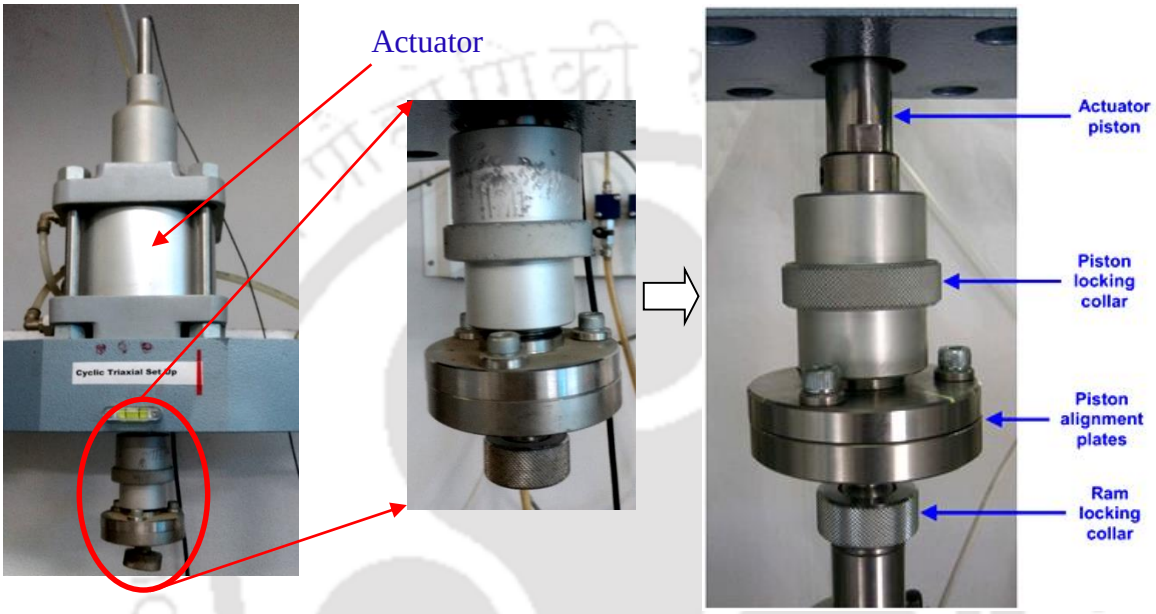

Fig. 3.7 Dynamic actuator and its components

3.3.4 Submersible load cell

Submersible load cell, of capacity 25 kN, is connected with top plate of triaxial cell through a load-cell ram as shown in Fig. 3.8. Subsequently, it is connected to the actuator with the aid of a ram locking collar (shown in Fig. 3.7) to transmit the cyclic or static loading onto the soil specimen. This load cell measures the load coming on the specimens during monotonic and cyclic shear tests.

3.3.5 Air water cylinder

The Air Water Cylinder (AWC), shown in Fig. 3.9, is an essential part of pneumatic triaxial systems. AWC chamber consists of an air bladder surrounded by water. As the air is pushed

inside the bladder with a targeted pressure, the same is transferred through the compressed water to the triaxial chamber. The targeted cell pressure and back pressure is applied via AWC onto and into the specimen, respectively. Two AWC are required, one for cell pressure channel and other for back pressure channel. The maximum working capacity of AWC is 1000 kPa.

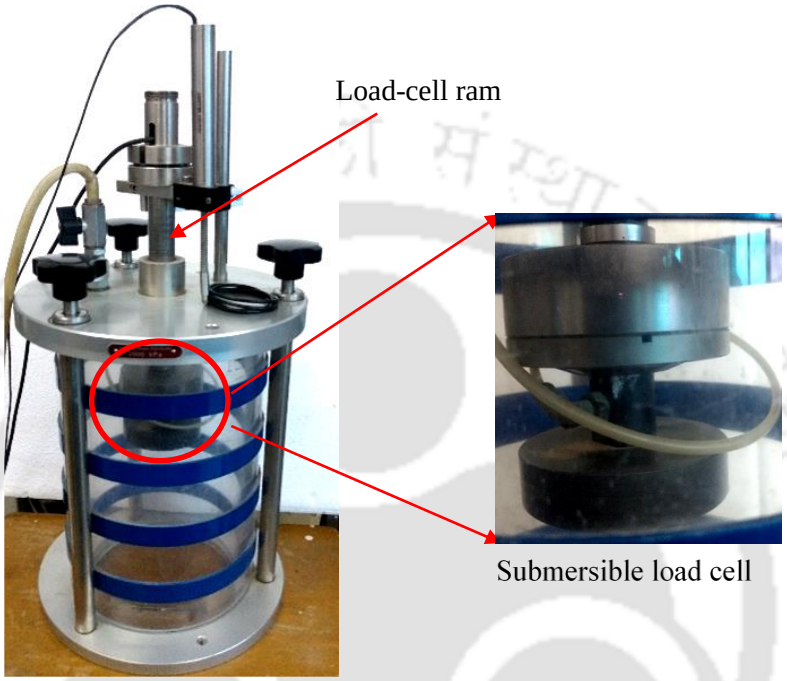

Fig. 3.8 Submersible load cell attached with triaxial cell

Fig. 3.9 Air Water Cylinder (AWC) unit

3.3.6 Automatic volume change device

The Automatic Volume Change (AVC) device comprises of a piston, sealed within a water filled chamber, and connected to a LVDT of capacity ±25 mm (Fig. 3.10). Flow of water through AVC unit causes a movement of the piston, and the response of the same is measured by the transducer. The output of the transducer is directly proportional to the volume of water flowing through AVC unit. AVC unit contains integral solenoid valves to allow automatic control of the flow direction, which are directly controlled by CDC unit and DYNATRIAX software.

Fig. 3.10 Automatic Volume Change (AVC) unit

3.3.7 Pressure transducers

Three different pressure transducers i.e. cell pressure, pore pressure and back pressure transducers, are depicted in Fig. 3.11, which are used to measure cell pressure, back pressure and pore-water pressure, respectively, during monotonic and cyclic loading. A solenoid valve is attached to each of the connections of the cell pressure and back pressure transducers for automatic opening and closure of the pressure lines. This solenoid valves are controlled by a compact dynamic controller (CDC) unit.

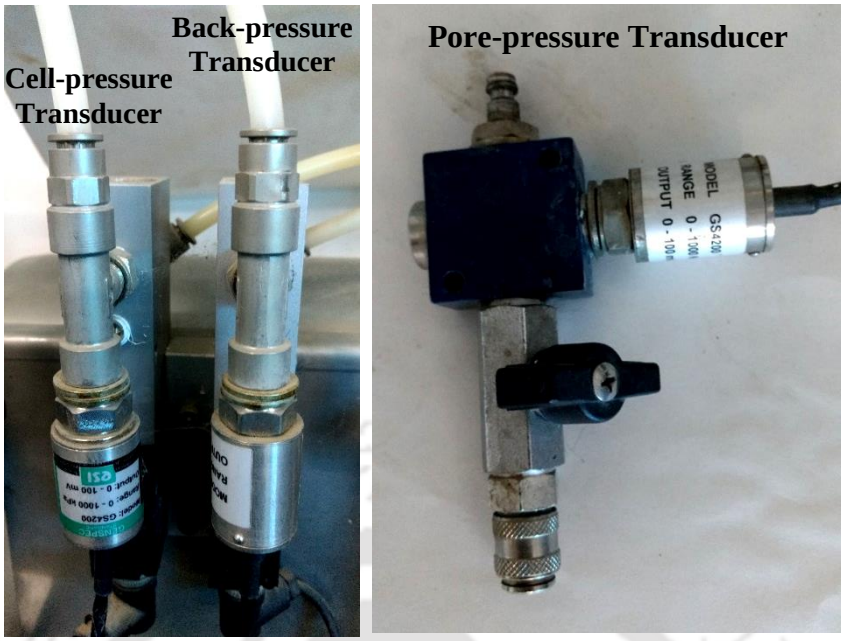

Fig. 3.11 Pressure transducers

3.3.8 Dry air receiver unit

The dry air receiver unit, shown in Fig. 3.12, is an interface between the air incoming to the system (from a compressed air source) and the air transmitted out to the servo-valves attached to the system. To control fluctuation of air during a cyclic test, it maintains a continuous supply of air without any change of pressure in the cell or the specimen. Two integral filters are provided at the inlet and outlet to remove any moisture from the air. The cell pressure transducers, back pressure transducers and servo-valves are mounted on this device. A regulator is provided at the inlet to control the pressure of the incoming air.

3.3.9 Compact dynamic controller

The Compact Dynamic Controller (CDC) unit is the operational hub of the cyclic triaxial system (Fig. 3.13a). All the components such as Tritech compression frame, actuator, solenoid valves, volume change devices, servo-valves and transducers are controlled and monitored during tests by CDC unit. The commands sent from DYNATRIAX software are received by CDC unit to control and manage the movement of the actuator and triaxial frame, the adjustment of the

pressure in the triaxial cell, opening and closure of the pressure lines, and flow direction in the automatic volume change (AVC) unit. CDC is fitted with three controllers to manage load/displacement, cell pressure and back pressure. This CDC unit is connected to the computer, and transfers transducer data to the computer, and vice-versa, via a data logger (Fig. 3.13b). The information received is further processed by DYNATRIAX software.

(a) Air-drier unit

(b) Dry air receiver unit

Fig. 3.12 Dry air receiver unit

Front view

Rear view

(a) Compact Dynamic Controller (CDC) unit

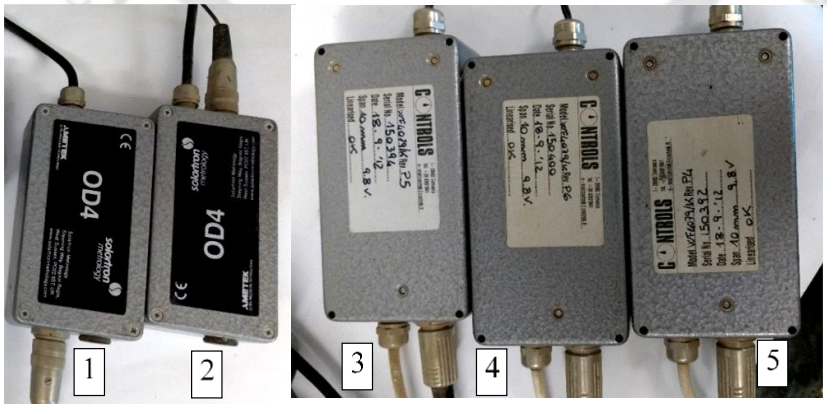

(b) Data logger for (1) actuator (2) external LVDT (3) on-sample LVDT1 (4) on-sample LVDT2 (5) on-sample LVDT3

Fig. 3.13 (a) Compact Dynamic Controller (CDC) unit (b) Data logger unit

Fig. 3.14 presents the schematic diagram of the cyclic triaxial setup, which reflects all the components along with their connections indicating the flow of operations for the proper functioning of the test apparatus. The arrows coming in and out of CDC unit, as presented in schematic diagram, reflects the importance of CDC unit in channelizing the information from DYNATRIAX software to the hardware components and vice-versa.

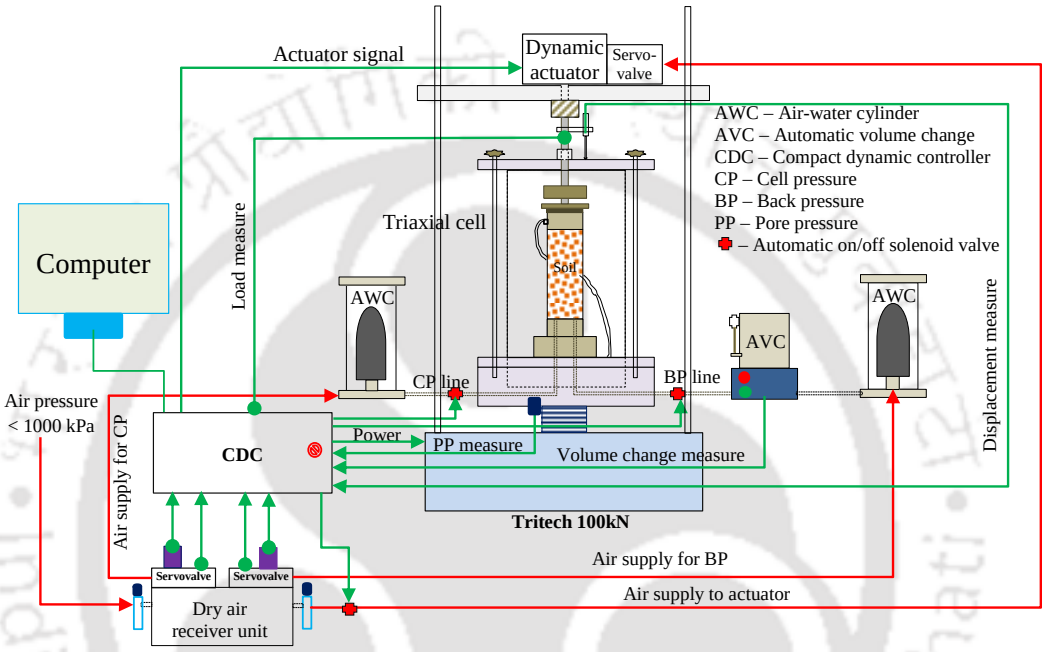

Fig. 3.14 Schematic diagram of a cyclic triaxial test setup

3.4 TESTING METHODOLOGY

This section deals with the methodology adopted to conduct the static monotonic and cyclic triaxial shear tests. This section elaborates the sample preparation technique, saturation technique, consolidation process and triaxial (static and shear) tests adopted for the present investigation.

3.4.1 Sample preparation

For sandy soil

Reconstituted solid cylindrical specimens, having diameter 70 mm and height 140 mm, were prepared for all the tests (ASTM D3999). Several sample preparation techniques such as dry

pluviation, moist tamping, and water sedimentation are common in practice for the preparation of reconstituted sand specimens (ASTM D3999; ASTM D5311; Ishihara, 1993; Kirar et al., 2012). Different methodologies of preparation of reconstituting specimens at same relative density can have different fabric structures and characteristics (Karg and Haegeman, 2009). Aforementioned all three methods were adopted in this study to prepare the specimens and saturation was checked accordingly, by measuring Skempton's *B*-value. Based on the *B*-value and the time required for saturation, as shown in Table 3.3, finally, dry pluviation technique was adopted to prepare the specimens.

The required amount of sand, based on the relative density, was poured in three layers through a cone shaped funnel into the specimen-forming mould (Fig. 3.15a,b). A vacuum pressure of 15-20 kPa was applied before removing the mould to maintain the verticality of the specimen (Fig. 3.15c). Subsequently, the triaxial cell was mounted on the base plate and then filled with de-aired water. After complete filling of de-aired water in triaxial cell, in order to maintain the verticality of the sample, a cell pressure equal to the vacuum pressure was applied, followed by simultaneous release of vacuum pressure (Ishihara et al., 1978a).

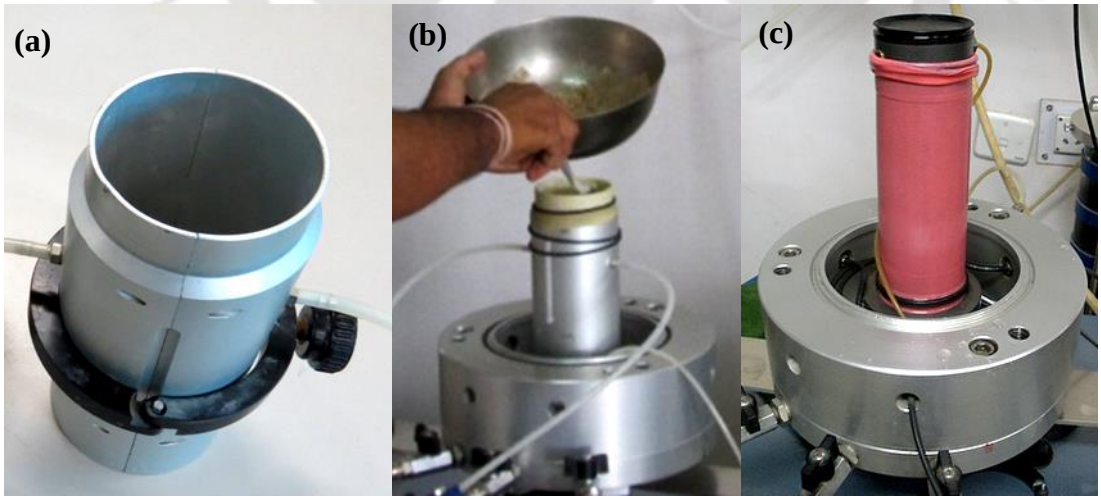

Fig. 3.15 (a) Split mould used for the preparation of sand specimen (b) Sand pouring into the mould (c) Prepared BS specimen

Table 3.3 Time taken to saturate sand specimen

Sl. No.	Methods of sample preparation	Saturation process	BP (kPa)	*B* – value	Time (hours)
1	Moist tamping (*water content* 5% *of weight*)	Apply BP, no CO_2	700	0.15 – 0.20	24
2	Dry deposition	Apply BP, no CO_2	700	0.15 – 0.20	24
3	Water sedimentation	Apply BP, no CO_2	500	0.85 – 0.90	24
4	Dry deposition	Apply BP followed by flushing deaired water through specimen	500	0.85 – 0.90	24
5	Dry deposition	Apply BP followed by flushing of CO_2 and de-aired water through the specimen	200	$\geq$ 0.98	1– 2

For cohesive soil

The remoulded cylindrical cohesive soil specimens of dimensions 70 mm diameter and 140 mm height was prepared in the mould (ASTM D3999). Fig. 3.16a shows the mould to prepare the cohesive soil (RS) specimens. To prepare the specimens, the dry soil of a specified weight was firstly mixed with the required amount of water. Once the water was uniformly mixed with the soil, the entire quantity of water-mixed soil was transferred into the mould from one end, while other end was enclosed with the collar (Fig. 3.16b). Thereafter, compaction was done from both ends by giving simultaneous equal rotation to the collars, maintaining uniform density of the specimen, till the specimen length of 140 mm was achieved. Sample prepared in mould was taken out by the help of extruder (Fig. 3.16c) and then kept on the base pedestal of triaxial frame. A membrane suction stretcher was used to place the rubber membrane over the mounted specimens.

A vacuum pressure of 15-20 kPa was applied before removing the mould to make proper contact between rubber membrane and circumferential boundary of the soil specimen. Subsequently, the triaxial cell was mounted on the base plate and then filled with water,

followed by application of cell pressure (CP) of 15-20 kPa and simultaneous release of vacuum pressure (Ishihara, 1993). The cell pressure was applied in this manner to prevent the intrusion and flow of CO_2 through the peripheral interface of rubber membrane and specimen boundary. The specimen preparation was followed by subsequent saturation and consolidation stages.

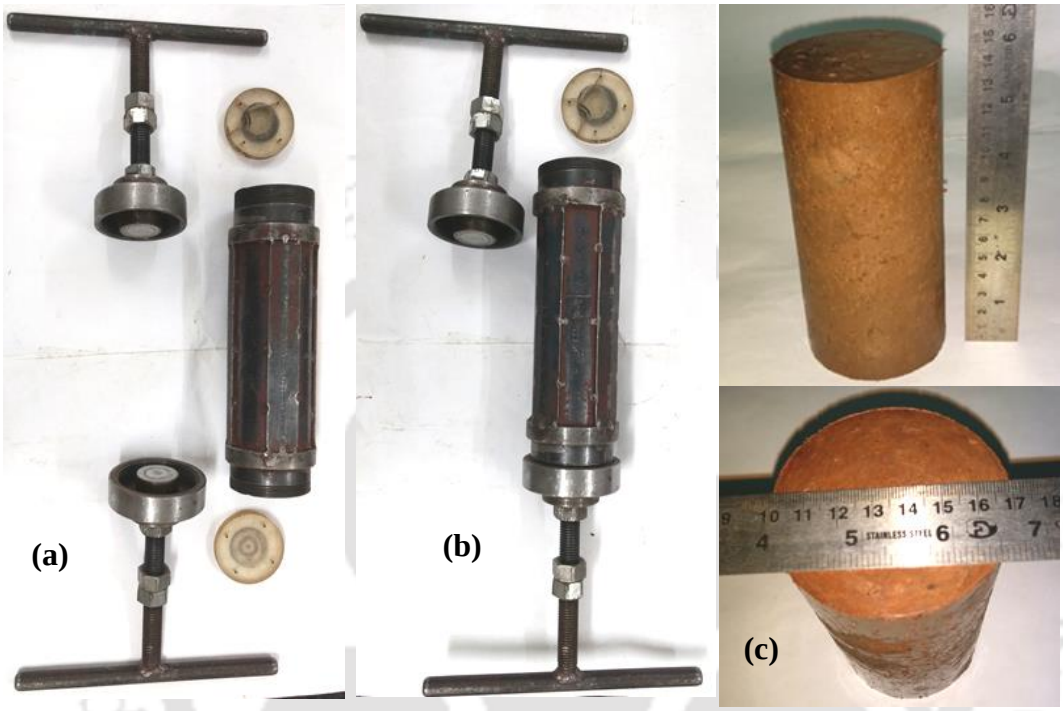

Fig. 3.16 (a) Mould for the preparation of RS specimen (b) Mould ready to be filled with water-mixed soil from one end, while the other end is fixed with the collar (c) Prepared RS specimen

3.4.2 Saturation

For sandy soil

The prepared specimen was then subjected to subsequent saturation, which is achieved from the complete dissolution of the air present in sample by passing de-aired water through the application of suitable back pressure (BP). The amount of BP required to dissolve the air depends upon the initial degree of saturation of the specimen. During the BP saturation methodology, the Skempton's pore pressure parameter (*B*-value) is checked to measure the degree of saturation at each increment of cell pressure (CP). The *B*-value is expressed as the

ratio of the increase of pore water pressure 'Δu' to the cell pressure increment '$\Delta\sigma_c$'. To determine the *B*-value, a cell pressure increment is applied while keeping the drainage valves closed (undrained condition) and the corresponding increment in the pore pressure is measured. When the increment of pore water pressure attains an equilibrium state, the *B*-value is calculated. *B*-value greater than or equal to 0.95 is an indication of degree of saturation nearly equal to 100% (Head, 1992). The *B*-value and corresponding degree of saturation is affected by compressibility, soil-texture, permeability, density and compactness of packing of the soil (Karg and Haegeman, 2009).

In the present study, in order to expedite the saturation process, the specimens were flushed with CO_2 for 10-15 minutes at a pressure lower than the applied initial cell pressure (~15-20 kPa) (as per Ishihara et al., 1978a). CO_2 was made to flow into the specimen through the bottom inlet pressure line of triaxial cell base plate, which then passes through the sample to reach the upper pressure line (connected to the bottom outlet pressure line of triaxial cell base plate via top cap). Since CO_2 is heavier, it replaces air present in the voids of the sample and is easily soluble in water than air. Subsequently, de-aired water was allowed through the CO_2 flushed specimen. The height of de-aired water tank was so maintained that the pressure head should be lower than the initial cell pressure of 15-20 kPa. To attain the saturation, the cell pressure (CP) and back pressure (BP) were then gradually increased in stages while maintaining an almost constant differential pressure of 10 kPa (Head, 1992). After each increment of CP, the *B*-value was estimated to check the saturation status. The specimen was considered to be completely saturated when the *B*-value was obtained to be greater than 0.95. The consolidated specimens were then subjected to monotonic and cyclic loading.

For cohesive soil

In order to expedite the saturation process, the specimen was flushed with CO_2 for 45 minutes to 1 hour at a pressure lower than 15-20 kPa, the initial CP (Ishihara, 1993). Subsequently, de-

aired water was passed through CO_2 flushed specimen. The water pressure head was maintained less than the existing cell pressure of 15-20 kPa. To attain the saturation, CP and BP were then gradually increased in stages while maintaining an almost constant differential pressure of 10 kPa. After each increment of CP, the Skempton's pore-pressure parameter (*B*) was estimated to check the saturation status. The specimen was considered to be completely saturated when the *B*-value was obtained to be greater than 0.96. The time taken in saturation for one specimen was 4-5 days, which is, from the application of CO_2 to achieving the *B*-value greater than 0.96.

After attaining saturation, the specimens, both cohesionless and cohesive soils, were isotropically consolidated to a targeted σ'_c by increasing CP while maintaining a constant BP. During the consolidation process, the specimen can be maintained at an isotropic or anisotropic state of stress according to the test requirement. For anisotropic consolidation, an additional axial stress is to be applied on the specimen. The effective stress can be applied either by increasing CP, or by decreasing BP, or by the combination of both (Head, 1992). In this study, the specimen was isotropically consolidated with increased CP while keeping constant BP, by allowing water to drain out into AVC system. After stabilization of incremental pore water pressure, the drainage valve was opened to allow the outflow of water. The drainage of water results in the decrease in volume and increase in the effective stress. During consolidation, the effective stress was estimated as the difference between CP and the residual pore pressure in the specimen, as shown in Fig. 3.17 (Head, 1992).

Theoretically, at the end of consolidation, the residual pore water pressure should become equal to BP; however, in experimental practice, such idealization is not achieved. Therefore, the desired effective confining stress on the specimens was considered to be achieved, when the difference between CP and pore pressure becomes equal to targeted value. The consolidation stage for cohesionless soil was considered to be completed when the excess pore water pressure nearly attained the applied BP. For cohesive soil, as the time required for excess

PWP to achieve BP is significantly high, the consolidation is considered to be completed if the volume change becomes constant or when 95% dissipation of the excess PWP is attained. The time needed in consolidation depends on the type of soil and its permeability.

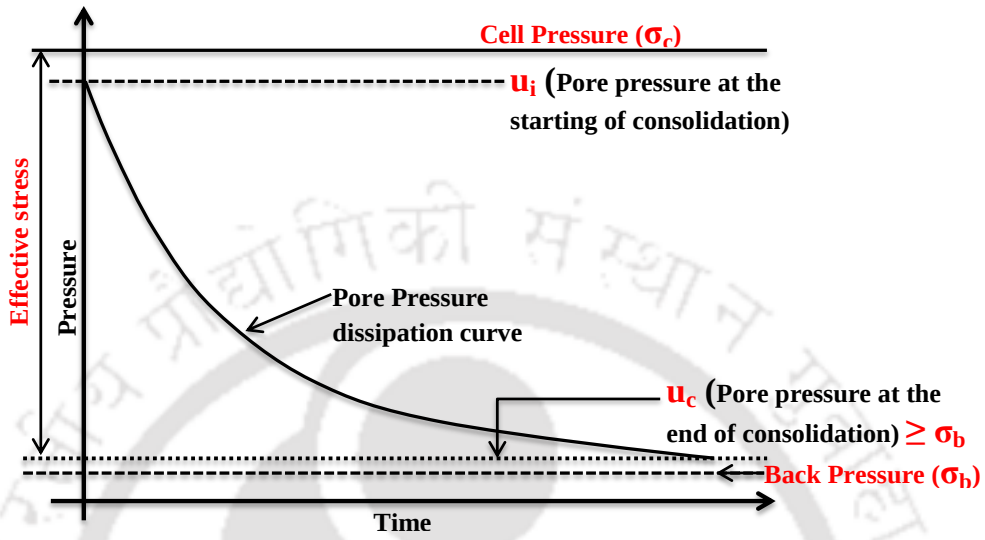

Fig. 3.17 Consolidation schematic of test specimen (after Head, 1992)

3.4.3 Triaxial shear tests

To comprehend the response of soils under different loading conditions such as static and dynamic, monotonic and cyclic triaxial tests respectively were performed on the sandy soil specimens prepared at different relative density (D_r = 30, 60 and 90%) and confining stress (σ'_c = 50, 100, 150 and 200 kPa). The cohesive soil specimens were either prepared at MDD-OMC conditions (as obtained from the compaction test) or at different water contents (8%, 15% and 25%) at a constant dry density of 1.5 g/cc. Static tests were performed in strain-controlled manner whereas, cyclic tests in both strain and stress-controlled manner.

Monotonic shear tests

Monotonic shear tests were conducted on dry and saturated cylindrical sand specimens. A displacement rate ranging from 0.005 mm/min to 1.2 mm/min were applied on consolidated specimens in undrained conditions, the details of which are listed in Table 3.4. Monotonic shear tests were also conducted on cohesive soil specimens at a displacement rate of 1.2 mm/min on

specimen prepared at different density and water contents, listed in Table 3.4. Since tests were undrained, the pore water pressure development in saturated specimens during application of deviator stress on the specimen was measured.

Table 3.4 Testing program for monotonic tests

Soil	D_r (%)	σ'_c (kPa)	Displacement rate (mm/min)
BS	30, 90	100	0.005 – 5.0
	30, 60, 90	50, 100, 150	1.2
RS	MDD-OMC, 1.5 g/cc and w = (8%, 15% and 25%)	50, 100, 150	1.2

Cyclic shear tests

Cyclic triaxial tests have been performed to evaluate the dynamic behaviour (dynamic properties and liquefaction potential evaluation) of soils using stress-controlled and strain-controlled shearing. For the evaluation of dynamic properties and liquefaction potential of sandy soil, strain- and stress-controlled cyclic triaxial tests were performed using sinusoidal wave (regular excitation) at different testing conditions. Tests were also conducted on sandy soil to observe the liquefaction potential when subjected to irregular (earthquake motion).For the evaluation of dynamic properties of cohesive soil, stress-controlled cyclic triaxial tests were performed using regular excitations.

Regular excitation

The actual acceleration time history of an earthquake is irregular, and the induced shear stresses or shear strains vary randomly both in magnitude and frequency during an earthquake (Ishihara and Yasuda, 1972, 1973, 1975). The laboratory experimental investigation to evaluate the response of soil using regular excitations were carried out considering an average equivalent uniform shear stress (in stress-controlled approach) or strain (strain-controlled approach) equal

to the 65% of the maximum shear stress or strain of the chosen strong ground motions (as per the simplified procedures suggested Seed and Idriss, 1971 and, Dobry et al., 1980).

Cyclic stress approach is based on the assumption that the loading expressed in terms of cyclic shear stresses; while, in cyclic strain approach, the earthquake-induced loading is expressed in terms of cyclic strains (Kramer, 1996). Therefore, to perform the strain-controlled cyclic tests, the representative values of cyclic shear strain ranging from 0.015%-7% was chosen, which cover the wide range of high cyclic strains. For the stress-controlled cyclic tests, different values of cyclic stress ratio (CSR = $\sigma_d/2\sigma'_c$), ranging from 0.05 to 0.4, was chosen to apply the load in stress-controlled manner. For any specific CSR, based on various confining pressures, the corresponding deviatoric stress (σ_d) was applied on the specimen, to identify the liquefaction in specimens for a given number of loading cycles.

Strain-controlled loading

For strain-controlled cyclic load test, firstly the desired single amplitude shear strain (γ_{SA}) was selected, as shown in Table 3.5, and, then required axial strains (ε_{SA}) were calculated using Eqn. 3.1. The resulting single amplitude deformation employed on the soil specimen was calculated using Eqn. 3.2.

$$\gamma_{SA} = \varepsilon_{SA}(1+\nu) \Rightarrow \varepsilon_{SA} = \gamma_{SA}/(1+\nu) \tag{3.1}$$

$$\varepsilon_{SA} = L_{SA}/\ L_S \Rightarrow L_{SA} = \varepsilon_{SA} \times L_S \tag{3.2}$$

where L_{SA} = single amplitude deformation (mm), L_s = length of test specimen (mm) and ε_{SA} = single amplitude axial strain (dimensionless). Fig. 3.18 presents a typical loading pattern (input) and output for regular strain-controlled loading pattern.

Table 3.5 Investigation parameters of the strain-controlled CT tests

Soil	D_r (%)	σ'_c (kPa)	f (Hz)	γ (%)
SBS	30	50	1	0.015, 0.045, 0.075, 0.15, 0.30,0.45,0.60, 0.75, 1.0, 1.5, 3.0
		100		0.045, 0.075, 0.15, 0.30,0.45,0.60, 0.75, 1.5
		150		0.045, 0.075, 0.15, 0.30, 0.45, 0.60, 0.75
	60	50	0.5, 1, 2, 3, 4	0.15, 0.60, 1.0, 1.5, 3.0, 4.5
		100		
		150		
	90	50	1	0.045, 0.075, 0.15, 0.30, 0.45, 0.60, 0.75, 1.5
		100		0.045, 0.075, 0.15, 0.30, 0.45, 0.60, 1.0, 1.5, 2.0
		150		0.045, 0.075, 0.15, 0.30, 0.45, 0.60, 0.75, 1.0, 1.5, 2.0
DBS	60	50	1	0.045, 0.075, 0.15, 0.30, 0.60, 0.75, 1.0, 1.5, 3.0, 4.5, 6.0,7.0
		100		0.045, 0.075, 0.15, 0.30, 0.45, 0.75, 1.5, 3.0, 5.0, 7.0
		200		0.075, 0.10, 0.30, 0.45, 0.60, 0.75, 1.5, 3.0, 4.5, 6.0

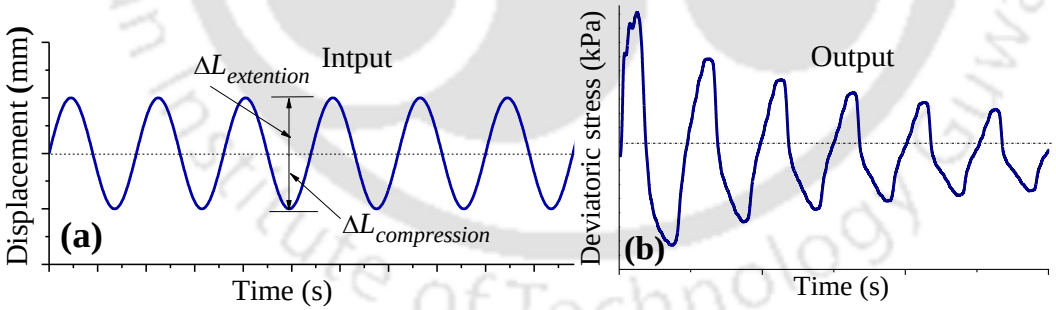

Fig. 3.18 (a) Typical loading pattern (input) and (b) Deviatoric stress variation (output) for a strain-controlled cyclic test

Stress-controlled loading

For stress-controlled cyclic load test, the magnitude of cyclic load (shown in Table 3.6) was firstly estimated, based on the desired cyclic stress ratio ($CSR_{desired}$). $CSR_{desired}$ is the ratio of the desired deviator stress to twice the effective consolidation stress. The magnitude of cyclic load

to be employed on the soil specimens were estimated using Eqn. 3.3.

$$P_c = 2 \times \sigma'_c \times CSR_{desired} \times A_c \tag{3.3}$$

where P_c = estimated cyclic load to be applied to the specimen, σ'_c = targeted effective stress, $CSR_{desired}$ = desired cyclic stress ratio ($\pm \sigma_d / 2\sigma'_c$) and A_c = area of specimen after consolidation. Fig. 3.19 presents a typical loading pattern (input) and output for regular stress-controlled loading pattern.

Table 3.6 Investigation parameters used in stress-controlled CT tests

Soil	D_r (%)	σ'_c (kPa)	f (Hz)	CSR
SBS	30, 60, 90	50, 100, 200	1	0.05, 0.1, 0.2, 0.3
	60	100	0.1, 0.5, 1, 2, 4	0.1, 0.2, 0.3, 0.4
RS	MDD-OMC, 1.5 g/cc & 8%*w*, 15%*w*, 25%*w*	100	1	0.1, 0.2, 0.3, 0.4

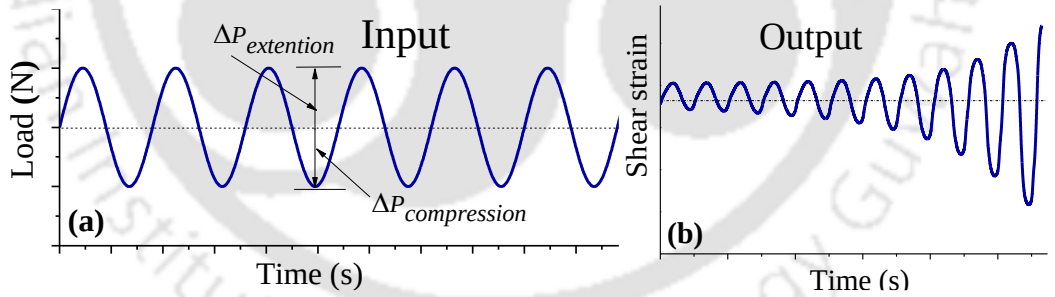

Fig. 3.19 (a) Typical loading pattern (input) and (b) Deviatoric stress variation (output) for a stress-controlled cyclic test

Selection of loading frequency for regular excitation

The selection of any particular frequency for regular excitation is a challenging task due to the significant variation of frequencies over a wide range. In the study of regular excitation, the sinusoidal wave pattern of stresses has been typically chosen for a frequency of 1 Hz for all tests. In the present study, the strain-controlled and stress-controlled cyclic tests have been conducted at for a frequency range 0.1–4 Hz, described in chapter 5. Bhattacharya (2007) has

reported that the predominant frequency range of earthquakes are 0.5-10 Hz. Based on the strain-controlled tests, Kumar at el. (2015) have also reported that the excess PWP increases with frequency up to 2 Hz, beyond which, it decreases. It was also reported that the shear modulus is not affected by the loading frequency, although the effect on damping ratio is significant. In addition to this, several literatures have reported about the effect of frequency over dynamic behaviour of soils (Teachavorasinskun et al., 2002; Yilmaz et al., 2004; Ravishankar et al., 2005; Jakka et al., 2010; Maheshwari et al., 2012b; Lombardi et al., 2014; Mohanty and Patra, 2016; Chattaraj and Sengupta, 2016a,b). Based on the experimental investigation and these literatures, the frequency of 1 Hz for cyclic loading can be recommended for the measurement of dynamic soil properties and liquefaction studies of sand.

Irregular excitations

Three different irregular stress time histories, computed from the acceleration histories of Bhuj (2001; PGA = 0.103g), Tezpur (2012; Scaled PGA = 0.36g) and Kobe (1995; PGA = 0.834g) strong motions, have been used to evaluate the dynamic response of soil. The acceleration time histories and their frequency domain representation obtained using Fast Fourier Transformations (FFT) of these three strong motions are presented in Fig. 3.20a and Fig. 3.20b, respectively. Frequency-domain representation indicates the distribution of energy content over a frequency band. It is observed that the significant energy content of Bhuj and Kobe strong motions are congregated over a frequency band of 0.5-4 Hz, while the same for Tezpur motion is found to be at 2-15 Hz. Dynamic earthquake loadings have been applied on the test specimen in terms of deviatoric stress history, which was evaluated by the Eqns. (3.4-3.7) proposed by Seed and Idrriss (1971). Fig. 3.20c shows the applied typical deviatoric irregular stress time histories of different ground motions with different PGA for a test specimen at effective confining stress of 100 kPa i.e. at an approximated confining depth of 10 m. The investigating parameters of the irregular seismic excitations are presented in Table 3.7.

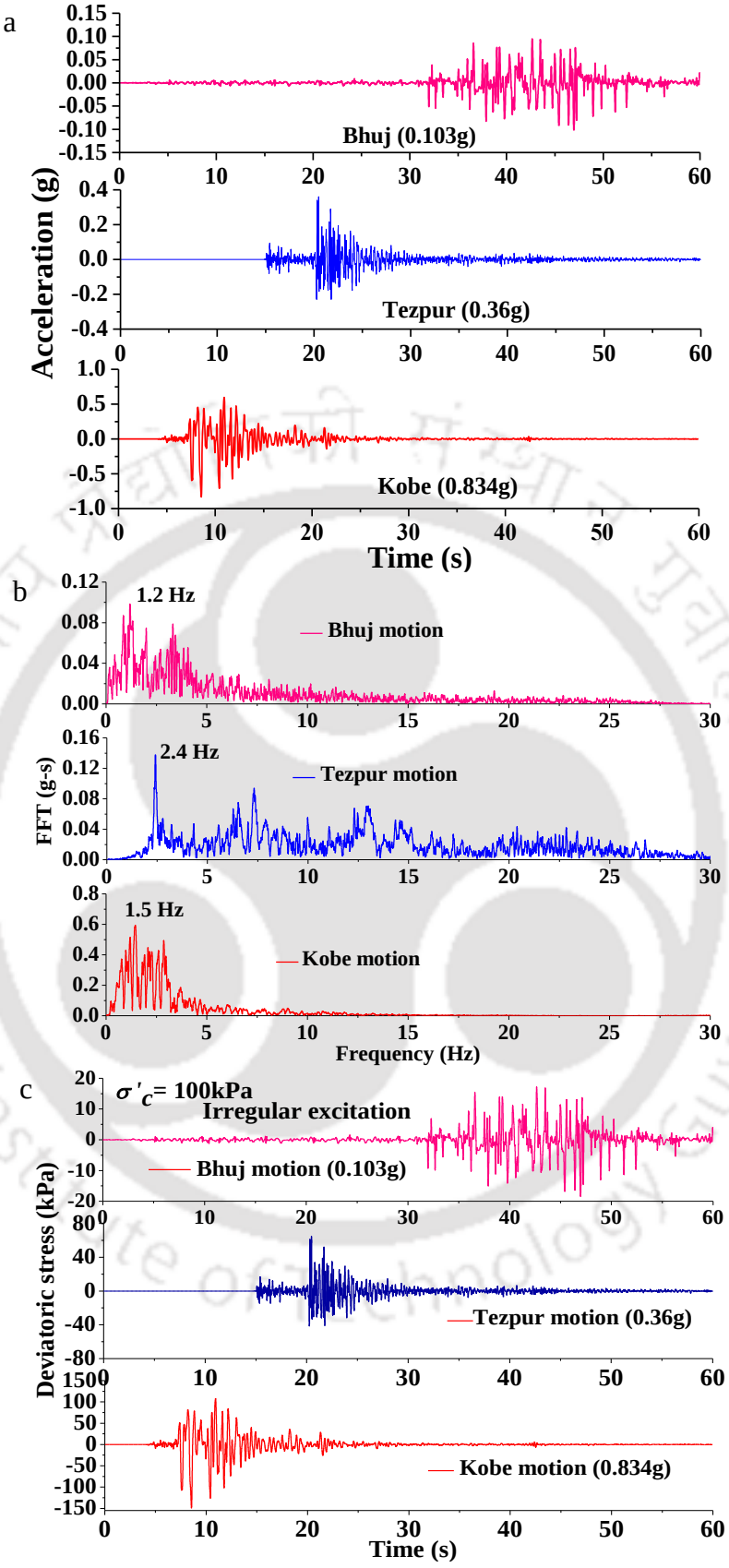

Fig. 3.20 (a) Acceleration time histories (b) Frequency domain representation (c) Typical irregular stress time histories of input motions

$$\tau = \frac{acc.(g)}{g} \times \sigma_v \times r_d \tag{3.4}$$

$$r_d = 1.0 - 0.00765z;\ for\ z \le 9.15m \tag{3.5}$$

$$r_d = 1.174 - 0.0267z;\ for\ 9.15 \le z \le 23m \tag{3.6}$$

$$\sigma_d = 2 \times \tau = 2 \times \frac{acc.(g)}{g} \times \sigma_v \times r_d \tag{3.7}$$

where, acc.(g) is the acceleration time history, σ_v is the total overburden vertical stress and r_d is the stress reduction factor (Eqns. 3.5-3.6). Since, the strong motions, used in this study, were recorded at ground level, r_d is considered to evaluate the stress at any particular depth 'z' (Youd et al., 2001). The different effective confining stress reflects that the soil specimens located at different confining depths below the ground level.

Table 3.7 Investigating parameters of the irregular seismic excitations

Soil	Irregular excitation	PGA (g)	Relative density D_r (%)	Confining depth (m)
BS	Bhuj Tezpur Kobe	0.103 0.360 0.834	30	5, 10, 15
	Bhuj Tezpur Kobe	0.103 0.360 0.834	30, 60, 90	10, 15
	Bhuj Tezpur Kobe	0.103	60	10
	Bhuj Tezpur Kobe	0.360	60	10

3.4.4 Measurement of local strains

To measure local strains mobilized due to elemental response of the soil specimen when subjected to static and dynamic loading, on-sample LVDT (Linear Variable Differential Transducers) were used. To achieve this objective, strain-controlled monotonic and strain-controlled cyclic triaxial tests were conducted on the sandy soil specimens prepared at two

relative densities (D_r = 30% and 90%) and three σ'_c (50 kPa, 100 kPa and 150 kPa). Before starting the test, fixity and calibration of the on-sample LVDTs are important tasks to achieve accurate response. The following sections deal with the assembly of the on-sample LVDTs to the specimen and calibration as well.

Assemblage of on-sample LVDTs on the specimen

Fig. 3.21 shows the photograph and schematic diagram of the assembly of submersible on-sample LVDTs to the soil specimen for the measurement of local strains. The attachment consists of two axially oriented LVDTs and one radially oriented LVDT; the entire attachment was placed at the mid-height of the specimen shown in Fig. 3.21a (Kumar et al., 2016). Simultaneous measurement of both axial as well as radial deformations would provide the Poisson's ratio of the soil specimen at different strain levels. Each axial transducer was initially fixed to the mounting block with the help of O-ring (Fig. 3.21a) and, then both axial transducers, along with the mounting blocks, were fixed to the specimen, with the aid of rubber bands. The axial LVDTs were placed diametrically opposite to each other, as shown in Fig. 3.21.

The rubber bands used to hold the mounting blocks in position has a width approximately 1 cm (shown in Fig. 3.21b), and are made up of the same material as the confining membrane used for the test specimen. The mounting blocks of each LVDT displace relative to one another as the specimen deforms, and allow free rotation to ensure accurate measurements of axial displacements during tests. As per the recommendation given in ASTM D3999, the thickness of membranes should not exceed 1% of the diameter of the specimen (i.e. 0.7 mm for the sol specimen of diameter 70 mm) such that no significant additional stresses are generated within the specimen. The thickness of the rubber band and the rubber membrane, as used for the present investigation, was in the range of 0.2–0.3 mm, which is well within the stated limit, thus eliminating the necessity of any membrane correction. The local axial strains in the specimens were estimated as the ratio of the average displacement measured by axial transducers to the

gauge length (i.e. initial distance between mounting blocks).

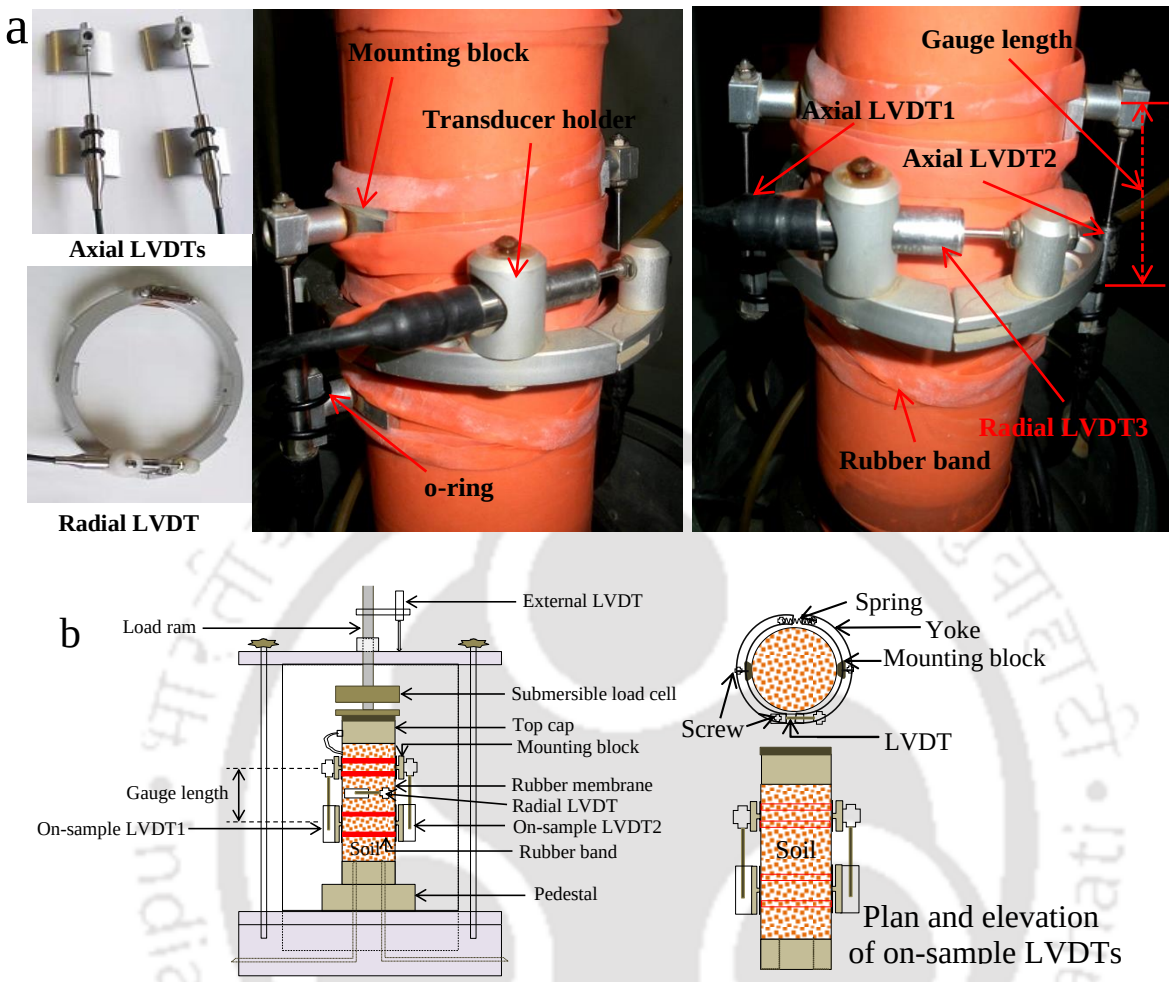

Fig. 3.21 (a) Soil specimen with on-sample LVDTs (b) Schematic diagram for the assemblage and fixities used in local strain measurement

On-sample LVDTs: Specification and calibration

Two LVDTs (LVDT1 and LVDT2) to measure axial deformation and one LVDT (LVDT3) for measuring radial deformation have been used as on-sample LVDTs for the determination of local strains. The on-sample LVDTs, used in the present study to measure the local strains, were supplied by Wykeham Farrance, and are fully functional in a water-submerged condition. The on-sample LVDTs requires a supply root-mean-square input voltage of 0.5 V–7 V r.m.s having 2-10 kHz sinusoidal frequency, while the calibrated supply voltage required is 5 V r.m.s having 5 kHz sinusoidal frequency at 30 mA power provision. Under the operating condition, the linearity or accuracy resides to 0.1% of the full range, allowing a tolerance phase shift of 10°

during a 5 V–5 kHz excitation; the optimum output load is obtained as 100 kΩ. The operating temperature of the transducer lies between -20°C to +125°C, having both zero temperature and span temperature coefficients to be ±0.01% full scale/°C. The on-sample LVDT remains sealed by an outer cable sleeve and can remain fully functional under an operating pressure 3.4 MPa. The on-sample LVDTs have been calibrated using the Geodatalog logger. The on-sample LVDTs have their own electrical zero and can be manually adjusted before starting the calibration. The calibration charts for the on-sample LVDTs are shown in Fig. 3.22, depicting the correlation between the measured values and predicted values.

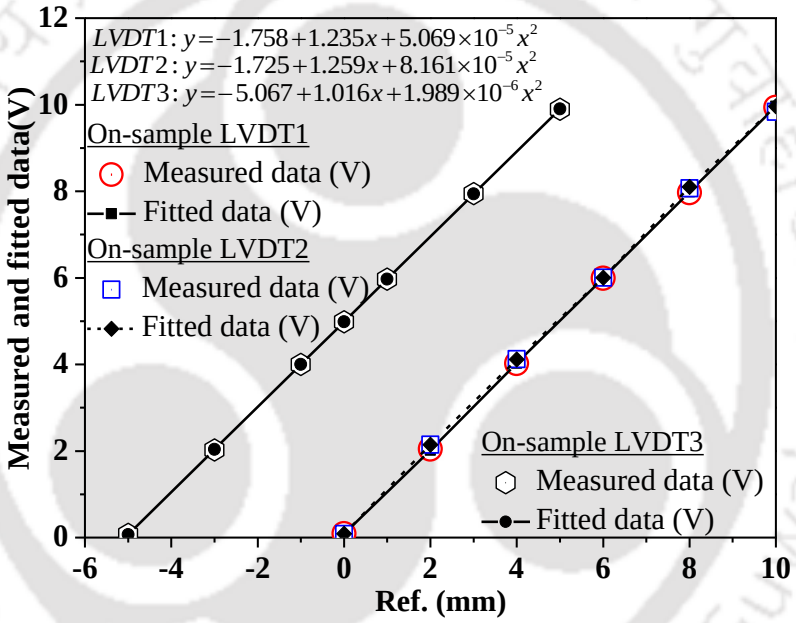

Fig. 3.22 Calibration curve of on-sample LVDTs

It can be observed that the predicted and measured voltages have excellent agreement and correspond to a negligible scatter on a 45° line. The measuring capacity of the axial and radial on-sample LVDTs are 0–10 mm. After attaching to the specimen, to measure the local strains at the start of the testing, LVDT readings were manually adjusted to zero. The water-submersible on-sample LVDTs allow the measurements of axial and radial deformations of the soil specimens to accuracy of 1 micron with any of the 16 bit data logging systems. The total buoyant weight of water-submerged on-sample LVDTs is 68 g, thus imposing an average

uniform stress of approximately 0.18 kPa on the central cross-section (70 mm diameter) of the undeformed specimen. Since, these excess stresses sue to the on-sample LVDTs are negligible in comparison to the range of applied effective stresses, the weight corrections were not accounted in the present study. Similar observations regarding the weight of the on-sample transducers have been mentioned by Cuccovillo and Coop (1997). The operating stress range of water-submersible on-sample LVDTs were is 0–3.4 MPa. Since, the applied confining stresses (range: 50 kPa–150 kPa), for the present study, were sufficiently less than the maximum operating stress limit, the on-sample LVDTs functioned efficiently during the experimental investigations. Scholey et al. (1995) and Cuccovillo and Coop (1997) have reported that the on-sample LVDTs respond accurately up to confining stress of 2 MPa under water-submerged conditions, while the response is accurate up to 70 MPa for oil-submerged conditions. The responses of the on-sample LVDTs during saturation and consolidation were found to be insignificant.

3.5 SUMMARY

This chapter presented the details of materials used in the study, i.e. cohesive soil, cohesionless soil, and their physical characterization as per the relevant standards. The cyclic triaxial test setup, its different hardware components and instrumentations, along with their function were described. Preparation of the soil specimens and the adopted techniques were also elaborated. Details of test parameters adopted and planning of experimental program with different testing methodologies are explained. The test methodologies followed to conduct the monotonic or cyclic tests, strain- or stress-controlled, using regular and irregular excitations, were also presented in brief. The on-sample LVDTs used in the present study to delineate the generation of local strains in the specimen is also presented. Further chapters describe the results obtained from various tests conducted as per the experimental program and planning.

Chapter 4 MONOTONIC SHEAR TESTS

4.1 INTRODUCTION

In most of the geotechnical engineering works, soil mass resist the shearing stresses, and in process, undergoes strain accumulation. The maximum shear stress taken by the soil before failure is represented as the ultimate shear strength of soil. If the shear stress exceeds the shear strength of soil mass, the foundation soil or the supported structures will fail due to strain localization and subsequently undergo coupled stress and deformation based failure. Depending on the rigidity of the soil mass, and the magnitude of loading, different degrees of strain can generate within the soil (low to high), resulting in the varying behavioral changes in soil properties at different strain levels. The response of soil at different strain rate, relative density and effective confining pressure were evaluated with the aid of monotonic compression shear tests. During shearing, the displacements were measured with the help of external and on-sample LVDTs and, the results have been presented and discussed in this chapter.

4.2 TESTING PROGRAM

Monotonic shear tests were conducted on dry and saturated cylindrical BS specimens as well as on RS specimens to comprehend the behaviour of both the soils. For BS specimens, tests were conducted at varying loading rate ranging from 0.005 mm/min to 5 mm/min for effective confining pressure of 100 kPa, while for RS specimens, 1.2 mm/min displacement rate was employed, the detailed of which are enlisted in Table 3.4. Since undrained tests were conducted, the pore water pressure generated during shearing was also measured and, then effective internal friction and cohesion (apparent cohesion) was evaluated.

This section discusses the response of dry and saturated BS and the RS, based on the outcome of monotonic shear tests. Monotonic compression shear tests were conducted for specimens prepared at different relative densities and subjected to varying confining pressure

and displacement rate. The response of soils at these testing conditions have been reported in terms of stress-strain variations, stress path, excess pore-water pressure ratio and variation of stiffness as recorded from the tests.

4.3 TESTS ON DRY COHESIONLESS SOIL

Monotonic compression tests have been performed on Dry Brahmaputra Sand (DBS) at a displacement rate of 1.2 mm/min, to observe the behaviour of soil under static loading and the results are presented in Fig. 4.1 to Fig. 4.4. Fig. 4.1 shows the variation of deviatoric stress with axial strain of DBS at a D_r = 60% and different σ'_c (i.e. 50 kPa, 100 kPa, 150 kPa). Higher confining pressure reflects higher deviatoric stress, since, the resistance to deform the soil specimen is higher at higher confining stress.

Fig. 4.2 shows the variations of deviatoric stress against confining stress, which is called as the stress path. Since, there is no pore water in the soil specimen depicted by Fig. 4.3, the stress path become a straight line reflected in Fig. 4.2. Fig. 4.4 depicts the variation of stiffness represented by secant modulus with axial strain at different confining pressure. It is seen from the figure that at lower axial strain, the secant modulus is higher when subjected to higher confining pressure, whereas, with the increase of axial strain, the difference between secant modulus at all three given confining stress reduces significantly. The secant modulus of a soil is generally used in many geotechnical applications. The secant elastic modulus for a soil is usually the slope of the line on the elastic stress - axial strain curve joining the points of zero deviator stress to the point having a deviator stress equal to one-half or one-third of the peak deviator stress (Lambe and Whitman, 1969).

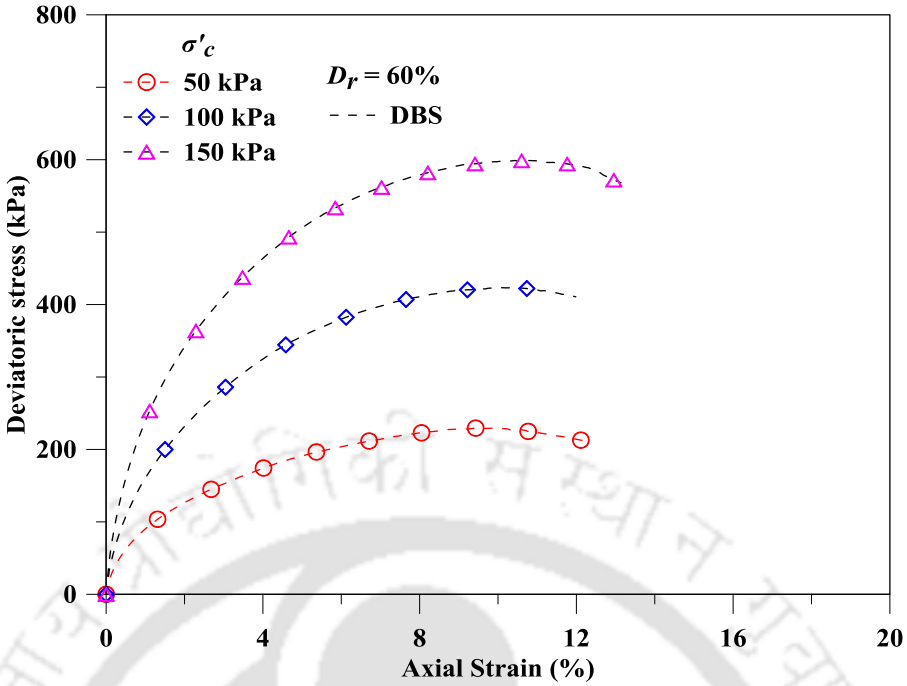

Fig. 4.1 Stress-strain variation for DBS subjected to different σ'_c

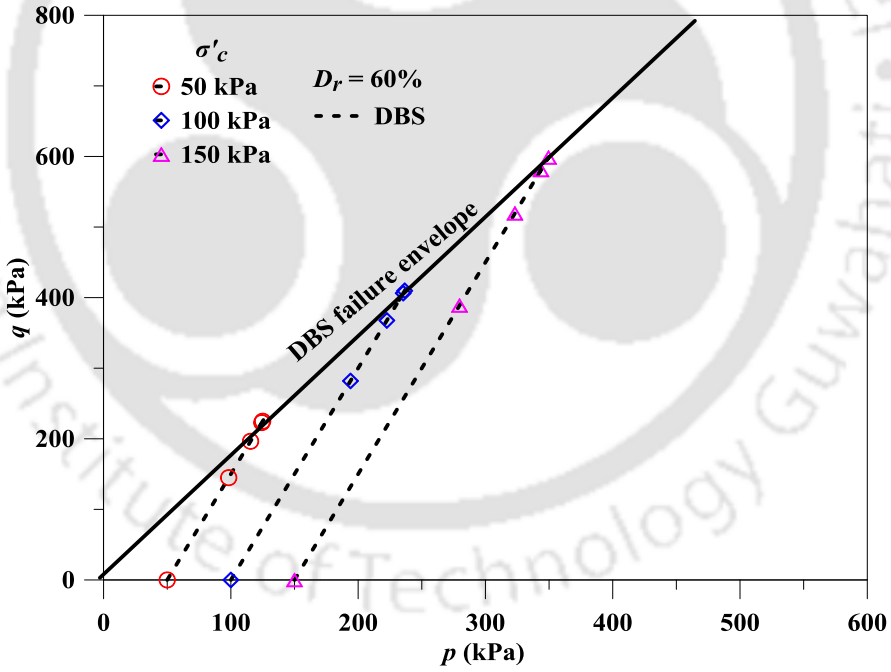

Fig. 4.2 Stress path plot for DBS subjected to different σ'_c

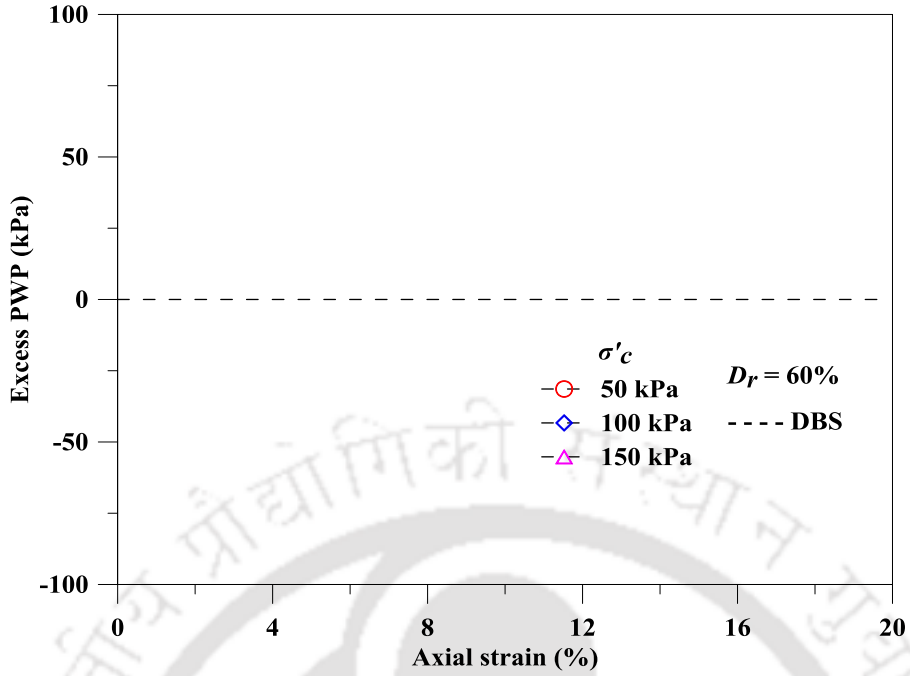

Fig. 4.3 Variation of excess PWP for DBS subjected to different σ'_c

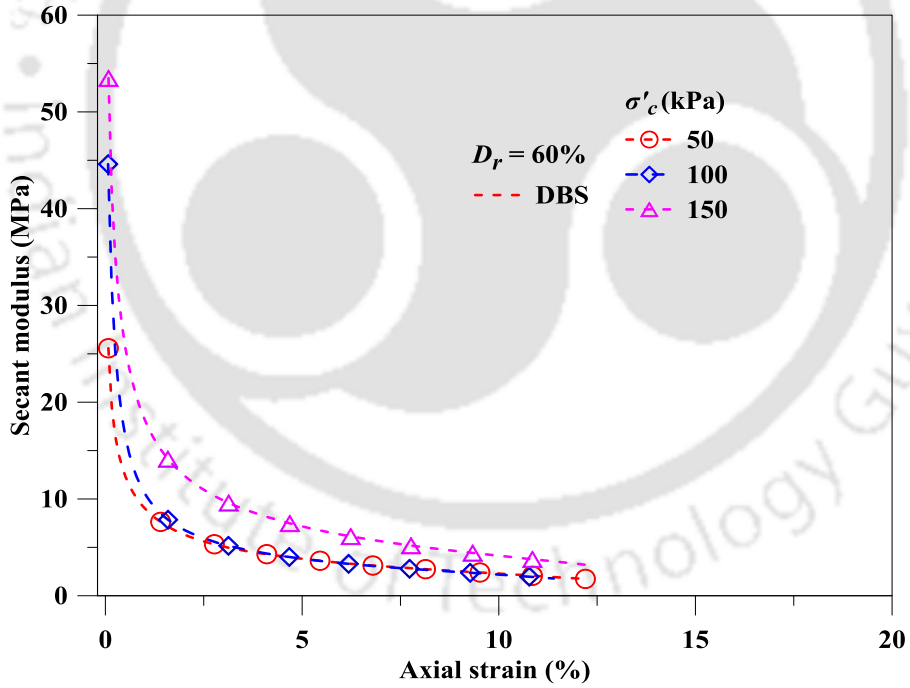

Fig. 4.4 Variation of secant modulus at different σ'_c for DBS subjected to different σ'_c

4.4 TESTS ON SATURATED COHESIONLESS SOIL

Saturated Brahmaputra Sand (SBS) was also tested under static loading, with a displacement rate of 1.2 mm/min, to observe the behaviour of soil under saturated conditions and identify the

behavioral changes during shearing. The results are presented in Fig. 4.5-Fig. 4.8. Fig. 4.5 shows the variations of deviator stress with axial strain for SBS at a D_r = 60% and different σ'_c (50, 100, 150 kPa). As obvious, at higher confining stress, the deviatoric stress is higher. Fig. 4.6 illustrates that the effective stress decreases initially, reflecting a contractive behaviour of sand, due to the increase of PWP. The contractive behaviour of soil along with the excess PWP development is more prominent at high confining pressure. Further increase of static loading causes increase in effective stress due to decrease in PWP (Fig. 4.7) which hints about soil-dilation behaviour with gradual redistribution of excess PWP within the soil specimen. The secant modulus under saturation conditions has also been reported in Fig. 4.8.

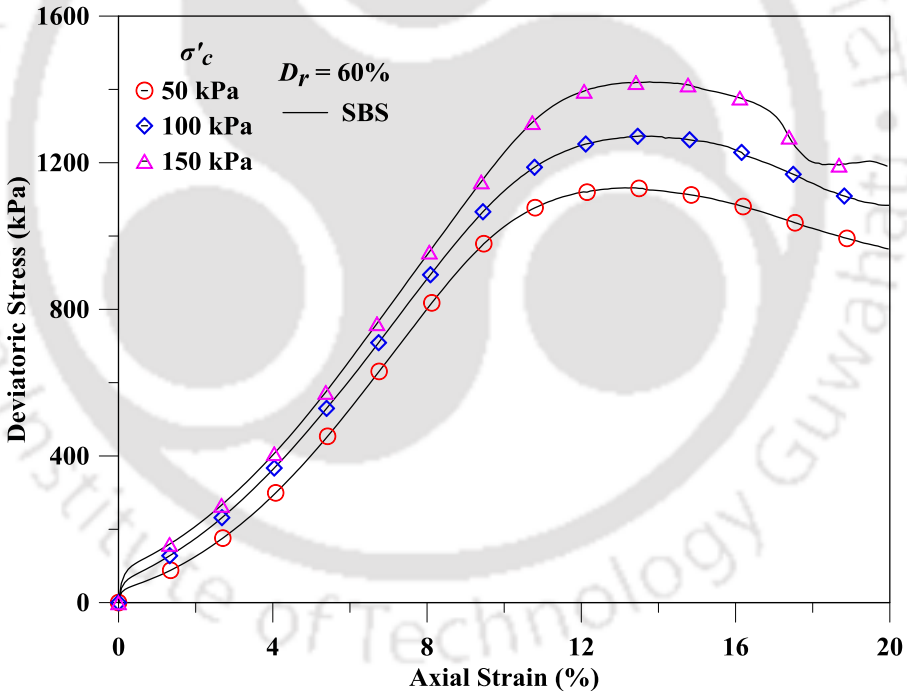

Fig. 4.5 Stress-strain variation for SBS subjected to different σ'_c

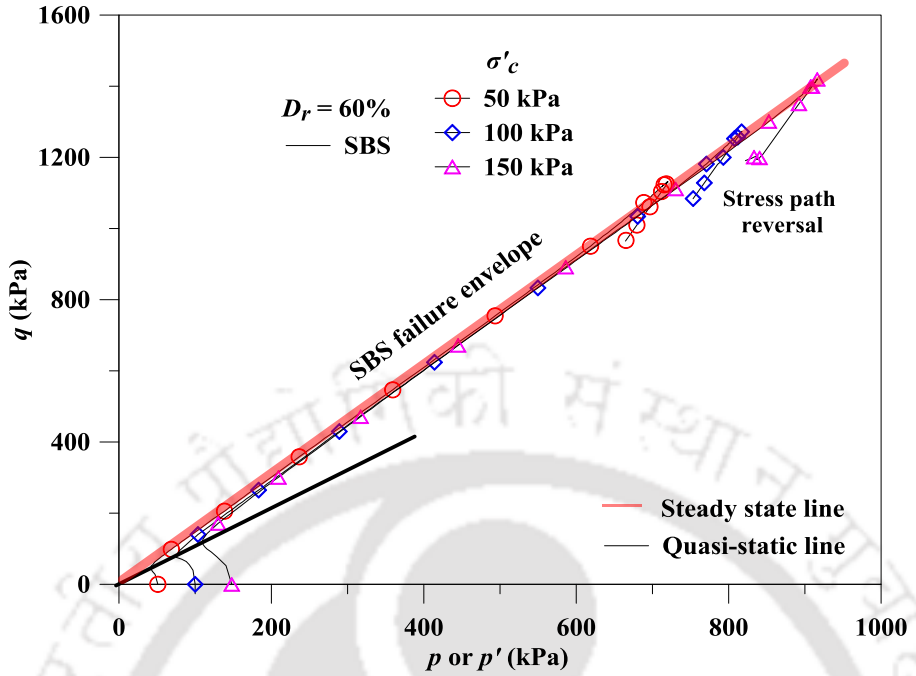

Fig. 4.6 Stress path plot for SBS subjected to different σ'_c

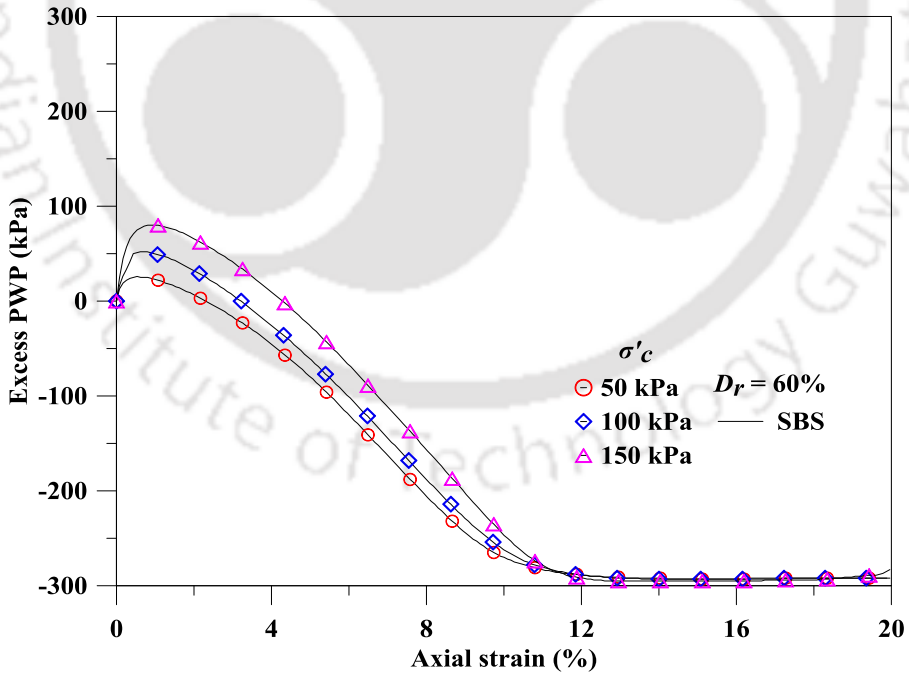

Fig. 4.7 Variation of excess PWP for SBS subjected to different σ'_c

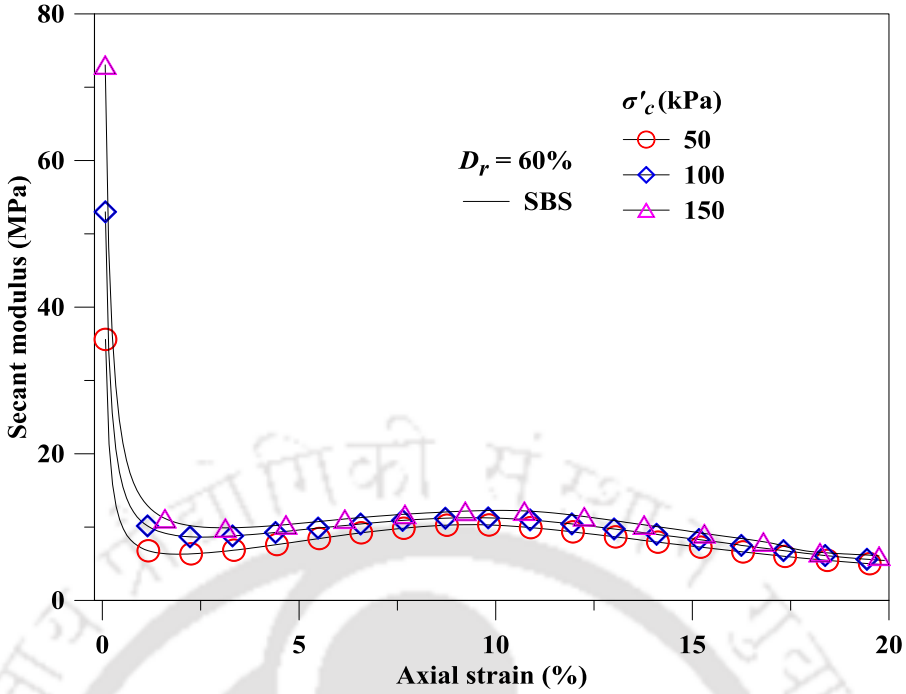

Fig. 4.8 Variation of secant modulus for SBS subjected to different σ'_c

4.4.1 Effect of confining pressure

To observe the effect of confining pressure, the tests have been conducted at three different effective confining pressures (σ'_c = 50 kPa, 100 kPa and 150 kPa) on the specimen prepared at D_r = 30% and subjected to a loading rate of 1.2 mm/min. The results are plotted in Fig. 4.9-Fig. 4.12. Fig. 4.9 shows that the strength i.e. resistance to deformation of the soil, increases with the increase of confining pressure. The maximum deviatoric stress ($\sigma_{d,max}$) attained by the SBS specimens for all three σ'_c was found at an axial strain of 20%. The $\sigma_{d,max}$ obtained at 50 kPa is approximately 26% lesser than that obtained at 100 kPa, whereas the same obtained at 150 kPa is nearly 7% higher than that of 100 kPa (Fig. 4.9). Fig. 4.10 illustrates that with the increase of confining depth (represented by confining pressure), the excess PWP increases. The increase in excess PWP up to strain levels ~ 1% in saturated sand under undrained monotonic loading revealed the possibility of static liquefaction (Castro, 1975; Kramer and Seed, 1988; Dash and Sitharam, 2011). Fig. 4.10 also describes that the soil do not behave like loose soil even at 30% relative density. Similar response has been observed by Ishihara (1993) for sand specimen

prepared at D_r = 16%, 38% and 64% tested at σ'_c = 60 kPa, 1000 kPa and 3000 kPa respectively. Thus, based on the observation by Ishihara (1993) and from the results obtained for soil specimens at D_r = 30% from the current investigation, it can be stated that even a loose sand (as per in its initial stress state) may behave like a dense sand depending upon the high confining stress. Further straining is responsible for the strength gain, due to decrease in excess PWP and corresponding increase in effective stress, thus hinting about soil-dilation behaviour with gradual redistribution of pore water pressure within the soil specimen. Since a residual amount of air still persists in the specimen at the end of saturation (Skempton, 1954), the shearing under undrained conditions shows decrease in excess PWP resulting an increase in degree of desaturation and matric suction (Fredlund and Rahardjo, 1993).

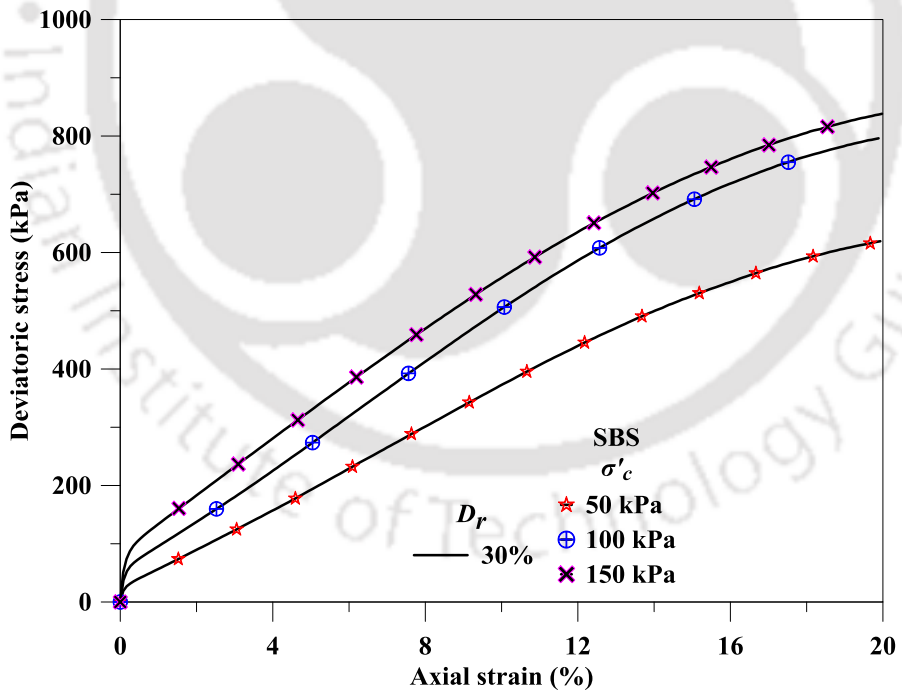

Fig. 4.9 Stress-strain response for SBS at D_r = 30%

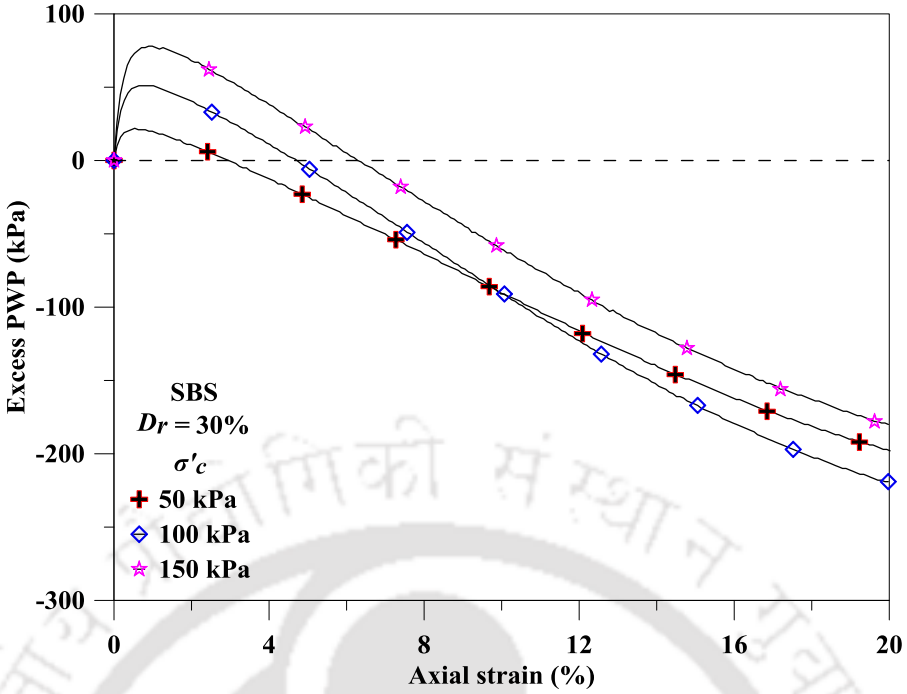

Fig. 4.10 Change in excess PWP for SBS at D_r = 30%

Fig. 4.11 reflects higher contractive behaviour of sand at high confining pressure. Further continuation of loading results pore pressure changes to negative and then the Skempton's pore pressure coefficient (A-parameter) becomes also negative. For any given soil, the A-parameter varies with the stresses and strains and its value may be quoted at failure (maximum deviator stress), at maximum effective principal stress ratio, or at any other required point (Skempton, 1954). From Fig. 4.12, it can be observed that the A-parameter depends on the confining stress, and initially up to ~1% of axial strain, it varies from +0.5 to +0.7 which shows the normally consolidated behaviour of soil; whereas, its variation to -0.35 reflects change in soil behaviour from over-consolidated to heavily over-consolidated state.

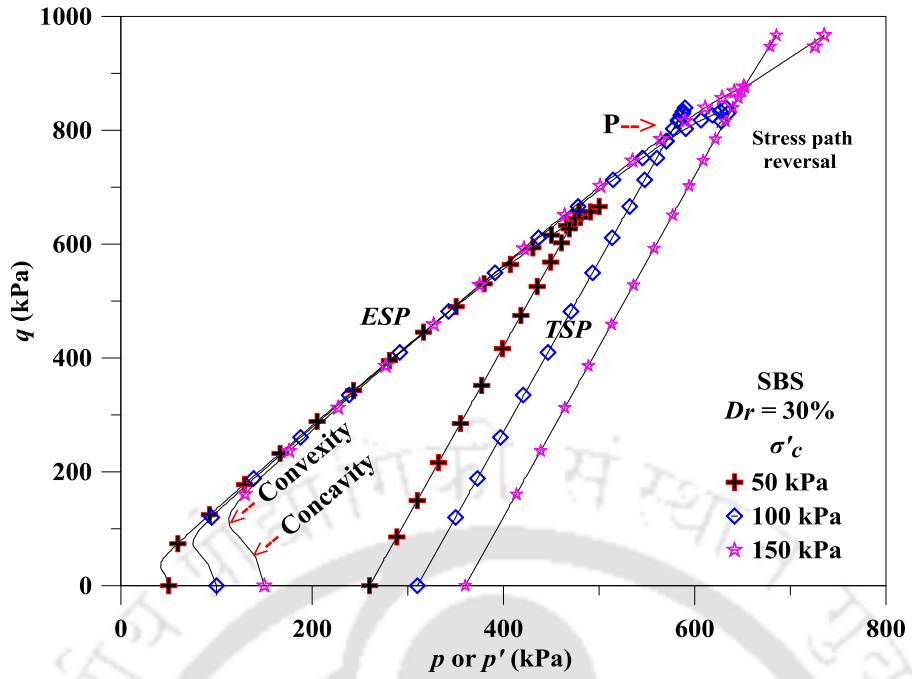

Fig. 4.11 Total and effective stress path for SBS at D_r = 30%

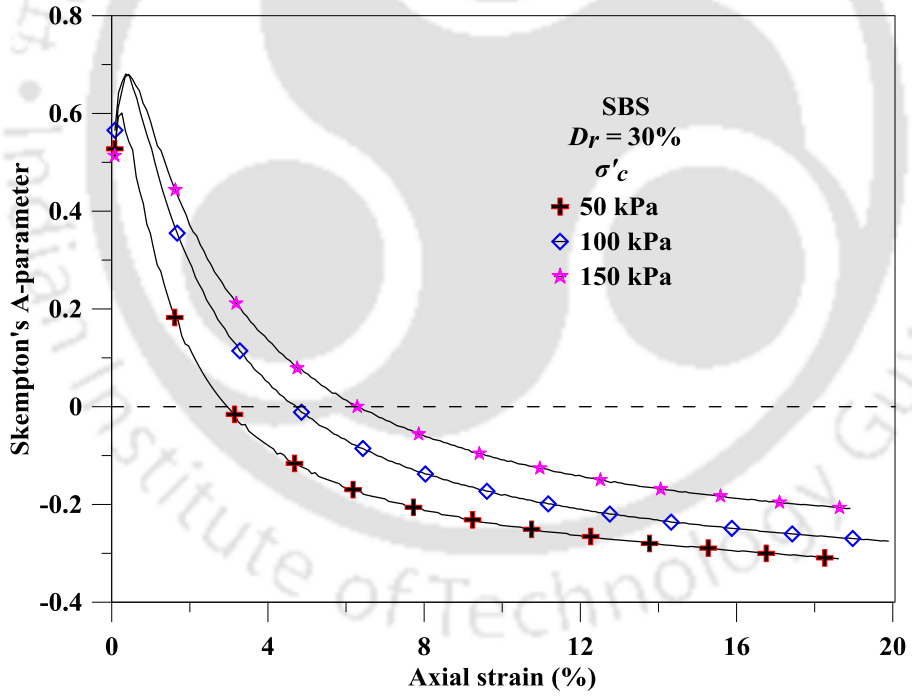

Fig. 4.12 Variation of Skempton's A-parameter for SBS at D_r = 30%

4.4.2 Effect of relative density

To emphasize the effect of D_r on stress-strain response of BS specimen, the tests have been conducted at four different D_r (10%, 30%, 60% and 90%) and targeted σ'_c = 100 kPa; the results

are presented from Fig. 4.13-Fig. 4.17. Fig. 4.13 depicts that with the increase of D_r, the maximum stress at failure of the specimens also increases. It was observed that the $\sigma_{d,max}$ and the associated strain levels are significantly affected by the variation of σ'_c and D_r. At any given σ'_c, the increase in $\sigma_{d,max}$ is substantial for the increase in D_r from 10% to 60%, whereas it is marginal for an increase in D_r from 60% to 90%. Hence, it can be stated that the effect of variation of σ'_c is more prominent for sands with lesser D_r, in the range of loose-to-medium dense sands.

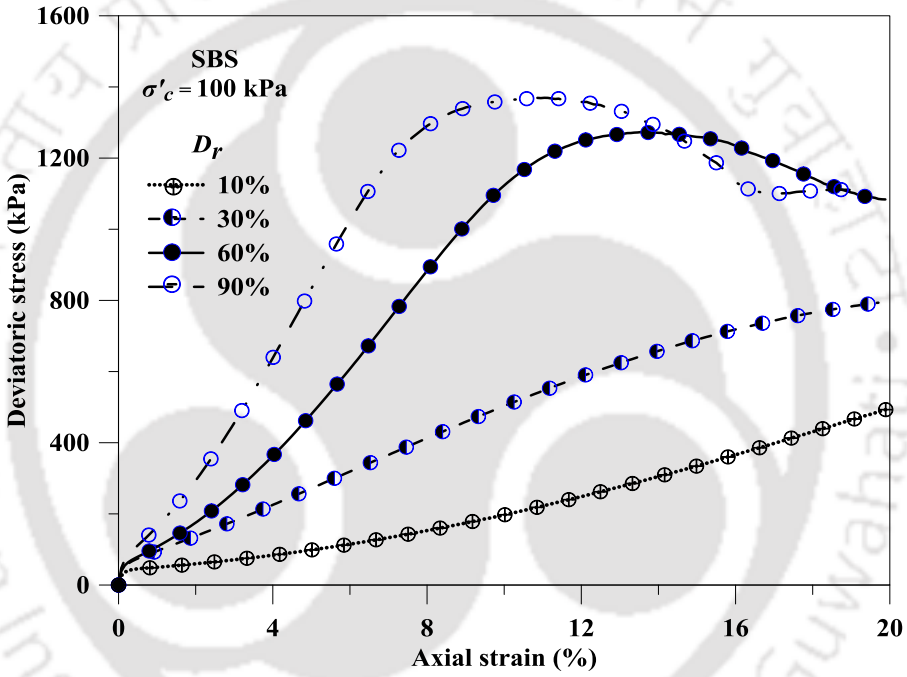

Fig. 4.13 Stress-strain response for SBS at different D_r

Fig. 4.14 presents the effective stress path for SBS at different D_r. Effective stress path (Fig. 4.14) becomes nonlinear at its yield point due to the nonlinear increase in the excess PWP under static loading, resulting in the concavity in effective stress path (Budhu, 2008). Fig. 4.15 illustrates the variations in excess PWP with axial strain for sands of various relative densities. It can be observed that the rate of increase in excess PWP, up to an axial strain of 0.5%, is almost same for all D_r. However, further increase in loading reflects, slower rate of decrease in excess PWP at D_r = 10%. It also shows that the rate of decrease in excess PWP increases with

increase in D_r. Fig. 4.16 also highlights that the D_r affects Skempton's A-parameter significantly. It reflects that the A-parameter varies with the change in state of soil and deviatoric stress (σ_d). Fig. 4.17 reflect that the secant modulus of soil is affected by D_r and σ'_c.

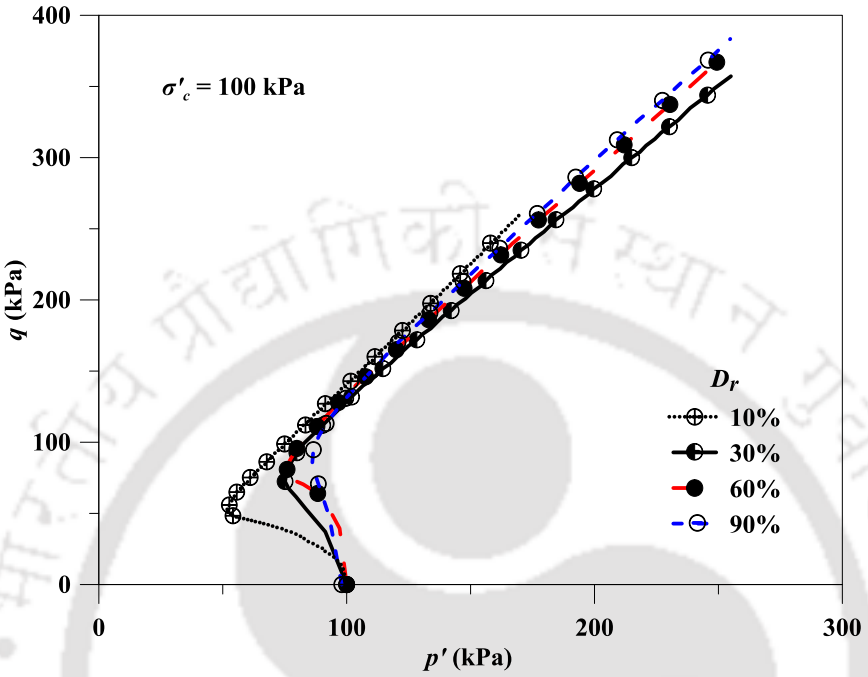

Fig. 4.14 Stress path plot for SBS at different D_r

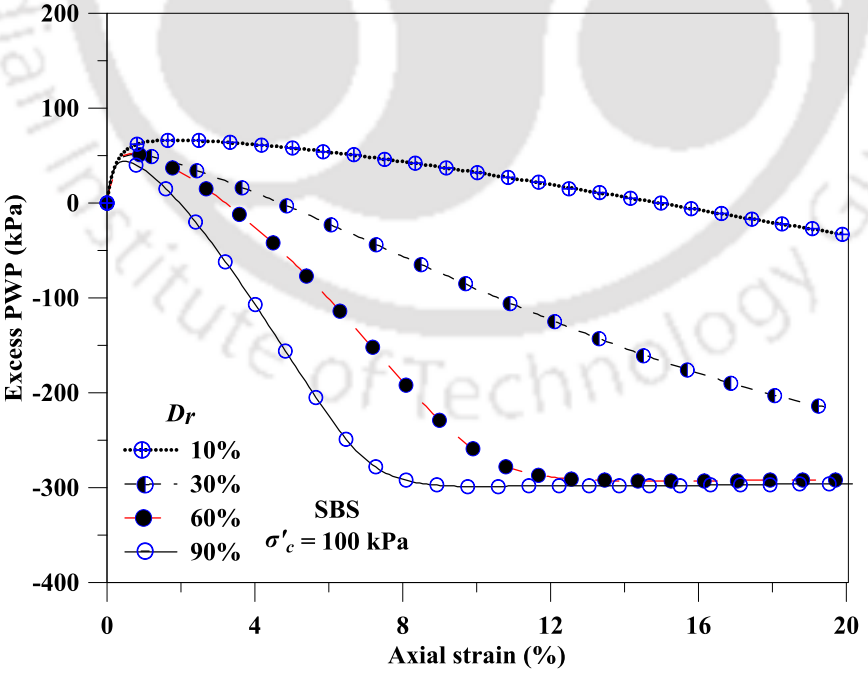

Fig. 4.15 Variation in excess PWP for SBS at different D_r

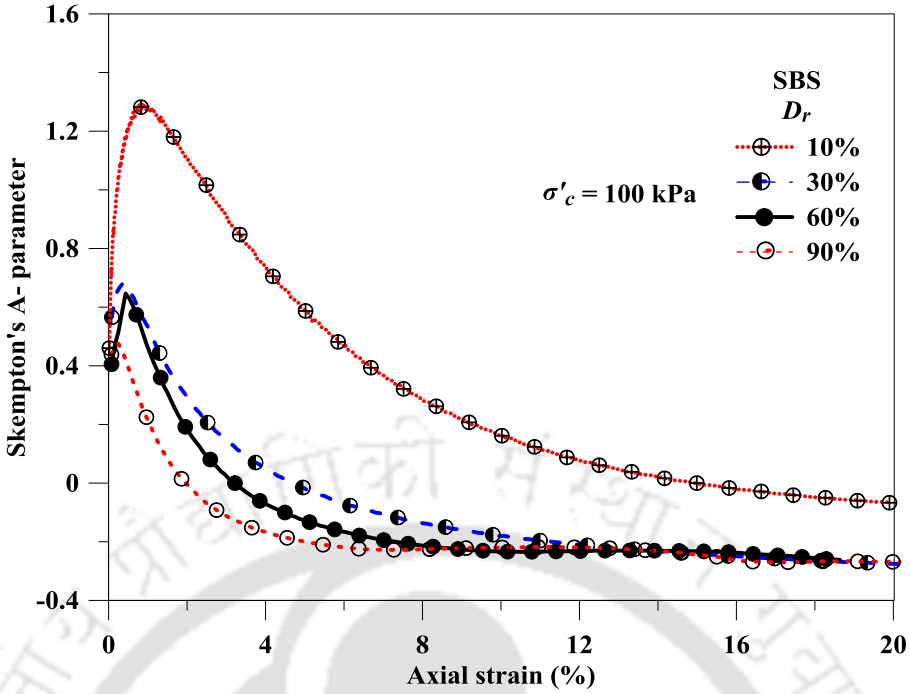

Fig. 4.16 Variation in Skempton's A-parameter for SBS at different D_r

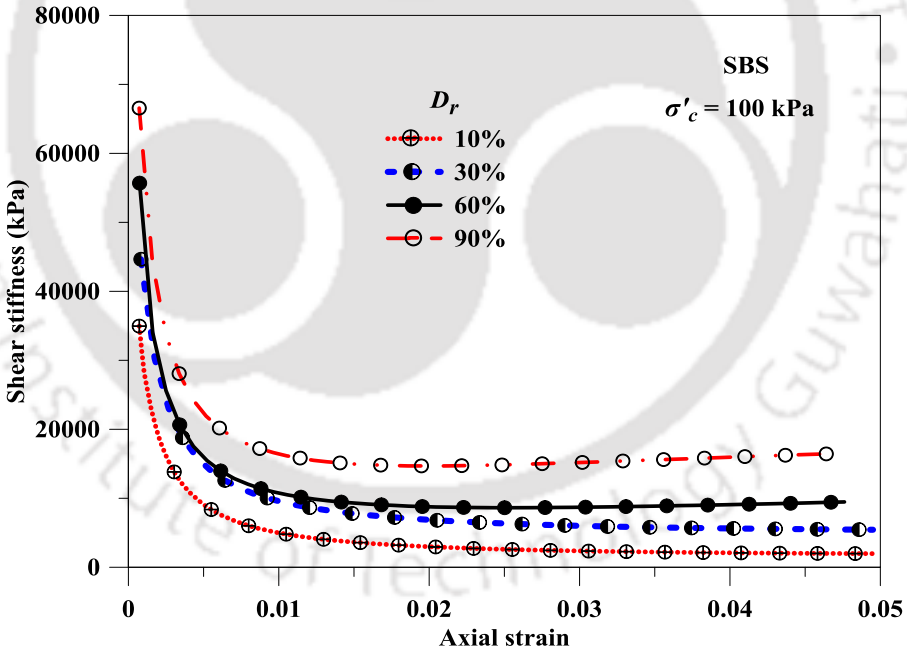

Fig. 4.17 Shear stiffness for SBS at different D_r

4.4.3 Effect of loading rate

Monotonic compression shear tests were performed at different loading rates ranging from 0.005 mm/min to 5.0 mm/min, on BS specimens reconstituted at three D_r (30%, 60% and 90%)

and σ'_c = 100 kPa. The results plotted in terms of stress-strain presented in Fig. 4.18, illustrates the effect of loading rate on compressive strength of SBS soil at two D_r (30% and 90%). It can be observed that the strength increases with the increase of loading rate up to 0.6 mm/min and 1.2 mm/min for D_r = 30% and 90 % respectively, beyond that the effect is very minimal. It can also be observed that with the increase of D_r from 30% to 90%, $\sigma_{d,max}$ at failure was increased by nearly 75% and, the axial strain reduced by approximately 50%. This $\sigma_{d,max}$ for D_r = 30% and 90% was considered corresponding to the axial strain of 20% and 10%, respectively. It can be stated that with the increase in D_r (from loose to very dense), the ductility of the soil gets partially compensated, since the higher interlocking of the particles at high D_r generates higher angle of internal friction (ϕ) and strength.

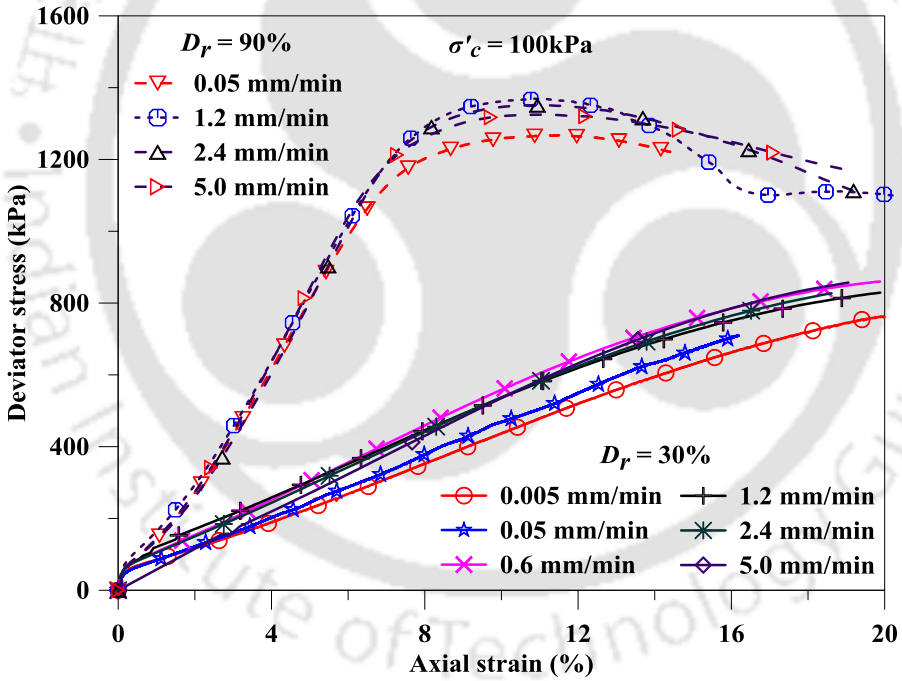

Fig. 4.18 Stress-strain response for SBS at different loading rates and D_r

Fig. 4.19 illustrates that $\sigma_{d,max}$ corresponding to D_r = 30% is increased by approximately 25% with the increase of loading rate up to 0.6 mm/min, beyond that it increased by ~2%; whereas, at D_r = 90%, the $\sigma_{d,max}$ increases approximately 9% with the increase of loading rate up to 1.2 mm/min, beyond that it decreased by ~ 4% for the stated range of loading rate.

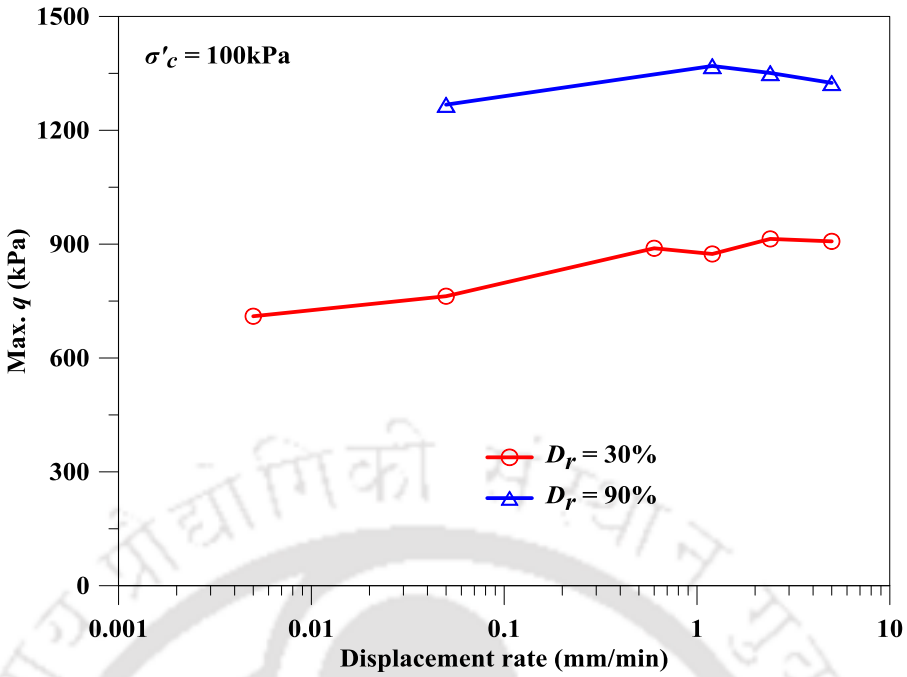

Fig. 4.19 Variations in maximum deviator stress for SBS at different loading rates

Secant modulus at two different D_r = 30% and 90% for different loading rates were presented in Fig. 4.20 and Fig. 4.21, respectively. From Fig. 4.20, it can be observed that the secant modulus of saturated sand decreases with the increase of loading rates up to approximately 1% strain levels, and becomes asymptotically constant thereafter. Based on Fig. 4.21, it can be stated that the secant modulus is also affected by D_r. Fig. 4.22 reflects the rise and redistribution of excess PWP during undrained monotonic compression tests at D_r = 30% and 90 %. It has been observed that at D_r = 30%, the rise of PWP at 0.005 mm/min is higher than that of 5.0 mm/min, and the redistribution of excess PWP is slower at 0.005 mm/min. The rise and redistribution of excess PWP at D_r = 90% was not found to be affected by loading rate. It can be observed from effective stress path plot (Fig. 4.23), that the soil shows more initial compression at slower displacement rate.

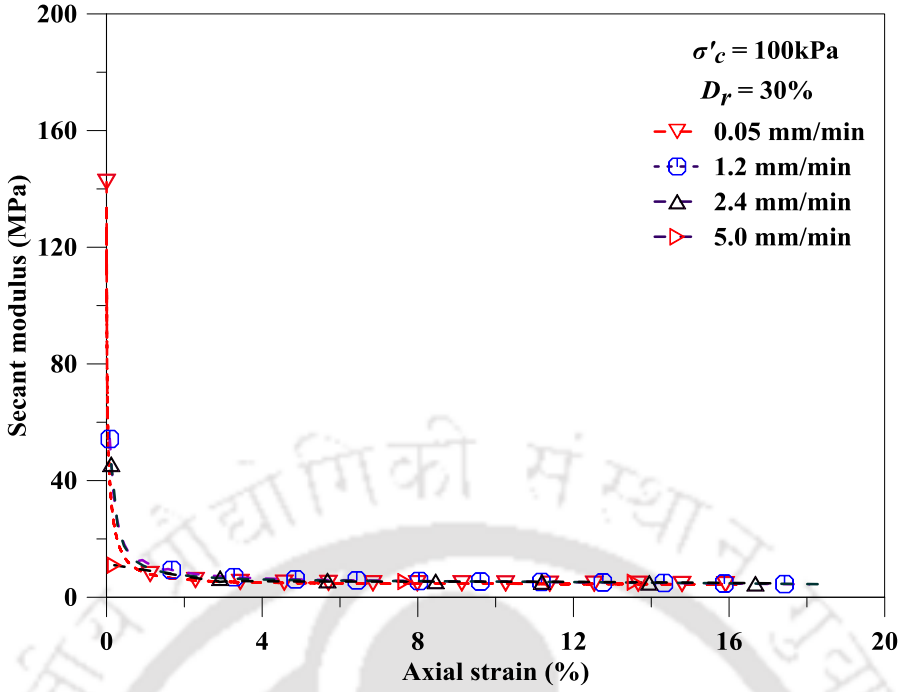

Fig. 4.20 Variation of secant modulus for SBS at D_r = 30% at different loading rates

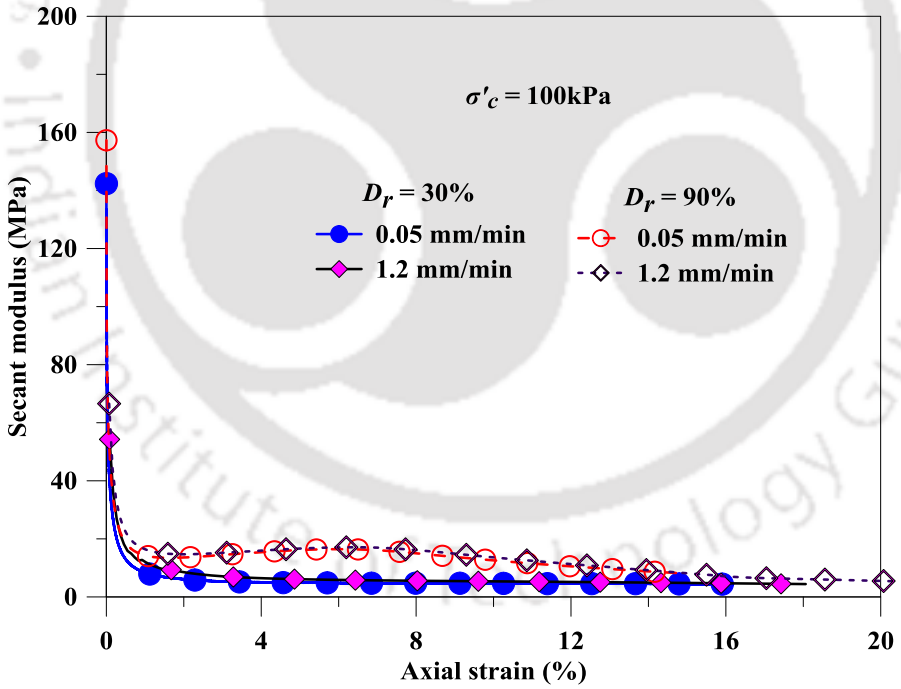

Fig. 4.21 Comparative variation of secant modulus of SBS at D_r = 30% and 90% for different loading rates

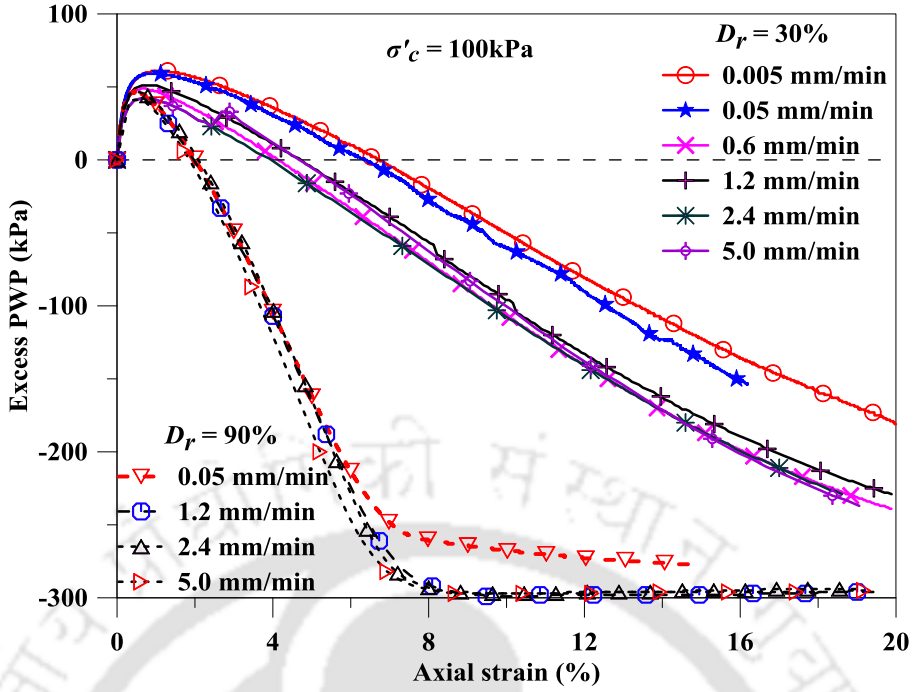

Fig. 4.22 Variation in excess PWP in SBS at different loading rates and D_r

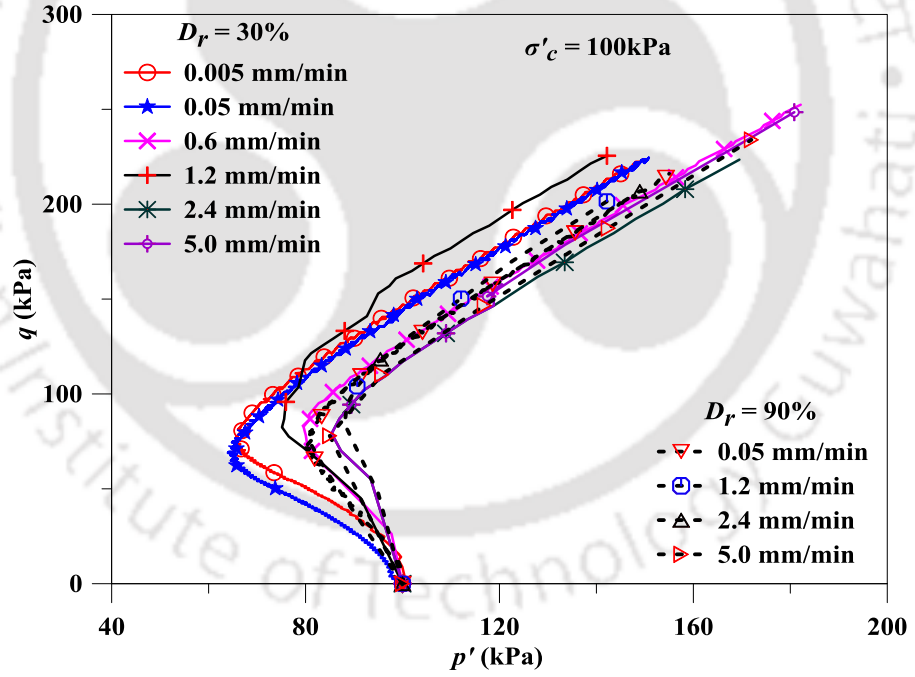

Fig. 4.23 Variation in stress path of SBS at different loading rates and D_r

4.4.4 Local strain measurements

Consolidated-Undrained (CU) monotonic triaxial tests were performed on the BS specimens to evaluate the elemental response of soil specimen using on-sample LVDTs. Fig. 4.24 provides

a comprehensive response of the BS soil based on the on-sample LVDT measurements. Fig. 4.24 (a-d) presents the variation of local (based on the on-sample LVDTs) and global axial strains (based on the external LVDT), while, Fig. 4.24(e-f) shows the variation of deviatoric stresses with both local and global axial strains. The importance of the on-sample LVDT measurements in the estimation of strain-dependent soil stiffness and Poisson's ratio is illustrated in Fig. 4.24g and Fig. 4.24h, respectively. The local axial strains were computed as an average of the longitudinal deformations obtained from the transducers LVDT1 and LVDT2. Fig. 4.24(a-b) show the response of the individual axial LVDTs throughout the time of shearing of the specimen. It can be observed that the responses of the axial transducers are not identical. Similar, non-identical responses from the two axial LVDTs, placed at the diametrically opposite ends of the sample, have been reported by Symes and Burland (1984). Such responses are attributed to bedding and tilting errors in the specimen during installation and shearing.

Fig. 4.24a depicts that higher incongruence develops during the shearing of specimens with low relative density (D_r = 30%), which may be due to system compliance, initial unprecedented seating or bedding errors, and progressive tilting of the specimen during shearing. Since, the soil specimen is in a relatively loose state, the initial bedding error might result in the initiation and subsequent continuous tilting of the specimen during the shearing process. For the specimen with higher relative density (D_r = 90%), it is observed that the response of the LVDTs are nearly similar, although not identical (Fig. 4.24b). In the initial part of shearing, owing to the possible initial bedding error, LVDT1 shows a lesser deformation than LVDT2. As the applied deviatoric stress increases, the bedding error gets compensated, and thus, the responses from LVDT1 and LVDT2 become identical at a particular time during the shearing. Beyond this time, the sample starts to show progressive tilting, and thus, nearly parallel displacement responses from the two LVDTs are obtained. Similar observations from on-sample LVDTs were represented by Symes and Burland (1984). Hence, it can be stated that

stiffer is the sample, the responses of the two LVDTs would be relatively similar. This can be observed as reported by Cuccovillo and Coop (1997), wherein shearing of a stiffer material yielded nearly identical response from the two LVDTs. Based on the responses obtained from the two LVDTs, for further calculations, an average axial displacement response is obtained as shown in Fig. 4.24(a-b). Brown and Snaith (1974) have also reported that the average response from the two on-sample LVDTs is effective in eliminating any error induced due to the tilting of the specimen.

Fig. 4.24c and Fig. 4.24d show the variations of both global and local axial strains with time, for specimens prepared at D_r = 30% and 90%, respectively. The global axial strains were estimated based on the external LVDT measurements, and is expressed as the ratio of change in length of the specimen to its initial length (i.e. 70 mm). On the other hand, the local axial strains were estimated based on the measurements from the on-sample transducers, and is expressed as the ratio of the change in the relative displacement of mounting blocks to the gauge length (i.e. 50 mm). Fig. 4.24(c, d) illustrates that the local axial strains are significantly lower than the applied global strain, in the order of 50% or more. This is attributed to the fact that the external transducer measures an average global displacement of the specimen. In reality, due to the presence of the varying boundary and confinement effects, displacement at different sections of the specimen will not be uniform. Hence, the local measurements will reflect a part of the globally measured deformation, which is illustrated in the stated figures. Moreover, the variation of local strains can be observed to be nonlinear in comparison to the observed perfectly linear global strains. This is due to the fact that the local measurement reflects the elemental response of the soil, while the global measurement portrays the applied displacement rate.

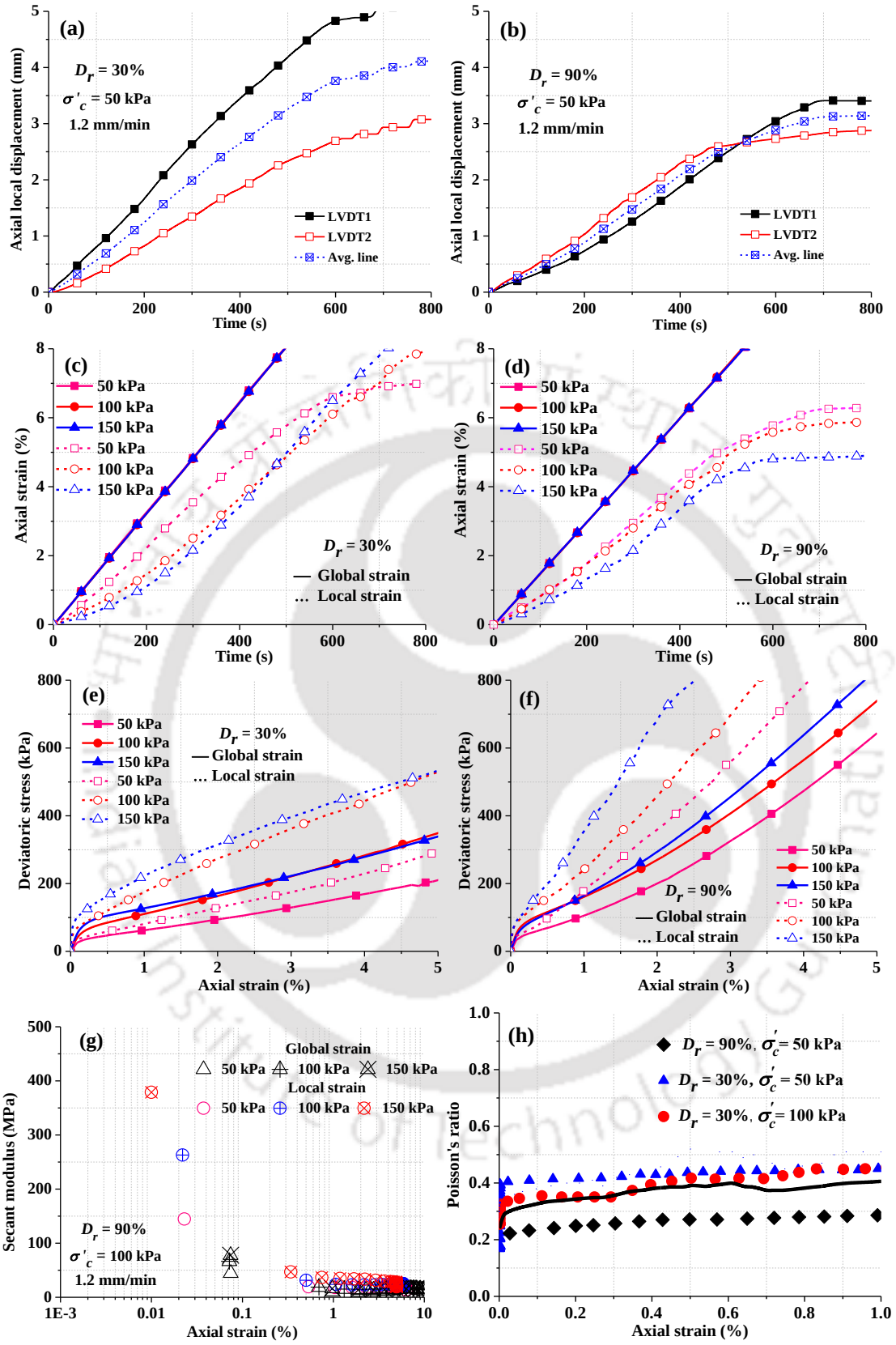

Fig. 4.24 Response of on-sample LVDTs at (*a*) D_r = 30% (*b*) D_r = 90%; Response of global and local LVDTs at (*c*) D_r = 30% (*d*) D_r = 90%; Stress-strain response (*e*) D_r = 30% (*f*) D_r = 90%; (*g*) Secant modulus based on global and local axial strain at D_r = 90% (h) Poisson's ratio at different D_r and σ'_c

Fig. 4.24e and Fig. 4.24f illustrates the variation of estimated deviatoric stresses at D_r = 30% and 90%, respectively, based on the measured global and local strains. The deviatoric stresses were evaluated as the ratio of load, measured from submersible load cell, to the corrected cross-sectional area (calculated as per Fratta et al., 2007), estimated from the corresponding global and local axial strains. Since, the measured global axial strain is comparatively higher than the local axial strains, as shown in Fig. 4.24(c, d), the estimated deviatoric stress based on the global strains would be lesser than that obtained using the local strain measurements; the same being illustrated in Fig. 4.24(e, f). Similar response have been illustrated for soils subjected to triaxial shearing as reported by Burland and Symes (1982), Symes and Burland (1984), Jardine et al. (1985) and Goto et al. (1991). Based on the variations of deviatoric stress and axial strain, the secant stiffness of soil was evaluated for the specimens sheared at a displacement rate of 1.2 mm/min, as shown in Fig. 4.24g. It was observed that for strains less than 0.1%, the secant stiffness estimated based on local strains sufficiently exceeds the same measured using global strains, in the order of 70% or higher. Similar observation has been reported in the literature (Cuccovillo and Coop, 1997; Yimsiri et al., 2005).

Fig. 4.24g also illustrates that the secant modulus is significantly affected by displacement rate. It was observed that the specimens, sheared with low displacement rates, show significantly higher stiffness when estimated using on-sample LVDT measurements, as compared to that obtained using external LVDT records. It is important to note that secant stiffness evaluated on the basis of global strains are nearly independent of the displacement rates, while the effect of the latter is largely predominant on the secant stiffness estimated from local strains. This observation signifies that the effect of displacement rate is prevalent on the elemental response of soil, rather than its overall average response. Based on the measured axial and radial deformations, Fig. 4.24h illustrates the typical variation of Poisson's ratio (ν) with varying axial strain levels. It is observed that Poisson's ratio (ν) lies within the range of 0.2-

0.45, with an average value of 0.35. Conventionally, based on the theory of elasticity, v = 0.5 is considered for the evaluation of stress-strain characteristics at undrained saturated conditions of the soils (Rollins et al., 1998). Literatures have reported that v can be even greater than 0.5 for soils exhibiting dilation during shearing (Bragg and Andersland, 1982) or has the presence of fine content (Suwal and Kuwano, 2012). For the present study, the strain-dependent Poisson's ratio obtained from the monotonic tests has been further used for the evaluation of cyclic shear properties.

Effect of stiffness of rubber band on stress-strain response

To attain proper attachment of the on-sample transducers to the soil specimen, a thin rubber band was used with the mounting block of LVDT as shown in Fig. 3.21. Although it has been reported in literature that the application of rubber membrane attachment on soil specimens, prepared under low relative density and subjected to low confining stresses, may lead to initial tilting (Jastrzebska and Kowalska, 2016), ample care has been taken to prevent such experimental circumstances. Even if the rubber band is made up of the same material as the membrane used to constrain the soil sample; the attachment of the same may provide an additional stiffness on the soil specimen during the test procedure, which, in turn, can affect the stress-strain behaviour. Fig. 4.25 and Fig. 4.26 highlight the overall effect of the rubber band attachment on the response of the soil specimen subjected to various test configurations. Fig. 4.25 shows the difference between the stress-strain responses of the soil specimen (prepared at D_r = 30% when subjected to two typical confining stresses (50 kPa and 100 kPa). When subjected to σ'_c = 50 kPa, the difference in peak deviatoric stress of the specimen (at an axial strain = 20%), obtained in the presence and absence of rubber strip attachments, is approximately 20%, while the same is 11% when subjected to σ'_c = 100 kPa. Fig. 4.26 shows the effect of D_r on the influence of rubber band for the test specimens tested at σ'_c = 100 kPa; the difference in peak deviatoric stress being approximately 9%. Hence, it can be stated that the

rubber band attachment has a negligible effect on the stress-strain and peak secant stiffness characteristics of the specimens prepared at higher relative density and subjected to higher confining stress.

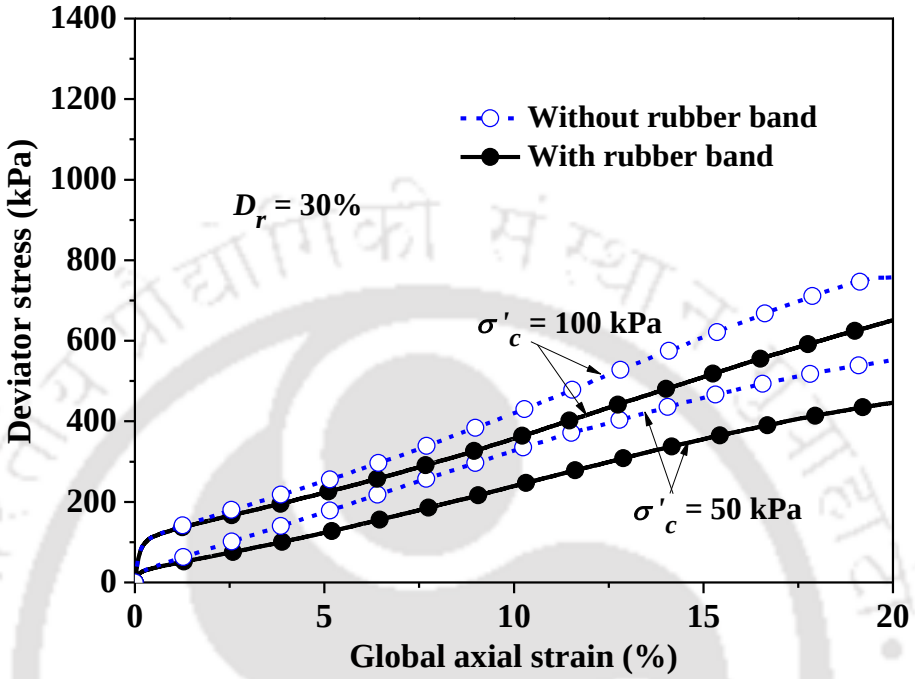

Fig. 4.25 Effect of rubber band attachment on stress-strain response of SBS at different σ'_c

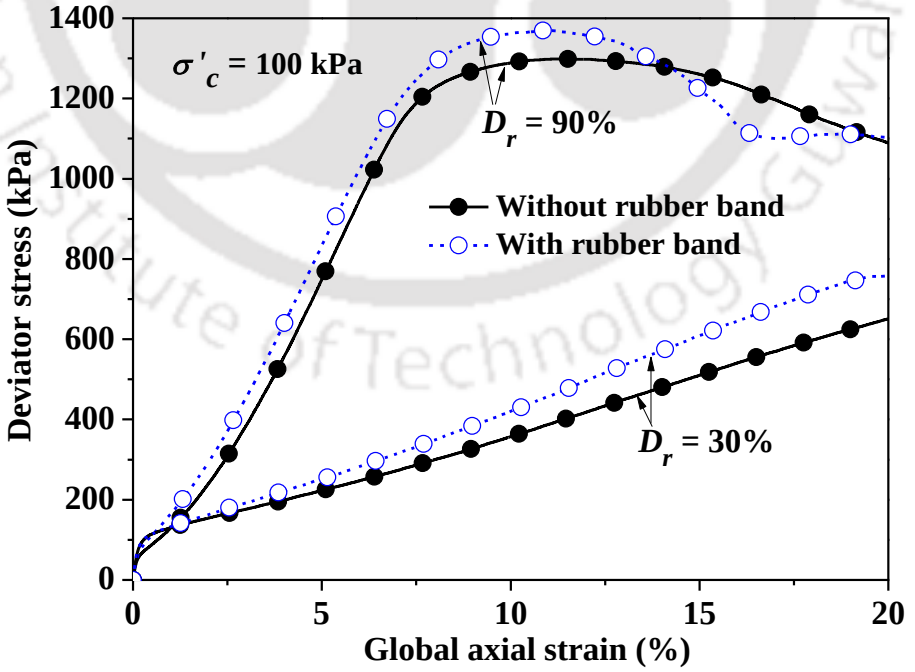

Fig. 4.26 Effect of rubber band attachment on stress-strain response of SBS at different D_r

Effect of loading rate on results based on the on-sample LVDTs data

Fig. 4.27 and Fig. 4.28 present the response of soil at a displacement rate of 0.0005 mm/min, 0.005 mm/min and 1.2 mm/min. Fig. 4.27 illustrate the stress-strain response of soil at these displacement rates, where significantly higher deviation of deviatoric stress was observed at lower displacement rate. It can also be observed from Fig. 4.27 that the deviatoric stress becomes higher from on-sample LVDT because of small local strain.

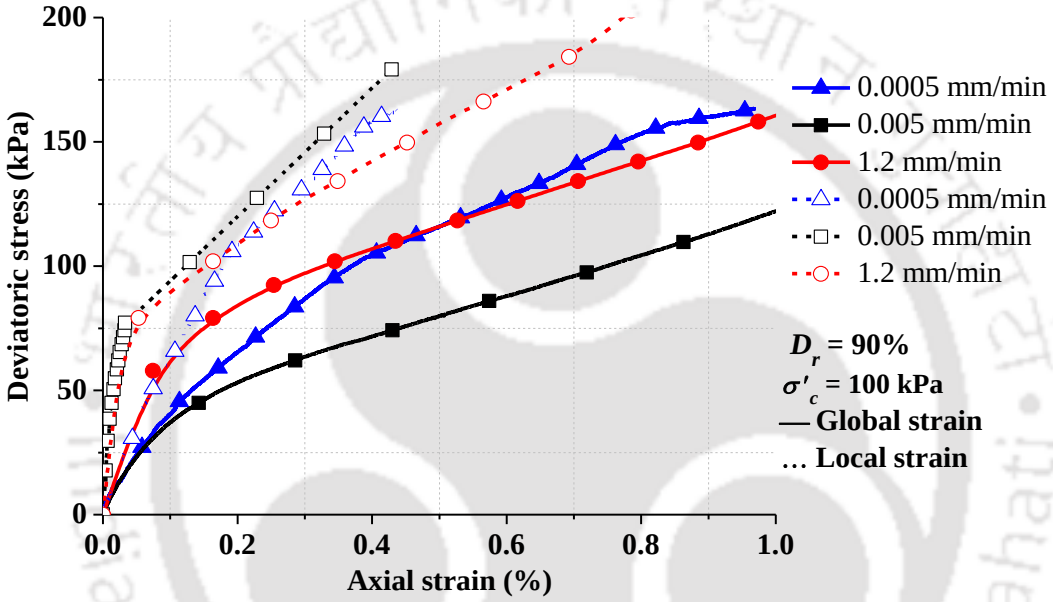

Fig. 4.27 Variation of stress-strain of SBS with global and local strains

Fig. 4.28 depicts the secant modulus variation at three displacement rates which shows loading rate significantly affects the soil stiffness. Specimen sheared with low displacement rate shows higher shear stiffness using on-sample LVDTs, whereas the same showed by external LVDT are significantly lower value. Soil stiffness becomes higher at higher displacement rate (1.2 mm/min) which is reflected by external LVDT, whereas, with on-sample LVDTs the same shows higher values at low displacement rate (0.0005 mm/min). The soil stiffness based on local strains were sufficiently higher, on the order of more than 50% at strain less than 0.1%, as shown in Fig. 4.28. Similar observation was made by Cuccovillo and Coop (1997), where the stiffness based on local strains (measured by on-sample LVDTs) was nearly

80% higher, at strain less than 0.1%, than that estimated using global strains; the triaxial shearing tests have been conducted at a confining pressure of 1.8 MPa on sandy specimens.

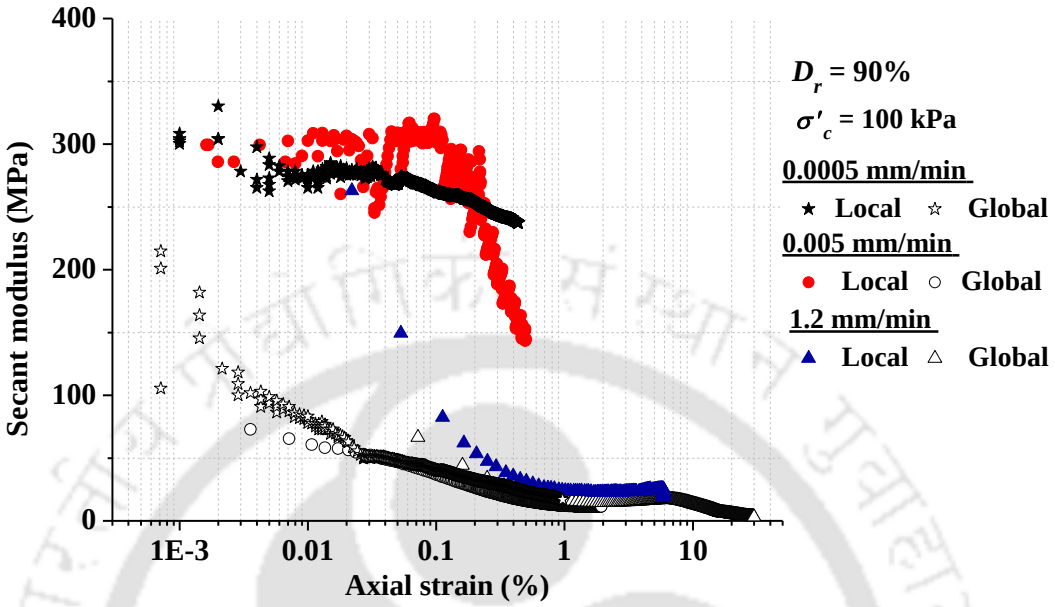

Fig. 4.28 Variation of secant modulus of SBS with global and local strains

4.5 COMPARATIVE BEHAVIOUR OF DRY AND SATURATED COHESIONLESS SOIL

Comparative results of both DBS and SBS are presented in Fig. 4.29-Fig. 4.32. Fig. 4.29 shows that the peak deviatoric stress achieved by SBS is higher than the DBS. This is attributed to the partial load borne by the water present in the pore of SBS, which is more incompressible with respect to the air present in pore of DBS. The angle of friction (ϕ) of SBS at a D_r = 60% in consolidated undrained condition was found to be approximately 32˚, which was relatively lesser (~2˚-3˚) than the DBS. Similar observation has also been reported by Lambe and Whitman (1969) and, Ranjan and Rao (1996). Thus, it can be noticed that the rise of excess PWP in undrained monotonic shear slightly affects the angle of friction and consequently strength due to the lubricating effect arising from pore-water water. The same can also be observed from the effective stress path plot (Fig. 4.30). The apparently small difference in angle of friction between dry and saturated state of soil cannot be neglected for problems related to

the failure of geotechnical structures, especially with regard to the slope stability and shear failures.

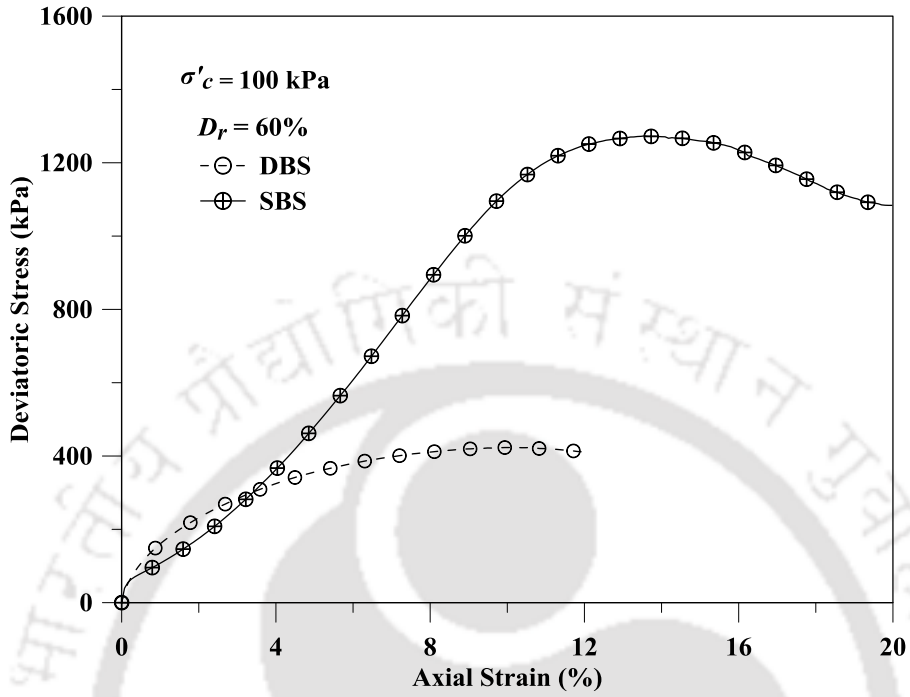

Fig. 4.29 Comparative stress-strain variation of SBS and DBS

Fig. 4.30 reflects that the effective stress is decreased initially, reflecting contractive behaviour of sand due to the increase in excess PWP and reaches the minimum deviator stress. The state of minimum deviator stress, where soil changes its behaviour form contractive to dilative, is called as state of phase transformation (Ishihara, 1993). The contractive behaviour and excess PWP development are more prominent at high confining pressure. Fig. 4.31 presents the variations in excess PWP during loading in SBS and DBS. Since, DBS represents the dry state of specimens, no PWP/excess PWP can be generated. However, SBS representing the saturated state of specimens, the excess PWP increases during loading up to axial strain of 0.6%. Further increase of static loading causes reduction in excess PWP, which hints about the gradual redistribution of excess PWP within the soil specimen. Fig. 4.31 also illustrates that although tests were undrained, a constant PWP is observed beyond the axial strain of 12%. Therefore, it can be stated that the cohesionless saturated sand specimen, even when tested

under undrained condition, can exhibit drained behaviour at very high axial strain. Fig. 4.32 illustrates the effect of saturation on the secant modulus of soil. The secant modulus at low axial strain is higher for saturated sand in comparison to the dry sand.

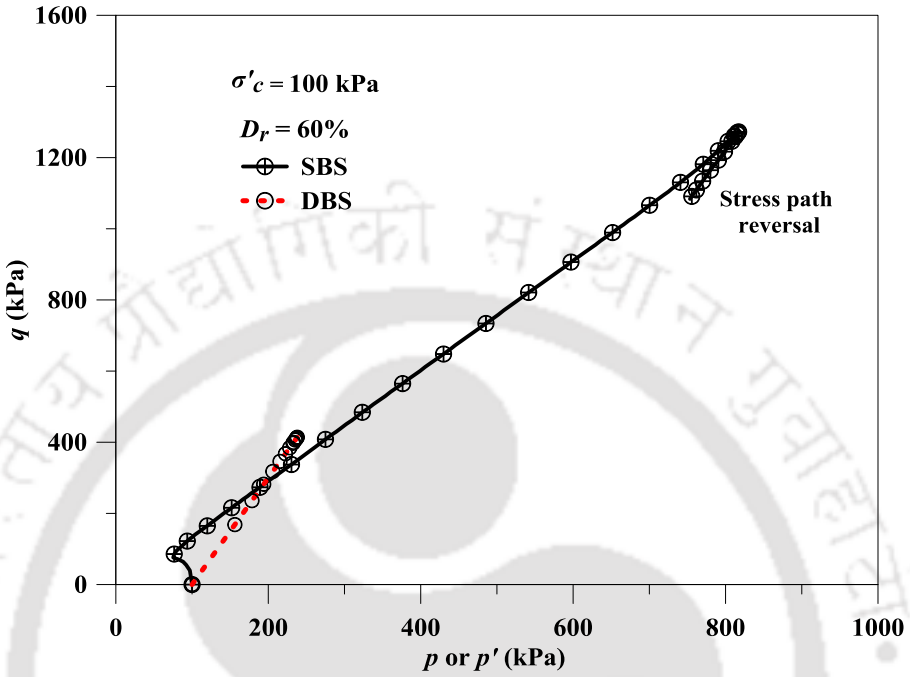

Fig. 4.30 Comparative stress paths plot for SBS and DBS

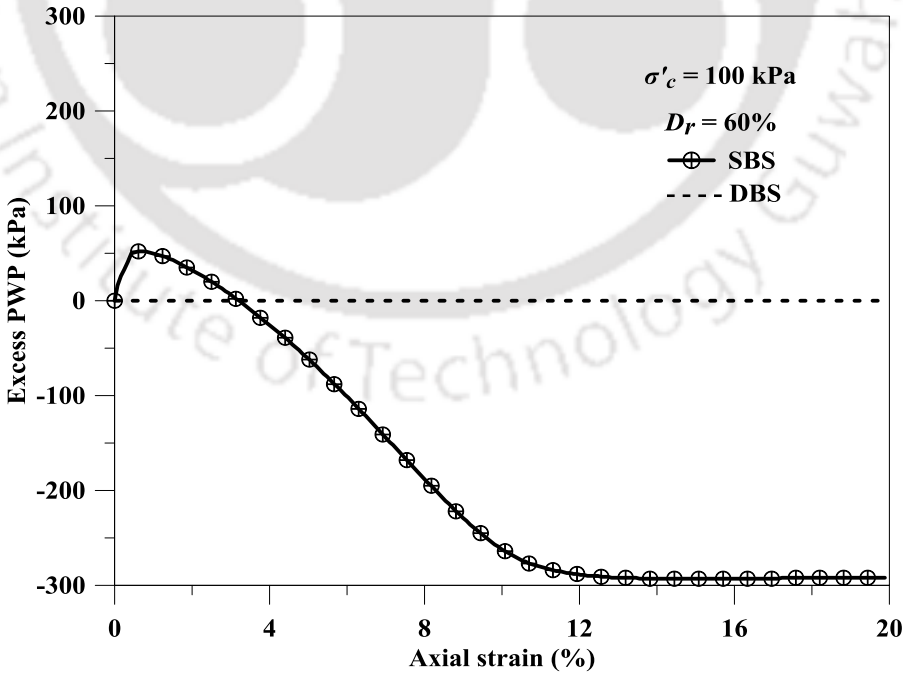

Fig. 4.31 Comparative variation of excess PWP of DBS and SBS

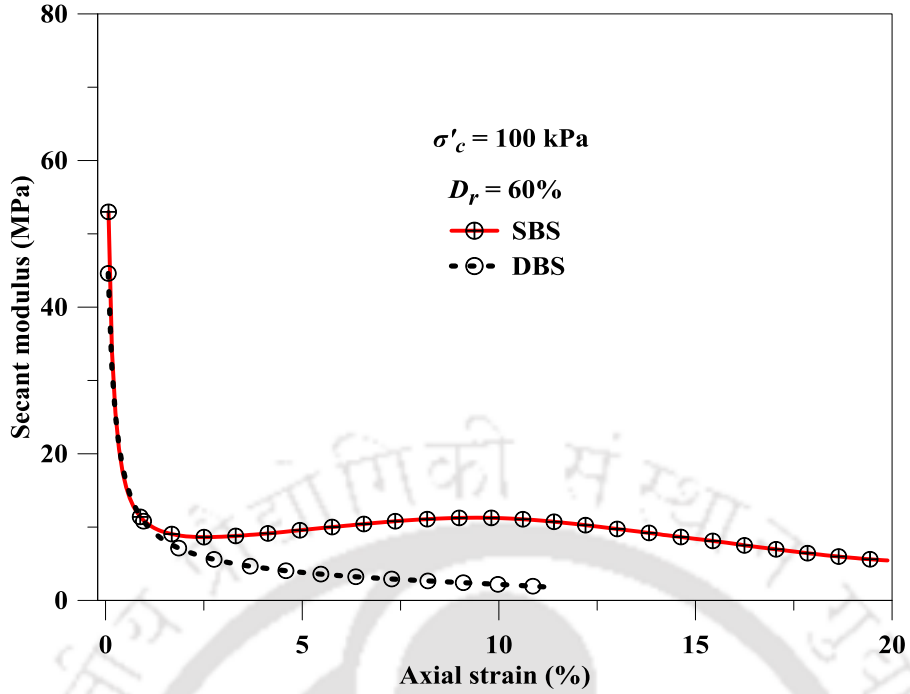

Fig. 4.32 Comparative variation of secant modulus of SBS and DBS

4.6 TESTS ON COHESIVE SOIL

Fig. 4.33 presents the variation in stress-strain responses at different σ'_c (50 kPa, 100 kPa and 150 kPa) for RS specimens. It can be stated that with the increase in σ'_c, σ_d also increases, which is similar to the results of BS specimens. To check the accuracy of results, the test was repeated on the similar specifications of RS specimen at σ'_c = 50 kPa and, a difference of nearly 10-15% in the results were observed. The deviatoric stress (σ_d) reaches a peak at an axial strain of approximately 20%. Based on the repeated tests at different σ'_c, the peak friction angle (ϕ) and cohesion of RS were found to be in the range of 22º-25º and 70-80 kN/m^2, respectively.

Fig. 4.34 presents the variations in excess PWP in RS specimens at different σ'_c. It can be observed that the excess PWP increases with strain, up to axial strain of 2%, beyond which it decreases and becomes negative. This is attributed to the overconsolidated behaviour of soil, since the RS specimens were prepared at MDD-OMC condition. Fig. 4.35 presents the stress path diagram at σ'_c = 50 kPa, 100 kPa and 150 kPa. At σ'_c = 50 kPa, it shows a reduction in the mean effective stress (p') until a value of 45 kPa and then increases which reflects the dilating

nature of soil. Similar behaviour of RS specimens were observed at σ'_c = 100 kPa and 150 kPa with p' = 82 kPa and 130 kPa, respectively.

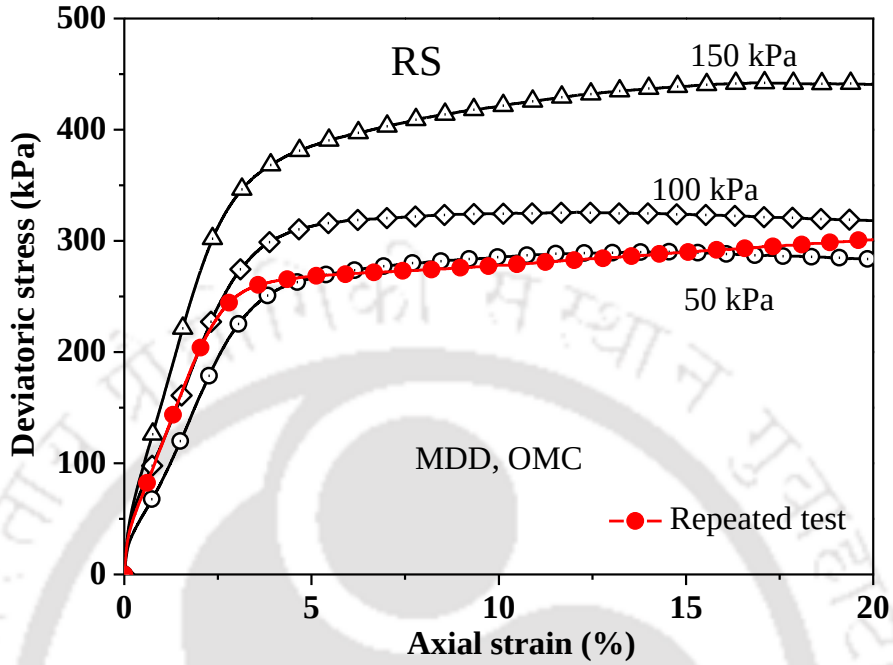

Fig. 4.33 Typical stress-strain response of RS specimen

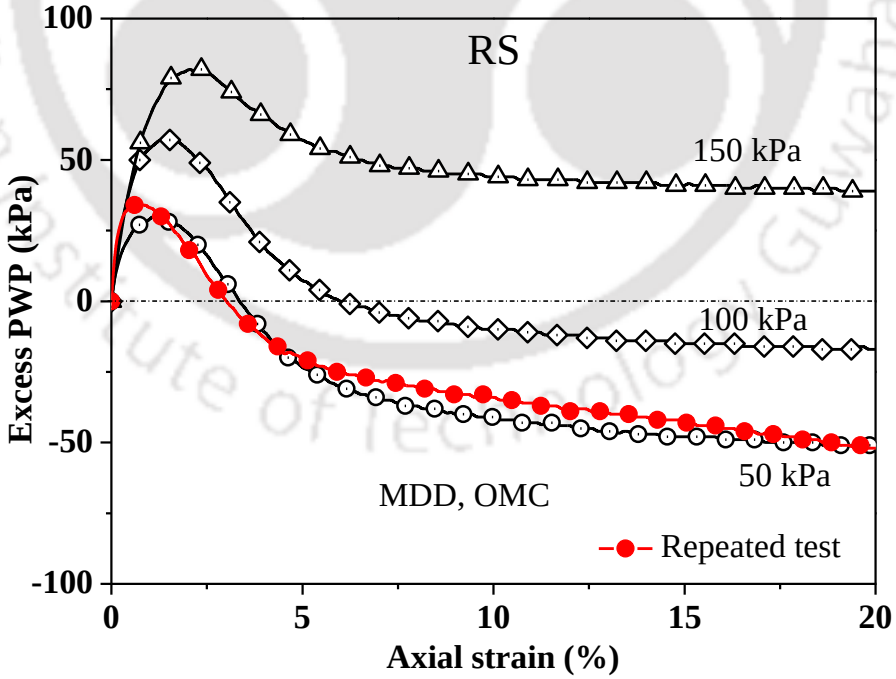

Fig. 4.34 Typical variation in excess PWP of RS specimen

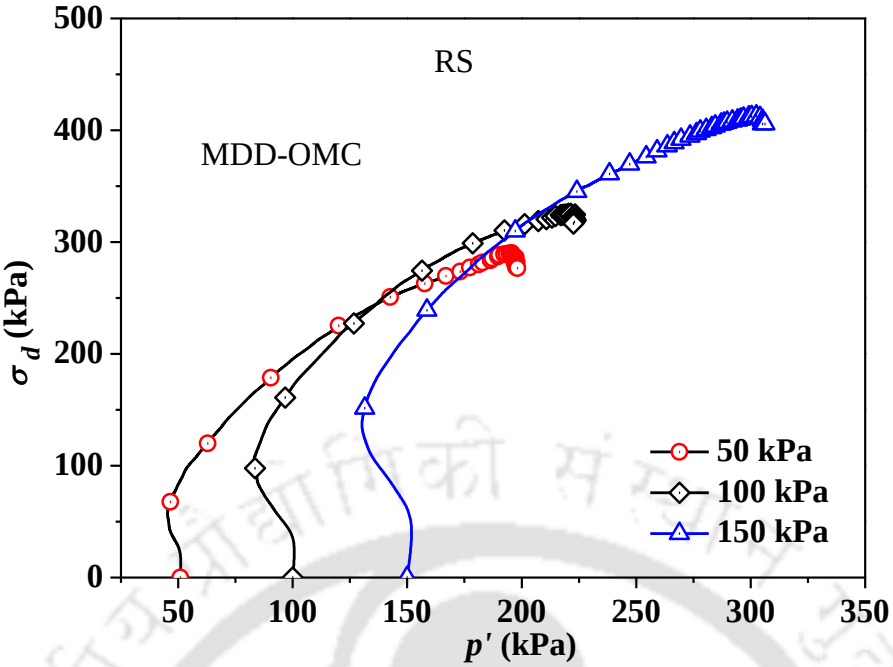

Fig. 4.35 Typical stress path plots for RS specimen

4.7 SUMMARY

Monotonic compression shear tests were carried out on the BS (dry and saturated conditions) as well as RS (saturated) soil specimens, to observe the behaviour of soil under different testing conditions such as confining stress, relative density, displacement rate. It was found that the behaviour of BS soil is significantly affected by saturation, confining stress, relative density, and displacement rate. Tests were also conducted on the saturated BS specimens to evaluate the global and local strains generated in soil specimens using external and on-sample LVDTs, respectively. The findings from the experimental investigation clearly highlight that in spite of applying a constant global strain on the soil specimen, there exists a variation of local strains in the soil specimens, manifested by the strain accumulation with time. Hence, the presumption of strain being constant throughout the sample, as considered conventionally, is improper. Poisson's ratio was also estimated from the displacement measured by radial and axial LVDTs. Tests conducted on RS shows stress dependency behaviour of soil.

Chapter 5 CYCLIC SHEAR TESTS: DYNAMIC PROPERTIES

5.1 INTRODUCTION

Since, dynamic properties (shear modulus and damping ratio) of soil governs the response of soil during dynamic loading, the evaluation of dynamic soil properties is an essential component for analysis of seismic effects and design of earthquake resistant structures. Cyclic triaxial shear test is a widely adopted laboratory experimentation to evaluate the dynamic properties and cyclic strength of the soils at different testing conditions allowing strain-controlled and stress-controlled tests. The dynamic properties of cohesionless soil (Brahmaputra sand, BS) and cohesive soil (Red soil, RS) are presented and discussed in this chapter. Dynamic properties of Dry Brahmaputra Sandy Soil (DBS) have been evaluated using strain-controlled approach based on the measurements of displacement from external LVDT. On the other hand, both strain-controlled and stress-controlled approaches have been used to evaluate the dynamic properties of Saturated Brahmaputra Sandy Soil (SBS) by measuring the displacement from both external LVDT and on-sample LVDTs. To evaluate the dynamic properties of cohesive soil (Red soil), stress-controlled stage loading was applied. During cyclic shear tests for the evaluation of dynamic properties of soils, the pore water pressure was also measured, which has been presented and discussed in Chapter 6. This chapter deals with the results obtained from strain-controlled and stress-controlled cyclic loading in the form of variations of shear modulus and damping ratio of both cohesionless and cohesive soils at different investigating parameters.

5.2 TESTING PROGRAM

Dynamic properties of SBS and DBS at various constant cyclic shear strain amplitudes ranging from 0.015% to 7%, and frequency of 0.1 Hz–4 Hz, have been evaluated at different relative density and effective confining stress, and are presented in Table 5.1. The same for SBS has

also been evaluated using constant stress cyclic loading represented by CSR = 0.1–0.4, at similar tests specifications listed in Table 5.2. The dynamic properties of Red soil (RS) have also been evaluated at different dry density and water content. Stress-controlled incremental loading (i.e. staged loading), depicted in Table 5.2, was applied on the cohesive soil specimens.

Table 5.1 Investigation parameters of the strain-controlled CT tests

Soil	D_r (%)	σ'_c (kPa)	f (Hz)	γ (%)
SBS	30	50	1	0.015, 0.045, 0.075, 0.15, 0.30,0.45,0.60, 0.75, 1.0, 1.5, 3.0
		100		0.045, 0.075, 0.15, 0.30,0.45,0.60, 0.75, 1.5
		150		0.045, 0.075, 0.15, 0.30, 0.45, 0.60, 0.75
	60	50	0.5, 1, 2, 3, 4	0.15, 0.60, 1.0, 1.5, 3.0, 4.5
		100		
		150		
	90	50	1	0.045, 0.075, 0.15, 0.30, 0.45, 0.60, 0.75, 1.5
		100		0.045, 0.075, 0.15, 0.30, 0.45, 0.60, 1.0, 1.5, 2.0
		150		0.045, 0.075, 0.15, 0.30, 0.45, 0.60, 0.75, 1.0, 1.5, 2.0
DBS	60	50	1	0.045, 0.075, 0.15, 0.30, 0.60, 0.75, 1.0, 1.5, 3.0, 4.5, 6.0,7.0
		100		0.045, 0.075, 0.15, 0.30, 0.45, 0.75, 1.5, 3.0, 5.0, 7.0
		200		0.075, 0.10, 0.30, 0.45, 0.60, 0.75, 1.5, 3.0, 4.5, 6.0

Table 5.2 Investigation parameters used in stress-controlled CT tests

Soil	D_r (%)	σ'_c (kPa)	f (Hz)	CSR
SBS	30, 60, 90	50, 100, 200	1	0.05, 0.1, 0.2, 0.3
	60	100	0.1, 0.5, 1, 2, 4	0.1, 0.2, 0.3, 0.4
RS	MDD 1.5 g/cc	100	1	0.1, 0.2, 0.3, 0.4

5.3 TESTS ON SATURATED COHESIONLESS SOIL

5.3.1 Strain-controlled cyclic loading

Strain-controlled CT tests were performed on isotropically consolidated specimens. Each test specimen was subjected to 40 cycles of sinusoidal strain-controlled loading (ASTM D3999). Fig. 5.1(b-d) exhibits the response obtained corresponding to the peak axial strain of 0.20% applied at f = 1 Hz (Fig. 5.1a) on a soil specimen at D_r = 30% and σ'_c = 100 kPa. Fig. 5.1b represents the exponential decay of deviator stress with increasing number of loading cycles (N) which is attributed to the progressive deformation of soil specimen. The increase in excess pore water pressure (PWP) generation is portrayed in Fig. 5.1c, which indicates the gradual increase of excess PWP ratio (r_u) to 1 (i.e. excess PWP = σ'_c).

Fig. 5.1d shows the reduction of mean effective stress, thus causing strength reduction due to increase in pore water pressure. Variation of deviator stress with axial strain (hysteresis loops) is presented in Fig. 5.1e, illustrating the degradation of dissipated energy and soil stiffness with increasing N, which is directly related to the accumulated PWP as well (Fig. 5.1c). The displacements obtained from external LVDT have been used to evaluate the strain properties. During an undrained cyclic loading, the rise of PWP in saturated sand causes the reduction of inter-granular forces resulting in the decrease of effective stress and soil stiffness (Seed and Lee, 1966; Matasovic and Vucetic, 1993). Similar results have been obtained from different cyclic tests conducted at varying levels of peak axial strain (ε), which have been subsequently used to evaluate the dynamic properties of the soils.

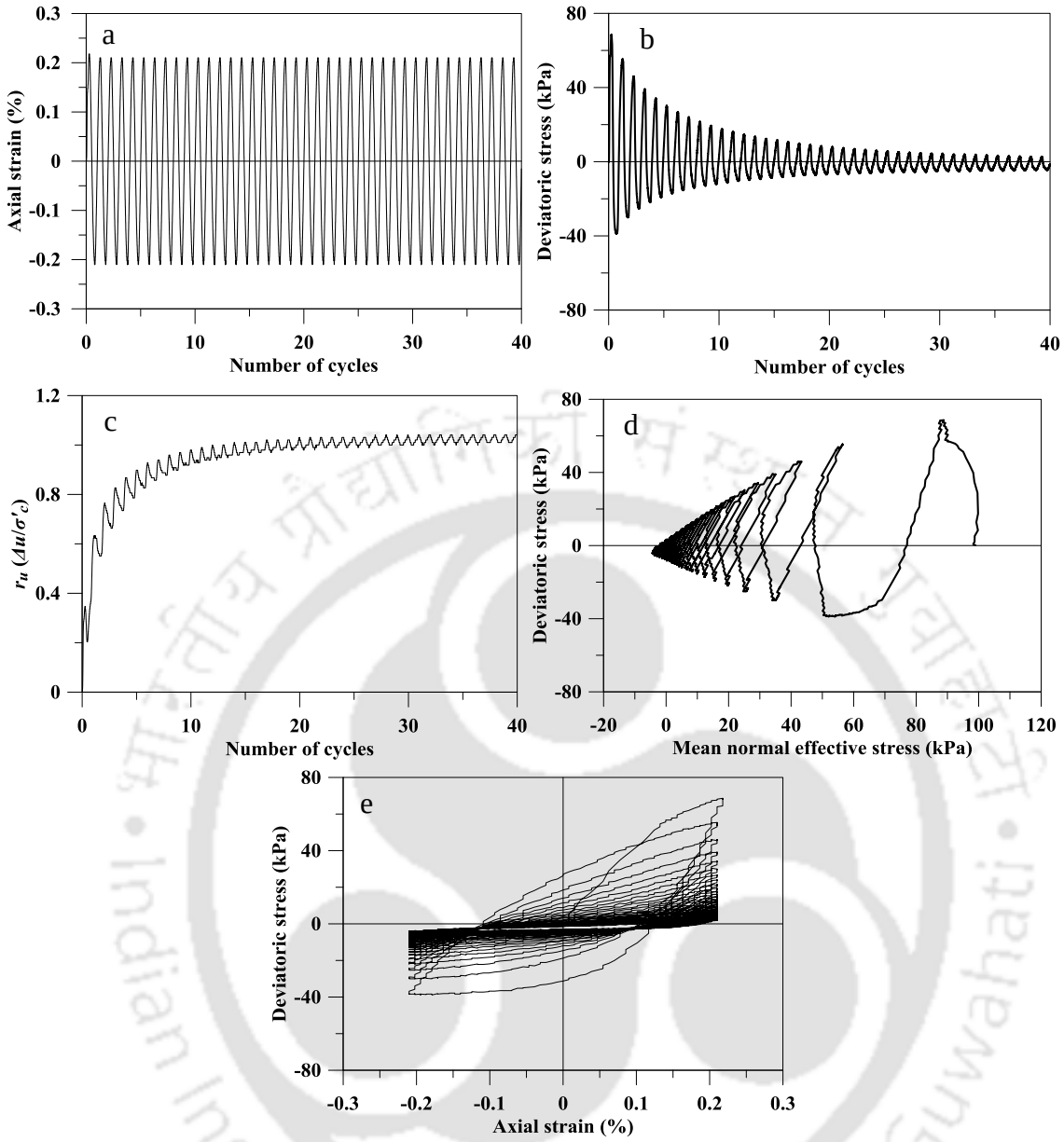

Fig. 5.1 Typical test results at ε = 0.20%, f = 1 Hz, σ'_c = 100 kPa and D_r = 30% (a) Axial strain vs N (b) Deviator stress vs N (c) PWP ratio vs N (d) Stress path plot (e) Hysteresis loops

Evaluation of dynamic properties

Out of all the loading cycles applied during the experimental investigation, dynamic properties of soil can be mathematically evaluated by considering any one particular hysteresis loop obtained from a specific loading cycle. Literature reported the use of different loading cycles to compute the dynamic soil properties, e.g. 10th cycle (Kokusho, 1980), 5th cycle (Seed et al., 1986), 3rd cycle (Okur and Ansal, 2007) and 1st cycle (Govindaraju, 2005; Okur and Ansal,

2007; Lanzo et al., 1997; Vucetic et al., 1998; Darendeli, 2001; Ravishankar et al., 2005; Sitharam et al., 2011; Kirar et al., 2012; Rollins et al., 1998). Matasovic and Vucetic (1993) have used separately the 1st cycle to calculate the shear modulus and 2nd cycle to compute damping ratio. The selection of the hysteresis loop was guided by the assumption that up to the n^{th} cycle, the hysteresis loop remained symmetrical. Fig. 5.2 (a-h) presents the hysteresis loops for initial two cycles, from the strain-controlled CT tests conducted at different peak shear strain levels. It is seen that the hysteresis loops becomes gradually asymmetric with increasing peak shear strain. Beyond γ = 0.15%, even the 1st cycle hysteresis loop is observed to be asymmetric (Fig. 5.2d-h). For the present study, the 1st cycle of loading and the corresponding hysteresis loop has been chosen for the evaluation of dynamic properties. Fig. 5.3 presents a typical Symmetrical Hysteresis Loop (SHL) along with the suggested conventional method to estimate the dynamic properties (ASTM D3999). In this method, the dynamic shear modulus (G) is evaluated from secant modulus (E_{sec}), obtained by the slope of the line joining the points of peak compressive and tensile stress-strain points; the damping ratio is evaluated from the stored strain energy by the triangle in the first quadrant (considering symmetricity for the entire loading cycle). However, in the case of Asymmetrical Hysteresis Loop (ASHL) as shown in Fig. 5.2(d-h), this method will not yield appropriate values as it will lead to the underestimation of damping ratio due to the consideration of higher strain energy for the entire loop. To take into the effect of actual strain energy and moduli values in compression and tension, true representation of asymmetric nature of hysteresis loop should be considered. In that case, dynamic soil properties are to be evaluated as described in Fig. 5.4, which is a regenerated version of the original methodology stated by Kokusho (1980). Therefore, for an ASHL, a modified method has been adopted to evaluate the shear modulus (G_a) and damping ratio ($D^{\#}$). Nevertheless, the conventional method, as stated for a SHL, has also been used to evaluate the shear modulus (G) and damping ratio (D), and is compared against those obtained from ASHL

for the sake of understanding the necessity of adopting the modified methodology.

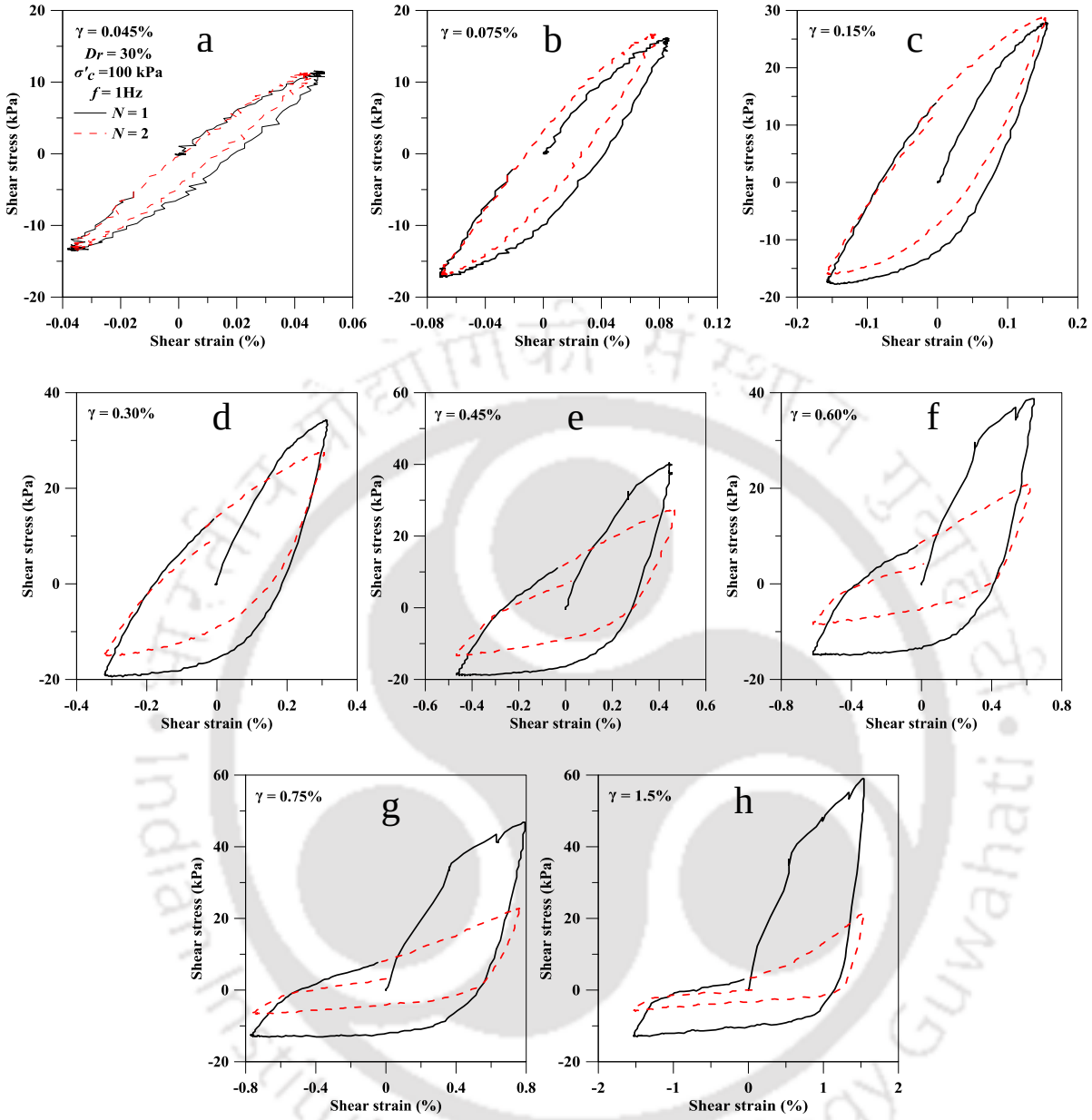

Fig. 5.2 (a-h) Typical shear stress-shear strain plots at different γ for initial two cycles at D_r = 30%, σ'_c = 100 kPa and f = 1 Hz

Evaluation of dynamic shear modulus

Based on the obtained experimental data, G for SHL and G_a for ASHL, are evaluated based on the descriptions provided in Fig. 5.3 and Fig. 5.4, respectively. Shear strain (γ) is evaluated by adopting Poisson's ratio (υ) = 0.5 (Kokusho, 1980; Rollins et al., 1998).

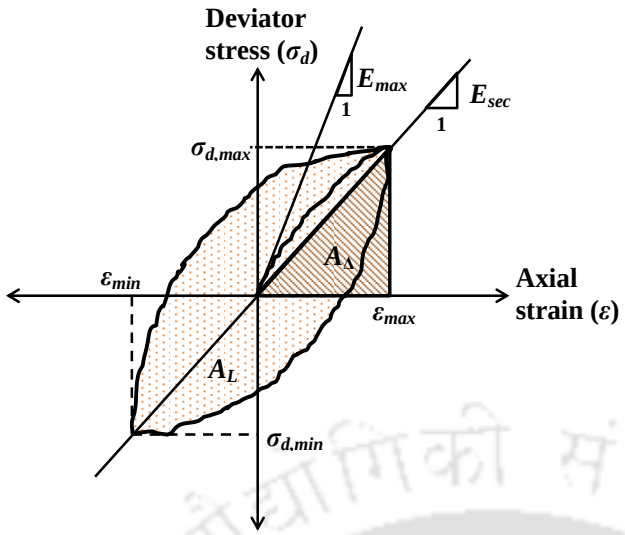

$$E_{sec} = \sigma_d / \varepsilon = \frac{\left(\sigma_{d,\max} - \sigma_{d,\min}\right)}{\left(\varepsilon_{\max} - \varepsilon_{\min}\right)}$$

$$G = E_{sec} / [2(1+\upsilon)]$$

$$\gamma = (1+\upsilon)\varepsilon$$

$$D = \frac{1}{4\pi} \times \frac{A_L}{A_\Delta}$$

Fig. 5.3 A typical symmetrical hysteresis loop (redrawn after Kramer, 1996)

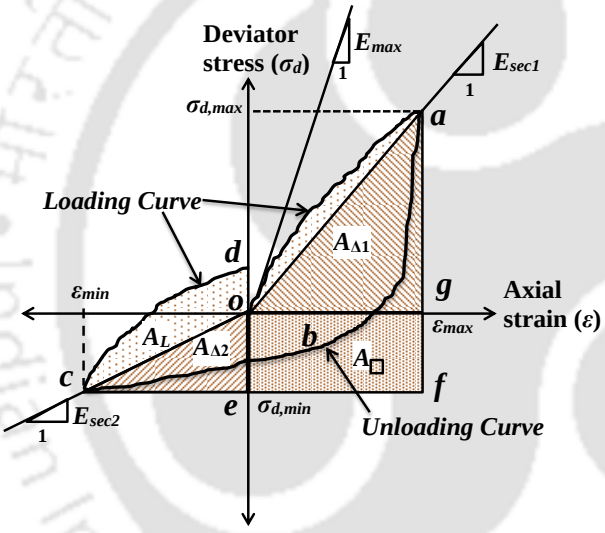

$$E_{sec,a} = \frac{E_{sec1} + E_{sec2}}{2}$$

$$G_a = E_{sec,a} / [2(1+\upsilon)]$$

$$\gamma = (1+\upsilon)\varepsilon$$

$$D^{\#} = \frac{1}{\pi} \times \frac{A_{L(o-a-b-c-d)}}{A_{\Delta 1} + A_{\Delta 2} + A_\square}$$

Fig. 5.4 A typical asymmetrical hysteresis loop

For BS specimens prepared at D_r = 30% and σ'_c = 100 kPa, Fig. 5.5 depicts the variation of G with N for different strain levels (γ = 0.045% to 0.60%). For $\gamma \geq 0.075\%$, a noticeable reduction in G is observed with increasing N. However, after a few loading cycles, depending on the strain level, the reduction becomes marginal. Fig. 5.6 presents the variations in G with γ for first loading cycle (N = 1) for SBS specimens at D_r = 30% and σ'_c = 50 kPa, 100 kPa and 150 kPa. It is observed that for a given shear strain amplitude, the shear modulus increases with the increase of σ'_c; similar observations were also reported by other researchers (Hardin and

Drnevich, 1972; Seed and Idriss, 1970; Govindaraju, 2005; Hanumantharao and Ramana, 2008; Kirar and Maheshwari, 2013; Chattaraj and Sengupta, 2016b). Fig. 5.6 also presents the results of repeated tests conducted with same testing conditions and methodology. Based on the repeated tests results, it can be stated that even if tests are repeated on the specimens of same specifications and following the same test methodology, the results are found to vary in the range of 5-15%, which is within the tolerance of experimental error. Fig. 5.7 represents the variation of shear modulus (G and G_a) with shear strain (BS specimens at D_r = 30% and σ'_c = 100 kPa). The results indicate that estimations of shear modulus from SHL and ASHL are practically same when evaluated from the 1st cycle, due to the similar mathematical averaging technique followed in both the approaches.

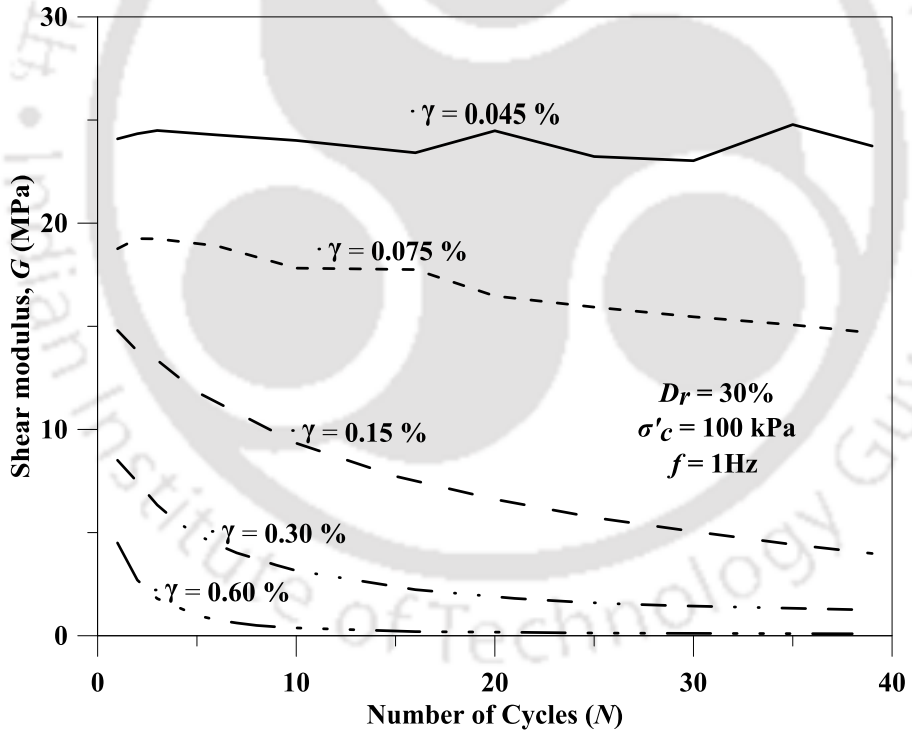

Fig. 5.5 Variation of shear modulus with N at different shear strains

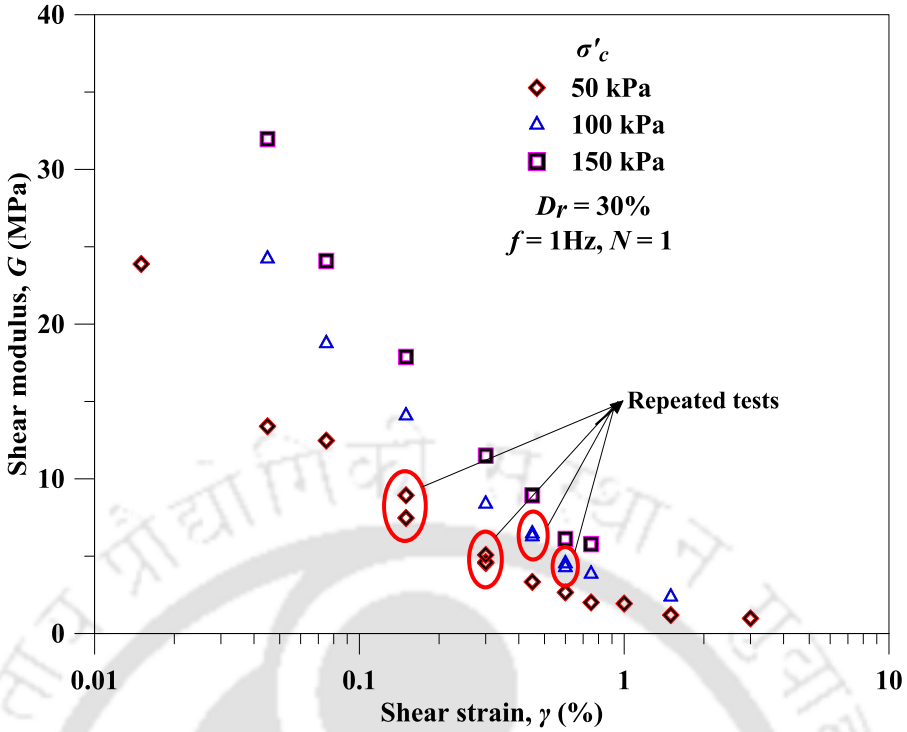

Fig. 5.6 Variation of shear modulus with shear strain based on ASHL

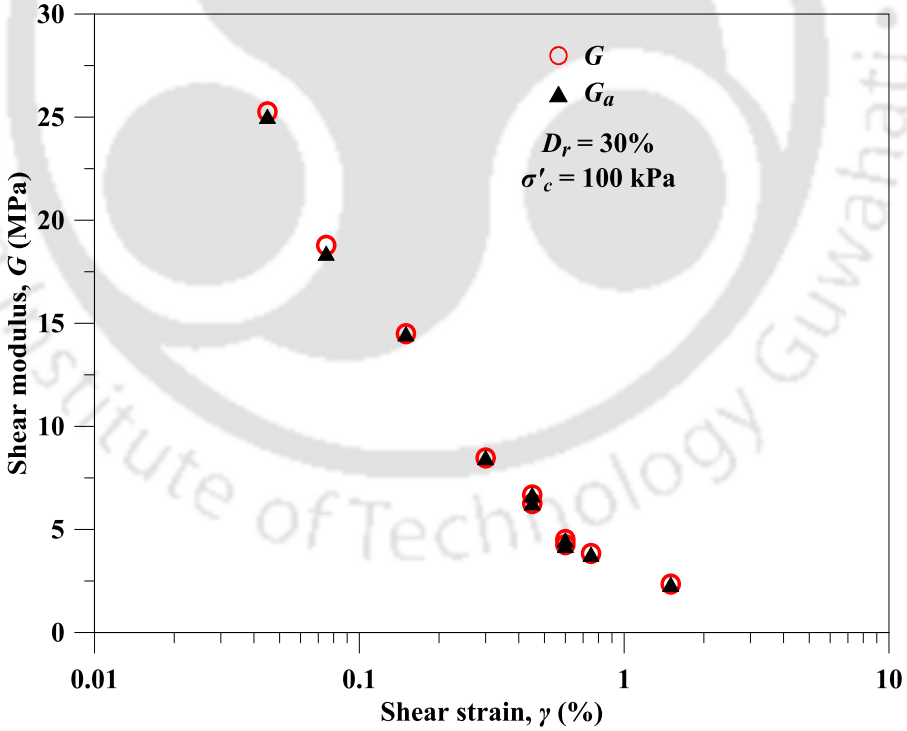

Fig. 5.7 Comparative variation of shear modulus with shear strain based on SHL and ASHL

A modulus reduction curve is used to represent the degradation of shear modulus with shear strain in terms of reduction in modulus ratio (G/G_{max}) (Kramer, 1996). G_{max} is the

maximum shear modulus of the soil that is generally defined at a very low shear strain ($\gamma \leq 5\times10^{-6}$) (Kramer, 1996; Okur and Ansal, 2007). For the present study, in the absence of availability of such experimental data at sufficiently low strain ($\gamma \approx 10^{-6}$), empirical correlation proposed by Chung et al. (1984) has been used for evaluating the G_{max} (Eqn. 5.1).

$$G_{\max}\left(\text{kPa}\right) = 523\,\frac{(OCR)^{k}}{(0.3+0.7e^{2})}\times p_a^{0.52}\times\left(\sigma'_c\right)^{0.48} \tag{5.1}$$

where, OCR is the over-consolidation ratio, k is an index parameter (0 for sands), e is the void ratio, p_a is the atmospheric pressure and σ'_c is the mean principal effective stress in kPa. Estimated G_{max} values for BS soil specimens at different D_r and σ'_c are presented in Table 5.3. The variation of G/G_{max} for BS with γ at different D_r and σ'_c are presented in Fig. 5.8. The scatter of the obtained data can be demarcated by upper- and lower-bounds, as represented by dotted lines in the figure. It can be observed that, at higher strain levels, the scatter of G/G_{max} gets significantly narrowed. For all practical purposes, the obtained estimates can be represented by an average G/G_{max} curve (Fig. 5.8).

Table 5.3 Estimated G_{max} for BS

σ'_c (kPa)	50	100	150
D_r (%)		G_{max} (MPa)	
30	49.64	69.24	84.12
60	57.73	80.52	97.82
90	67.25	84.12	113.95

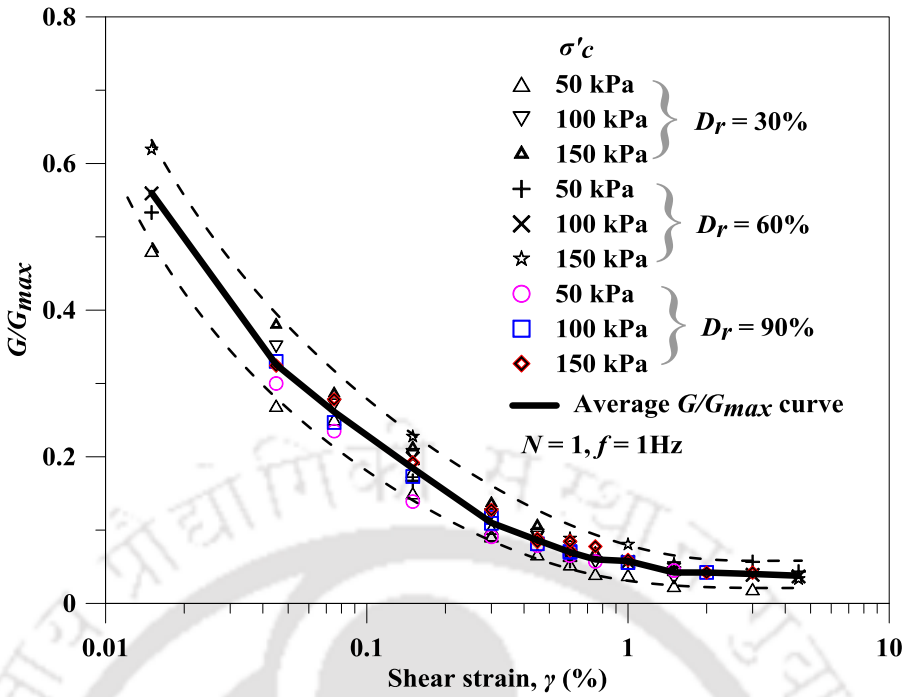

Fig. 5.8 Variation of G/G_{max} with γ at different σ'_c and D_r

The average G/G_{max} curve for BS has been compared with the G/G_{max} curves for different types of sandy soils available in the literature, and is presented in Fig. 5.9. In spite of a similar trend, the G/G_{max} estimates of BS show lower values in comparison to the classical curves (Seed and Idriss, 1970; Kokusho, 1980; Vucetic and Dobry, 1991); although, it is in close agreement to those reported for Indian soils (Govindaraju, 2005; Hanumantharao and Ramana, 2008; Kirar and Maheshwari, 2013). From Fig. 5.10, it can be stated that each type of soil have its own characteristic behaviour based on its PSD and other properties such as liquid limit, plastic index, percentage fines and hence, the dynamic properties of each soil are also subjected to variation. Thus, from Fig. 5.9, it can be stated that the non-judicious adoption of any particular standard modulus reduction models (Seed and Idriss, 1970; Kokusho, 1980; Vucetic and Dobry, 1991) for any soil will lead to incorrect estimation of the dynamic behaviour. It should be customary that the dynamic properties of each soil be judiciously determined before its application for any practical geotechnical engineering problems.

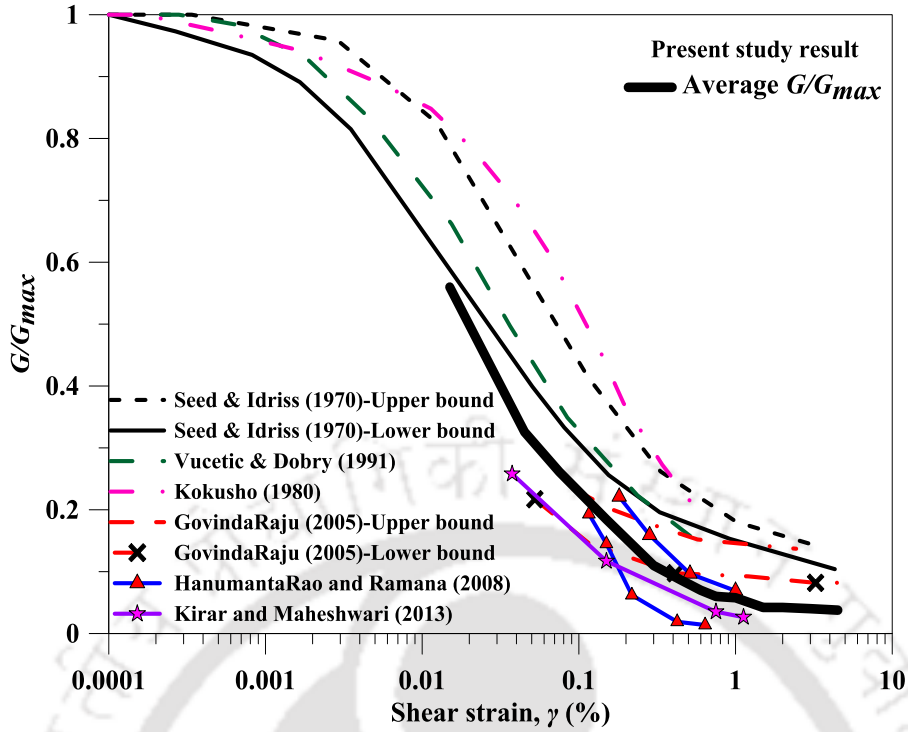

Fig. 5.9 Comparison of G/G_{max} for different soils

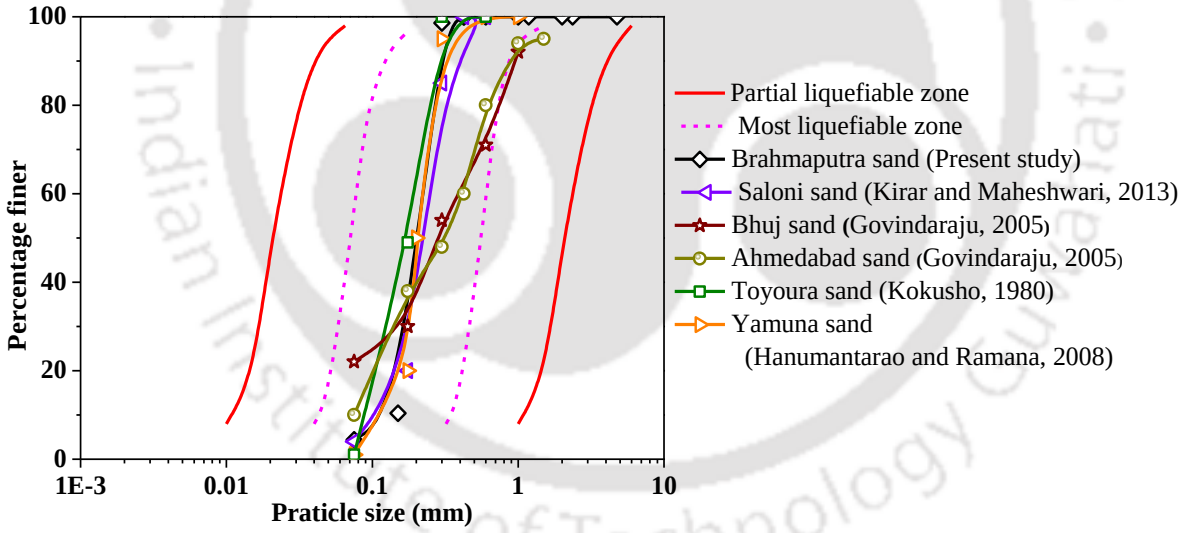

Fig. 5.10 Particle size distribution of different soils

Evaluation of damping ratio

Fig. 5.11 illustrates the variations of damping ratio with N, computed using both conventional (D) and the modified method ($D^{\#}$) (as shown in Fig. 5.3 and Fig. 5.4, respectively). For the evaluation of $D^{\#}$, the stored strain energy in one complete cycle has been considered (represented by the hatched polygon in Fig. 5.4), which comprises of two triangles and a

rectangle having the area $A_{\Delta 1}$, $A_{\Delta 2}$ and $A_{\square}$ respectively. A_L is the area enclosed by the hysteresis loop and is expressed in Eqn. (5.2) (Kreyszig, 2010), where ε_i and σ_i are the axial strain and deviator stress (i = 1 to n, where n is number of points used to construct the hysteresis loop).

$$A_L = \frac{1}{2}\left|(\varepsilon_1 \times \sigma_2 - \varepsilon_2 \times \sigma_1) + (\varepsilon_2 \times \sigma_3 - \varepsilon_3 \times \sigma_2) + - - - + (\varepsilon_1 \times \sigma_n - \varepsilon_n \times \sigma_1)\right| \quad (5.2)$$

It is observed that for $\gamma \leq 0.075\%$, the differences between D and $D^{\#}$ are insignificant, which is primarily attributed to the nearly symmetric hysteresis loops at these low shear strains for all loading cycles. Significant difference is noted between D and $D^{\#}$, at $\gamma \geq 0.15\%$, where $D^{\#}$ is found to be noticeably higher than D, due to enhanced asymmetric nature of the hysteresis loops at these strain levels (Fig. 5.2). This observation inadvertently indicates that the estimation of damping ratio following conventional method is too conservative, and the modified method should be adopted. For a typical variation of damping ratio (γ = 0.60%, Fig. 5.11e), it can be observed that the estimated values of D and $D^{\#}$ become closer, thus suggesting formation of near-symmetrical loops approximately beyond 30th cycle. Similar observations are made for the damping ratios obtained for other peak shear strains (γ > 0.60%, Fig. 5.11f).

Fig. 5.12-Fig. 5.17 depict the variations of damping ratio (D and $D^{\#}$) with shear strain for test specimens prepared at different D_r and σ'_c. Fig. 5.12 shows the effect of σ'_c on D and $D^{\#}$ for SBS specimens at D_r = 30%. It can be observed that specimens subjected to lower σ'_c (50 kPa) depicts higher damping ratio in comparison to that obtained at higher σ'_c (100 and 150 kPa), the latter observation is attributed to the relatively higher stiffness imparted in the specimens due to higher confinement. The damping ratio is not found to vary noticeably for σ'_c greater than 100 kPa.

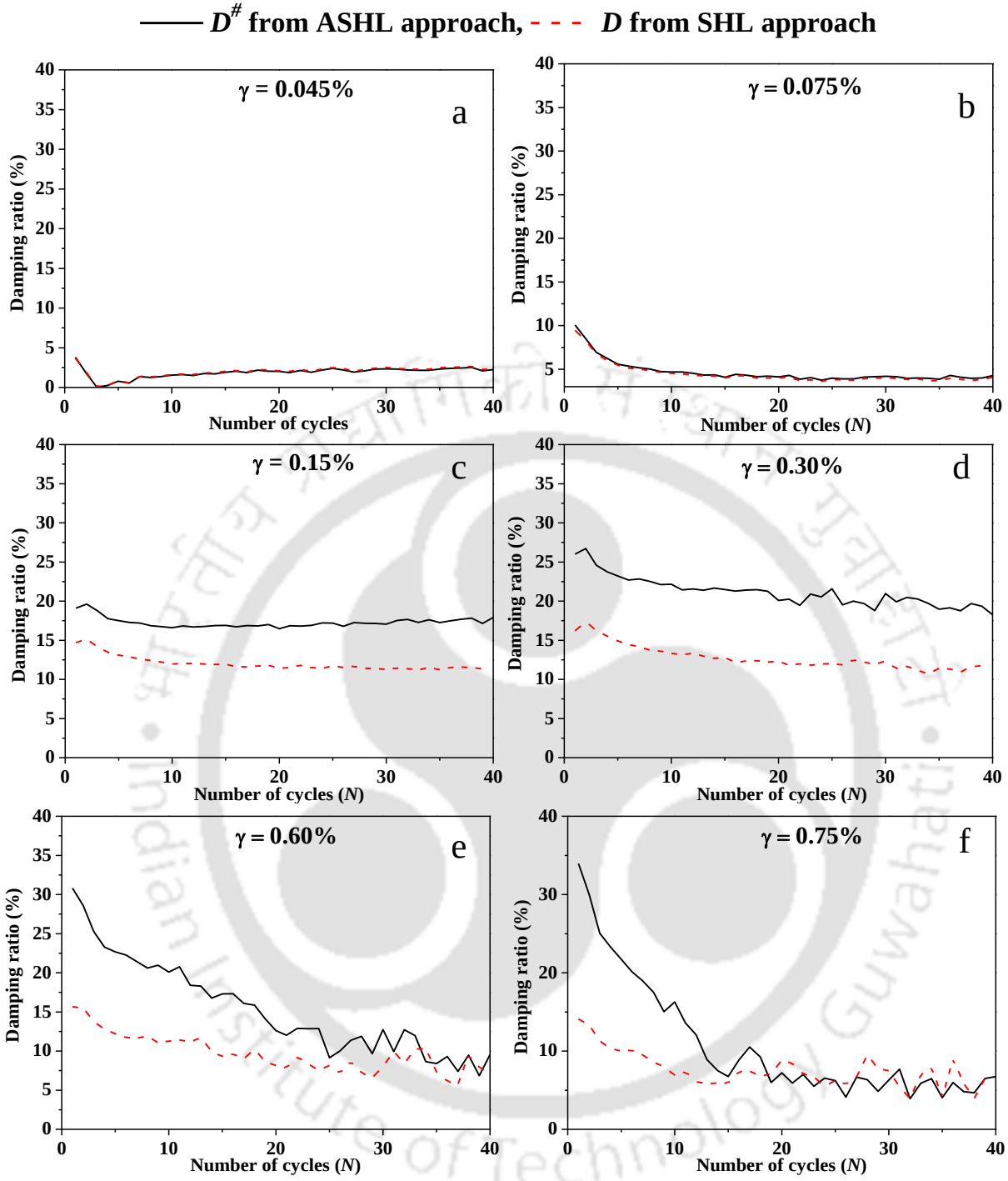

Fig. 5.11 (a-f) Variation of $D^{\#}$ and D with N for γ = 0.045-0.75%

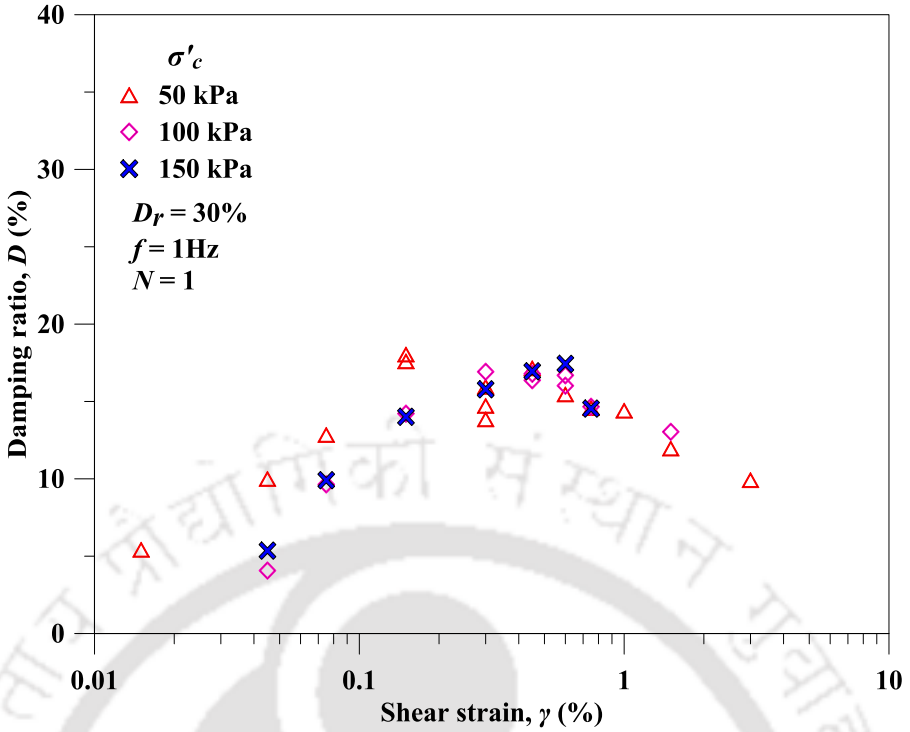

Fig. 5.12 Variation of D with γ at different σ'_c

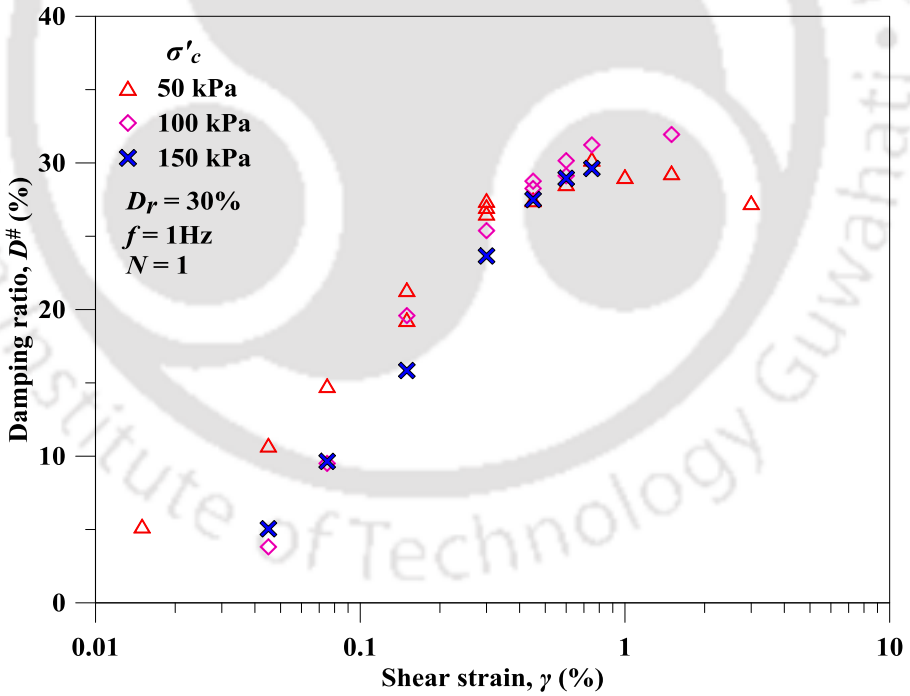

Fig. 5.13 Variation of $D^{\#}$ with γ at different σ'_c

It can also be noted that D (Fig. 5.12) attains a peak magnitude at a γ = 0.5%, while $D^{\#}$ (Fig. 5.13) attains the peak magnitude at $\gamma \approx 1\%$. Beyond the stated peak values, a significant reduction in damping ratio is observed at higher strain levels which are noticeably different

from that observed in the damping ratio curves from earlier studies (Seed and Idriss, 1970; Iwasaki et al., 1978; Kokusho, 1980; Kokusho et al., 1982; Seed et al., 1986; Chang et al., 1989; Woods, 1991; Vucetic and Dobry, 1991; Ishibashi and Zhang, 1993; Stokoe et al., 1995; Sitharam and Govindaraju, 2003; Govindaraju, 2005; Hanumantharao and Ramana, 2008; Kirar and Maheshwari, 2013). It should be noted that, for the earlier studies, tests were conducted up to strain levels of about 1%. Very few researchers have provided the experimental evidence of estimated damping ratio beyond 1% shear strain (Kiku and Yoshida, 2000; Brennan et al., 2005; Mashiri, 2014; Matasovic and Vucetic, 1993), which followed a similar trend as obtained in the present study. The effect of D_r on the damping ratio obtained from SHL and ASHL are presented in Fig. 5.14 and Fig. 5.15, respectively. Both figure portrays that up to $\gamma \approx 0.5\%$, D_r has an insignificant effect on D and $D^{\#}$ estimated for BS specimens subjected to σ'_c = 100 kPa.

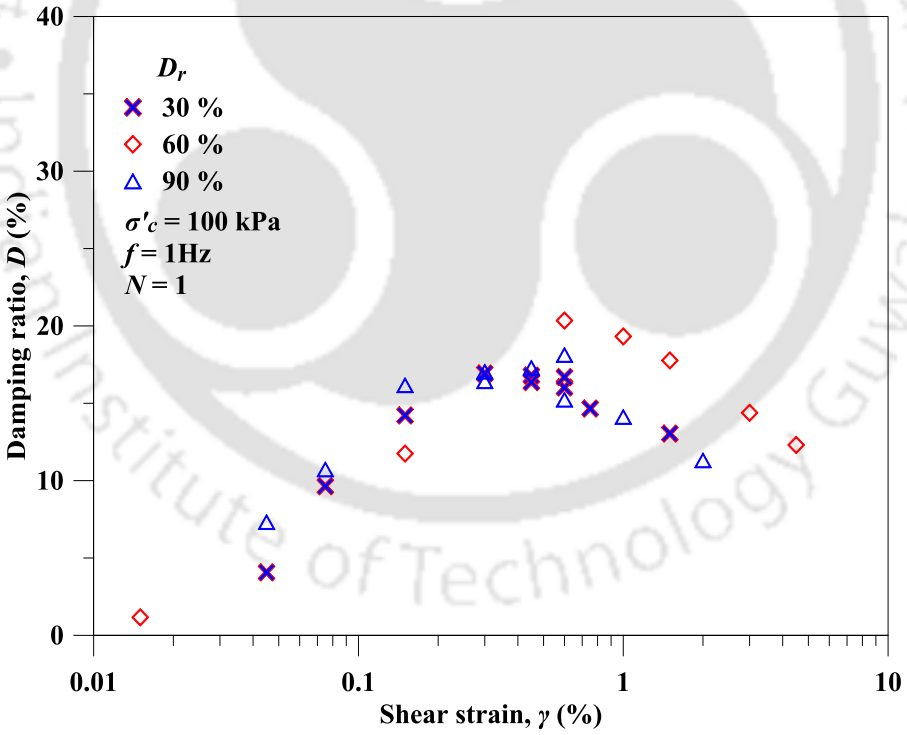

Fig. 5.14 Variation of D with γ at different D_r

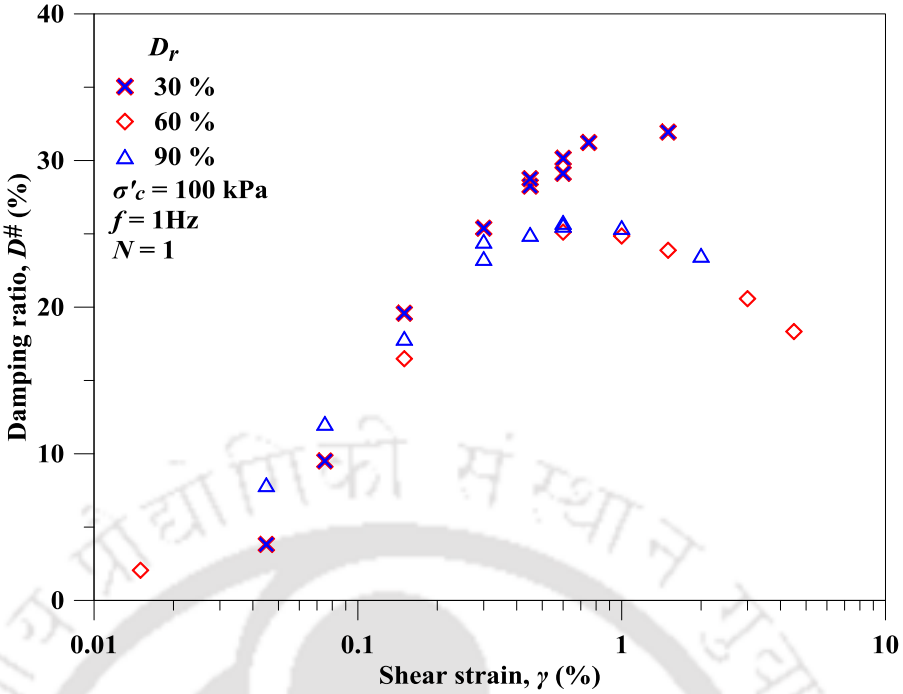

Fig. 5.15 Variation of $D^{\#}$ with γ at different D_r

For all practical purposes, Fig. 5.16 presents the average trends of the estimated D and $D^{\#}$ for SBS specimens prepared at different D_r and σ'_c. It is observed that, the average trend of $D^{\#}$ exceeds D by 40-70%, with higher deviation at higher strain levels beyond 0.50%. From the overall observations of Fig. 5.12-Fig. 5.16, it can be stated that the modified method to estimate damping ratio is significantly important and that the conventional method largely underestimates the actual damping developed in the specimen, especially at higher strain levels. Most of the existing literature reports the estimated damping ratio up to $\gamma \leq 1\%$, and the same is extrapolated to estimate the damping ratio for beyond 1% (such as in the existing commercial software for ground response analyses or any other seismic studies). However, the present study unambiguously reflects that the damping ratio exhibits non-conventional behaviour $\gamma \geq 1\%$, where a noticeably decreasing trend is observed rather than the conventionally assumed increasing or asymptotic variation. Hence, the current observation provides a better phenomenological understanding and a scope of improvement of the existing methods utilizing damping ratio curves beyond γ = 1% by defining a curvilinear variation for the entire strain

range tested for the present study. The obtained variation of damping ratio from the present study has been compared with the data available in the literatures as shown in Fig. 5.17. It can be observed that most of the earlier researchers have restricted the data up to a γ of 1%. The data from present study also follows the observed trend (within 1%). Based on the present observation related to the variation of damping ratio over the entire strain range, it can be stated that using the damping ratios for $\gamma \leq 1\%$, is not judicious to extrapolate the trend of damping ratio beyond 1%, and that a new functional variation of the same should be developed in order to use the same for purposes of geotechnical engineering involving wider range of shear strain.

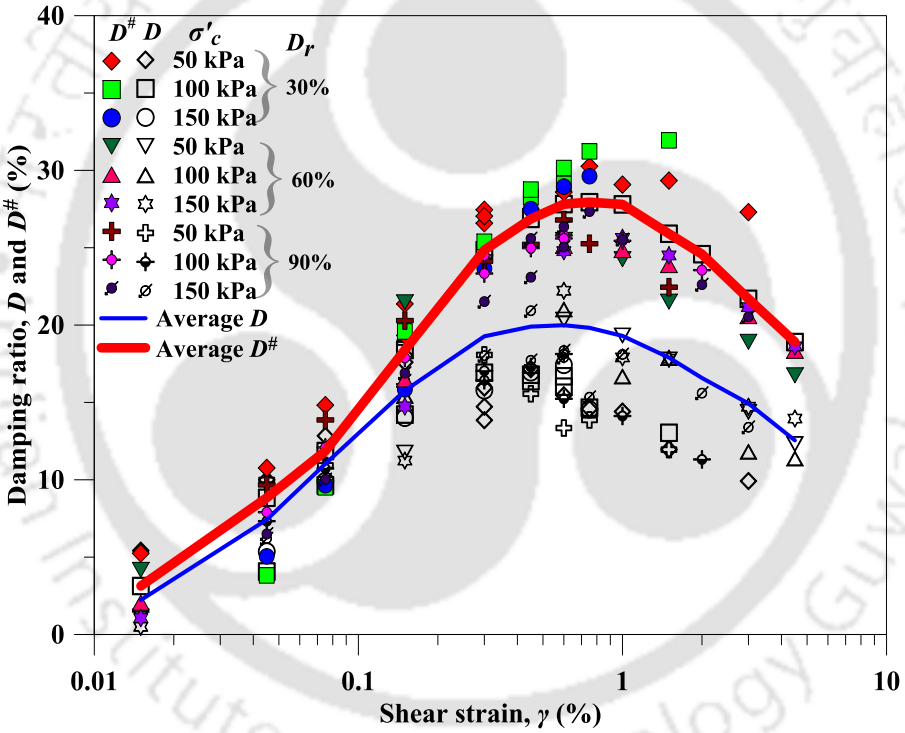

Fig. 5.16 Comparison of D and $D^{\#}$ of SBS

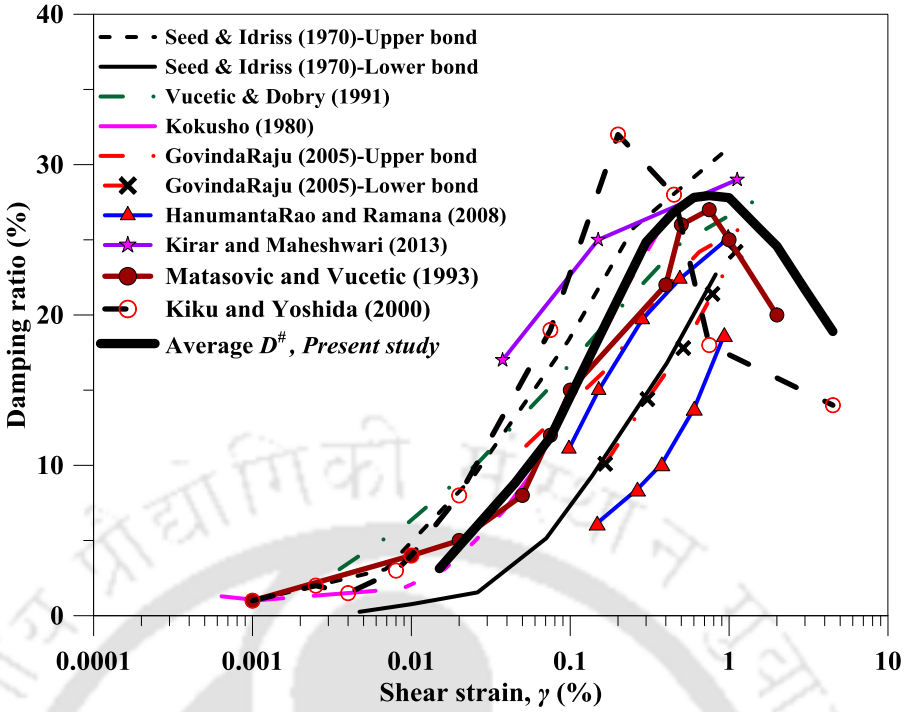

Fig. 5.17 Comparison of damping ratio of different soils from available data in literature

Effect of loading frequency on strain-controlled dynamic shear properties

The effect of loading frequency on the shear modulus and damping ratio, evaluated for first cycle, are presented in Fig. 5.18 and Fig. 5.19, respectively. Fig. 5.18 depicts that the higher confining pressures reflects higher shear modulus, while the loading frequency is not observed to cast a prominent influence on the magnitude of dynamic shear modulus. Fig. 5.19, however represents a significant effect of frequency on the magnitude of damping ratio. For a particular peak axial strain (γ = 0.15%), from trend line plot, it can be observed that the increase in frequency results in a noticeable decrement in the damping ratio; however scatter data points show the increase of damping ratio up to 1 Hz and then decreases with loading frequency. This decrease in the damping ratio is attributed to the increasing intensity of the inter-particle interaction intensity with increasing loading frequency which leads to enhanced friction resulting in a faster dissipation of energy in very small time interval. Thus, it can be noted that the BS specimens subjected to sinusoidal stress history of 1 Hz loading frequency, incorporate the viscous effect of pore-water on the dynamic response of BS.

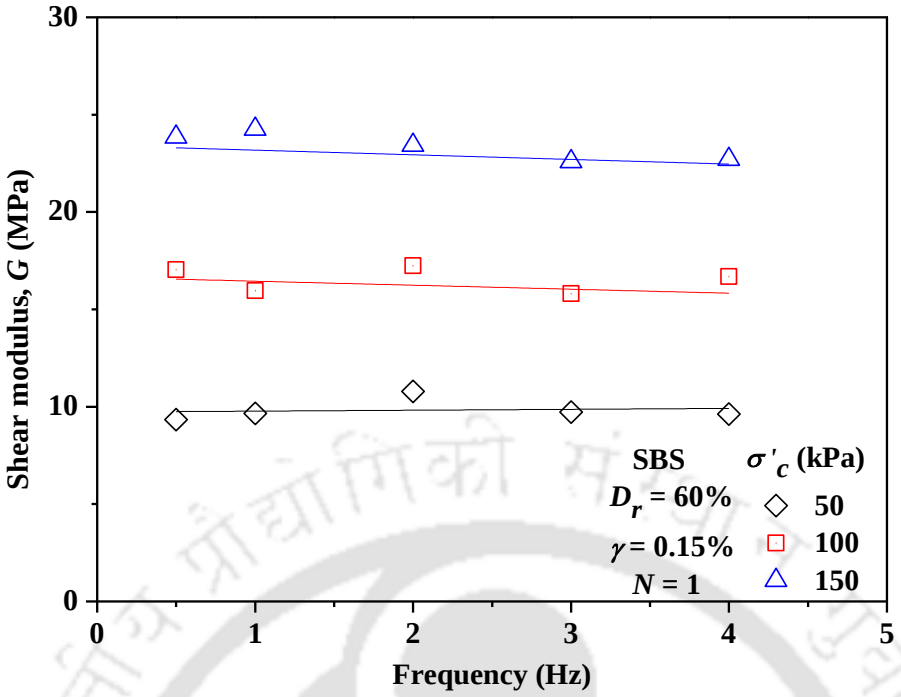

Fig. 5.18 Effect of loading frequency on shear modulus

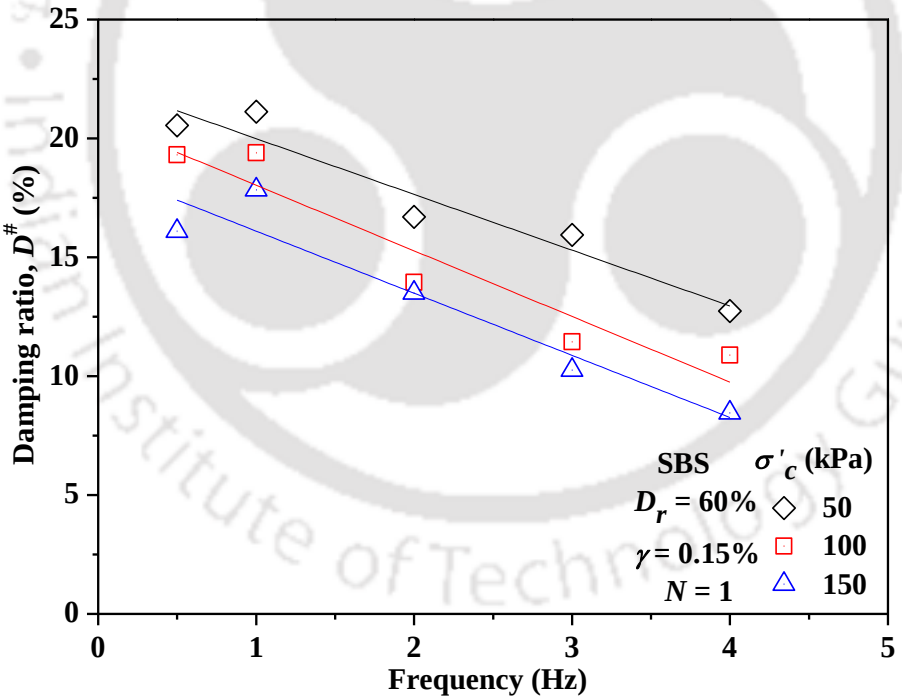

Fig. 5.19 Effect of loading frequency on damping ratio

Fig. 5.20 illustrate the variation of excess PWP ratio with number of loading cycles at different frequencies. It has been observed from Fig. 5.20, that the excess PWP ratio increases with number of loading cycles and loading frequency. However, the excess PWP ratio increases

up to 2 Hz and further decreases, which suggests that the rate of generation of excess PWP decreases at higher loading frequency. This is attributed to the slower rate of the generation of excess PWP at higher frequency due to less time in the repetition of stress cycles. The obtained excess PWP in first loading cycle are presented in Fig. 5.21, which reflect that the lesser amount of excess PWP developed at higher loading frequency resulting lower in damping ratio. Variation of shear modulus and damping ratio with shear strain for loading frequency range 0.5-4.0 Hz and σ'_c range 50-150 kPa are presented in Fig. 5.22 and Fig. 5.23, respectively. It can be observed from Fig. 5.22, that the effect of frequency on shear modulus is insignificant for a particular σ'_c, whereas the damping ratio, presented in Fig. 5.23, beyond shear strain of 1% decreases for all loading frequencies at all σ'_c.

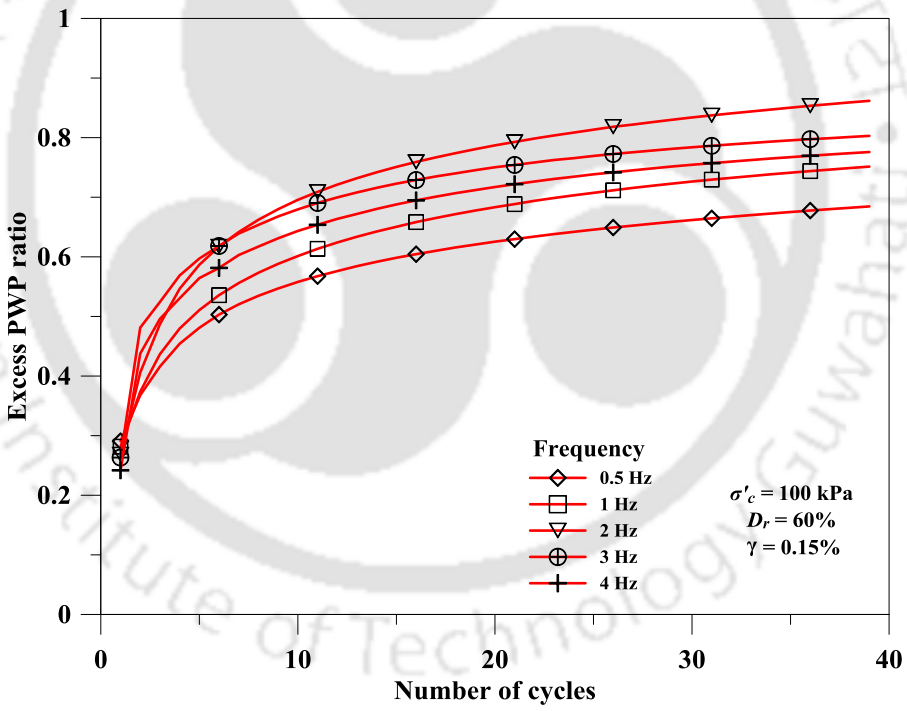

Fig. 5.20 Variation of excess PWP ratio with number of loading cycles at different loading frequencies

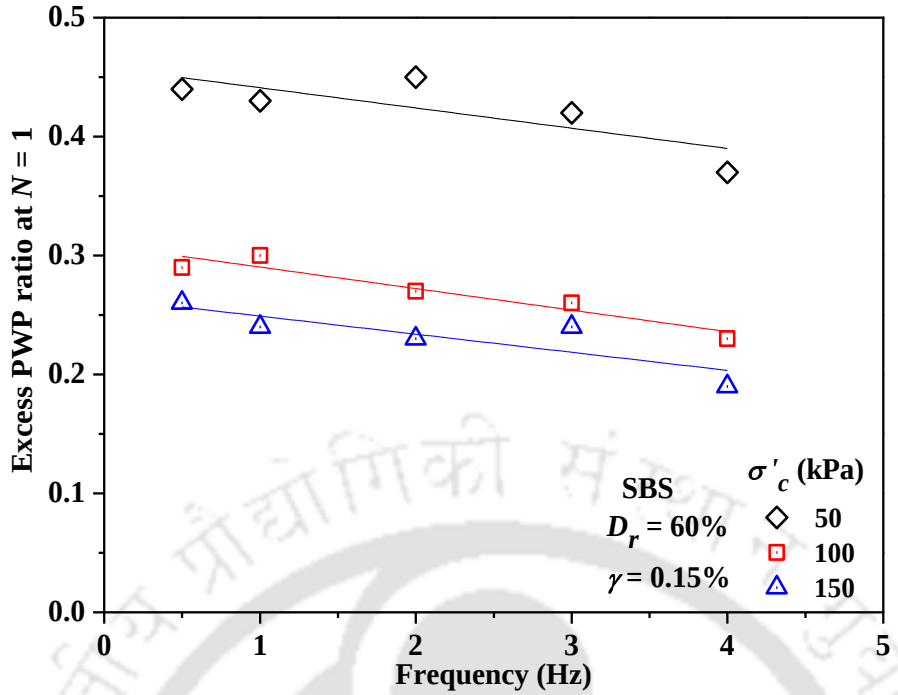

Fig. 5.21 Variation of excess PWP ratio with loading frequency for N = 1

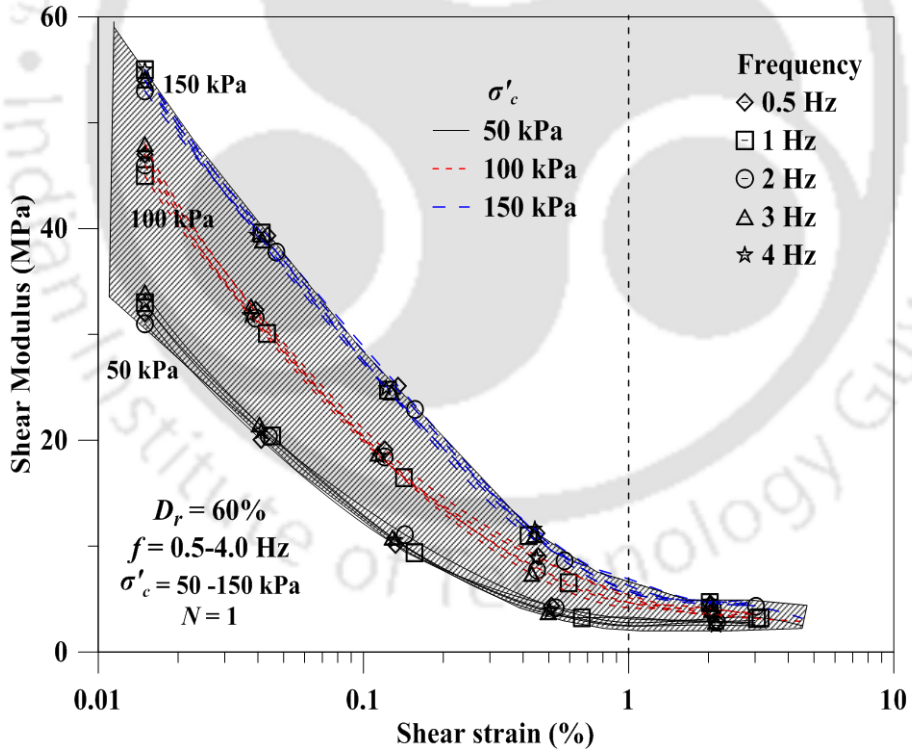

Fig. 5.22 Variation of shear modulus with shear strain for f = 0.5–4.0 Hz and σ'_c = 50–150 kPa

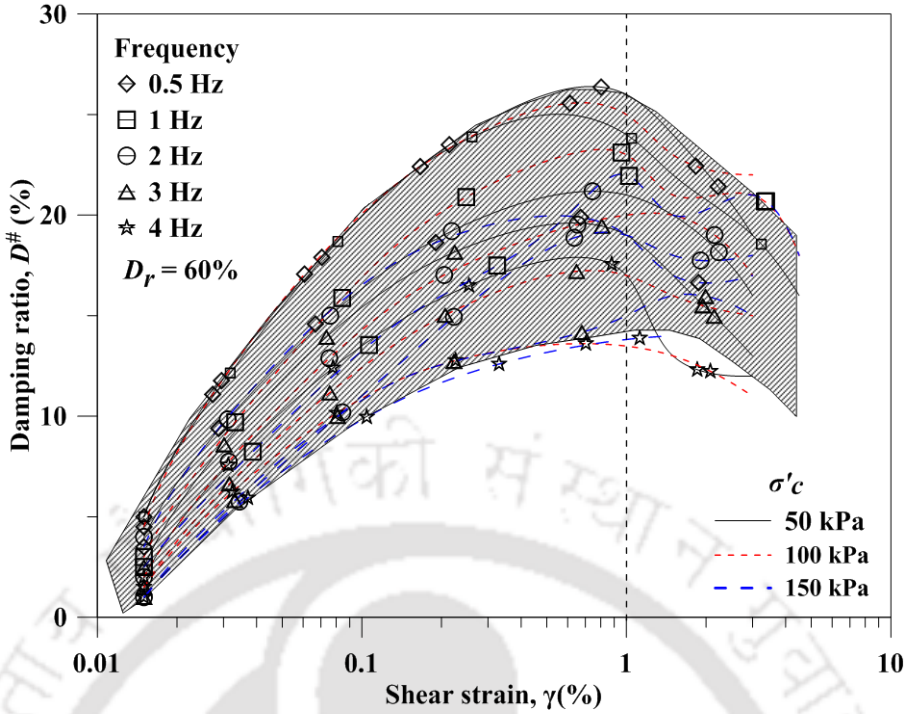

Fig. 5.23 Variation of damping ratio with shear strain for f = 0.5–4.0 Hz and σ'_c = 50–150 kPa

5.3.2 Dynamic properties of saturated cohesionless soil using on-sample LVDTs

Strain-controlled cyclic triaxial tests have been performed on the SBS considering different peak shear strain levels, the remaining test conditions and sample specifications being similar as that of monotonic test described in Chapter 3. The external and on-sample LVDTs have been used to capture the global and local deformation, respectively, during the cyclic loading of soil specimens. Fig. 5.24 represents the variation of the applied axial strain (obtained from external LVDT) and the local axial strains (obtained from on-sample LVDT) obtained for the tests conducted with different applied peak axial strains (0.03%, 0.2% and 0.66%). Fig. 5.24 illustrates that the axial strain, applied uniformly on the top of specimen, does not get uniformly transferred at the mid-height of the specimen, which is in contrary to the assumptions made in the conventional analysis. Moreover, it can be observed that with time, there is an accumulation of strains in the soil specimens. This reflects that in spite of constant strain applied globally (externally) on the specimen, the on-sample transducers are capable of highlighting the

variation and accumulation of local strains, when attached at different sections of the specimen.

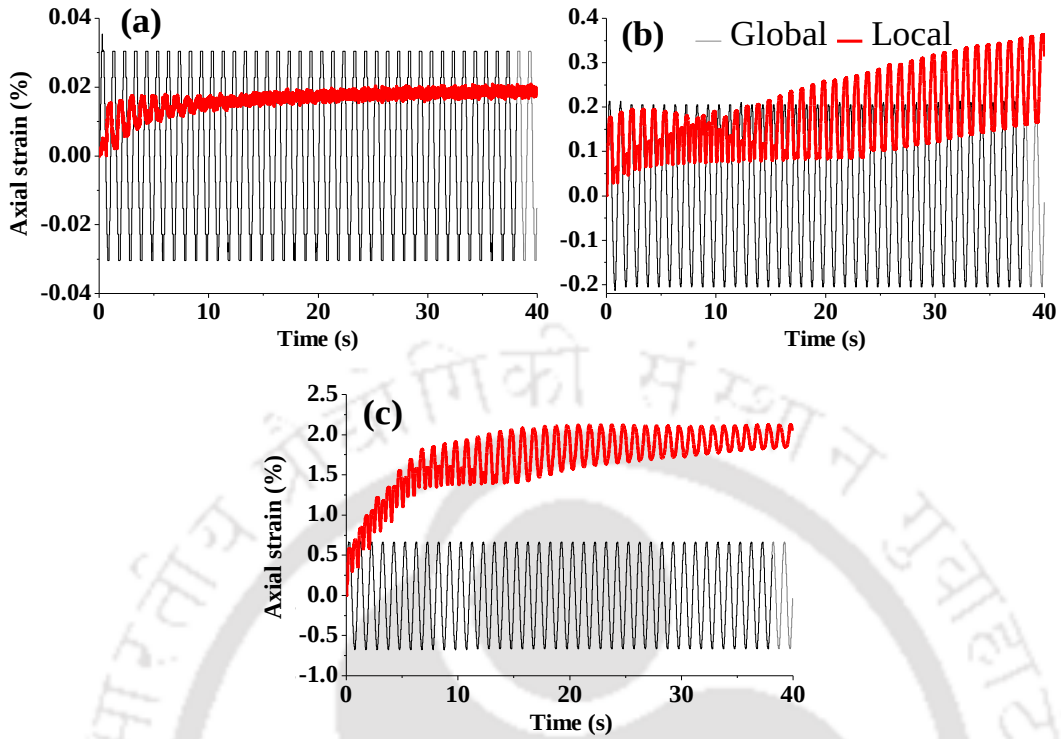

Fig. 5.24 Strain time histories from external and on-sample LVDTs at peak axial strains (a) 0.03% (b) 0.2% (c) 0.66%

Fig. 5.25 represents the stress-strain response of the soil specimens based on both the global and local strain measurements. As obvious, the peak global strain, measured by the external LVDT, is found to be constant for each of the tests. However, for each particular test configuration, the measured local strains are found to be significantly varying throughout the test, and are noticeably different than the applied global strain. Hence, it is understood that along the length of the specimen, distribution of axial strain takes place due to elemental response of particles, which result in such deviation between the local and global strains. Thus, evaluation of the soil stiffness, based on the presumption that global strain is uniform all along the soil sample, will yield conservative results. Hence, it would be judicious enough to utilize the measured local strains for the estimation of the shear stiffness of the soil sample, as the stiffness is also bound to vary along the length of the sample.

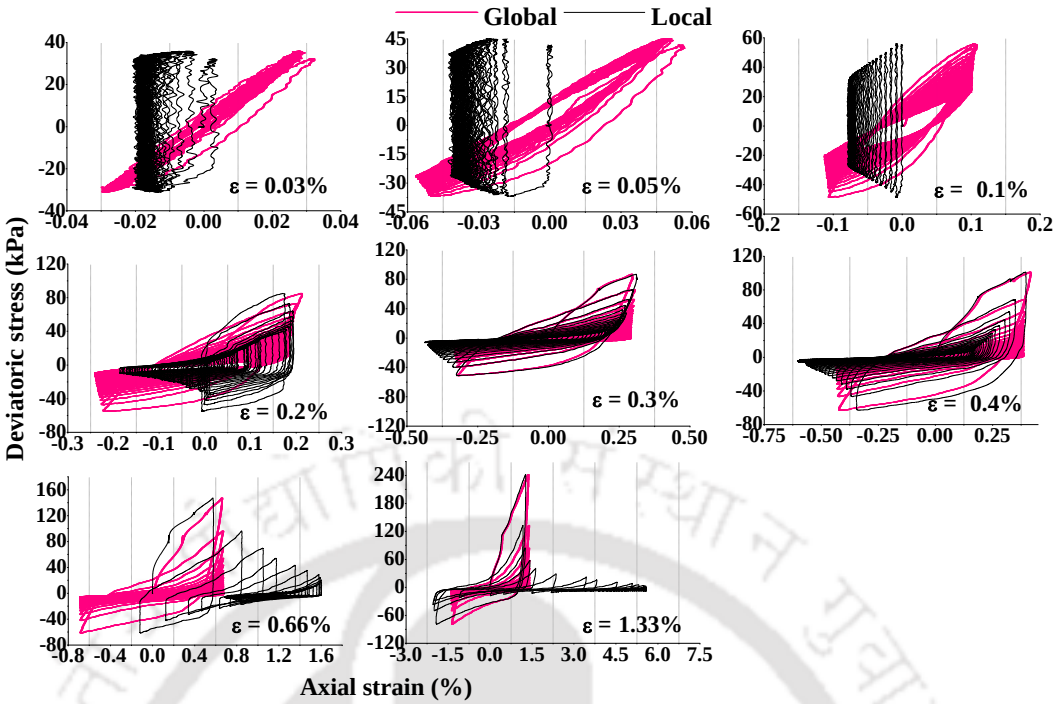

Fig. 5.25 Stress-strain plots based on external and on-sample LVDTs at D_r = 90%, σ'_c = 100 kPa and f = 1 Hz

Fig. 5.26 represents the importance of the measurement of local strains to estimate the shear modulus. It can be observed that the on-sample LVDTs are able to measure low shear strains induced in the specimen, and thus, the shear modulus evaluated at these local strains can be considered as maximum shear modulus (G_{max}). The shear strain (γ) shown in Fig. 5.26 was evaluated from the axial strain (ε) using Eqn. (5.3) (ASTM D3999), and the Poisson's ratio was considered to be 0.5 for saturated undrained specimens (Rollins et al., 1998).

$$\gamma = \varepsilon \times (1+\nu) \tag{5.3}$$

Fig. 5.26 also depicts that the variations of shear modulus evaluated from the external LVDT. It can be observed that beyond cyclic shear strain amplitude of 0.1%, the shear modulus obtained from the measurements of on-sample and external LVDT are in extremely close agreement, thus indicating that the on-sample transducers are also capable enough in manifesting the measurement of the shear modulus at higher strain ranges as well. Table 5.4

lists the values of G_{max} as well as the secant shear modulus (G, computed from 1st cycle of the test) for different test conditions based on both local and global strains. Researchers have performed low-strain tests on fine sands and proposed standard correlations for the estimation of G_{max} (Chung et al., 1984; Hardin and Drnevich 1972; Kokusho 1980). It is observed from Table 5.4 that the G_{max} obtained from the present experimental investigation are in appreciable agreement with those obtained using the above-mentioned standard correlations.

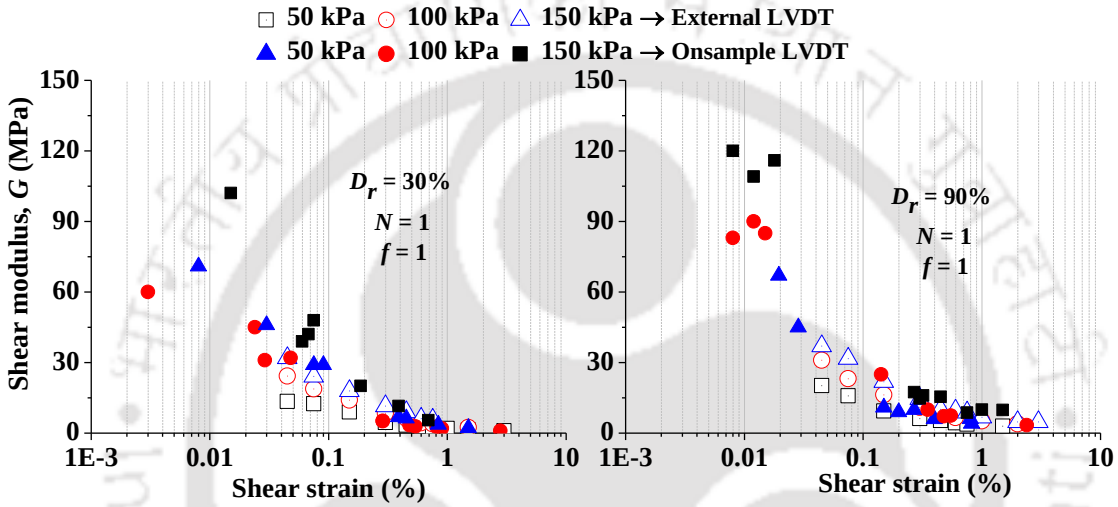

Fig. 5.26 Comparative plot of shear modulus of SBS based on the external and on-sample LVDTs

Table 5.4 Estimated G_{max} values for BS

Parameter		σ'_c (kPa)	50		100		150	
		D_r (%)	30	90	30	90	30	90
Shear modulus (G, MPa)	Present study	G (based on External LVDT, γ = 0.045%)	13	20	24	31	32	37
		G_{max}.(value based on On-sample LVDT)	60	70	71	91	102	120
	Low-strain tests on fine	Chung et al. (1984)	50	67	69	94	84	114
		Hardin and Drnevich (1972)	59	79	83	112	102	137
		Kokusho (1980)	61	90	86	127	105	156

Fig. 5.27 illustrate the variation of modulus reduction curve, represented by G/G_{max}, based on both global and local strains. The estimated G_{max} based on the measurements from on-sample LVDTs was used to normalize G (i.e. the secant modulus obtained either from global strain or local strain measurements). Fig. 5.27 shows the variation of G/G_{max} for BS, as obtained from the on-sample LVDT measurements, and the same has been compared with that obtained from external LVDT measurement from test specimens subjected to high cyclic strains (Kumar et al., 2017). Based on the agreeable match beyond a shear strain of 0.1%, it can be stated apart from obtaining the shear modulus at low strains (approximately 3×10^{-3} % to 0.1 %), the on-sample LVDTs can be effectively used even to obtain the same at high strain range (greater than 1.0%). Based on the application of on-sample transducers for cyclic triaxial testing, Gookin et al. (1996) have also reported the modulus reduction curve over a wide range of strain for Monterey No. 30 sand prepared (D_r = 89%), and the same has been illustrated in Fig. 5.27. Thus, these findings highlight the importance of the use of on-sample LVDT for the measurement of local strains which can be used to obtain the dynamic response of cohesionless soil over a wide range of strain.

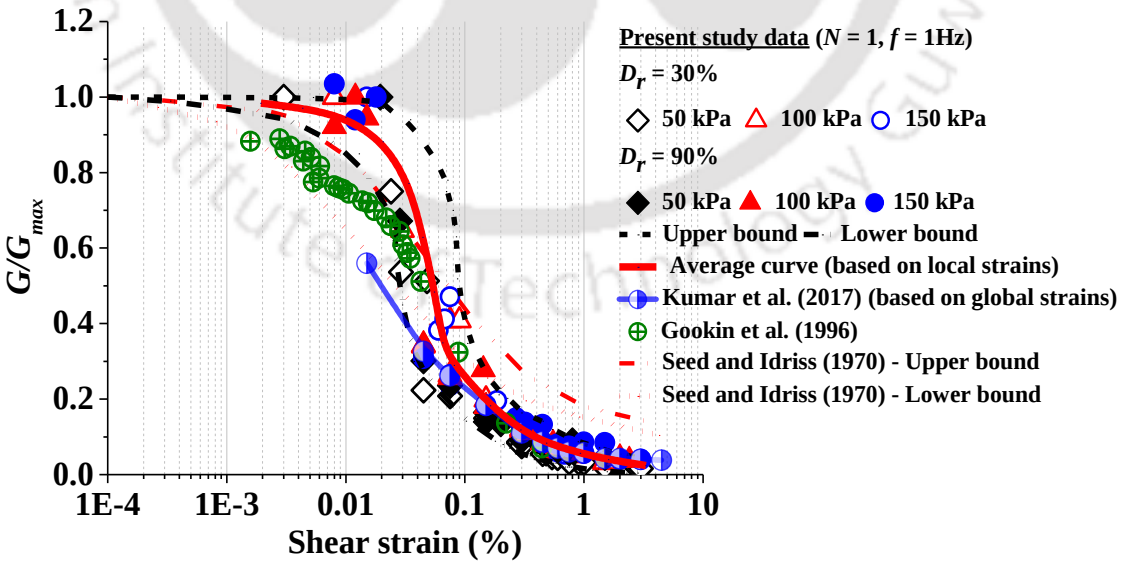

Fig. 5.27 Comparative modulus reduction of SBS based on external and on-sample LVDTs

5.3.3 Stress-controlled cyclic loading

Typical results obtained for SBS, from the stress-controlled cyclic triaxial tests at cyclic stress ratio (*CSR*) = 0.1, D_r = 60%, σ'_c = 100 kPa, f = 1 Hz are shown in Fig. 5.28. Fig. 5.28a presents the variations in deviator stress with number of loading cycle (N) up to 40 cycles which causes deformations in the soil specimen. Fig. 5.28b shows the output in terms of variation of axial strain with N, exhibiting strain accumulation over the loading period. Fig. 5.28c illustrates the development of excess PWP ratio ($r_u = \Delta u/\Delta\sigma_{3c}$) due to the applied loading, which causes initiation of liquefaction of soil based on the criterion $r_u = 1$. Fig. 5.28d shows the stress-strain response obtained during cyclic loading, which was subsequently used to evaluate the dynamic properties such as the shear modulus (G) and the damping ratio ($D^{\#}$) of SBS, based on the stress-controlled approach.

Evaluation of shear modulus and damping ratio

Dynamic shear properties of SBS soil have also been evaluated based on stress-controlled cyclic loading, following a methodology similar to the strain-controlled loading. Fig. 5.29 and Fig. 5.30 shows the results of dynamic shear properties of SBS soil at D_r = 60%, σ'_c = 100 kPa and f = 1 Hz for different Cyclic Stress Ratio (CSR) ranging from 0.1–0.4. Fig. 5.29 depicts that the shear modulus drastically decreases with the increase of CSR and shear strain. It has been observed that, for CSR = 0.1, the shear modulus values for all 40 cycles are almost same, which reflects that the hysteresis loop remains almost symmetrical and does not exhibit softening with number of loading cycles (shear modulus is evaluated from the slope of the hysteresis loop). The significant degradation of shear modulus was observed at CSR = 0.2, 0.3 and 0.4, from nearly 25 MPa, 12 MPa and 5 MPa to less than 1 MPa, respectively, due to asymmetric nature of hysteresis loop and softening up of the specimen with loading cycles. It can also be seen that the significantly higher shear strains are experienced by the soil specimen in first loading cycles due to higher σ_d of 20kPa, 40 kPa, 60 kPa and 80 kPa at CSR = 0.1, 0.2, 0.3 and 0.4, respectively.

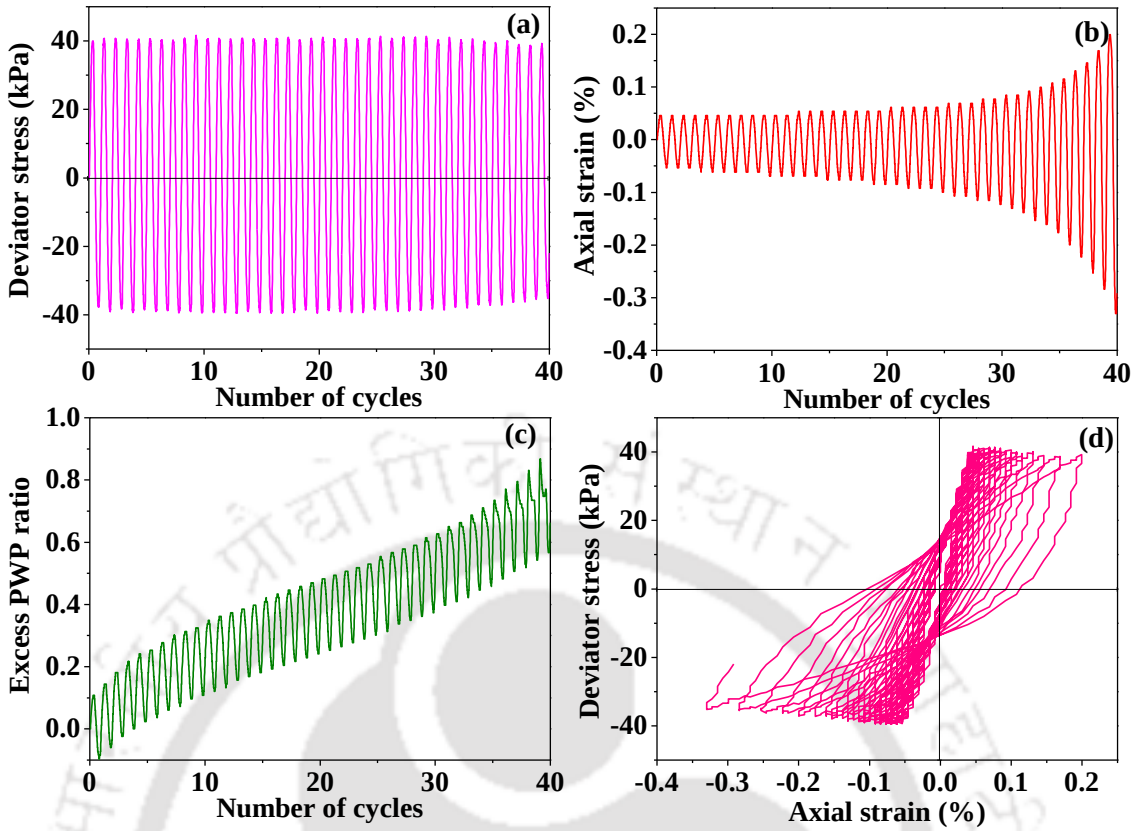

Fig. 5.28 (a-d) Typical test results obtained from stress-controlled cyclic triaxial test of SBS

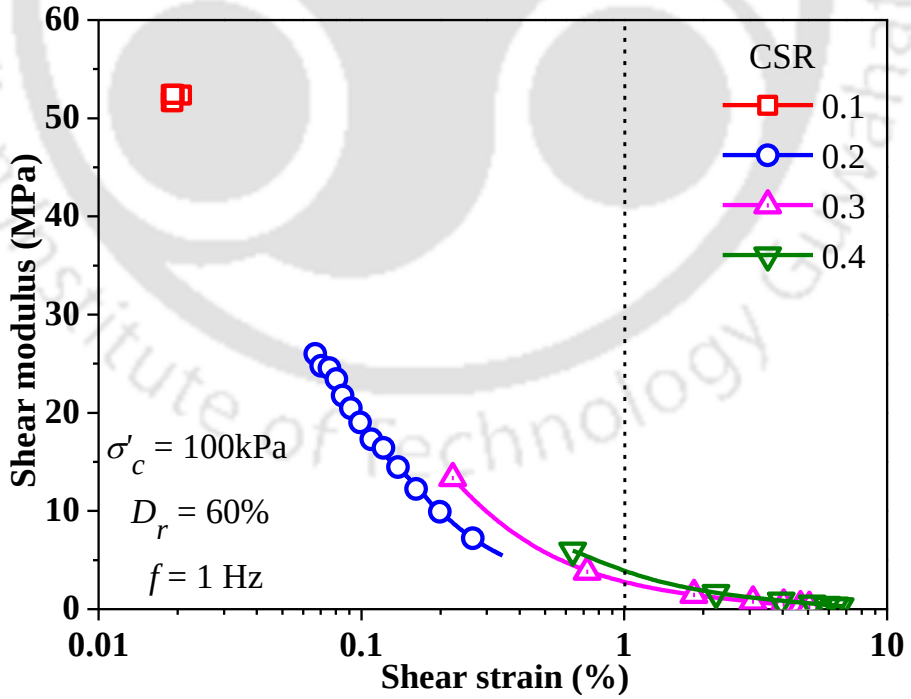

Fig. 5.29 Variation of shear modulus of SBS with shear strain from stress-controlled loading

Fig. 5.30 depicts the variations in damping ratio with shear strain at different CSR ranging from 0.1-0.4. Damping ratio, D and $D^{\#}$, was evaluated based on the both symmetrical and asymmetrical approach, respectively. It is seen that, for CSR = 0.1, D and $D^{\#}$ are almost same, due to the formation of symmetrical hysteresis loop at all 40 loading cycles. At CSR = 0.2, it was been seen that the D and $D^{\#}$ up to γ = 0.2% are nearly same, and beyond γ = 0.2%, D exceeds from $D^{\#}$. This condition arises, when loop is not symmetrical because the symmetrical approach estimates lesser stored strain energy by considering the area of triangle in first quadrant, as shown in Fig. 5.31 and Fig. 5.32, for N = 1 and 23, respectively. Damping ratio calculated by symmetrical approach is overestimated because the area of stored strain energy (calculated by area of triangle) in the first quadrant is less at N = 1 than the third quadrant. However, in strain-controlled approach, D was observed to be lesser than $D^{\#}$ because the area of stored strain energy (calculated by area of triangle) in the first quadrant was higher at N = 1 than the third quadrant, and thus D was underestimated. Thus, based on the both strain-controlled and stress-controlled, it can be stated that the asymmetrical approach can evaluate the precise damping ratio because of the accurate estimation of stored strain energy during the loading cycle. The degradation in damping ratio beyond γ = 1.0% has been observed, which is similar to the strain-controlled cyclic loading.

Fig. 5.33 presents the variations in γ with N at different *CSR*. It is seen that, at CSR = 0.1, the amount of γ till 40 cycles are substantially less i.e. less than or equal to 0.02%, whereas, γ was observed nearly ~ 1.0%, 1.75% and 2.4% for CSR values 0.2, 0.3 and 0.4, respectively. Fig. 5.34 presents the variations in r_u with N at different *CSR*. At CSR = 0.1, the magnitude of r_u is nearly 0.1 at the end of 40 cycles, which is attributed to the development of very low shear strain (almost constant γ = 0.02%). However, at CSR $\geq$ 0.2, significant variation in r_u was observed during cyclic loading, depicted in Fig. 5.34. The excess PWP ratio (r_u) reached 1, at 4^{th}, 7^{th} and 28^{th} number of loading cycles when γ was nearly ~ 1.0%, 1.75% and 2.4% for CSR

values 0.2, 0.3 and 0.4, respectively. Fig. 5.35 presents the development of r_u along with γ accumulation. It shows that r_u increases with the increase in γ and, higher γ poses higher vaue of r_u, for a constant D_r and σ'_c. The accumulation of γ and development of r_u depends on the soil type, stress applied or tests conditions.

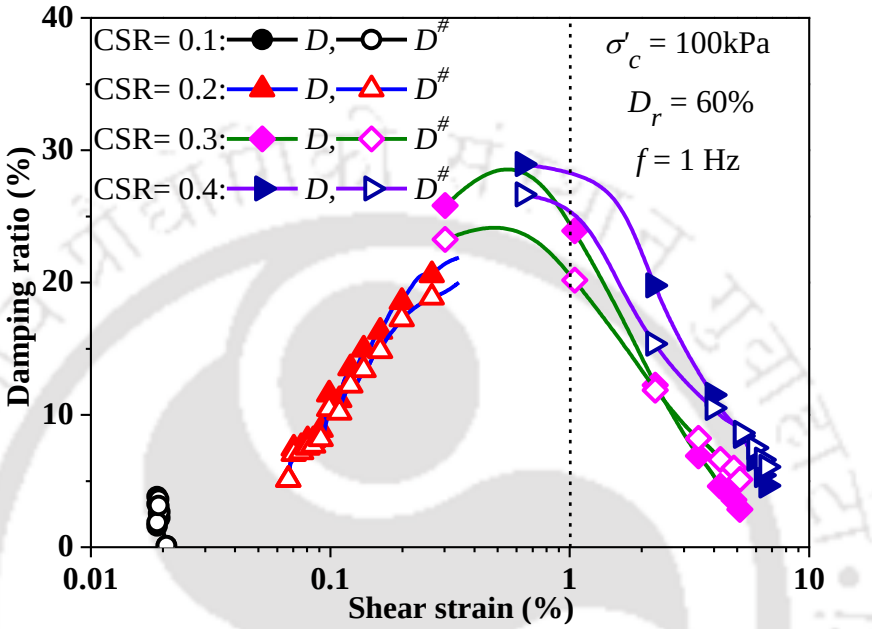

Fig. 5.30 Variation of damping ratio of SBS with shear strain from stress-controlled loading

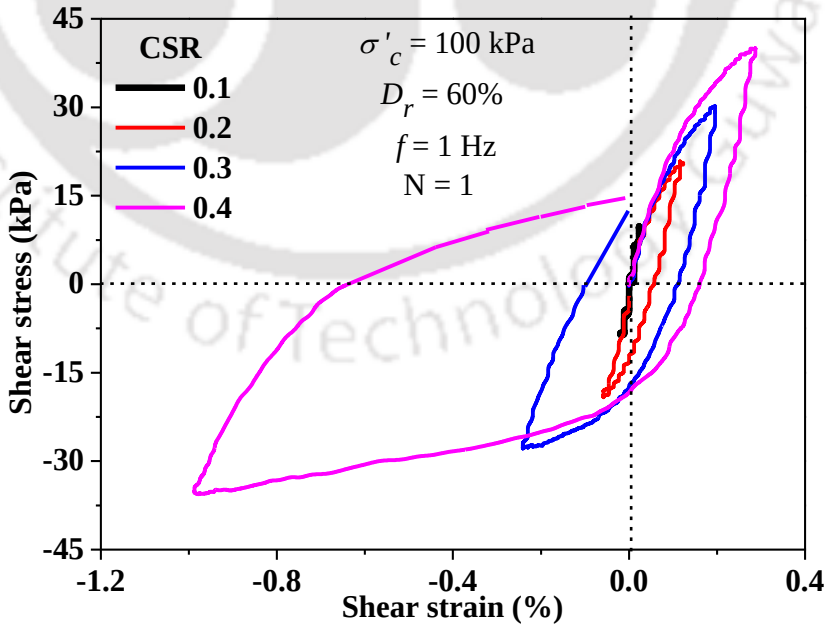

Fig. 5.31 Hysteresis loop at $N = 1$ for different *CSR*

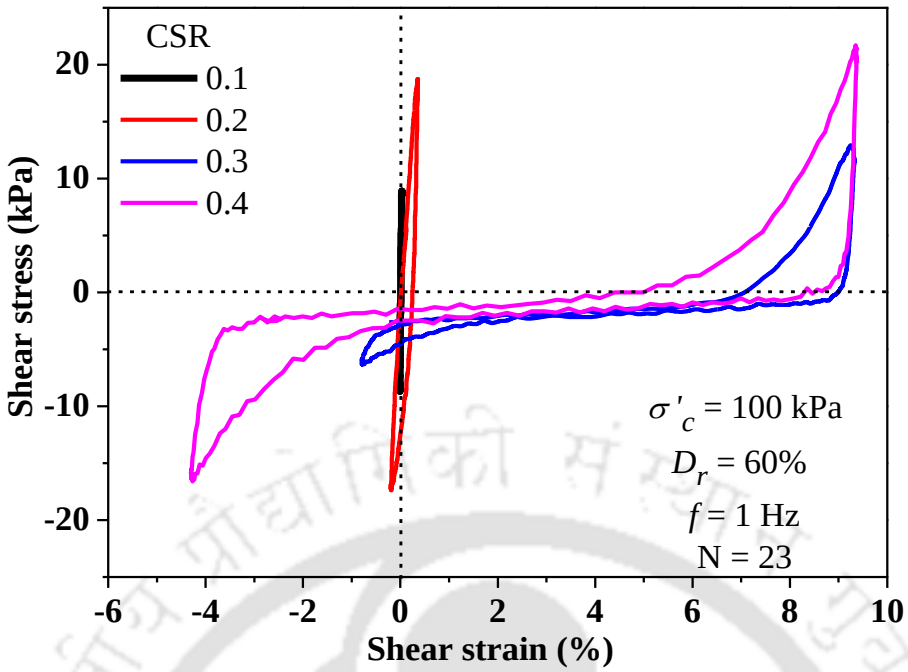

Fig. 5.32 Hysteresis loop at N = 23 for different *CSR*

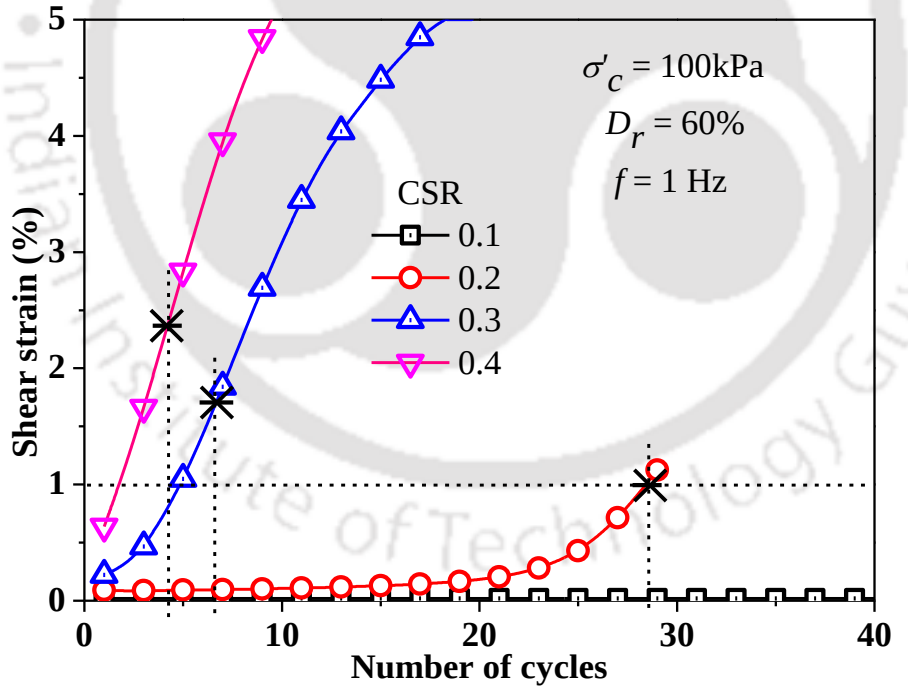

Fig. 5.33 Variation of shear strain with number of cycles for different *CSR*

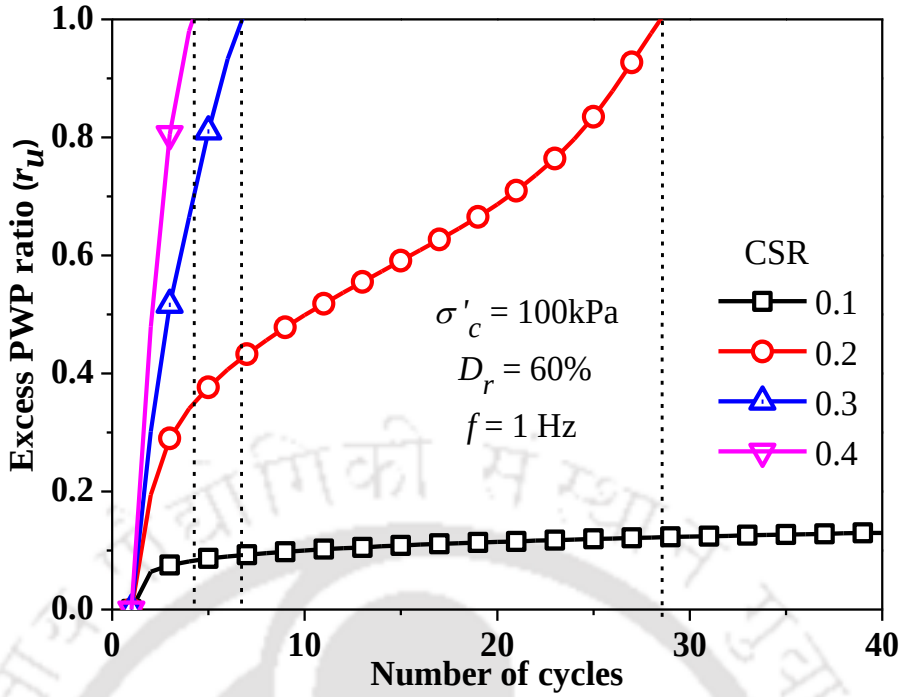

Fig. 5.34 Variation of excess PWP ratio with number of cycles for different *CSR*

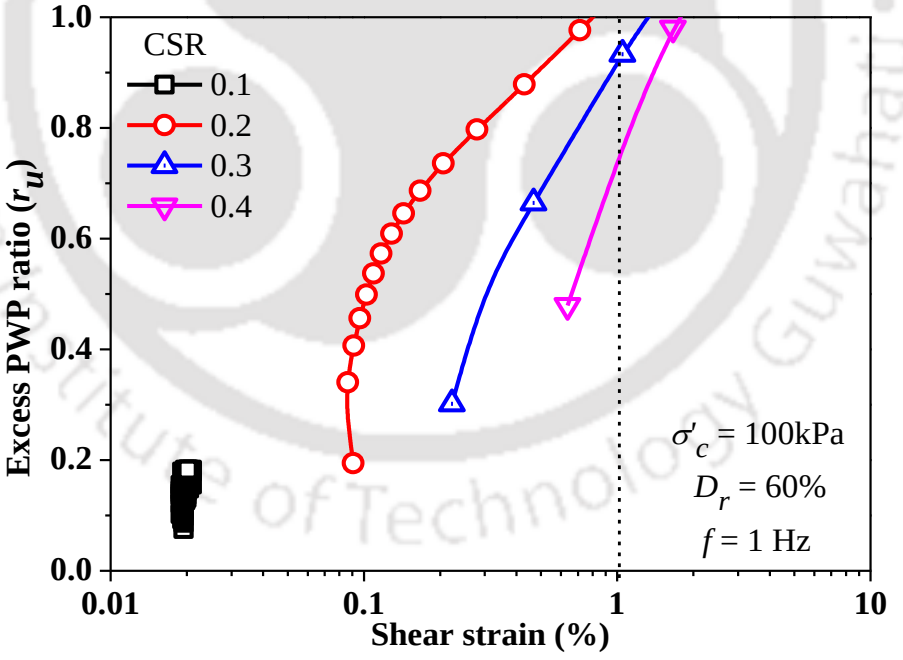

Fig. 5.35 Variation of excess PWP ratio with shear strain for different *CSR*

Effect of loading frequency on stress-controlled dynamic shear properties

The effects of loading frequency on the variations of shear modulus and damping ratio have

also been studied using stress-controlled cyclic loading. Fig. 5.36-Fig. 5.38 depicts the results at different loading frequency ranging from 0.1 Hz to 4 Hz for *CSR* = 0.2 at D_r = 60% and σ'_c = 100 kPa. It is seen from Fig. 5.36, that the shear modulus and damping ratio are significantly affected by loading frequency. It has also been seen that the shear modulus increases up to the frequency of 1 Hz and decreases afterward, whereas damping ratio follow decreasing trend. In contrary to this, Dash and Sitharam (2016) reported that the shear modulus decreases and damping ratio increases with increase in frequency from 0.1 Hz to 0.5 Hz because of the increase in excess pore water pressure from 0.1 Hz to 0.5 Hz at first loading cycle. To observe the effect of excess pore water pressure ratio and shear strain developed on shear modulus and damping ratio at first loading cycle for different loading frequencies, plots are presented in Fig. 5.37.

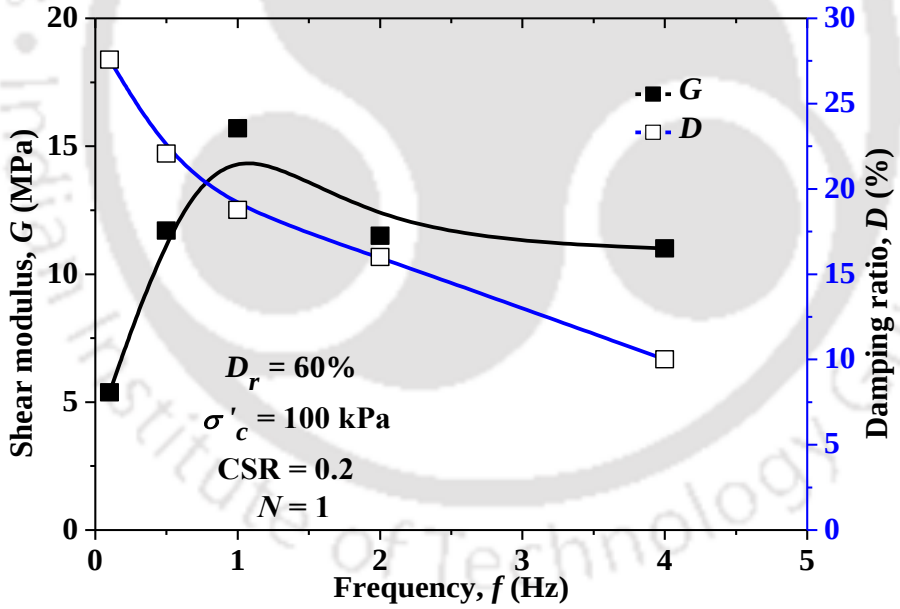

Fig. 5.36 Variations of shear modulus and damping ratio with loading frequency for *N* = 1

It can be seen from Fig. 5.37, that the excess pore water pressure ratio and shear strain, for *f* = 0.1 Hz, are significantly higher than the other frequency resulting lower shear modulus and higher damping ratio. The shear modulus, at *f* = 1 Hz, is higher and corresponding excess pore water pressure ratio and shear strain are lower from other loading frequency. Fig. 5.38

describes that the rate of generation of excess pore water pressure affected significantly by frequency of cyclic loading. The loading frequency of 1 Hz shows lesser rate of generation of excess pore water pressure compared to other frequency.

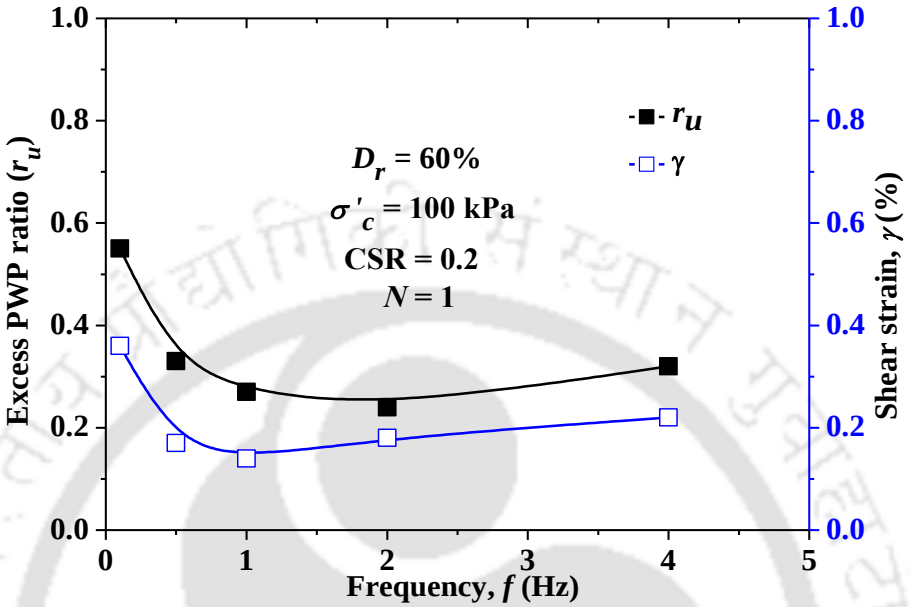

Fig. 5.37 Variations of r_u and shear strain with loading frequency for N = 1

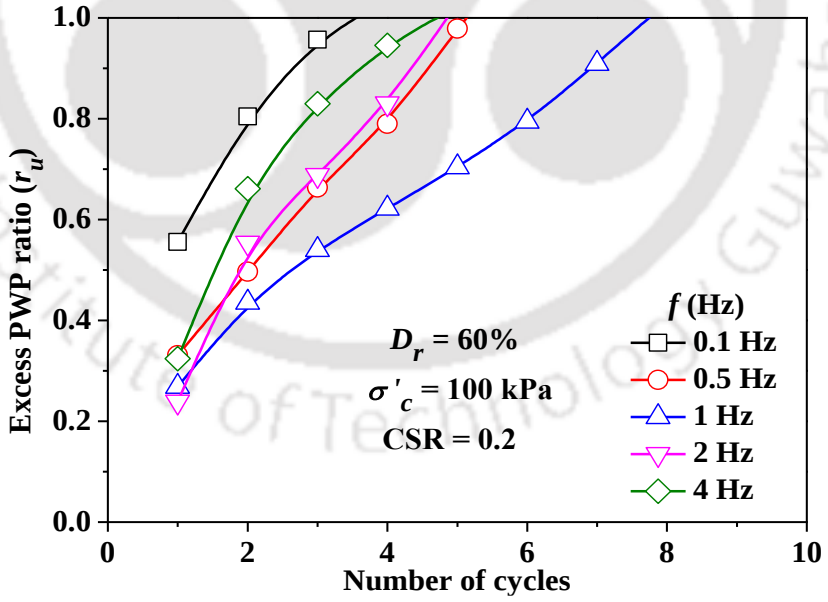

Fig. 5.38 Variations of r_u with number of loading cycles at different loading frequencies

5.3.4 Comparison of strain-controlled and stress-controlled tests results

Fig. 5.39 and Fig. 5.40 presents the variations in shear modulus and damping ratio, respectively,

from strain-controlled tests conducted at different γ (considering only first cycle, N = 1) and from stress-controlled tests conducted for different *CSR* (considering all hysteresis cycles, N = 1-40). Fig. 5.39 presents the variations in shear modulus with γ obtained from both strain-controlled and stress-controlled approach. It is seen that the results follow similar degradation pattern with minimal difference from each other. Fig. 5.40 shows the variations in damping ratio ($D^{\#}$) with γ obtained from both stress-controlled and strain-controlled approach. It can be noted that $D^{\#}$ attains the peak magnitude at $\gamma \approx 1\%$ from both the approaches. From the results of damping ratio variations, it can be concluded that the damping ratio varies with similar trend form both strain and stress-controlled approach, and hence the dynamic soil properties can be evaluated by both the approaches. However, due to asymmetry in hysteresis loop after few loading cycles, the stress-controlled approach misrepresents the precise estimation of dynamic properties. In such condition, strain-controlled approach can give accurate dynamic properties for any constant shear strain amplitudes. Beyond the peak shear strain of 1%, a significant reduction in damping ratio is observed at higher strain levels which are noticeably different from that observed in the damping ratio curves from earlier studies (Seed and Idriss, 1970; Iwasaki et al., 1978; Kokusho, 1980; Seed et al., 1986; Vucetic and Dobry, 1991; Stokoe et al., 1995; Govindaraju, 2005; Kirar and Maheswari, 2013). It should be noted that, for the earlier studies, tests were conducted up to strain levels of about 1% only by strain-controlled approach. Very few researchers have provided the experimental evidence of estimated damping ratio beyond 1% shear strain based on strain-controlled approach which followed a similar trend as obtained in the present study (Kiku and Yoshida, 2000; Brennan et al., 2005; Mashiri, 2014; Matasovic and Vucetic, 1993).

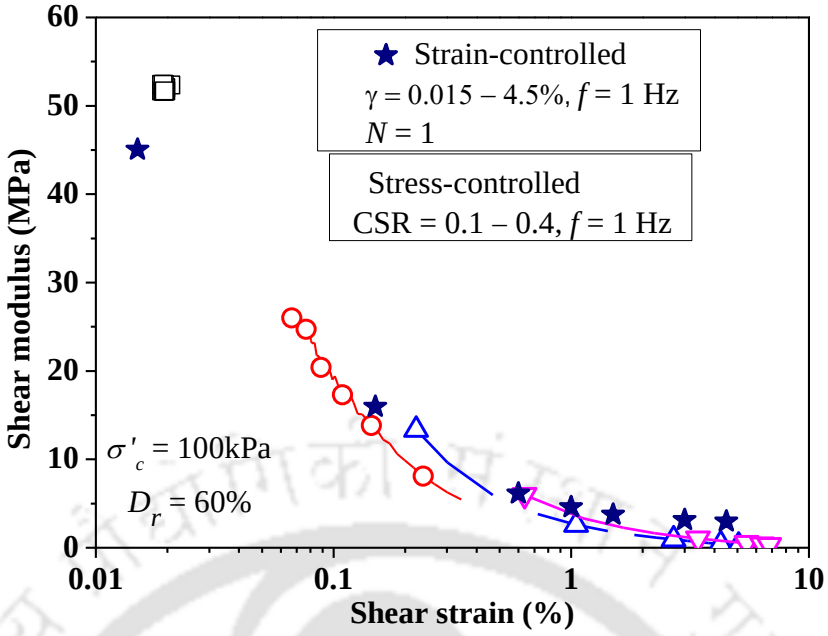

Fig. 5.39 Variation of shear modulus obtained from strain- and stress-controlled excitations

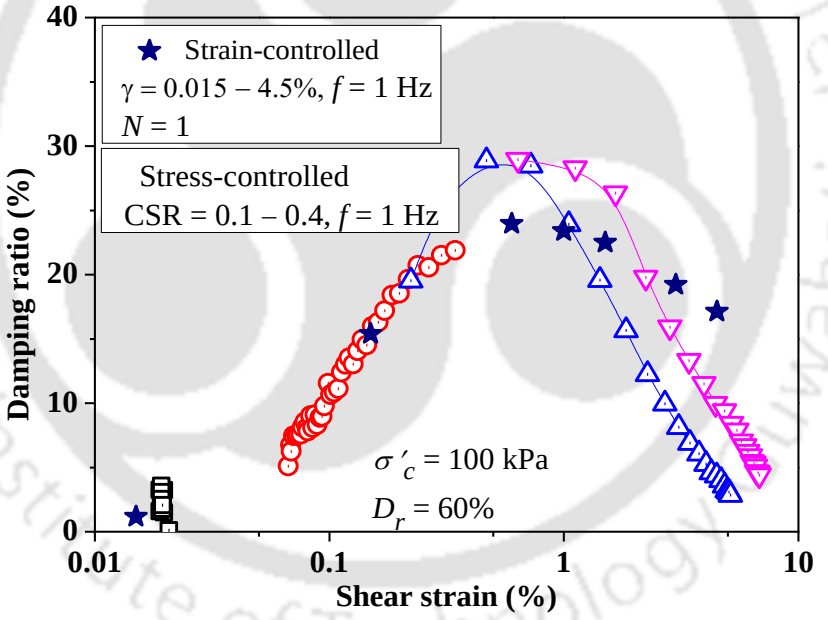

Fig. 5.40 Variation of damping ratio obtained from strain- and stress-controlled excitations

5.4 TESTS ON DRY COHESIONLESS SOIL

Strain-controlled cyclic triaxial tests were conducted on dry cohesionless soil (DBS) specimens. A typical plot of input and output of DBS specimen at an axial strain of 0.20% subjected to f = 1 Hz for 40 cycles and effective confining pressure (σ'_c) of 100 kPa is presented in Fig. 5.41. Fig. 5.41a depicts the applied axial strain on to the specimen. Fig. 5.41b shows the variation of

deviator stress with number of cycles, which is responsible for the increase in stiffness due to particle rearrangement in each loading-unloading cycle. Fig. 5.41c shows the pore water pressure variation; since the soil is dry, the development of excess PWP will be zero. Fig. 5.41d shows the stress path variation because of zero pore water pressure. Fig. 5.41e shows the hysteresis loop during cyclic loading reflects the dissipation of energy only due to friction associated with movement of the sand particles.

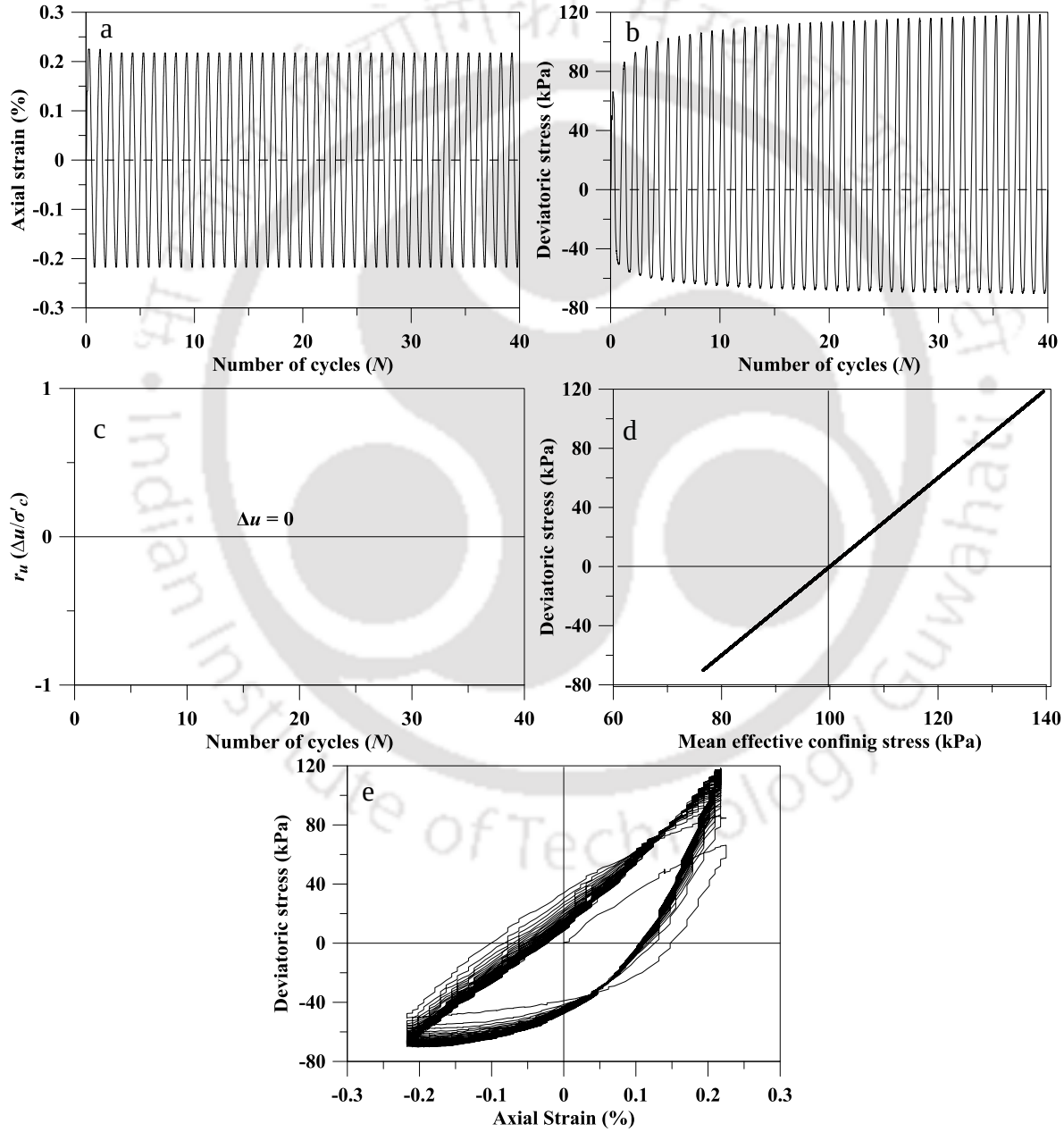

Fig. 5.41 (a-d) Typical test results of DBS at ε = 0.20%, f = 1 Hz and σ'_c = 100 kPa

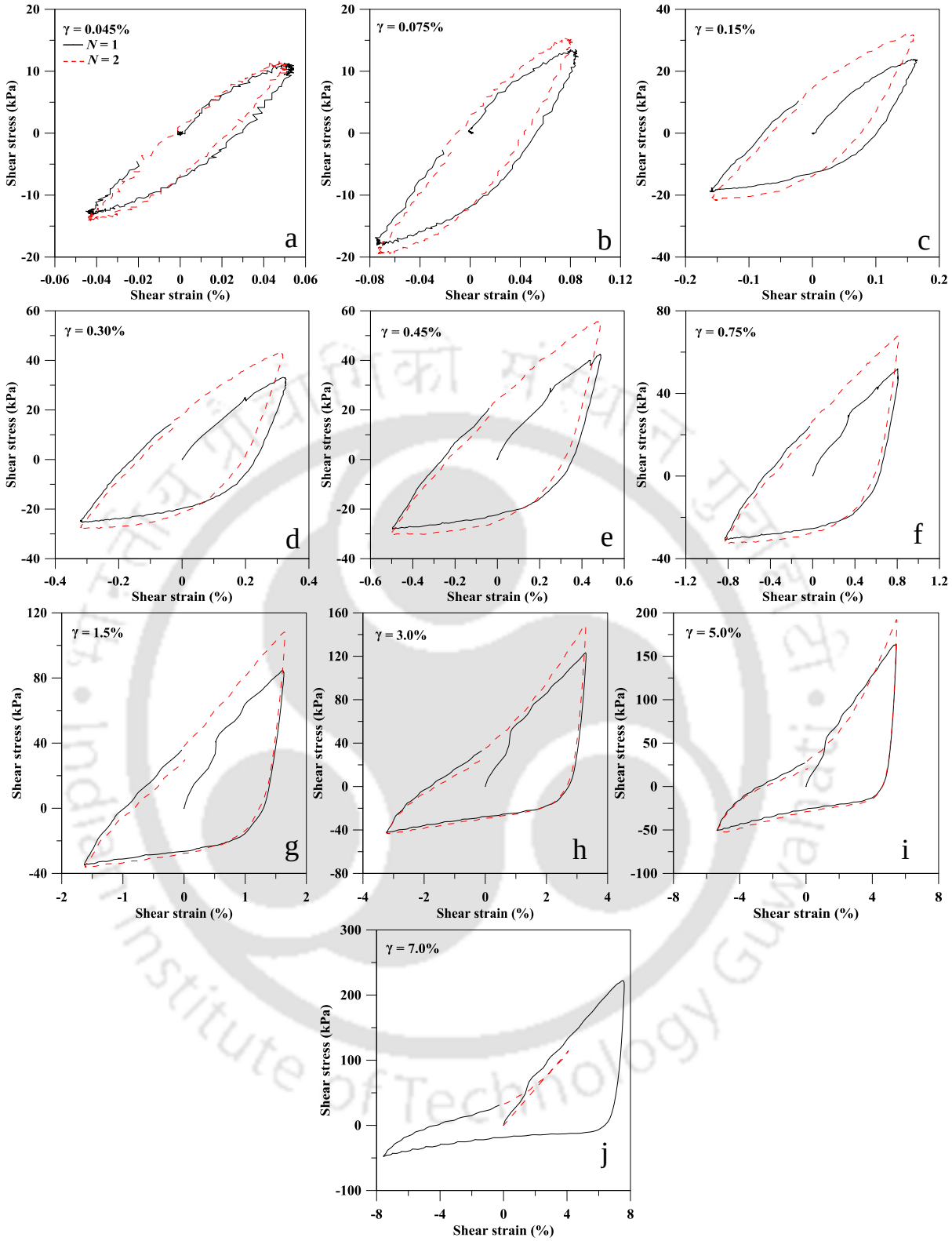

Fig. 5.42 (a-j) Typical shear stress-shear strain plot for SBS at different γ for initial two cycles at D_r = 60%, σ'_c = 100 kPa and f = 1 Hz

Fig. 5.42(a-j) presents the hysteresis loops for initial two cycles obtained from the strain-controlled CT tests conducted on DBS at different peak shear strain levels. It is seen that the

hysteresis loops becomes gradually asymmetric with increasing peak shear strain, similar to the SBS tests. Beyond γ = 0.15%, the 1st cycle hysteresis loop is observed to be asymmetric, as can be noted from the stark dissimilarity in shear stress magnitude in compression and tension side (Fig. 5.42d-j). Thus, in the present study, only the 1st cycle of loading and the corresponding hysteresis loop has been chosen for the evaluation of dynamic properties, as described in section 5.3.1.

Effect of shear strain and confining pressure on dynamic shear properties

The variation of shear modulus and damping ratio of DBS for 1st loading cycle are presented in Fig. 5.43 and Fig. 5.44, respectively. Fig. 5.43 reflects the rapid decrease of shear modulus with the increase of shear strain amplitudes (γ), and increase in the same with the increase of confining pressure at any particular shear strain amplitude.

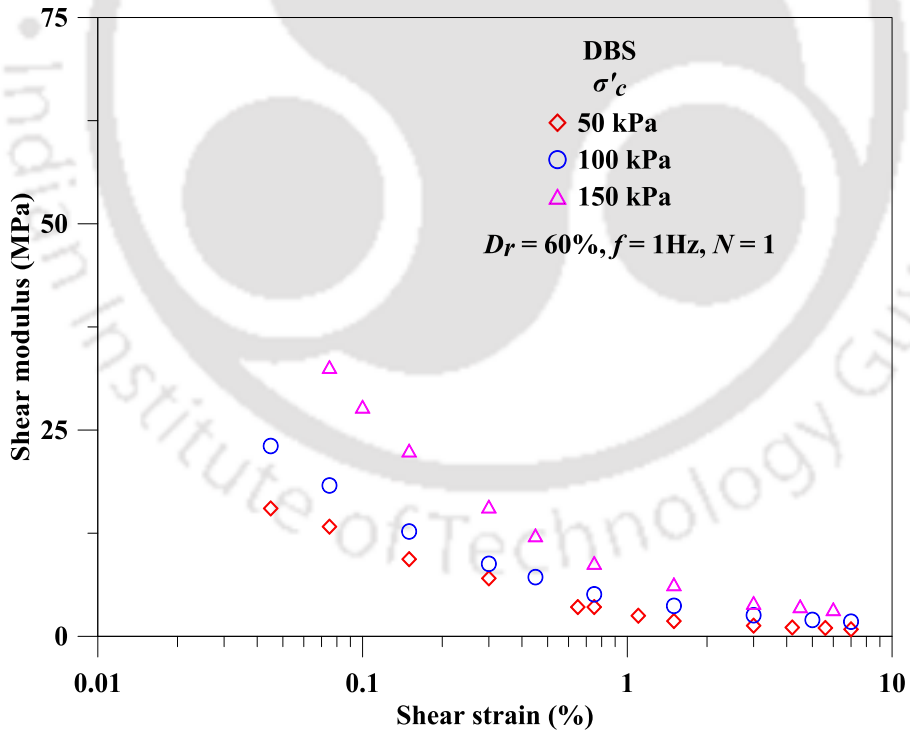

Fig. 5.43 Variation of shear modulus of DBS with shear strain at different σ'_c from strain-controlled tests

Fig. 5.44 indicates that the soil damping is strongly influenced by both the shear strain amplitude and effective confining pressure. It shows the variations in damping ratio of DBS

with shear strain using symmetrical (D) and modified ($D^{\#}$) approach. It has been observed that $D^{\#}$ is significantly higher than D and exhibits an asymptotic trend. The damping ratio (D) exhibits non-conventional behaviour beyond shear strain of 1%. From the scatter plot of D and $D^{\#}$ at σ'_c = 50 kPa, 100 kPa and 150 kPa, it can be stated that the effect of σ'_c is not significant over the tested range of shear strain. Therefore, an average line was plotted for practical purposes. It can be observed that for DBS, $D^{\#}$ is greater than D. The difference between $D^{\#}$ and D is around 20-40% in between the range of shear strain 0.15%-0.50% and this difference increase more than 100% with the increase of shear strain beyond 0.50% (Fig. 5.44).

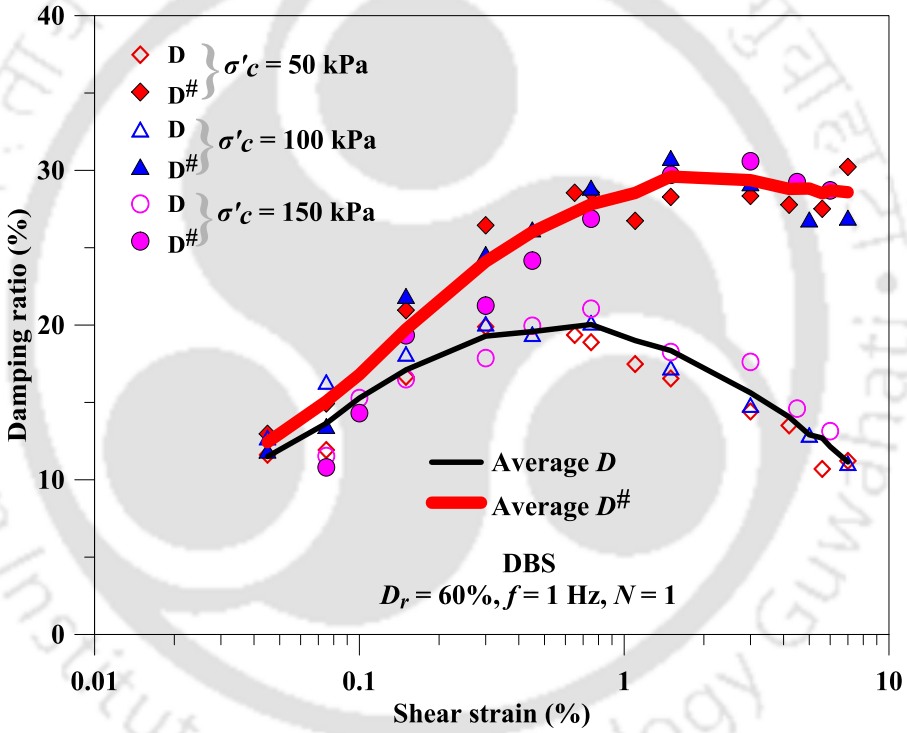

Fig. 5.44 Variation of damping ratio of DBS with shear strain at different σ'_c from strain-controlled tests

5.5 COMPARISON OF STRAIN-CONTROLLED TESTS RESULTS OF DRY AND SATURATED COHESIONLESS SOIL

A typical comparative plot of hysteresis loop obtained for SBS and DBS at two consecutive loading cycles are presented in Fig. 5.45. It describes that the amount of dissipated energy (E_d) of SBS is decreased with increase of loading cycles, i.e. from N = 1 to 2, since excess pore

water pressure increases during loading resulting in the decrease of the effective stress. In DBS, E_d increased with loading cycles, i.e. from N = 1 to 2, since in dry state, the soil particles forms a dense matrix through rearrangement of the particles during cyclic loading. E_d is directly proportional to the area inside of stress-strain loop, as shown in Fig. 5.45.

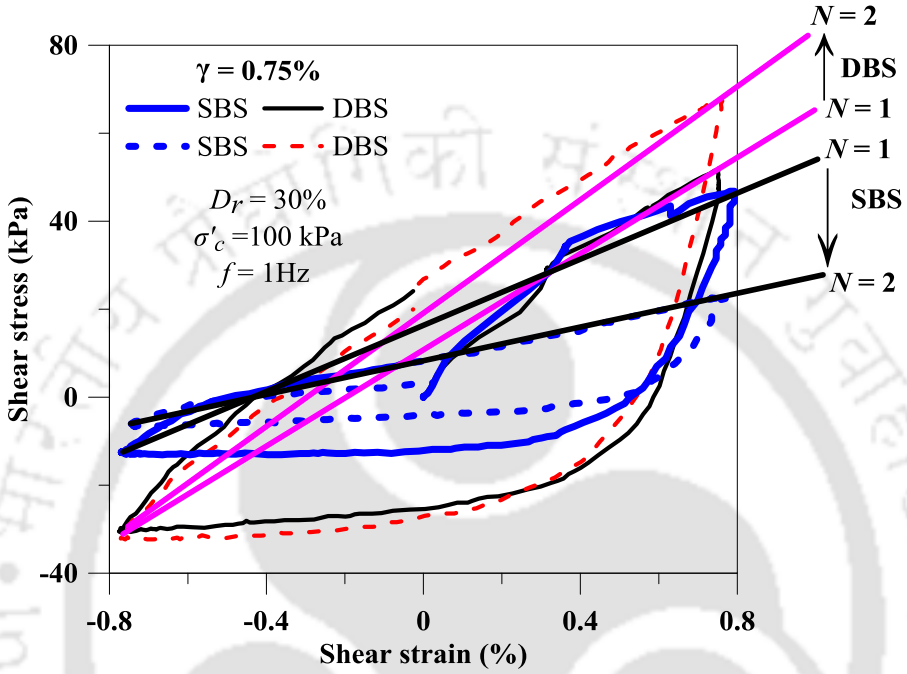

Fig. 5.45 Typical comparative hysteresis loops for SBS and DBS at two consecutive loading cycles (N = 1 to 2)

Effect of loading cycles on shear modulus and damping ratio

The variations of shear modulus of DBS and SBS with number of cycles are presented in Fig. 5.46. According to the Fig. 5.46, the shear modulus of DBS increases with the increase of number of cycles because of the densification of sand during cyclic loading. It is observed from Fig. 5.46 that the shear modulus increases significantly up to 20 cycles, beyond which the effect is marginal. It was also seen that the shear modulus of SBS decreases with the increase of number of cycles due to rise of excess PWP. The rise of excess PWP under undrained condition causes reduction of stiffness due to the loss of inter-granular contact between the particles. On the contrary, no generation of PWP in DBS result in increase of shear modulus due to densification of the dry soil. It can be noted that the shear modulus (for γ = 0.15%) of DBS and

SBS is nearly of same magnitudes at the first loading cycle, which indicates that the generation of excess PWP negligibly affects the shear modulus of sand at first cycle.

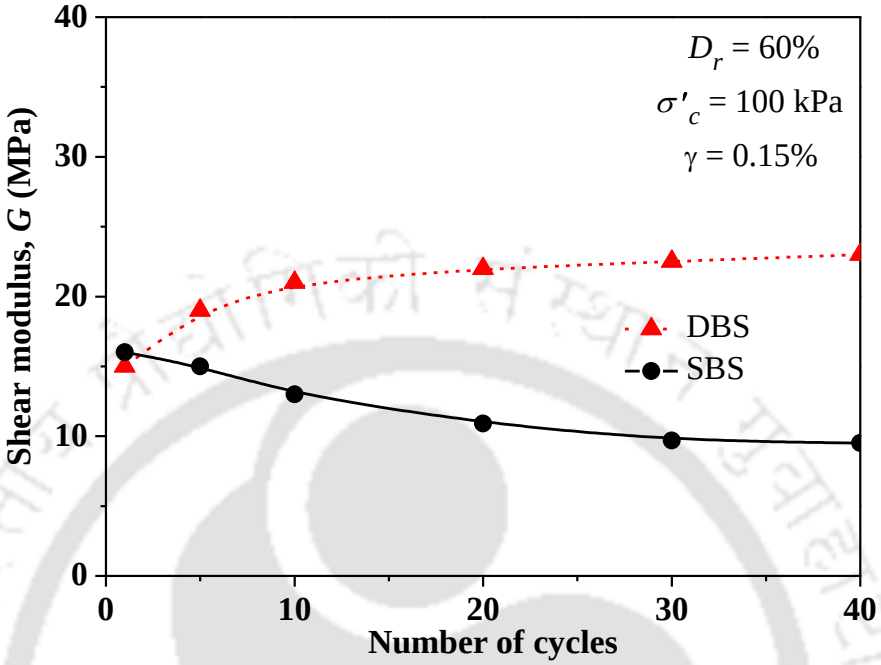

Fig. 5.46 Comparative variation of shear modulus for SBS and DBS with number of cycles from strain-controlled tests

The variation of damping ratio with number of cycles for DBS and SBS specimens are presented in Fig. 5.47. Fig. 5.47 indicates that the damping ratio of DBS decrease with number of cycles, which is conversely to the trend of carination of shear modulus of DBS with number of cycles. It clearly means that the damping ratio of soil decreases with the increase of soil stiffness. The damping ratio obtained from modified method is higher than conventional method. In Fig. 5.47, the variation in damping ratio of SBS with number of cycles has also been presented. It can be observed that the damping ratio of SBS decreases initially till 15 cycles, and then marginally increases; this is attributed to the development of excess PWP and consequently initiation of liquefaction at the 15th cycle. It can also be stated from Fig. 5.46 and Fig. 5.47 that the shear modulus and damping ratio of SBS at any particular cycles, depends on the excess PWP build up at that particular cycle.

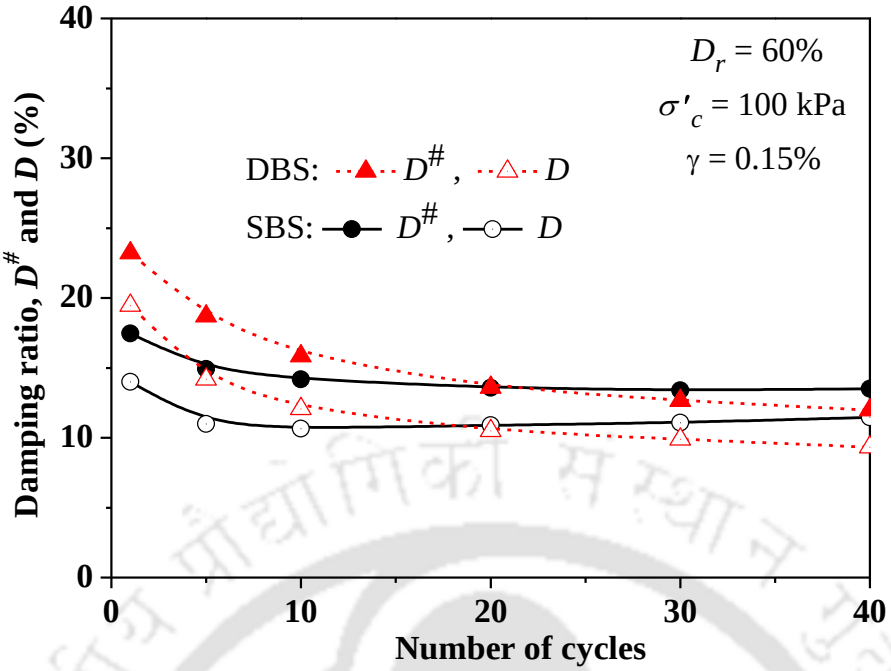

Fig. 5.47 Comparative variation of damping ratio for SBS and DBS with number of cycles from strain-controlled tests

Effect of shear strain and confining pressure on shear modulus

The variations in shear modulus of DBS and SBS are presented in Fig. 5.48, which emphasizes that for both the cases, the trend of variation of shear modulus with shear strain amplitudes and confining pressure are almost the same. Fig. 5.48 clearly indicates that the effect of saturation of the shear modulus is insignificant. Fig. 5.49 depicts the variations of G/G_{max} of both DBS and SBS. It shows that the variation of G/G_{max} is in very narrow range of scatter for 1st loading cycle. It can be observed from Fig. 5.48 and Fig. 5.49 that, the shear modulus (G) and modulus reduction (G/G_{max}), respectively, are negligibly affected by saturation at 1st loading cycle.

Effect of shear strain and confining stress on damping ratio

Fig. 5.50 presents the effects of γ and σ'_c on damping ratio of SBS obtained for first cycle, whereas Fig. 5.51 presents the same for both DBS and SBS. Fig. 5.50 indicates that the soil damping ratio is strongly influenced by γ, whereas marginally by σ'_c (for the tested range 50 kPa-150kPa). It also shows the variations in damping ratio for SBS with shear strain using

symmetrical (D) and modified ($D^{\#}$) approach. It is seen that $D^{\#}$ of SBS is greater than its D. The difference between $D^{\#}$ and D is nearly 0-30% in between the range of shear strain 0.015%-4.5%. Fig. 5.50 also reflects that $D^{\#}$ exhibits non-conventional behaviour beyond shear strain of 1% whereas the same has not been observed for DBS, as shown Fig. 5.44. Similar observations on the damping ratio of saturated sand have also been reported by few researchers (Kiku and Yoshida, 2000; Rollins et al., 1998). This significant reduction in damping ratio may be due to high pore-water pressure generation in first cycle causing significant loss in frictional energy in sand skeleton because of the reduction in inter-particle contacts at these high shear strains (Matasovic and Vucetic, 1993; Mashiri, 2014). Fig. 5.51 presents the comparative plot of the variations in $D^{\#}$ for both DBS and SBS. It shows that the $D^{\#}$ of DBS is greater than SBS. The difference in $D^{\#}$ of DBS and SBS is nearly 5% at γ = 0.045% and increased with increase in γ (up to γ = 5%). Thus, it can be stated that that the saturation significantly affects $D^{\#}$ at high strain level.

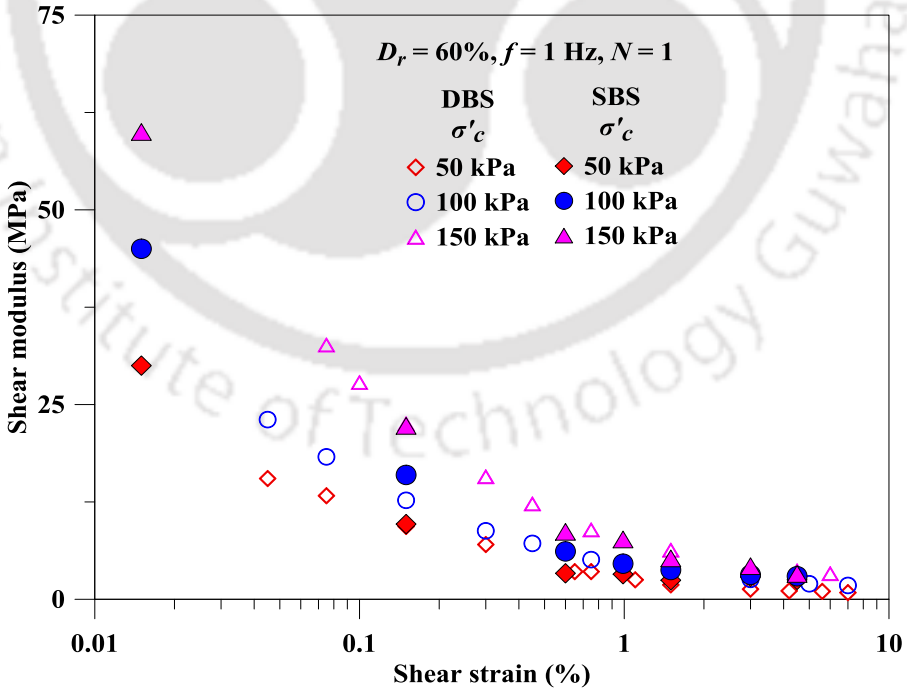

Fig. 5.48 Comparative variation of shear modulus for DBS and SBS with shear strain at different σ'_c from strain-controlled tests

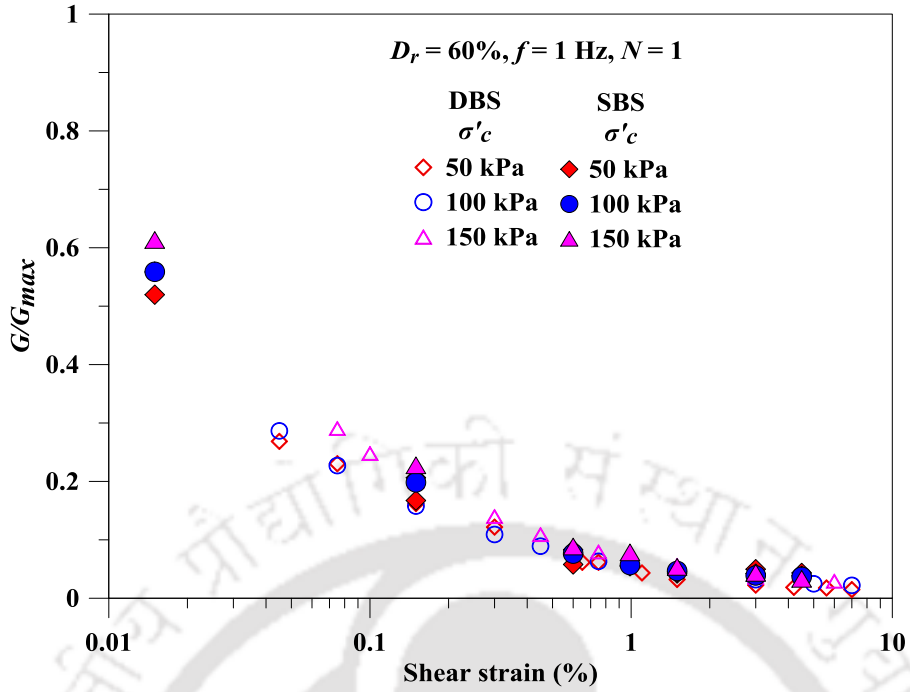

Fig. 5.49 Comparative variation of modulus reduction for DBS and SBS with shear strain at different σ'_c from strain-controlled tests

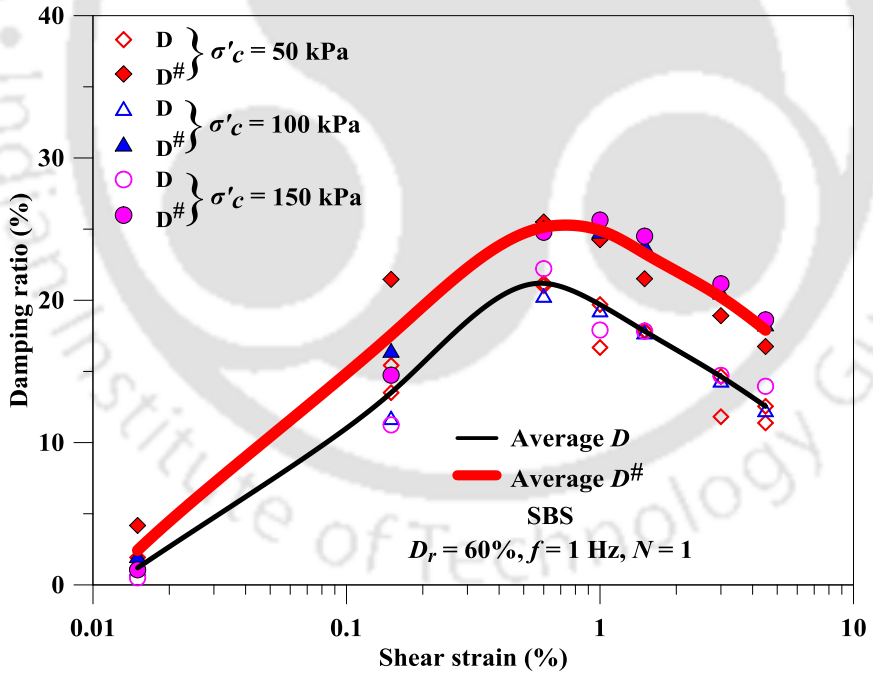

Fig. 5.50 Variation of damping ratio of SBS with shear strain at different σ'_c from strain-controlled tests

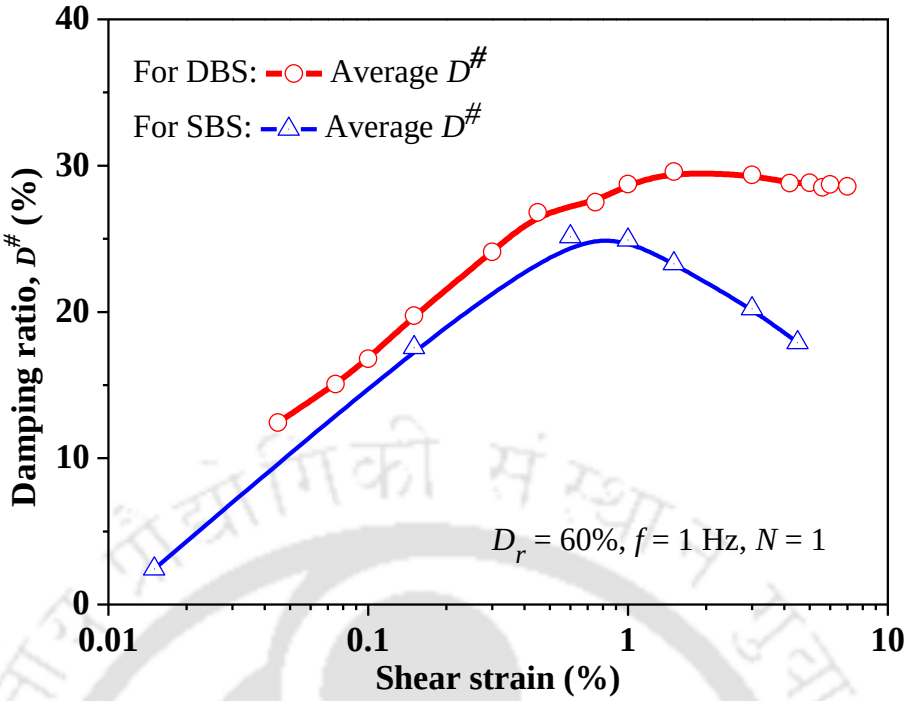

Fig. 5.51 Comparative variations in damping ratio for DBS and SBS from strain-controlled tests

Comparison with Seed and Idriss (1970) model

The experimentally obtained results of modulus ratio (G/G_{max}) and damping ratio (D and $D^{\#}$) is compared with the Seed and Idriss (1970) results and are presented in in Fig. 5.52 and Fig. 5.53, respectively. Seed and Idriss (1970) has given a range of shear modulus and damping ratio curves for sandy soil which is frequently used in software like SHAKE2000 (Ordonez, 2011) and DEEPSOIL (Hashash et al., 2016) for ground response analysis. It can be observed from Fig. 5.52 that in an average, the Seed and Idriss (1970) model overestimate the modulus reduction values by nearly 80%. Fig. 5.53 depict the variations in damping ratio ($D^{\#}$) of DBS and SBS with shear strain and also compared with Seed and Idriss (1970). It can be observed that the damping ratios (D and $D^{\#}$) of both DBS and SBS, evaluated from asymmetrical approach, are accommodated within the range of Seed and Idriss (1970) up to shear strain of 1%. It is seen that $D^{\#}$ of DBS is higher than $D^{\#}$ of SBS, in the order of 5-20% from γ = 0.045-1%, while the difference is greater 70% for γ greater than 1%. However, D of DBS shows higher values than that of SBS in the γ range 0.045-1%. Fig. 5.53 also shows that D of both DBS and

SBS obtained by conventional approach is negligibly affected by saturation for γ beyond 1%.

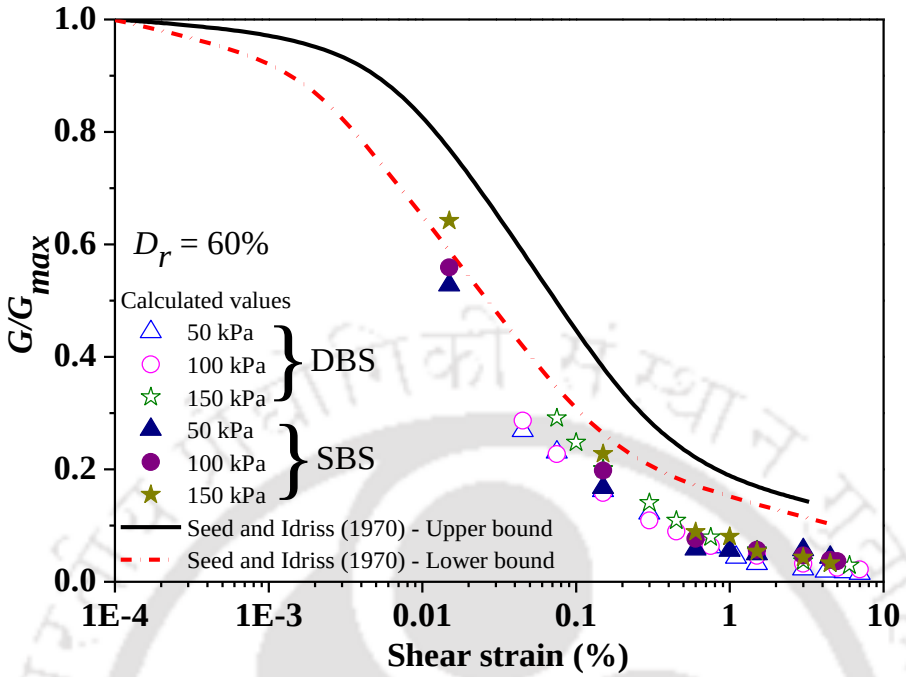

Fig. 5.52 Comparative modulus reduction curves obtained from present investigation and existing literatures

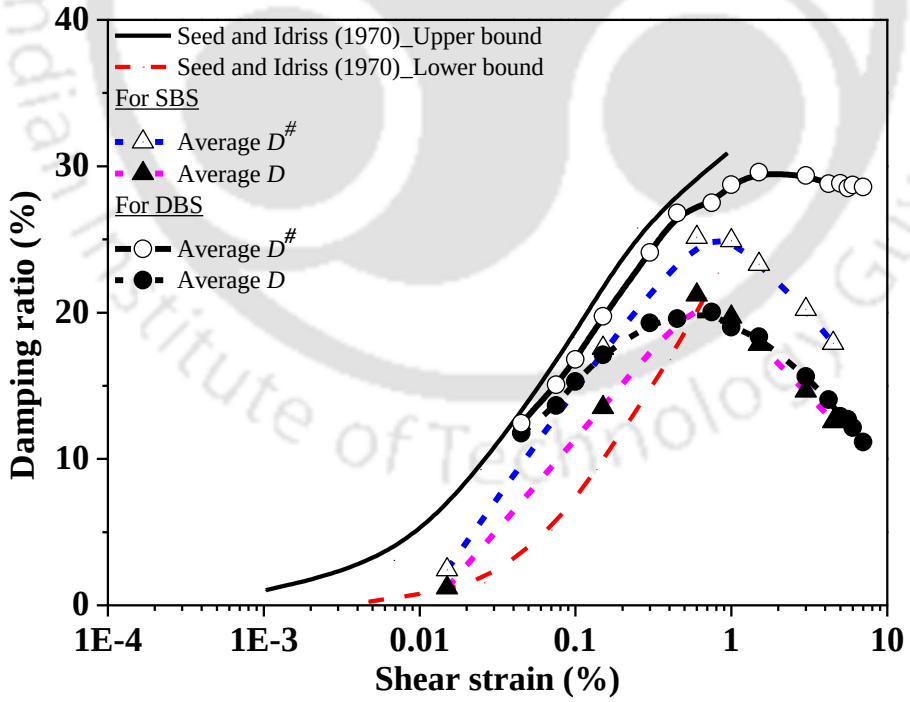

Fig. 5.53 Comparative damping ratio curves obtained from present investigation and existing literatures

From both the Fig. 5.52 and Fig. 5.53, it can be stated that even though the standard soil curves are in practice for common purposes, the dynamic characterization of soil for any particular site is necessary to be estimated and correspondingly, the estimated values should be used for conducting seismic studies.

5.6 TESTS ON COHESIVE SOIL

Stress-controlled cyclic loading tests have been conducted to evaluate the shear modulus and damping ratio of cohesive soil. Since, strain-controlled test requires a new test specimen for each constant peak strain amplitudes, the stress-controlled loading is a good choice to evaluate the dynamic properties of soil, where a single test specimen can be subjected to various strain levels. In this study, staged loading were applied on the specimens in stress-controlled manner as presented in Fig. 5.54. Yoshida (2015) has also reported that the single stage test (i.e. strain-controlled test) is not performed in Japan for engineering practice, because it requires many test specimens. In other word, staged-loading represents the realistic approach to evaluate the dynamic response and properties of soil, since, the same soil can experience different stress levels, either due to the main shock followed by significant aftershocks, or minor foreshocks followed by main shock during an earthquake event.

A typical plot of the response of cohesive soil during staged loading is presented in Fig. 5.55. It reflects that with the increase of shear strains, the shear modulus of cohesive soil decreases, while the damping ratio increases. The increase in pore water pressure with shear strains has also been observed, however a reduction in the pore water pressure is noticed at the time gap between staged loadings. This is attributed to time gap between the subsequent stages, in which there remains ample possibility of the redistribution of excess pore water pressure within the soil sample.

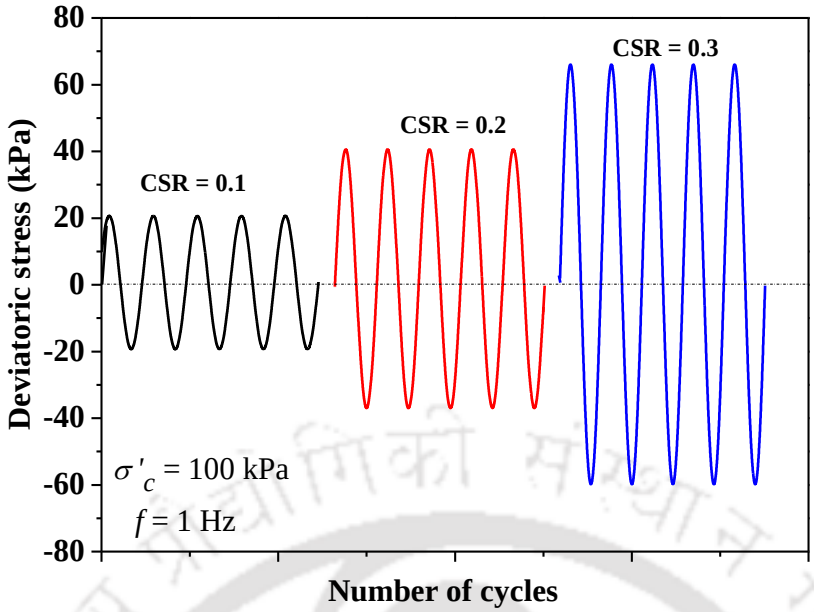

Fig. 5.54 Stress-controlled stage cyclic loading applied on RS specimen

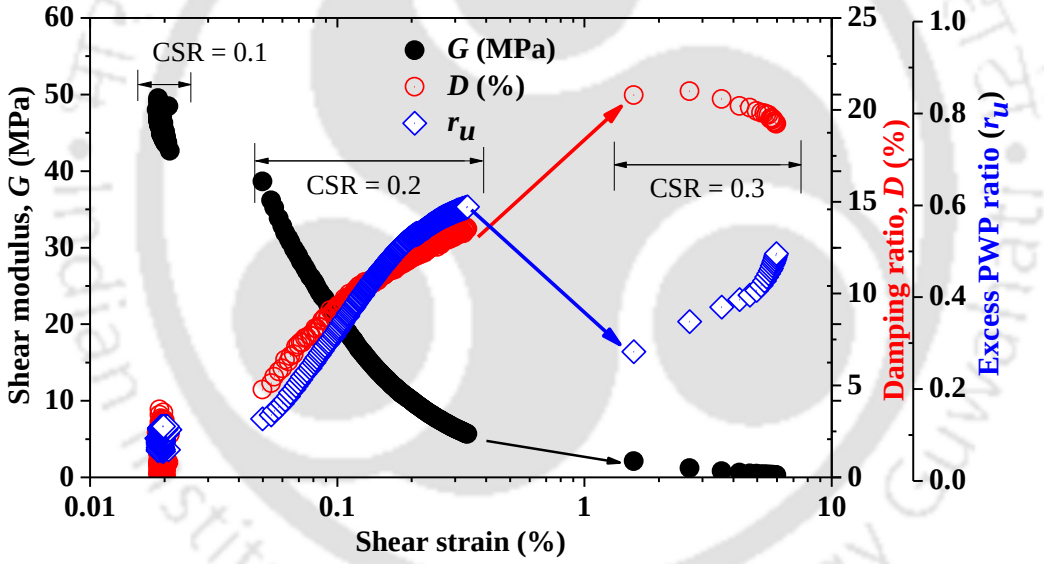

Fig. 5.55 A typical representation of the variations of G, D and r_u obtained from stage cyclic loading of RS specimen

Stress-controlled tests has been conducted at different cyclic shear stress amplitude ranging from 20 kPa to 80 kPa, represented by CSR = 0.1-0.4. The tests have been conducted at σ'_c = 100 kPa, with loading frequency of 1 Hz, on the specimens prepared at varying water content and dry density. Similar methodology like sandy soil, explained earlier, has been adopted to evaluate the dynamic shear modulus (G) and damping ratio ($D^{\#}$) of cohesive soil. Fig. 5.56 represents the shear stress-strain hysteresis loop at different number of loading cycles

i.e. from N = 1–20. It has been seen that the hysteresis loops obtained from stress-controlled at different number of loading cycles are almost symmetrical for N = 1–10 beyond which there is a development of asymmetric nature of the loop.

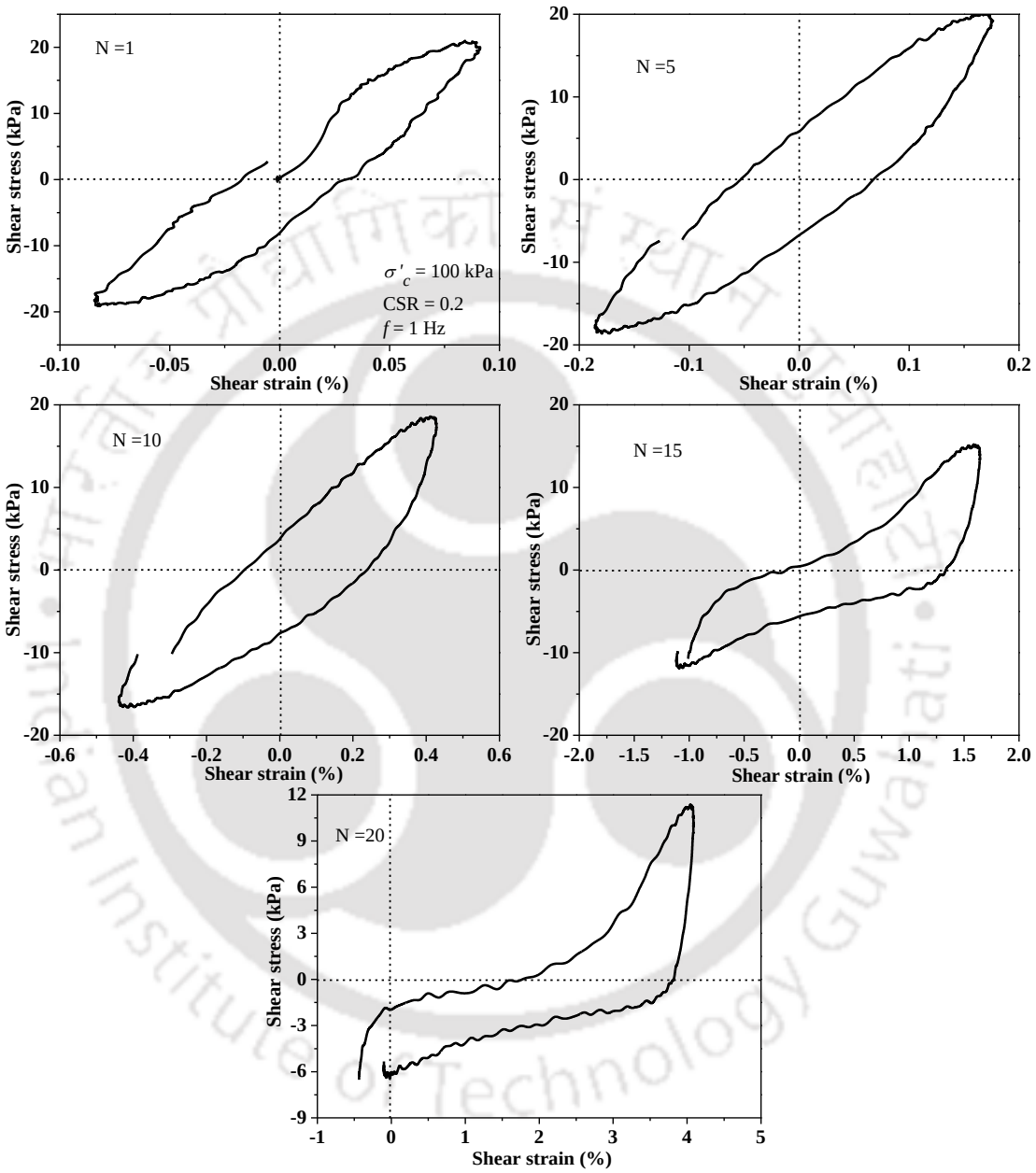

Fig. 5.56 Hysteresis loop obtained at different loading cycles in stress-controlled loading of RS specimen

Fig. 5.57 depicts that the variation in shear modulus obtained from stress-controlled stage loading. It is observed that the compaction state of RS has negligible effect on its shear modulus. Fig. 5.58 presents the modulus reduction and damping ratio curves for RS. To obtain the

normalized modulus reduction curve, presented in Fig. 5.58, G_{max} for RS has been evaluated from the empirical correlation proposed by Hardin and Drnevich (1972). The evaluated modulus reduction curve and damping ratio of RS soil can be applicable for ground response analysis. In this study, the average values of both modulus reduction and damping ratio curve have been used further in ground response analysis.

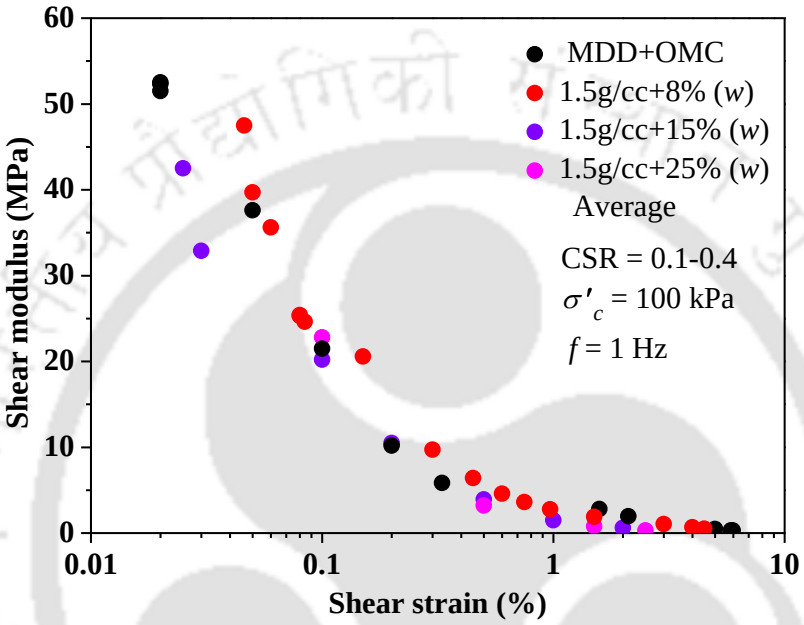

Fig. 5.57 Variation of shear modulus of RS obtained from stress-controlled tests

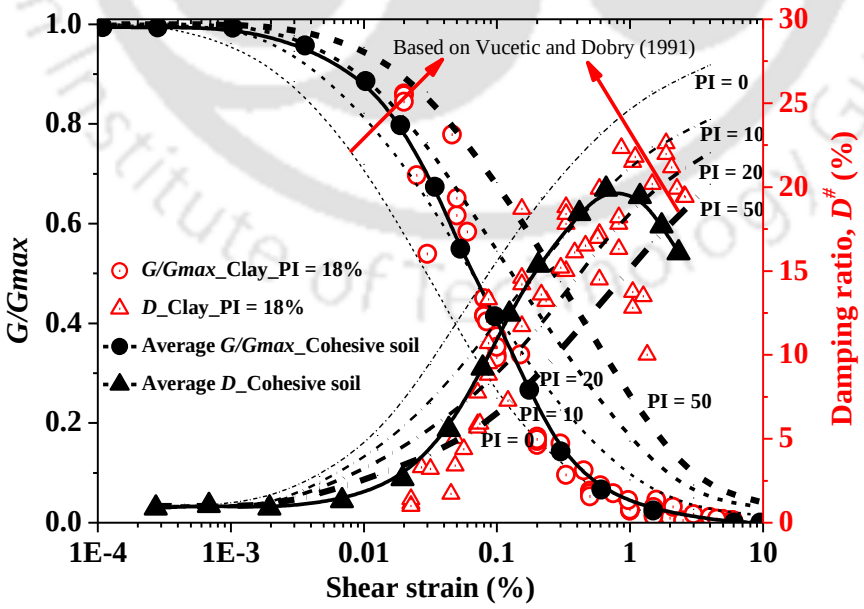

Fig. 5.58 Variation of G/G_{max} and damping ratio of RS obtained from stress-controlled tests

5.7 SUMMARY

Strain and stress-controlled cyclic triaxial tests have been conducted on cohesionless and cohesive soil to evaluate the dynamic properties at a wide range of shear strains. Hysteresis loops at different loading cycles manifested the dynamic behaviour of the soil and exhibited noticeable asymmetric nature especially at higher strain levels. Since conventional methods do not account for such asymmetry in the estimation of the dynamic properties of the soil, a modified method of the evaluation of the same has been adopted. It is observed that, on an average $D^{\#}$ (damping ratio based on the asymmetrical hysteresis loop) exceeds D (damping ratio based on the symmetrical hysteresis loop) by 40-70%, with higher deviation exhibited at higher strain levels beyond 0.50%. On-sample LVDTs emphasized the variations in soil stiffness and locally mobilized strains due to elemental response of soil particles. The local strain measurements were able to determine the shear modulus and damping ratio of the specimen for a wide range of strain, encompassing both low-strain (~3×10^{-3}%) and high-strain (~5%) ranges.

Chapter 6 CYCLIC SHEAR TESTS: LIQUEFACTION EVALUATION

6.1 INTRODUCTION

Any cyclic loading on saturated soils initiates the development of excess pore water pressures which will affect the effective stresses and there by the strength of the soil. Complete loss of shear strength due to the development of excess pore water pressures (PWP) i.e., liquefaction condition is the major contributor in earthquake related damages. This chapter deals with the liquefaction evaluation of sandy soil using regular and irregular seismic excitations through strain-controlled and stress-controlled cyclic triaxial tests. The obtained results are presented in terms of variations of PWP and shear strain with loading cycles.

6.2 TESTING PROGRAM

To evaluate the liquefaction potential of BS soil, cyclic triaxial tests were conducted in strain- and stress-controlled approach with regular and irregular excitations. The test parameters of strain- and stress-controlled tests with regular excitations were mentioned in Table 5.1 and Table 5.2, respectively. Test parameters for stress-controlled tests with irregular excitations were listed in Table 3.7.

6.3 STRAIN-CONTROLLED TESTS WITH REGULAR EXCITATIONS

Regular excitation is a simple and approximated way to find the behaviour of soils under actual irregular excitations. This section discusses the results in terms of excess PWP and cyclic stress ratio (CSR), obtained from the strain-controlled cyclic tests at different γ, σ'_c and D_r (40 cycles at f = 1 Hz). Excess PWP is finally presented in terms of normalized PWP ratio, $r_{u,}$ (= PWP/ σ'_c). The effect of these parameters on the response of the soil sample subjected to a cyclic strain-controlled approach have been discussed.

Variations in r_u with number of cycles at different γ, σ'_c and D_r

Fig. 6.1 shows the cyclic variations in r_u with number of cycles (N) at different γ for D_r = 30% and σ'_c = 100 kPa, which indicate nonlinear increase of excess PWP with number of cycles. For shear strain value of 0.3%, r_u value reached one at about 12 cycles, indicating the attaining the liquefaction state. For shear strain values of 0.045% and 0.075%, the generated excess PWP ratios are within 0.6. The figure also shows that, though the average (or maximum) r_u values are increased with shear strain, the cyclic variations of r_u at any cycle are decreased with the increase in shear strain value. The dotted lines present the maximum value of excess PWP, which has been further used in the analysis and corresponding interpretations. It can be observed that the probability of soil liquefaction increases with the increase of γ and N. In other words, at any particular σ'_c, for identical N, the tendency of the specimen to liquefy the specimen increases with the increase in applied γ at any particular σ'_c. It has been observed that the higher γ results in quicker initiation of liquefaction, i.e. the condition r_u = 1 is attained in lesser N.

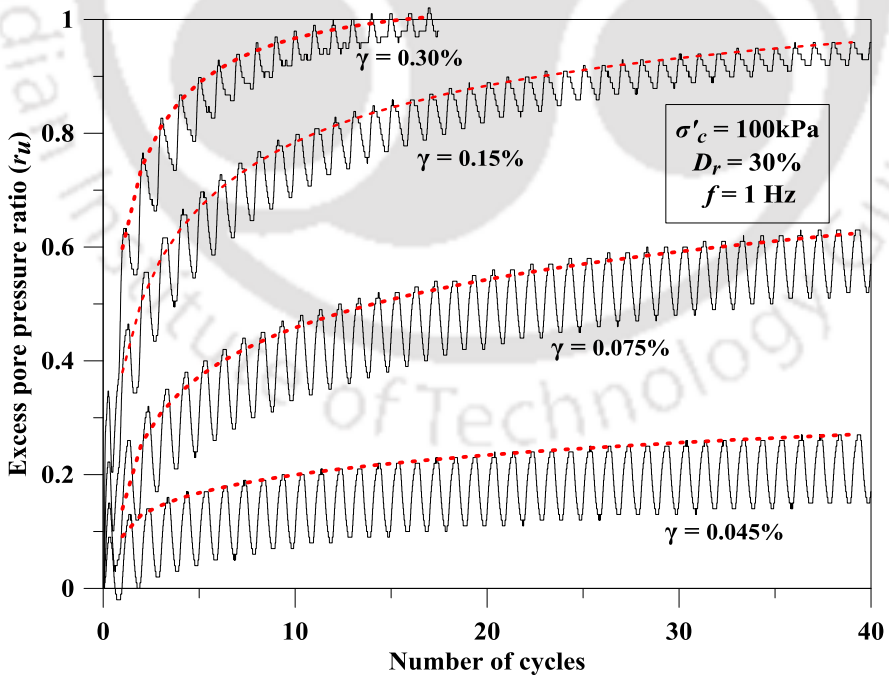

Fig. 6.1 Variation of r_u with N from a cyclic strain controlled test of SBS

Fig. 6.2 presents the variation in maximum r_u in each cycle with N at different γ. It shows

that with the increase in γ, i.e. from 0.045% to 0.75%, the liquefaction resistance decreases. The r_u value was observed to be nearly 0.2, 0.55, 0.95, 1, 1, 1 and 1 at γ = 0.045%, 0.075%, 0.15%, 0.30%, 0.45%, 0.60% and 0.75%, respectively. Tests were also conducted at γ > 0.75% as listed in Table 3.5 of Chapter 3, which showed that the BS specimen, prepared at D_r = 30% and subjected to σ'_c = 100 kPa, attains $r_u \geq 0.90$ in 1st cycle for $\gamma \geq 0.75\%$. This show the onset of liquefaction at the very 1st cycle. It can also be noted that more number of cycles (N) are required to initiate liquefaction for soil specimen subjected to γ less than 0.60%. Similar responses were observed for the specimen prepared at D_r = 60% and 90%, when soil specimens subjected to σ'_c = 50 kPa and 150 kPa.

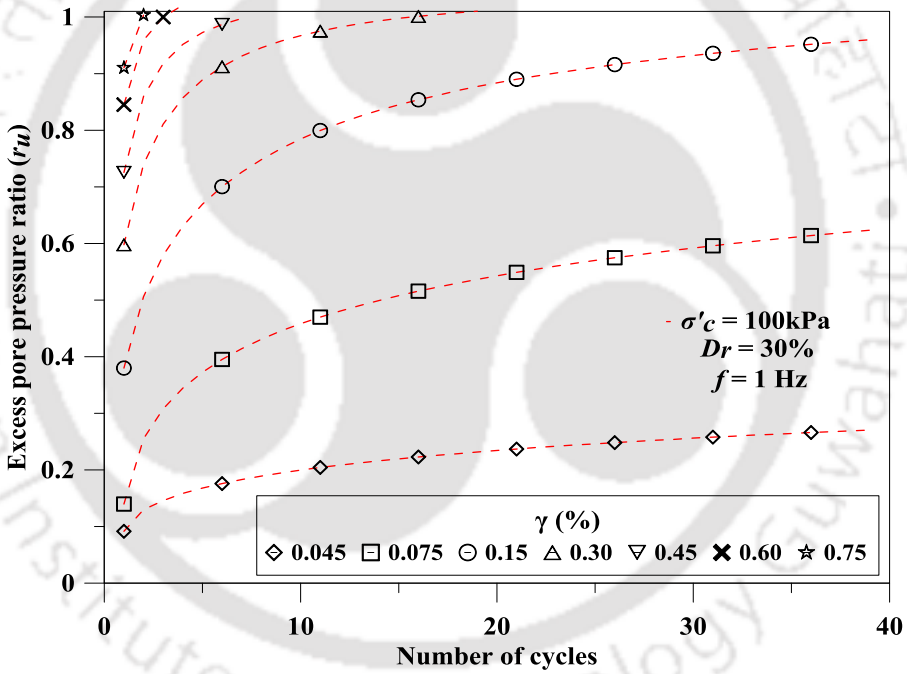

Fig. 6.2 Variation of maximum r_u with N at different γ

Fig. 6.3 presents the variations of r_u at different σ'_c for BS specimens prepared at D_r = 30%. It also shows the variations of r_u at γ = 0.075% and 0.15%. For γ = 0.075%, maximum r_u value is 0.8 at σ'_c = 50 kPa, while it is 0.53 at σ'_c = 150 kPa, whereas for γ = 0.15%, the maximum r_u value reached 1 at 30 cycles for σ'_c = 50 kPa, while r_u = 0.90 at 30 cycles for σ'_c = 150 kPa. Thus, the figure indicates that for a given shear strain value and number of cycles, the r_u values

decreased with increase in σ'_c. Fig. 6.3 also shows that, for identical number of cycles (N) and σ'_c, the tendency to liquefy the specimen increases with increase of γ.

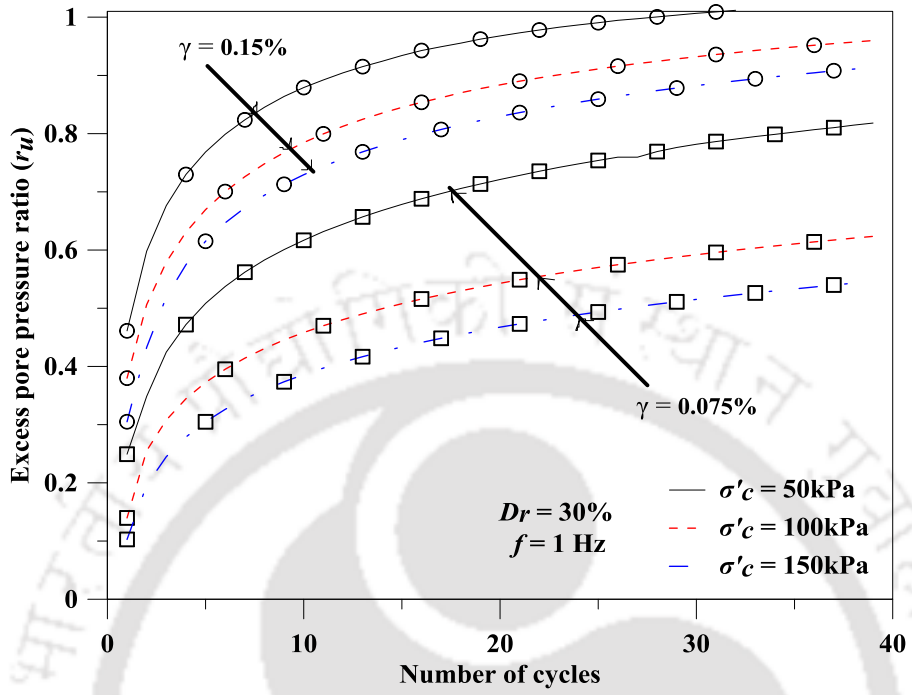

Fig. 6.3 Variation of maximum r_u with N at different σ'_c and γ

Fig. 6.4 illustrates the variation in r_u for test specimens prepared at different D_r i.e. 30%, 60% and 90% and tested at σ'_c = 50 kPa with γ of 0.075% and 0.15%. It reflects that the r_u decreases with the increase of D_r for a constant γ and σ'_c. At γ = 0.075%, BS specimen shows maximum r_u = 0.8 and 0.7 at 40 cycles, for D_r = 30% and 90%, respectively, whereas at γ = 0.015%, the maximum r_u was observed to be 1.0 (at 32 cycles) and 0.9 (at 40 cycles), for D_r = 30% and 90%, respectively. Therefore, it can be stated that the initiation of liquefaction is significantly affected by D_r as well as γ. It is also seen that for any constant γ (0.075% or 0.15%), r_u is nearly same at first cycles for all three D_r.

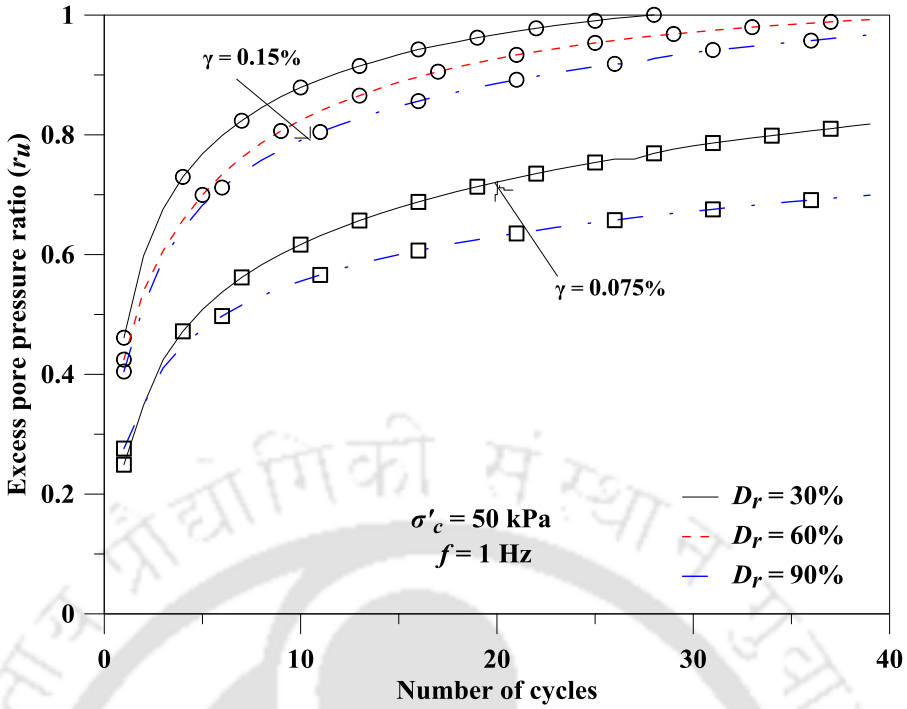

Fig. 6.4 Variation of maximum r_u with N at different D_r and γ

Variations in shear stress and *CSR* at different γ, σ'_c and D_r

Fig. 6.5 shows the variations in shear stress ($\tau = \sigma_d/2$) with number of cycles (N) at different γ (Fig. 6.5a), σ'_c (Fig. 6.5b) and D_r (Fig. 6.5c). The figure also shows the same in terms of cyclic stress ratio (CSR = $\sigma_d/2\sigma'_c$). Fig. 6.5a shows the variations in shear stress (τ) and *CSR* with N at different γ, for constant σ'_c = 50 kPa and D_r = 30%. The decrease in shear stress reflecting strength reduction of soil with loading cycles, is due to the increase in excess PWP in the soil specimen. Fig. 6.5a also illustrates that, for first cycle, τ and CSR is significantly higher for higher magnitudes of γ, and the same decreased continuously with subsequent loading cycles and finally reaches to zero in case of liquefaction of the soil. Fig. 6.5b presents the variations in τ with N at different σ'_c for constant D_r = 30% and γ = 0.15%. τ was observed to be nearly 15 kPa, 30 kPa and 35 kPa for 1st cycles at σ'_c = 50 kPa, 100 kPa and 150 kPa, respectively, whereas *CSR* was found to be nearly 0.3, 0.3 and 0.22 for 1st cycles at σ'_c = 50 kPa, 100 kPa and 150 kPa, respectively. Therefore, it can be stated that for a constant D_r (30%) and γ (0.15%), higher σ'_c impart higher τ on BS specimens, whereas, *CSR* is negligibly affected by the variation of σ'_c.

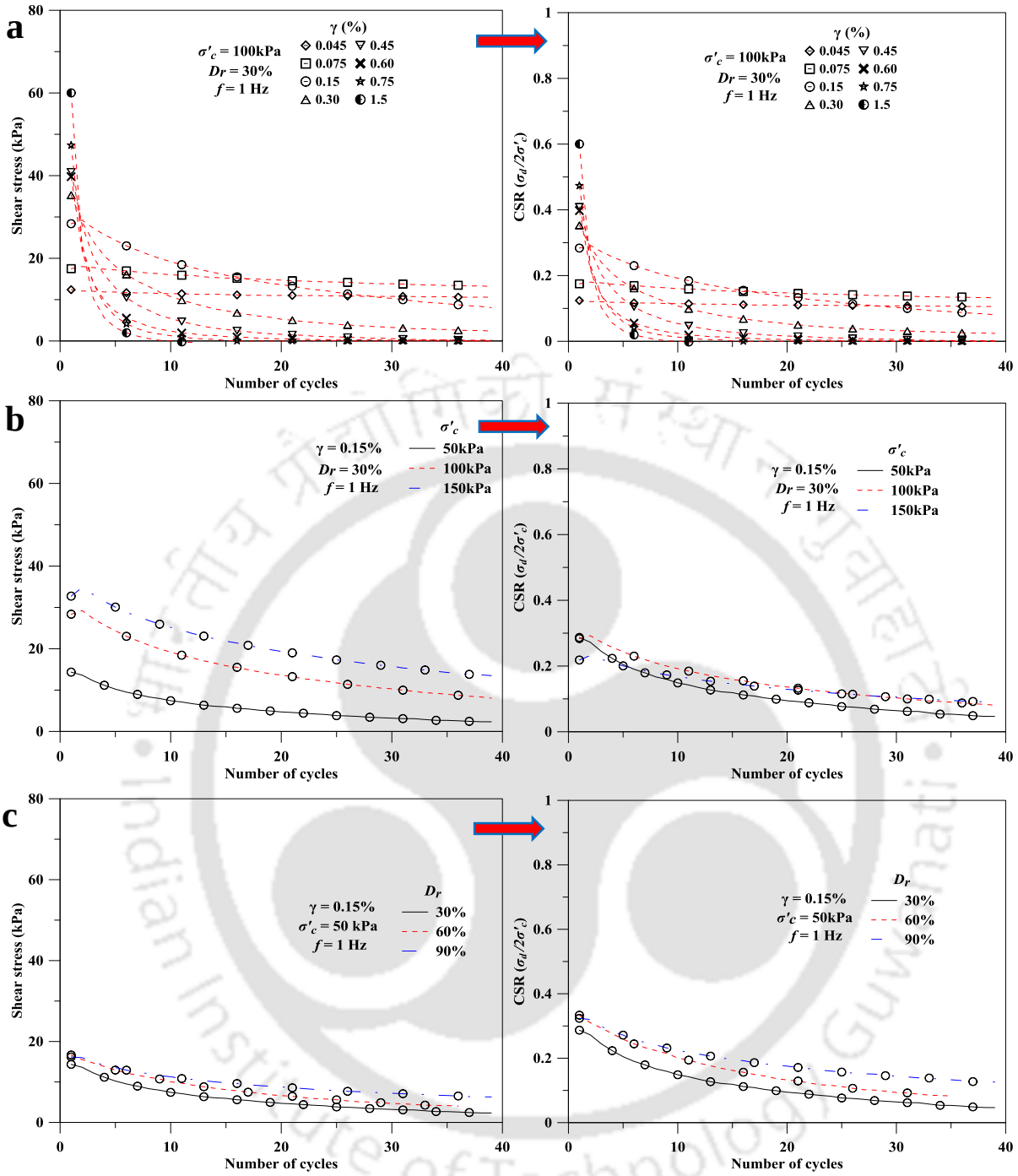

Fig. 6.5 Variation of shear stress and CSR with N at different (a) γ (b) σ'_c (c) D_r

Fig. 6.5c presents the variations in shear stress (τ) and *CSR* with N at different D_r for constant σ'_c = 50kPa and γ = 0.15%. The τ was observed to be nearly 14 kPa, 16 kPa and 16 kPa for 1st cycles at σ'_c = 50 kPa, 100 kPa and 150 kPa, respectively, whereas *CSR* was found to be nearly 0.29, 0.33 and 0.33 for 1st cycles at σ'_c = 50 kPa, 100 kPa and 150 kPa, respectively. Therefore, it can be stated that the both τ and *CSR* are almost free from σ'_c dependency, for a

constant σ'_c (50 kPa) and γ (0.15%).

Cyclic stress ratio (*CSR*) generally used to define the cyclic strength of soil, is an index to define the stresses applied on the soil specimens against the effective confining stress (σ'_c) in stress-controlled loading. In strain-controlled loading, the amount of stress applied on the soil specimens at σ'_c and γ, is evaluated in terms of *CSR*. The developed maximum *CSR* at first cycle for different γ, D_r and σ'_c are presented in Table 6.1. It is observed that *CSR* increases with the increase in γ for D_r = 30% and σ'_c = 50 kPa, because the developed deviator stresses (σ_d) in first cycle increases with the increase of γ. Table 6.1 also presents that the number of cycles (N) required for the specimen to attain the initiation of liquefaction (N_L), corresponding to γ and developed *CSR*. It is seen that with the increase in *CSR*, the liquefaction resistance of BS specimen decreased as reflected by the attained values of r_u. The *CSR* values decreases with the increase of σ'_c from 50 kPa to 150 kPa) for constant D_r and γ. Similar results are observed for σ'_c = 100 kPa and 150 kPa (Table 6.1). The results obtained for D_r = 60% and 90%, and σ'_c = 50 – 150 kPa were similar to D_r = 30% and σ'_c = 50 – 150 kPa. Therefore, the discussions are not provided due to resemblance. For all D_r and σ'_c, it is observed that the developed deviator stress (σ_d) is much higher than the initial σ'_c at γ greater than 0.75%, therefore the evaluated *CSR* (= $\sigma_d/2\sigma'_c$) becomes equal to or greater than 0.5. Based on Table 6.1, the developed *CSR* attains a value of 0.5 with r_u = 1 at almost $\gamma \approx 1.0\%$, which can be considered as a limiting value of γ ($\approx$ 1.0%) for N_L. Beyond this limiting γ, when *CSR* becomes greater than 0.5, soil is not able to resist even a single loading cycle and thus soil column was observed to collapse/fail because of extensive increase in excess PWP i.e. nearly equal to or greater than the initial σ'_c. Kramer (1996) was reported that the soil shows flow failure criteria when σ'_c is lesser than the applied stress. Thus, from the present study, it can be observed that the BS specimen shows initiation of liquefaction for different D_r and σ'_c, when the CSR becomes nearly equal to 0.5.

Table 6.1 Parameters of the strain-controlled cyclic triaxial tests

D_r (%)	σ'_c (kPa)	γ (%)	0.015	0.045	0.075	0.15	0.30	0.45	0.60	0.75
30	50	σ_d (kPa)	6	15	25	30	41	41	49	48
		CSR	0.06	0.15	0.25	0.30	0.41	0.41	0.49	0.48
		N_L	NL	NL	NL	16	4	4	2	1
		r_u	0.08	0.54	0.8	1	1	1	1	1
	100	σ_d (kPa)		25	35	57	71	79	82	95
		CSR		0.13	0.18	0.29	0.36	0.40	0.41	0.48
		N_L		NL	NL	NL	16	7	4	1
		r_u		0.27	0.62	0.96	1	1	1	1
	150	σ_d (kPa)		31	46	66	96	105	112	138
		CSR		0.1	0.15	0.22	0.32	0.35	0.38	0.46
		N_L		NL	NL	NL	18	9	5	3
		r_u		0.25	0.55	0.91	1	1	1	1
60	50	σ_d (kPa)	9.6			41			47	
		CSR	0.096			0.41			0.47	
		N_L	NL			40			3	
		r_u	0.07			0.99			1	
	100	σ_d (kPa)	13			64			95	
		CSR	0.065			0.32			0.47	
		N_L	NL			NL			7	
		r_u	0.045			0.75			1	
	150	σ_d (kPa)	12			85			117	
		CSR	0.04			0.28			0.39	
		N_L	NL			NL			8	
		r_u	0.015			0.68			1	
90	50	σ_d (kPa)		20	32	36	49	66	83	85
		CSR		0.20	0.32	0.36	0.49	0.66	0.83	0.85
		N_L		NL	NL	NL	10	3	1	1
		r_u		0.47	0.70	0.97	1	1	1	1
	100	σ_d (kPa)		34	43	58	87	90	103	
		CSR		0.17	0.22	0.29	0.44	0.45	0.52	
		N_L		NL	NL	NL	28	12	4	
		r_u		0.35	0.61	0.86	1	1	1	
	150	σ_d (kPa)		40	56	73	106	120	130	170
		CSR		0.14	0.19	0.24	0.35	0.40	0.44	0.57
		N_L		NL	NL	NL	32	20	8	7
		r_u		0.30	0.52	0.89	1	1	1	1

Note:- N_L – number of cycles to liquefy the specimen; NL – not liquefied in 40 cycles; σ_d (kPa) – deviatoric stress employed on the specimens at first cycle for given γ; *CSR* – cyclic stress ratio at first cycle; r_u – excess PWP ratio

6.4 STRESS-CONTROLLED TESTS WITH REGULAR EXCITATIONS

Stress-controlled regular excitation is a simple representation of irregular excitation, which implies the equivalent number of regular loading cycles for any irregular excitation. In the present study, based on the Eqn. (3.7) proposed by Seed and Idriss (1971), *CSR* values from

0.05 to 0.4 were used for regular excitation tests to study the liquefaction parameters of the BS soil. Test results were presented in terms of accumulation of γ and excess pore water pressure (u_e) generation. Excess pore-water pressures (u_e) are represented as excess pore-water pressure ratio ($r_u = u_e / \sigma'_c$). Typical plots of the responses obtained from stress-controlled tests are presented in Fig. 6.6-Fig. 6.9. Fig. 6.6 shows the variations in σ_d with mean effective at CSR = 0.1, 0.2, 0.3 and 0.4, for the specimens prepared at D_r = 60% and σ'_c = 100 kPa. It illustrates that the σ_d applied on the soil specimens increases with the increase of *CSR*, which lead to the quick liquefaction of soil. It is also seen that the effective stress path becomes tapered when initiation of liquefaction occurred in the soil specimen. The number of cycles (*N*) of repetitive load corresponding to the applied *CSR* is responsible for the development of r_u (shown in Fig. 6.7) and accumulation of γ (presented in Fig. 6.8). Fig. 6.7 presents the variations in r_u with *N* at different *CSR*. It was noticed that the specimen subjected to *CSR* = 0.1 does not show initiation of liquefaction even up to 500 cycles which is due to significantly lower amount of strain accumulation. However, other values of *CSR* = 0.2, 0.3 and 0.4 showed initiation of liquefaction (r_u = 1) at *N* = 29, 7 and 4, respectively. For the sake of comparison with other *CSR* values, the same has been presented up to 40 cycles (Fig. 6.7 and 6.8). Fig. 6.8 reflects the variations in accumulated γ with *N* at different *CSR*. It shows that γ reached 1.0%, 2.0% and 2.5% at *CSR* values 0.2, 0.3 and 0.4, respectively when BS specimens shows r_u = 1.

Fig. 6.9 shows the variations in *CSR* with number of cycles (*N*) at D_r = 60% and σ'_c = 100 kPa. It is seen that the BS specimen shows liquefaction at *N* = 4, 7 and 29 for *CSR* = 0.4, 0.3 and 0.2, respectively, whereas at CSR = 0.1, no liquefaction was observed till 500 cycles. Therefore, mark for CSR = 0.1 is not presented in Fig. 6.9. Thus, it can be stated that the BS specimen liquefies in lesser *N*, when subjected to higher *CSR*. This is attributed to the higher σ_d applied on the specimen at higher *CSR*. Several other tests have been conducted at different D_r, σ'_c and CSR, and results are presented in the following section.

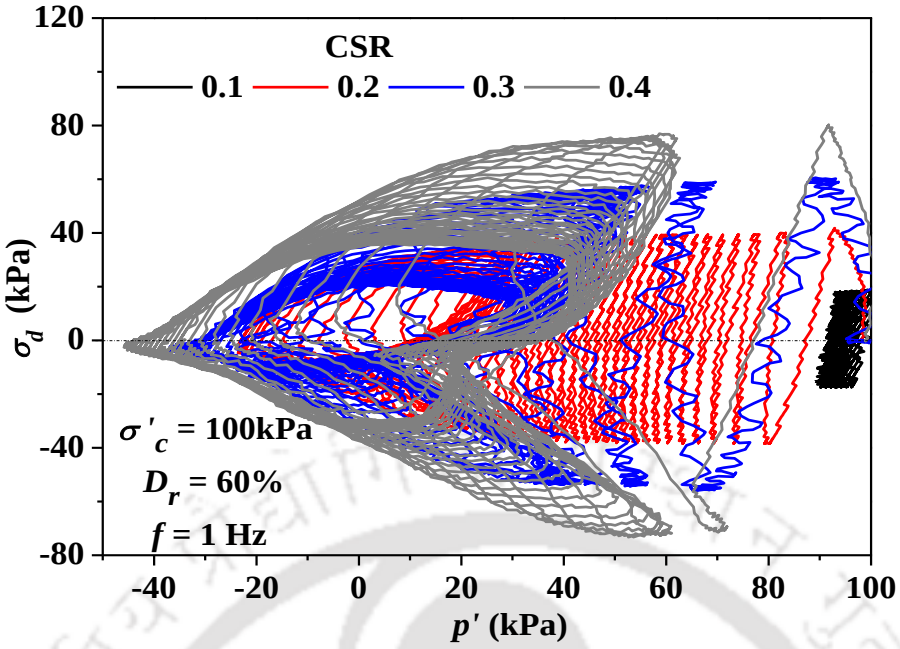

Fig. 6.6 Stress path plot from stress-controlled tests of SBS at various CSR

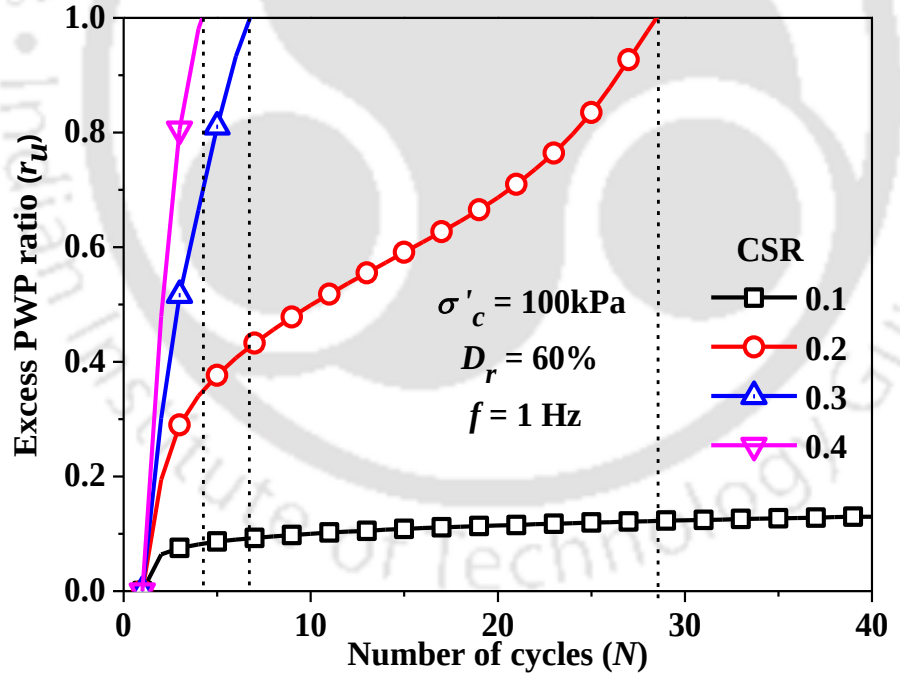

Fig. 6.7 Variation in r_u with number of cycles at different *CSR* obtained from stress-controlled test

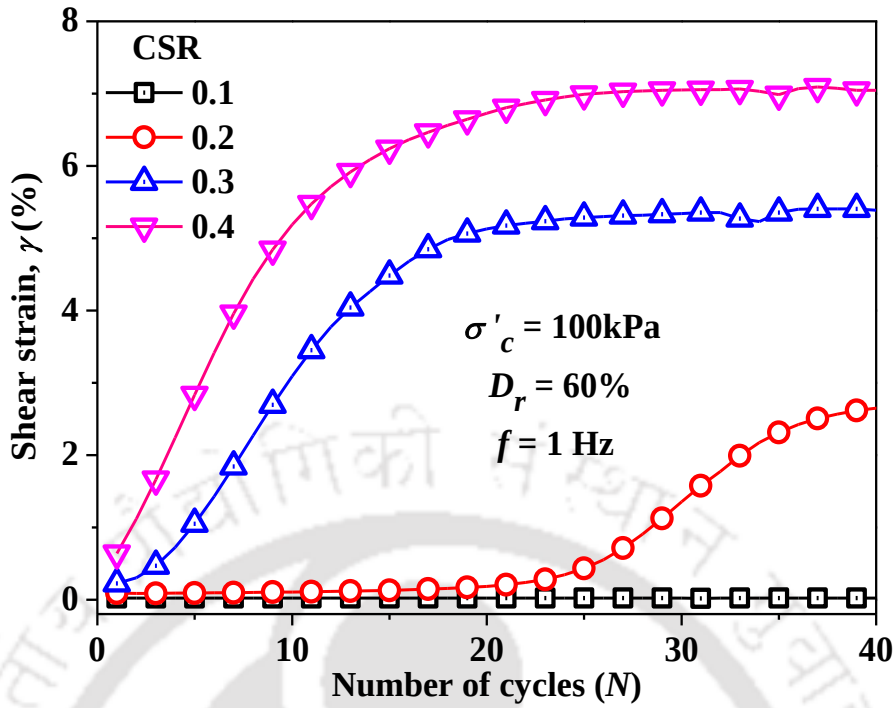

Fig. 6.8 Variations in γ with number of cycles at different *CSR* obtained from stress-controlled test

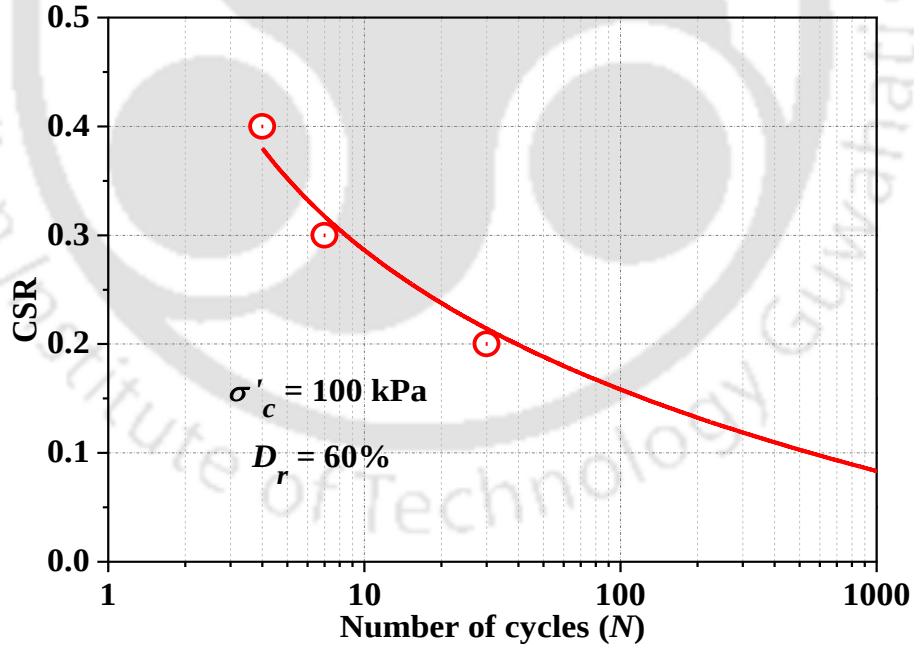

Fig. 6.9 Variation of CSR with number of loading cycles obtained from stress-controlled test

Variation of r_u and γ with loading cycles at different σ'_c and *CSR*

Fig. 6.10 presents the r_u responses of BS specimens (D_r = 30%; σ'_c = 50, 100 and 200 kPa) for

different *CSR* ($\sigma_d/2\sigma'_c$) values ranging from 0.05 to 0.3. It was observed that the specimens with *CSR* = 0.2 exhibits initiation of liquefaction at *N* = 10, 4 and 3 for σ'_c = 50, 100 and 200 kPa, respectively; whereas for *CSR* = 0.3 the same reflected at *N* = 2 and 1.5 for σ'_c = 50 and 100 kPa, respectively. Fig. 6.10 illustrates that the liquefaction was not reported for *CSR* = 0.05 and 0.1 till 100 cycles at σ'_c = 50 kPa. The specimens showed liquefaction at 122nd and 62nd number of loading cycles when subjected to *CSR* = 0.1 for σ'_c = 100 and 200 kPa, respectively. Thus, it can be stated that the liquefaction in BS specimens is more pronounced with the increase of σ'_c. This is attributed to the simultaneous increase in γ and σ_d on the soil specimens with the increase of σ'_c. Simatupang and Okamura (2017) have also observed that the liquefaction resistance decreases with increase in σ'_c, for a particular CSR value, which indicates a stress level dependency of liquefaction. Similar observations has also been reported by Wang et al. (2017).

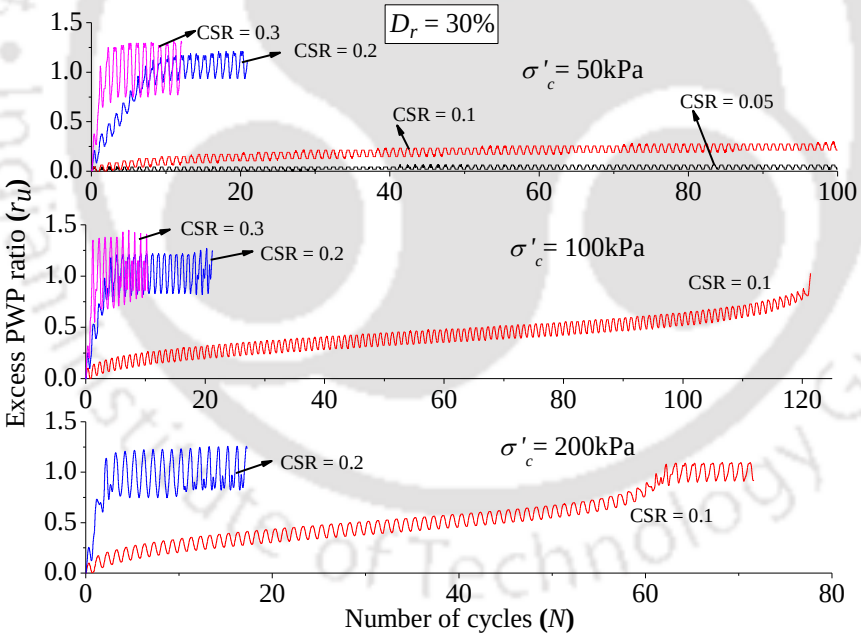

Fig. 6.10 Variation of r_u with *N* at different σ'_c and *CSR* for D_r = 30%

Fig. 6.11 illustrates the accumulation of γ during cyclic loading at D_r = 30% and different σ'_c subjected to different *CSR* ranging from 0.05 to 0.3. It reflects that, for *CSR* = 0.2, the accumulated γ were 0.45%, 2.5% and 6.8% when initiation of liquefaction occurs at σ'_c = 50, 100 and 200 kPa, respectively; whereas for *CSR* = 0.3 the accumulated γ was greater than 1%

for σ'_c = 50 and 100 kPa. It also shows that the liquefaction was not observed at *CSR* = 0.05 and 0.1 for σ'_c = 50 kPa; and the accumulated γ was ~ 0.02% till 500 cycles. The accumulated γ was 0.5% and 1.5%, when liquefaction initiated in the samples (prepared at D_r = 30% and subjected to *CSR* = 0.1) at $N = 122^{nd}$ and 62^{nd} subjected to σ'_c = 100 and 200 kPa, respectively. Thus, it can be stated that, for same *CSR*, the σ_d and γ increases substantially with the increase in σ'_c and, consequently the number of cycles required for the onset of liquefaction decreases. Under this circumstance, it is obvious that lesser number of loading cycles will be required to attain the state of liquefaction for specimens subjected to high σ'_c. Field experience, during past earthquakes, revealed that the liquefaction has mainly occurred at shallow depth (i.e. <15 m), whereas, laboratory experiment reflects that the liquefaction resistance of soil with respect to confining stress depends upon the testing conditions (Seed and Idriss, 1971, Elgamal et al., 1996). Tumi (1983) and Govindaraju (2005) were reported that the liquefaction resistance of sandy soil decreases and increases with the increase of σ'_c using stress-controlled approach, while the same increases during a strain-controlled approach. Experimental and numerical investigations also revealed that the liquefaction may occur at depths greater than 15 m depending upon peak ground acceleration and soil conditions (Seed and Idriss, 1971; Elgamal et al., 1996; Byrne et al., 2004; Sreng et al., 2015; Qu et al., 2016). Therefore, the results presented in this section, can be used as an artefact to understand the behaviour of sand specimens subjected to regular cyclic excitations.

Fig. 6.12 presents the response of BS soil specimens for D_r = 60% at σ'_c = 50, 100 and 200 kPa. The specimen at different σ'_c was subjected to different cyclic stress amplitudes, defined by different *CSR* values from 0.05 to 0.3. It is observed that the specimen tested at *CSR* = 0.2, reflect initiation of liquefaction at *N* = 30, 9 and 3 for confining stress 50, 100 and 200 kPa, respectively; whereas for *CSR* = 0.3 the same reflect at *N* = 3 and 2 for confining stress 50 and 100 kPa, respectively. It also shows that the liquefaction was not reported at CSR = 0.05

and 0.1 even in 500 cycles, however, for the sake of comparison the graph is plotted for 100 cycles. It was also observed that the liquefaction resistance decreases with the increase of σ'_c for any particular *CSR* (for example, *CSR* = 0.2), thus indicating the stress level dependency since σ_d increases with the increase in σ'_c.

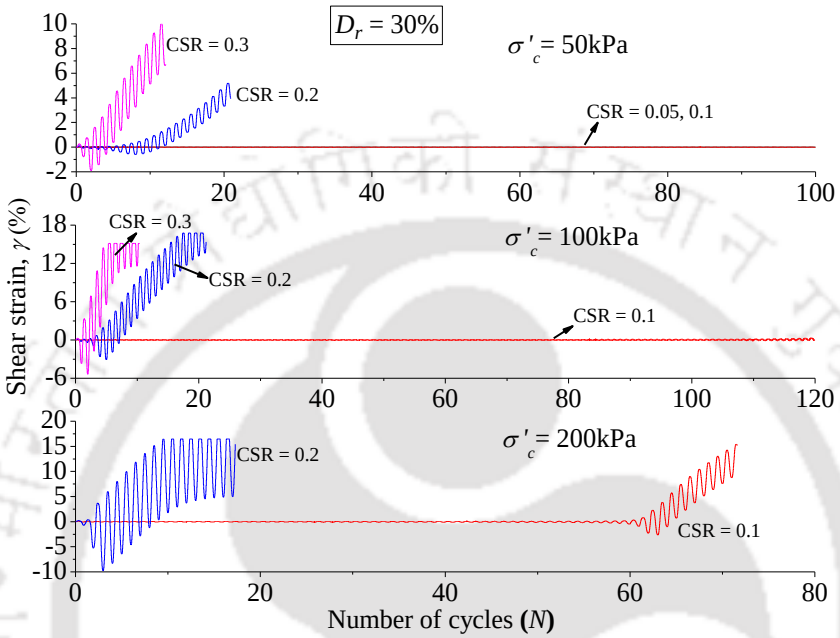

Fig. 6.11 Variation of γ with N at different σ'_c and *CSR* for D_r = 30%

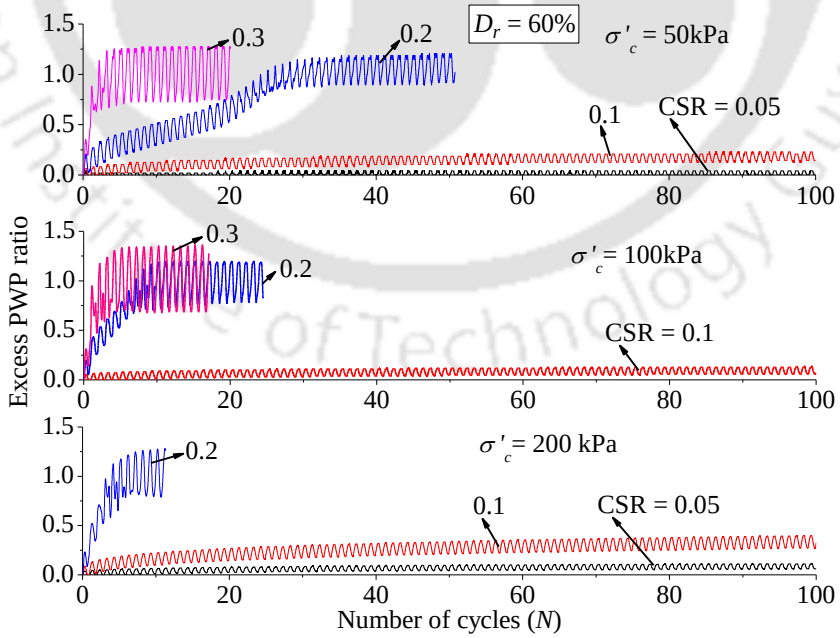

Fig. 6.12 Variation of r_u with N at different σ'_c and *CSR* at D_r = 60%

Fig. 6.13 illustrates the γ accumulation during cyclic loading at D_r = 60% and tested for *CSR* range 0.05-0.3. It reflects that, for *CSR* = 0.2, the γ was greater than 0.5% when initiation of liquefaction occurred, for all σ'_c = 50, 100 and 200 kPa; whereas for *CSR* = 0.3 the γ was 0.75% for σ'_c = 50 and 100 kPa. It also shows that the liquefaction was not reported at *CSR* = 0.05 and 0.1, and the accumulated shear strain was ~ 0.02%. For same *CSR*, it is seen that with the increase in σ'_c, σ_d increases substantially and consequently *N* required for the onset of liquefaction decreases. The summary of results regarding the number of cycles and shear strain generated at the onset of liquefaction obtained at different σ'_c is presented in Table 6.2.

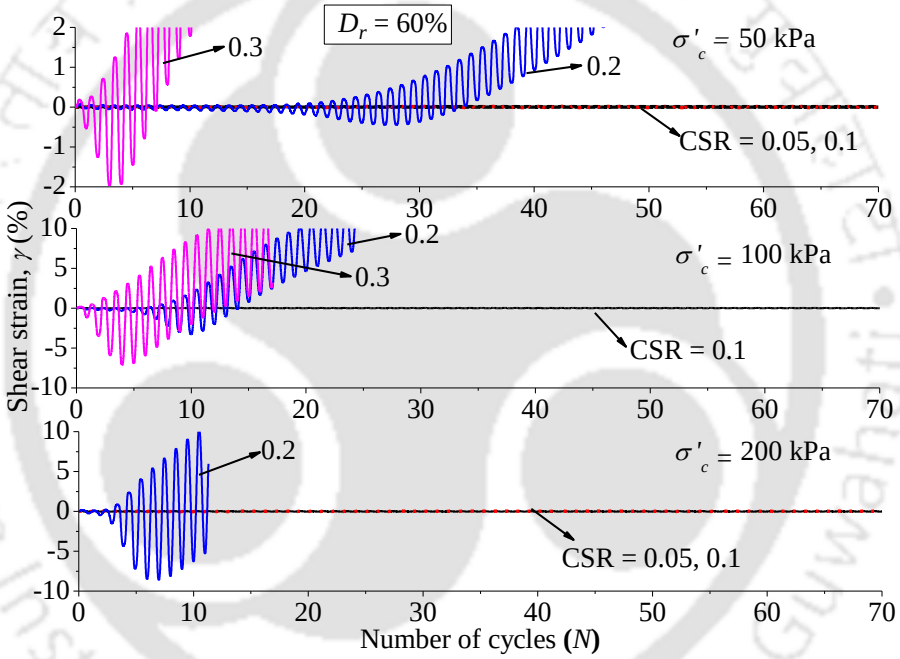

Fig. 6.13 Variation of γ with *N* at different σ'_c and *CSR* at D_r = 60%

Table 6.2 clearly shows that, for a constant D_r (60%), the liquefaction resistance of soil decreases with increase in CSR and σ'_c. It also shows that the initiation of liquefaction occurred at different confining depth (i.e. σ'_c), when accumulation of γ exceeded 0.5%. Thus, based on the stress-controlled tests, it can be stated that the accumulation of γ is also one of the major contributory factor along with the generation of excess PWP to the initiation of liquefaction in saturated sand.

Table 6.2 Summary of results regarding the number of cycles and shear strain generated at the onset of liquefaction for SBS subjected to regular excitation and at different σ'_c

D_r (%)	σ'_c (kPa)	Number of cycles (N) to liquefaction and shear strain (γ)	*CSR* 0.05	0.1	0.2	0.3
60	50	N	*NL*	*NL*	30	3
		γ (%)	0.02	0.02	0.5	0.75
	100	N	*NL*	*NL*	10	2
		γ (%)	0.02	0.02	0.75	0.75
	200	N	*NL*	*627*	4	
		γ (%)	0.02	0.5	0.75	

NL – No liquefaction till 500 cycles

Variation of r_u and γ with loading cycles at different D_r and *CSR*

Fig. 6.14 presents the behaviour of SBS specimens, in terms of variations in r_u and γ, prepared at different D_r subjected to varying *CSR* (i.e. 0.05-0.3) for 100 regular excitation cycles. Although, the tests have been conducted up to 500 cycles for *CSR* = 0.05 and 0.1. It was observed that the specimens prepared at any D_r, and subjected to low magnitude *CSR* (for example, *CSR* = 0.05 and 0.1), does not exhibit liquefaction till 500 cycles whereas, specimens subjected to higher *CSR* magnitudes (for example, *CSR* = 0.2 and 0.3) manifested the occurrence of liquefaction. Fig. 6.14 also illustrates that at D_r = 30% and σ'_c = 50 kPa, the specimens at *CSR* values 0.2 and 0.3 liquefied at N = 10 and 2, respectively. Similar behaviour is portrayed at other D_r. It can be observed that the number of cycles required to exhibit liquefaction increases with the increase in D_r of the specimen. In other words, it can be stated that the liquefaction potential decreases with increasing D_r or compactness of the soil.

Fig. 6.15 presents the response of BS soil specimens prepared at D_r = 30%, 60% and 90% at σ'_c = 50 kPa. The specimen at different D_r was subjected to different cyclic stress amplitudes defined by different *CSR* values from 0.05 to 0.3 as shown in Fig. 6.15. It is observed that for D_r = 30%, the specimen with CSR values of 0.05 and 0.1 exhibit substantially low magnitudes of shear strain. It can also be noticed that at D_r = 30%, 60% and 90%, BS portrays onset of liquefaction at *CSR* = 0.2 in N ~ 10, 30 and 50 cycles, respectively, when the corresponding

shear strain reaches ~ 0.5%. $\gamma \geq 0.5\%$ was again observed at $CSR = 0.3$ for samples prepared at D_r = 30%, 60% and 90%, when initiation of liquefaction observed at N ~ 2, 3 and 10 cycles, respectively. Summary of the outcomes from the tests at different D_r are presented in Table 6.3. Similar to the Table 6.2, it can also be stated that the initiation of liquefaction occurred at different D_r, when accumulation of γ exceeded 0.5%. Dobry and Abdoun (2015) also reported that γ needed to trigger the liquefaction, for clean sand, was in the range of 0.4%-3%.

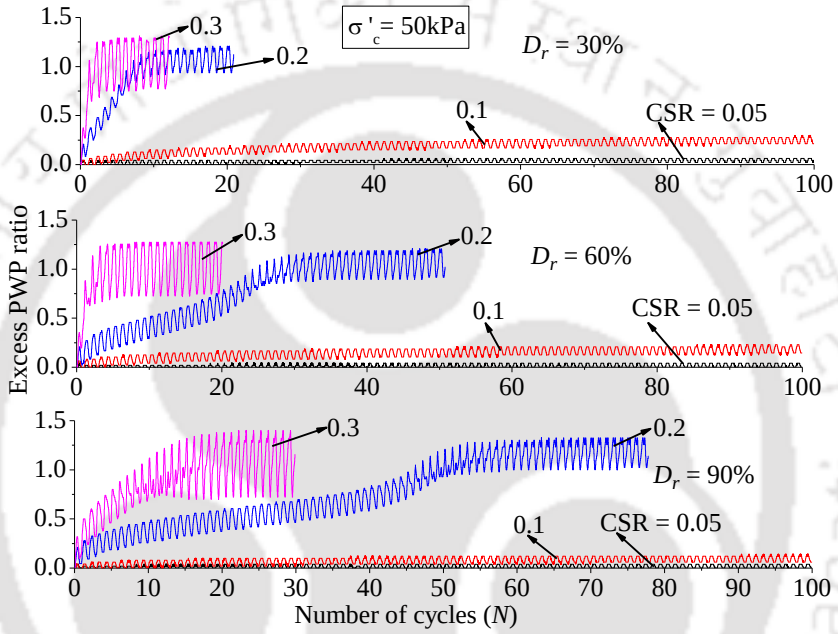

Fig. 6.14 Variation of r_u with N at different D_r and CSR at σ'_c = 50 kPa

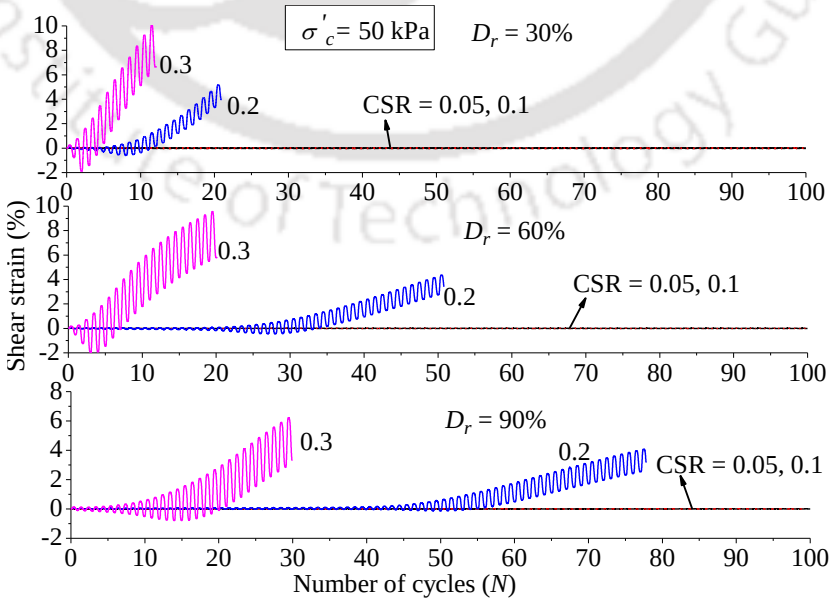

Fig. 6.15 Variation of γ with N at different D_r and CSR at σ'_c = 50 kPa

Table 6.3 Summary of results regarding the number of cycles and shear strain generated at the onset of liquefaction for SBS subjected to regular excitation and prepared at different D_r

σ'_c (kPa)	D_r (%)	Number of cycles (N) to liquefaction and shear strain (γ)	CSR			
			0.05	0.1	0.2	0.3
50	30	N	*NL*	*NL*	10	2
		γ (%)	0.02	0.02	0.6	0.75
	60	N	*NL*	*NL*	30	3
		γ (%)	0.02	0.02	0.5	0.75
	90	N	*NL*	*NL*	30	3
		γ (%)	0.02	0.02	0.5	0.5

NL – No liquefaction till 500 cycles

Effect of simultaneous increase of D_r and σ'_c

Fig. 6.16 presents the response of BS specimens in terms of r_u with simultaneous increase of D_r and σ'_c for *CSR* range 0.05-0.3. It is observed that for *CSR* = 0.2 and 0.3, the specimens prepared at D_r = 30% and σ'_c = 50 kPa required lesser number of stress cycles to attain liquefaction, in comparison to the specimen prepared at D_r = 60%, σ'_c = 100 kPa and D_r = 90%, σ'_c = 200 kPa. Based on the comparison from previous Section 6.4, it can be stated that the liquefaction potential decreases with the increase of D_r, while the same increases with the increase of σ'_c. The tests have also been conducted for *CSR* = 0.05 at D_r = 30%, σ'_c = 50 kPa; and for *CSR* = 0.1 at D_r = 30%, σ'_c = 50 kPa; D_r = 60%, σ'_c = 100 kPa and D_r = 90%, σ'_c = 200 kPa up to 500 loading cycles. It was observed that the specimen prepared at any D_r and σ'_c, and subjected to *CSR* = 0.05 and 0.1, does not exhibit liquefaction in 500 loading cycles. However, the specimen subjected to higher *CSR* magnitude (0.2 or 0.3) manifested the occurrence of liquefaction. Fig. 6.16 illustrated that the specimens D_r = 30% and σ'_c = 50 kPa showed liquefaction at the 8th and 2nd cycles for the *CSR* values 0.2 and 0.3, respectively. The BS specimen prepared at D_r = 60% and σ'_c = 100 kPa showed liquefaction at the 10th and 3rd cycles for the *CSR* values 0.2 and 0.3, whereas, liquefaction was observed at the 12th and 5th cycles at D_r = 90% and σ'_c = 200 kPa for the *CSR* values 0.2 and 0.3, respectively.

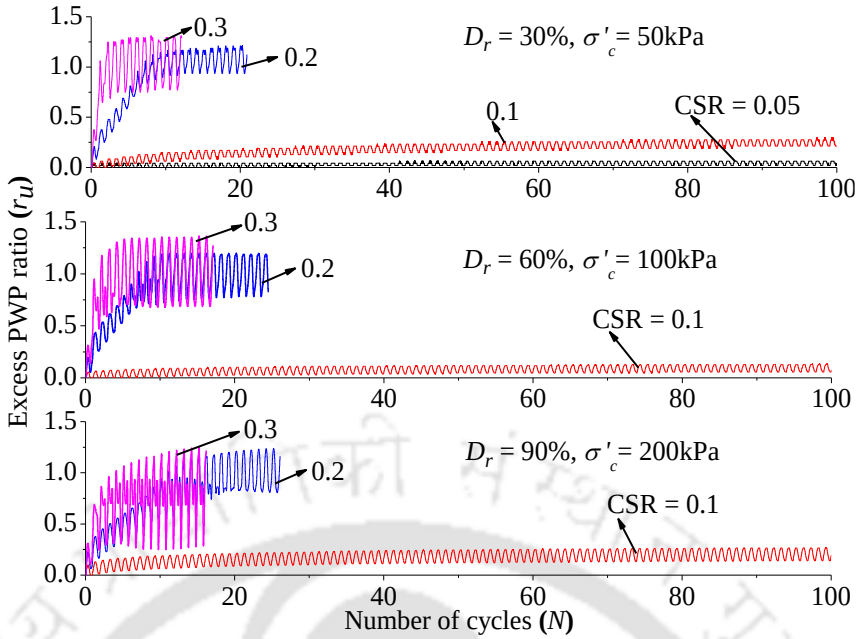

Fig. 6.16 Variation of r_u with N for simultaneous increase of D_r and σ'_c

Fig. 6.17 presents the γ accumulation in the BS specimens at different D_r and σ'_c subjected to different *CSR* from 0.05 to 0.3. It can be seen that the specimens prepared at D_r = 30% and σ'_c = 50 kPa exhibited substantially low magnitudes of shear strain (≈ 0.2%) at *CSR* values 0.05 and 0.1, and no liquefaction was observed. At *CSR* = 0.2, the BS specimens prepared at D_r = 30%, σ'_c = 50 kPa; D_r = 60%, σ'_c = 100 kPa and D_r = 90%, σ'_c = 200 kPa portrayed onset of liquefaction at N = 8, 10 and 12 cycles, respectively, where the corresponding γ reached ~ 0.5%. $\gamma \geq 0.5\%$ was again observed at *CSR* = 0.3 for D_r = 30%, 60% and 90%, when initiation of liquefaction was observed at N ~ 2, 3 and 5 cycles, respectively.

Fig. 6.18 presents the variation in *CSR* with number of loading cycles required to liquefy (N_L) the SBS specimens prepared at D_r = 30%-90% and subjected to σ'_c = 100 kPa. It shows that, for any constant *CSR* (for example, *CSR* = 0.2), the liquefaction resistance increases with the increase in D_r (i.e. from D_r = 20% to 90%). It is also illustrated that, for any constant D_r, the liquefaction resistance decreases with the increase in *CSR* (i.e. from 0.15 to 0.3). Thus, it can be stated that BS soil in loose state is highly vulnerable to liquefaction even at low magnitudes of shaking (based on *CSR* value), whereas it is relatively resilient at higher D_r.

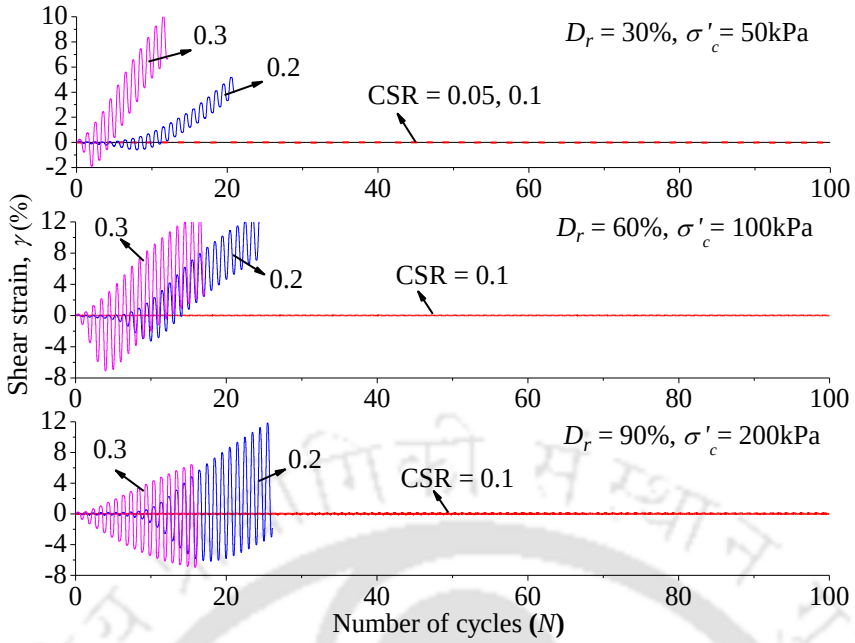

Fig. 6.17 Variation of γ with N for simultaneous increase of D_r and σ'_c

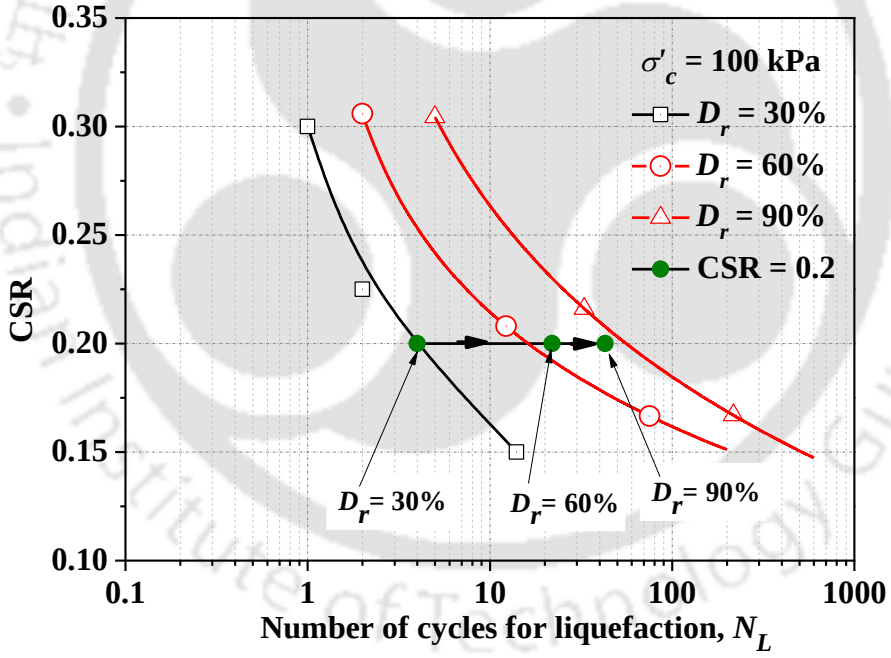

Fig. 6.18 Variation of *CSR* with N_L

Fig. 6.19 presents the variations in r_u (obtained from stress-controlled approach) with N/N_L (N/N_L is the cycle ratio; where N is number of cycle and N_L is the number of cycles at which liquefaction is manifested). Such the pore-pressure model are commonly being used in ground response analysis (GRA) tools such as SHAKE2000 and DEEPSOIL and, numerical

analysis tool such as FLAC and PLAXIS, to perform GRA studies. The results obtained from both the approaches were compared with the data available in literature (Lee and Albaisa 1974, Seed et al. 1975 and Polito et al. 2008). It can be clearly observed that the stress-controlled tests data of the present study does not come under the boundaries proposed by the aforementioned researchers, which might be due to the different particle sizes or different testing conditions.

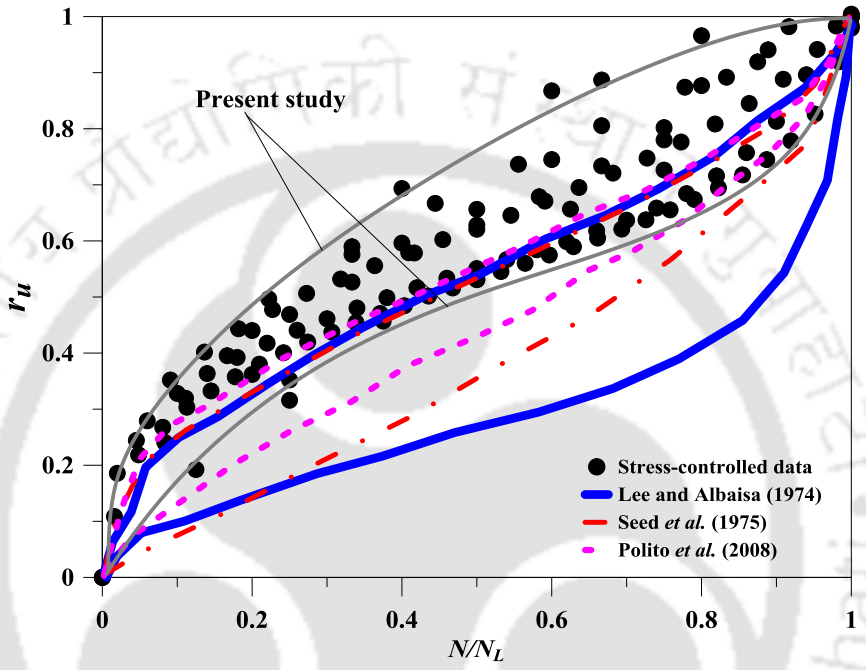

Fig. 6.19 Pore pressure models (relationship between r_u and N/N_L) proposed from present study in comparison to the existing literature

Fig. 6.20 presents the variations in r_u (obtained from stress-controlled approach) with γ, and are compared with the upper and lower boundaries of the same proposed by Cetin and Bilge (2012). Cetin and Bilge (2012) estimated r_u values, based on stress-controlled cyclic testing, corresponding to the occurrence of the maximum shear strain either at liquefaction state or at the end of specified cycles, whichever is reached earlier. The difference between the outcomes of the present study and that reported by Cetin and Blige (2012), revealed that the variations in r_u with γ depends on the particle sizes of the soils and testing conditions. It can also be concluded that the soils manifest the occurrence of liquefaction i.e. $r_u = 1$, when the γ exceeds 1%.

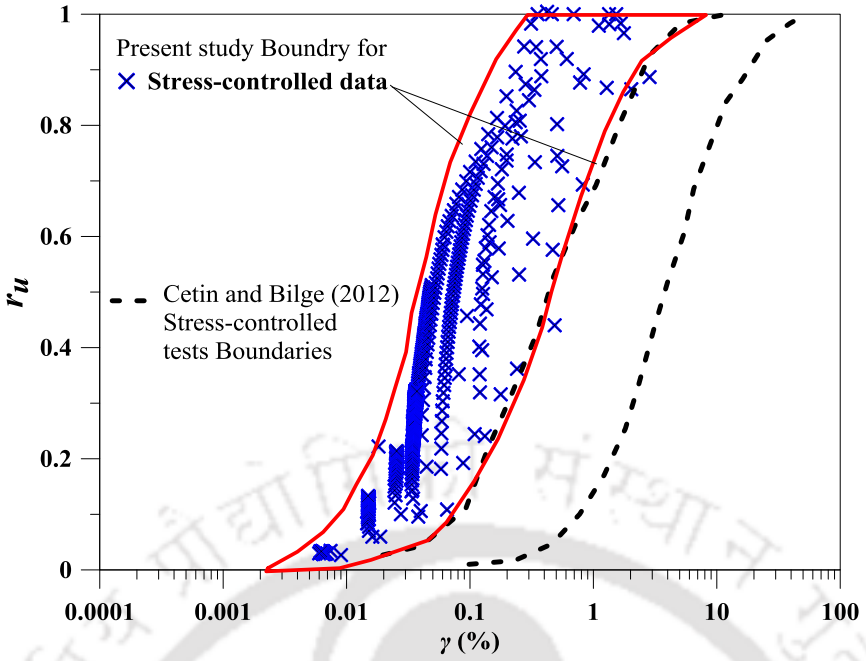

Fig. 6.20 Relationship between r_u and γ based on the stress-controlled approach obtained from the present study and that reported by Cetin and Bilge (2012)

6.5 STRESS-CONTROLLED TESTS WITH IRREGULAR EXCITATIONS

Irregular excitations such as earthquakes result different levels of strains and excess PWP generated in the soils. Therefore, to observe the behaviour of BS specimens under irregular excitations three strong motions of namely Bhuj, Tezpur and Kobe earthquakes were chosen. Test specimens were prepared at different D_r (i.e. 30, 60 and 90%) and were subjected to different σ'_c (i.e. 50, 100 and 150 kPa) representing the approximate soil confining depths to be 5, 10 and 15 m, respectively. Cyclic loading was applied on the BS specimens in the form of irregular excitations as explained in Section 3.4.3.

Effect of relative density

Relative density (D_r), representing the compactness of soil specimen and an indicative of the degree of inter-particle interaction, plays a major role in defining the dynamic behaviour of cohesionless soils. The effect of D_r on the onset of liquefaction of the BS specimens at a σ'_c = 100 kPa and subjected to different stress histories are presented in Fig. 6.21. Fig. 6.21a presents

the responses of BS specimens subjected to Bhuj motion. It can be observed that r_u decreases with the increase in D_r. The maximum r_u values of 0.13, 0.09 and 0.08 were obtained for test specimens at D_r of 30%, 60% and 90%, respectively. Owing to the higher ratio of soil particles in a fixed volume representing lesser void ratio and denser state of specimens, quantity of induced excess PWP decreased with the increase in D_r during the dynamic shaking. As a consequence, tests conducted at higher D_r revealed lesser γ accumulation (< 0.04%). Similar observations are illustrated in Fig. 6.21b and Fig. 6.21c, when the BS specimens were subjected to Tezpur and Kobe motions, respectively, although depicting larger γ and r_u. Specimens when subjected to Bhuj motion, no liquefaction was observed ($r_u << 1$), however, the specimens exhibited liquefaction ($r_u = 1$) when subjected to both Tezpur and Kobe motions due to increase in PGA. Further, it can be observed that the accumulation of excess PWP was very quick, when subjected to Tezpur and Kobe motions, and resulted quick or instant liquefaction phenomena. This feature is attributed to the impulsive nature of Tezpur and Kobe strong motions, where the PGA was reached suddenly, unlike the Bhuj motion, which showed a gradual attainment of PGA (Fig. 3.20). Maximum shear strains (γ_{max}) were observed to be in the range of 0.5-0.7% for the specimens subjected to Tezpur motion (Fig. 6.21b), while the strain range was observed to be 5-15% for Kobe motion (Fig. 6.21c) due to the enhancement in PGA value. From Fig. 6.21(a-c), it can be noticed that the rate of strain accumulation and excess PWP generation reduced with the increase of D_r for a constant σ'_c. Thus, it is evident that D_r has a significant role in governing the onset of liquefaction of cohesionless specimens subjected to seismic shaking.

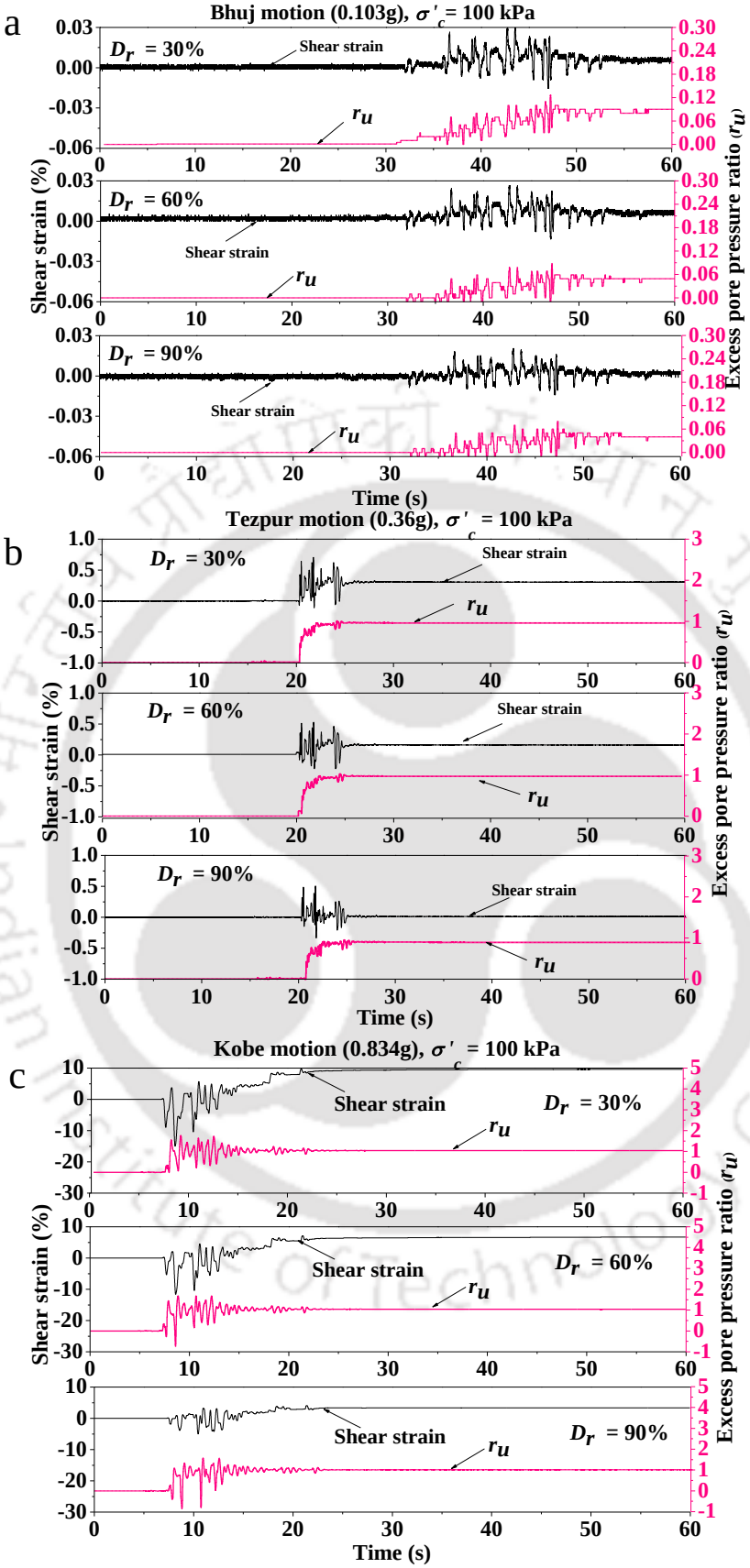

Fig. 6.21 Accumulation of shear strain and excess PWP ratio in SBS specimens at σ'_c = 100 kPa for different D_r and subjected to (a) Bhuj (b) Tezpur (c) Kobe strong motions

Table 6.4 enumerates the findings of the experimental investigations conducted on BS specimens prepared at different D_r. It can be noticed that for a given earthquake motion, the variations in D_r from 30% to 90% shows reduction in maximum shear strain (γ_{max}) values. The γ_{max} obtained from Bhuj motion at D_r = 30%, 60% and 90% are 0.032%, 0.03% and 0.02%, respectively; γ_{max} obtained from Tezpur motion are 0.70%, 0.52% and 0.50% respectively while, for Kobe motion γ_{max} are 15%, 12% and 8%, respectively. Therefore, it can be stated that γ_{max} decreases with the increase in D_r (from 30% to 90%) for all Input motions. It is also seen that the BS specimens subjected to Bhuj motion show $r_{u,max}$ = 0.13, 0.09 and 0.08 for D_r = 30%, 60% and 90%, respectively, and therefore, no liquefaction is observed. However, BS specimens subjected to Tezpur motion and Kobe motion exhibited liquefaction. $r_{u,max}$ is the maximum excess PWP ratio reached, when soil specimens are subjected to strong motions. It can be observed that the specimen prepared at D_r = 90% attained a near-liquefaction state with $r_{u,max}$ = 0.9, whereas the specimen prepared at D_r = 60% showed a distinct onset of liquefaction ($r_{u,max}$ = 1.0); although, the difference in γ_{max} are marginal, 0.5 and 0.52, respectively. From this observation, it can be stated that the shear strain equal to 0.5% manifests the onset of liquefaction for these set of tests and the corresponding maximum cyclic stress ratio (CSR_{max}) being 0.32. Table 6.4 clearly indicates that the specimens with higher D_r depict lower r_u. This effect is more pronounced at lower PGA level. At higher PGA levels, though there is significant reduction in γ_{max}, and the liquefaction condition becomes inevitable as r_u reaches 1.0. Variations in the shear modulus (G), evaluated as a ratio of the maximum shear stress to the maximum shear strains, at different D_r, for different strong motions are also presented in Table 6.4. It can be seen that G obtained from Bhuj motion at D_r = 30%, 60% and 90% are 28.75 MPa, 30.67 MPa and 46.0 MPa, respectively. Referring to G values presented in the table, it can be stated that the G increases with the increase in D_r.

Table 6.4 Summary of investigations on BS specimens prepared at different D_r and subjected to various strong motions

Input motion	D_r (%)	σ'_c (kPa)	CSR_{max}	γ_{max} (%)	τ_{max} (kPa)	G (MPa)	$r_{u,max}$	Liquefaction
Bhuj (0.103g)	30	100	0.092	0.032	9.2	28.75	0.13	No
	60			0.03		30.67	0.09	
	90			0.02		46.00	0.08	
Tezpur (0.36g)	30	100	0.327	0.70	32.7	4.66	1.0	Yes
	60			0.52		6.27	1.0	
	90			0.50		6.52	0.9	
Kobe (0.834g)	30	100	0.756	15.0	75.6	0.50	2.0	Yes
	60			12.0		0.63	1.7	
	90			5.00		1.51	1.5	

Effect of confining depth

Fig. 6.22 presents the effect of confining depth has been presented in terms of different σ'_c, and the resulting shear stresses due to a given earthquake motion. In this attempt, the test specimens prepared at D_r = 30% are considered for different confining depths. Fig. 6.22 shows the results of such BS specimens subjected to different irregular excitations. Fig. 6.22a illustrates the accumulation of shear strain (γ) and development of r_u in BS specimen subjected to Bhuj motion (PGA = 0.103g). It is observed that $\gamma_{max} \approx$ 0.01%, 0.03% and 0.03% at confining depths of 5 m, 10 m and 15 m, respectively. An increase in the confining depth implies that the specimens were subjected to higher shear stress, which resulted in increased shear strain. Maximum excess PWP ratio observed to be very low ($r_{u,max}$ = 0.1<< 1) which is due to the low *CSR* values (0.097, 0.092 and 0.078 at 5, 10 and 15m depth due to 0.103g PGA). It can also be observed that the specimens at two different depths, 10 and 15 m (with σ'_c = 100 and 150 kPa) showed identical response in terms of shear strain and excess PWP, which is again attributed to the low PGA level. BS specimens at different depths subjected to scaled Tezpur motion (PGA = 0.36g) with *CSR* ranging between 0.28-0.35 exhibited higher peak shear strains in the range of 0.06-1.8% (Fig. 6.22b). Specimens subjected to σ'_c of 100 kPa and 150 kPa exhibited a clear onset of liquefaction as r_u reaches nearly 1, while it is significantly lesser ($r_{u,max}$ = 0.25 << 1) for σ'_c = 50 kPa. This behaviour indicates that a BS stratum in the field located at a particular depth,

corresponding to the above stated range of σ'_c (i.e. 100-150 kPa), is likely to liquefy. It is also observed that as the specimen liquefies; a significant residual shear strain is manifested indicating the strength reduction of soil. Similar response of larger residual shear strain (> 6%) has also been reported from ground response analysis studies using SHAKE and DEEPSOIL (Suetomi and Yoshida, 1998; Kumar et al., 2014a,b). As indicated from Fig. 6.22c, when subjected to Kobe motion (PGA = 0.834g with CSR range of 0.65-0.80), BS specimens at any of the confining pressures exhibited r_u = 1 and a substantial residual shear strain (> 5%), thus clearly exhibiting the occurrence of liquefaction in the specimen. From the above illustration, it can be stated that the behaviour of BS specimens at different confining pressure is indicative of their supposed behaviour at different depths in the field subjected to strong motions.

Table 6.5 summarizes the results demonstrating the effects of confining depth (i.e. σ'_c) and PGA levels of chosen strong motions. It can be seen that γ_{max} obtained from Bhuj motion at σ'_c = 50 kPa, 100 kPa and 150 kPa are 0.01%, 0.03% and 0.03%, respectively. γ_{max} values for Tezpur motion are 0.06%, 0.70% and 1.8%, while the values for Kobe motion are 8%, 15% and 18%, respectively. Thus, it can be stated that the accumulation of shear strain increases with the increase in σ'_c as well as PGA. The variations in $r_{u,max}$ with the variations in σ'_c and PGA were also estimated and presented in Table 6.5. Table 6.5 also presents the variations in stiffness (i.e. shear modulus, G) at different σ'_c and PGA. It is seen that G obtained from Bhuj motion at σ'_c = 50 kPa, 100 kPa and 150 kPa are 48.5 MPa, 30.67 MPa and 39.0 MPa, respectively. It can be stated that G is significantly affected by increase of σ'_c and PGA. Moreover, it can be stated that BS specimens manifest the onset of liquefaction beyond a PGA value of 0.36g when γ_{max} exceeds 0.50%. Furthermore, at particular D_r and confining depth, the input motion of higher PGA reflects higher strain accumulation. Table 6.5 also illustrates that for a particular D_r, generation of excess PWP or liquefaction susceptibility of soil increases with the increase of confining depth for all input motions.

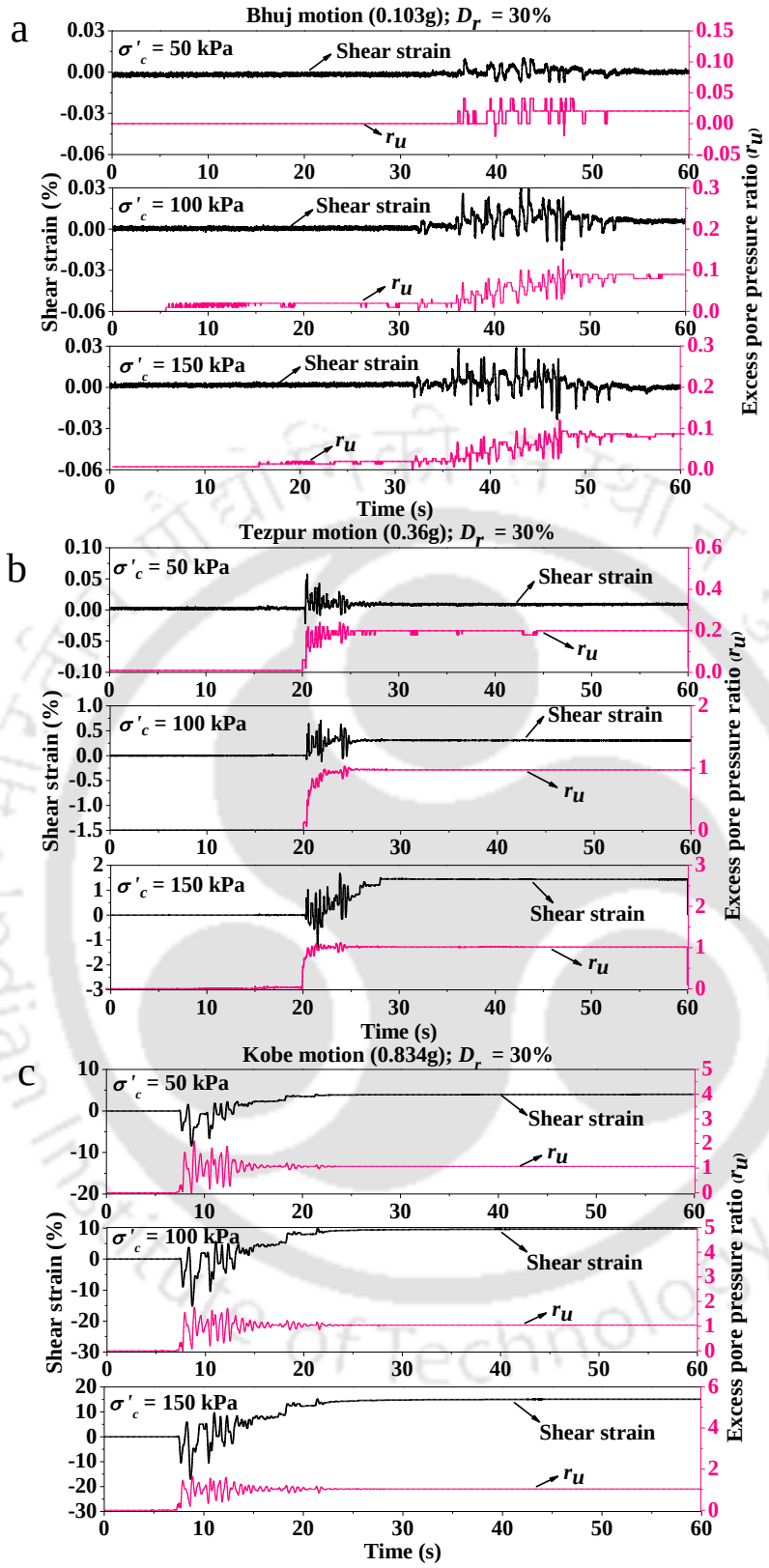

Fig. 6.22 Accumulation of shear strain and excess PWP ratio in SBS specimens at D_r = 30% and different σ'_c for (a) Bhuj (b) Tezpur (c) Kobe strong motions

Table 6.5 Summary of investigations on BS specimen subjected to different σ'_c and strong motions

Input motion	σ'_c (kPa)	D_r (%)	CSR_{max}	γ_{max} (%)	τ_{max} (kPa)	G (MPa)	$r_{u,max}$	Liquefaction
Bhuj (0.103g)	50	30	0.097	0.01	4.85	48.50	0.05	No
	100		0.092	0.03	9.2	30.67	0.13	
	150		0.078	0.03	11.7	39.00	0.13	
Tezpur (0.36g)	50	30	0.346	0.06	17.3	28.84	0.25	No
	100		0.327	0.70	32.7	4.67	1.00	Yes
	150		0.278	1.80	41.7	2.32	1.20	
Kobe (0.834g)	50	30	0.802	8.00	40.1	0.50	2.25	Yes
	100		0.756	15.0	75.6	0.50	1.75	
	150		0.645	18.0	96.7	0.54	1.75	

Effect of simultaneous increase of D_r and σ'_c

Previous sections presented the tests results obtained for the remoulded specimens prepared at D_r = 30%, 60% and 90% with varying σ'_c, separately, which reflects that the availability of soil of a particular D_r (for example, D_r = 30%) at a depth of 5 m, 10 m and 15 m where σ'_c = 50 kPa, 100 kPa, 150 kPa, respectively. This section illustrates the response of soil presents at a different depth and, varies in both σ'_c along with D_r, simultaneously. Fig. 6.23 illustrates the effect of both σ'_c and D_r simultaneously, wherein higher D_r of the test specimen was considered at a larger depth (i.e. 50 kPa and 30% at 5 m depth, 100 kPa and 60% at 10 m, 150 kPa and 90% at 15 m depth). Adoption of such parameters may be more realistic to the field scenario. In this case, $r_{u,max}$ was found to be 0.04, 0.1 and 0.1 at test conditions σ'_c = 50 kPa, D_r = 30%; σ'_c = 100 kPa, D_r = 60% and σ'_c = 150 kPa, D_r = 90%, respectively. γ_{max} was observed to be 0.12, 0.2 and 0.27, corresponding to the aforementioned testing conditions, respectively. The results indicate that γ and r_u increases with the increase in both σ'_c and D_r. Further, it can be concluded that in comparison to D_r, σ'_c has more pronounced effect on the enhancement of the liquefaction potential of soil. It is to be understood that soils at higher confining depth will require more σ_d to achieve the onset of liquefaction (as indicated by laboratory investigations). However, such high σ_d at higher depths will not be available in the field when subjected to strong motion, and

the zone of liquefaction is thus restricted more at shallower depths. The confining depths considered in the present study, as such, pertain to shallower depth (≤15 m), and hence, does not violate the field experience.

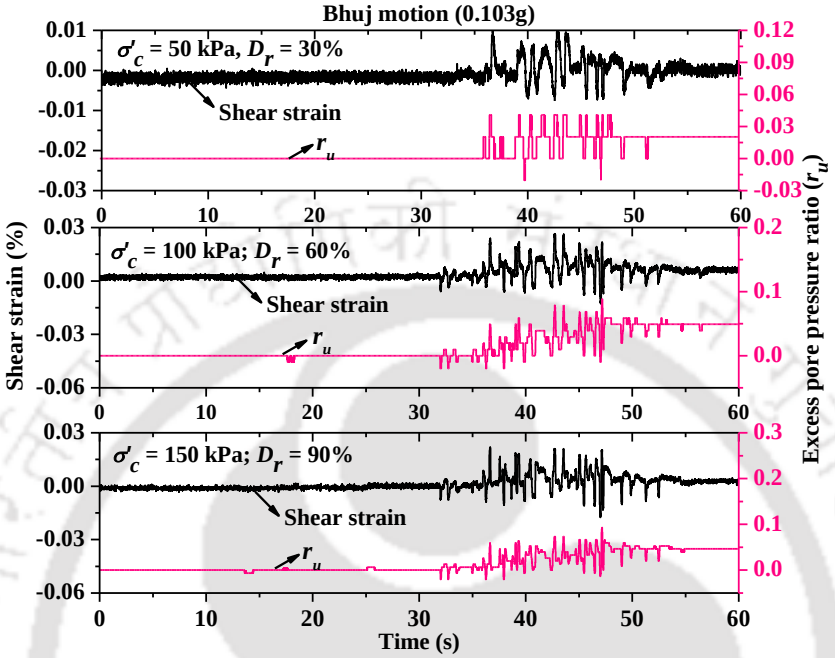

Fig. 6.23 Accumulation of shear strain and excess PWP ratio in SBS specimens subjected to Bhuj motion of PGA 0.103g for simultaneous variation in D_r and σ'_c

Effect of similarly scaled strong motions

This section discusses the results obtained from BS specimens with different strong motions scaled to specific PGA (0.103g and 0.36g). Fig. 6.24 presents the effect of the three earthquake motions (of same PGA) on BS specimens prepared at D_r = 60% and subjected to σ'_c = 100 kPa (10 m depth). Fig. 6.24a illustrates that when BS specimens subjected scaled PGA of 0.103g, none of the scaled ground motions initiate the liquefaction. Though, PGA is same, the specimens exhibited different amplitudes of γ_{max} under different excitations. γ_{max} was obtained in the following order of Bhuj (0.103g)>Kobe (0.103g)>Tezpur (0.103g). This is due to the Arias intensity and specific energy density of the earthquake motions, which also follow the similar trend as that obtained for γ_{max} i.e. Bhuj (0.103g)>Kobe (0.103g)>Tezpur (0.103g). Ground motions [Bhuj(0.103g), Tezpur(0.36g) and Kobe(0.834g)] when scaled to 0.36g (Fig.

6.24b), exhibited liquefaction in the soil sample. The variations in γ_{max} for 0.36g motions were found in the similar order as that of 0.103g.

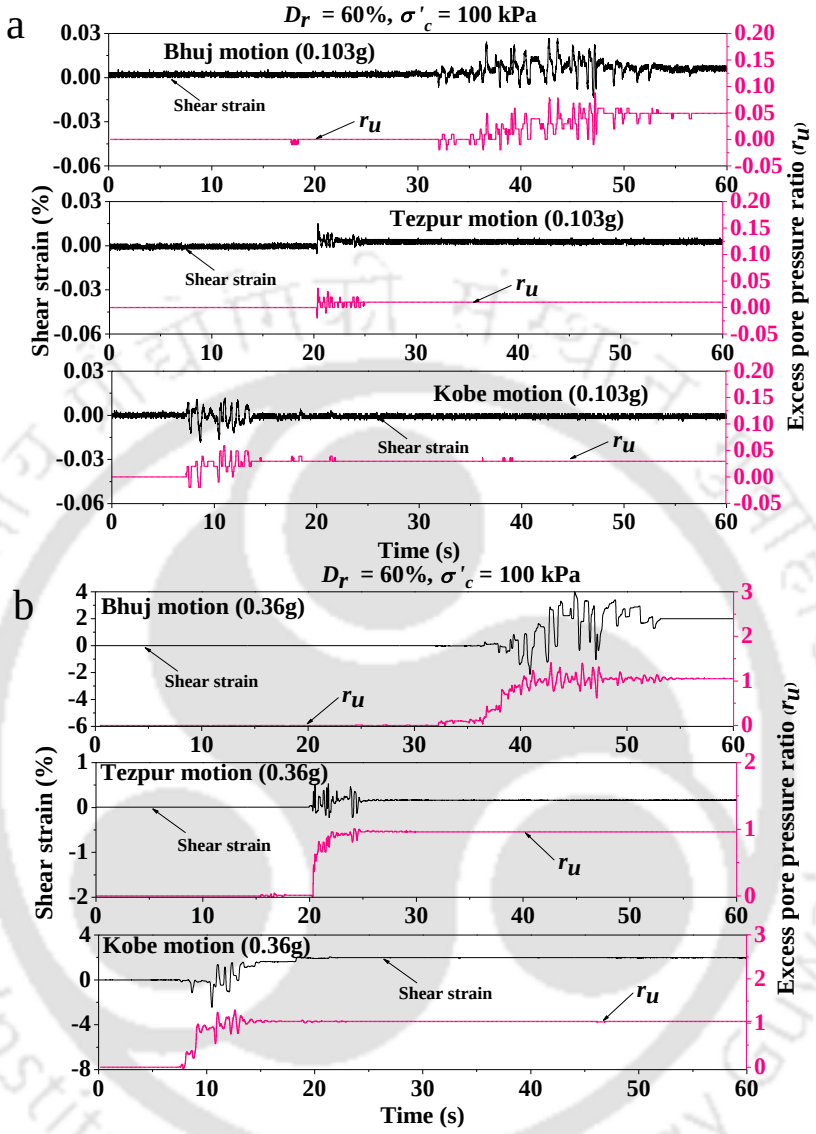

Fig. 6.24 Accumulation of shear strain and excess PWP ratio in SBS samples prepared at D_r = 60% and σ'_c = 100 kPa, and subjected to scaled earthquake motions of PGA 0.103g and 0.36g

The overall behaviour of the specimens can be clearly observed from the summary of the results presented in Table 6.6. It can be noted that BS specimens prepared at particular D_r and σ'_c, subjected to the similarly scaled strong motions, results in different magnitudes of maximum shear strain due to the variation in the associated strong motion parameters. From Table 6.6, it can be stated that Tezpur motion shows lowest values of γ_{max} and $r_{u,max}$ in comparison to the Bhuj and Kobe motion, the highest magnitudes being manifested by the Bhuj

motion. The reason for such behaviour is attributed to the varying strong motion parameters (Table 6.7) such as arias intensity, specific energy density, which exhibited similar trend of variation as that observed from the response of test results. Other strong motions parameters such as predominant period, mean period, bracketed duration and significant duration (Table 6.7) might have a direct or indirect effect on the observed responses. Sassa and Yamazaki (2017) have reported the influence of waveforms and durations of earthquakes on soil liquefaction. However, the study of individual parametric effects is outside the scope of the present attempt.

Table 6.6 Summary of results subjected to scaled ground motions with same PGA

Input motion	Scaled PGA(g)	D_r (%)	σ'_c (kPa)	CSR_{max}	τ_{max} (kPa)	γ_{max} (%)	G (MPa)	$r_{u,max}$	Lique-faction
Bhuj						0.026	35.38	0.09	
Tezpur	0.103	60	100	0.092	9.2	0.015	62.00	0.036	No
Kobe						0.019	48.42	0.06	
Bhuj						4.00	0.817	1.40	
Tezpur	0.36	60	100	0.327	32.7	0.52	6.29	1.00	Yes
Kobe						2.50	1.30	1.26	

Table 6.7 Ground motion parameters of scaled PGA of 0.103g and 0.36g

Parameters	Bhuj	Tezpur	Kobe	Bhuj	Tezpur	Kobe
	(0.103g)			(0.36g)		
Predominant period (s)	0.26	0.14	0.36	0.26	0.14	0.36
Mean period (s)	0.59	0.23	0.64	0.59	0.23	0.64
Bracketed duration (s)	55.18	30.72	21.92	55.18	30.72	21.92
Significant duration (s)	14.84	9.04	8.38	14.84	9.04	8.38
Arias intensity (m/s)	0.268	0.074	0.14	3.12	0.9	1.73
Specific energy density (cm^2/s)	438.56	8.7	128.57	5351	106.6	1570.4
v_{max}/a_{max} (s)	0.136	0.03	0.105	0.136	0.03	0.105

6.6 SUMMARY

This chapter presented the liquefaction potential of cohesionless soil (BS) based on the strain-controlled and stress-controlled tests. Regular excitations were used in strain-controlled approach, whereas in stress-controlled approach both the regular (sinusoidal) and irregular (Bhuj, Tezpur and Kobe strong motions) excitations were used. Tests were conducted using different investigating parameters such as γ, D_r and σ'_c. The variations in the generation of excess PWP and accumulated γ during cyclic loading, causing onset of liquefaction, were reported. Based on the results of BS specimens subjected to strain-controlled regular excitation, it can be concluded that the liquefaction resistance increases with the increase in D_r as well as σ'_c for any constant γ. It was also observed that r_u obtained at first cycle is significantly affected by σ'_c, although negligibly affected by D_r. It can also be concluded that the developed *CSR* attains a value of 0.5 with $r_u = 1$ at $\gamma \approx 1.0\%$, which can be considered as a limiting value ($\approx$ 1.0%) onset of liquefaction. Beyond this limiting γ, when *CSR* becomes greater than 0.5, soil is not able to resist even a single loading cycle and thus soil column was observed to instantly collapse/fail because of extensive increase in excess PWP i.e. nearly equal to or greater than the initial σ'_c. Thus, from the present study, it can be reported that the BS specimen shows quick initiation of liquefaction for different D_r and σ'_c, when CSR becomes nearly equal to 0.5.

Based on the results obtained from stress-controlled sinusoidal excitation, it can be concluded that the liquefaction resistance of BS soil affected by D_r and σ'_c. It was observed that γ approximately reached the magnitudes of 0.5-0.75% during the initiation of liquefaction. Based on the results of stress-controlled irregular excitation, it can be concluded that the BS specimens, prepared at any D_r, will show quick liquefaction under the following optimum conditions: PGA > 0.36g, CSR > 0.3 and $\gamma_{max} \geq 0.75\%$. Thus, based on the aforementioned result and discussions, it can be stated that the liquefaction potential of a cohesionless specimen is significantly affected by D_r, σ'_c, PGA of strong motion, γ and stress amplitude.

Chapter 7 GROUND RESPONSE ANALYSIS

7.1 INTRODUCTION

This chapter deals with the application of the findings from the experimental investigations. Ground response analysis (GRA) is one of the important studies to foresee the potential consequences of an earthquake prior to its occurrence. The response of the soil mass and any supported structure is governed by the regional seismicity, source mechanism, soil-structure interaction and local geology. This chapter discusses the outcomes of the one-dimensional equivalent linear GRA conducted for Guwahati city. The responses have been assessed using the experimentally evaluated strain-dependent dynamic properties (i.e. modulus reduction and damping ratio curve, as illustrated in Chapter 5) of the locally available soils, and the same has been compared to the response obtained using standard and commonly adopted models for dynamic properties of soils (e.g. Seed and Idris, 1970; Vucetic and Dobry, 1991). In order to assess the soil responses, the results are presented in terms of peak ground acceleration (PGA), Fourier amplification ratio (FAR), peak spectral acceleration (PSA) and variations in strain along with the depth.

7.2 STUDY REGION

Guwahati city, situated at 26.18°N (latitude) and 91.75°E (longitude) (shown by star mark in Fig. 7.1a), is the largest metropolitan city of Assam, also called as 'Gateway of the North-East India'. Based on the census (2011), this city is one of the fastest growing cities in India with a population of about 1 million. The city, outspread over an area of 215 km^2, is situated between the banks of the Brahmaputra River and foothills of the Shillong plateau. The topography of the Guwahati region consists of several hills and isolated hillocks made of Precambrian granitic rocks with varying altitude from 50-60 m above the mean sea level (MSL). Based on the past earthquake data, tectonic setup and regional geology, the city is surrounded by six seismic

blocks i.e. Shillong Plateau, Assam Valley, Eastern Himalaya, Mishmi Thrust, Bengal Basin and Indo-Burmese Range, as shown in Fig. 7.1(b) (Raghukanth et al., 2008). The city has experienced several devastating earthquakes of different magnitudes ranging from M5 to M8.7 (Nath et al., 2008). Thus, accounting the prevalent seismicity level encountered in the area, one-dimensional (1-D) GRA has been conducted for Guwahati city. Three different earthquake motions, namely Bhuj, Tezpur and Kobe strong motions having peak ground acceleration (PGA) of 0.103g, 0.36g and 0.834g respectively, has been chosen for the said purpose.

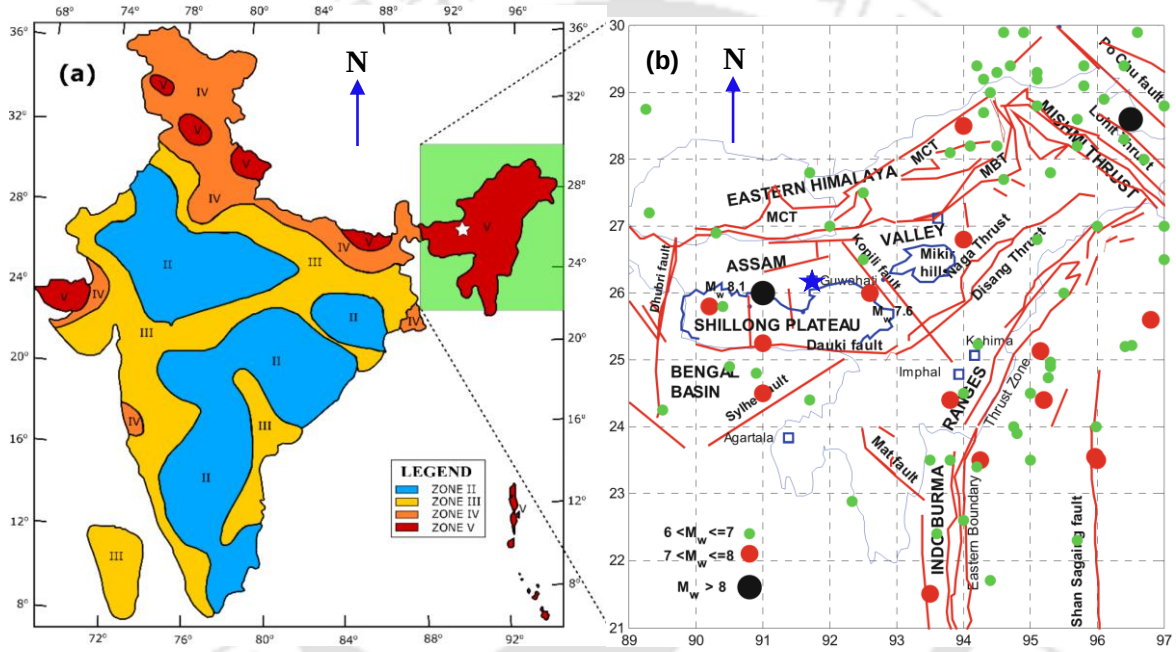

Fig. 7.1 (a) Seismicity of India and study region (IS 1893: 2002) (b) Seismic fault details nearby the study region (Raghukanth and Dash, 2010)

7.3 SITE CHARACTERIZATION

The characteristics of geological layers, especially up to a depth of 30 m from the ground surface, plays a dominant role in earthquake geotechnical engineering, since the amplification or de-amplification of the ground motion are predominantly controlled by these geologically surficial layers (Nandy, 2007). In the present study, extensive geotechnical site investigation data are collected for the Guwahati city and analyzed for their response when subjected to various strong motions. The location map of boreholes is presented in Fig. 7.2. At these

locations, both borehole investigation data and laboratory test data were used to collate the relevant information required for GRA, namely the index properties of soil deposits, thickness of subsoil strata and the Standard Penetration Test (SPT) *N* values. The SPT-*N* values were further used to estimate the shear wave velocity profiles of the substrata using standard correlation as proposed by Maheswari et al. (2010).

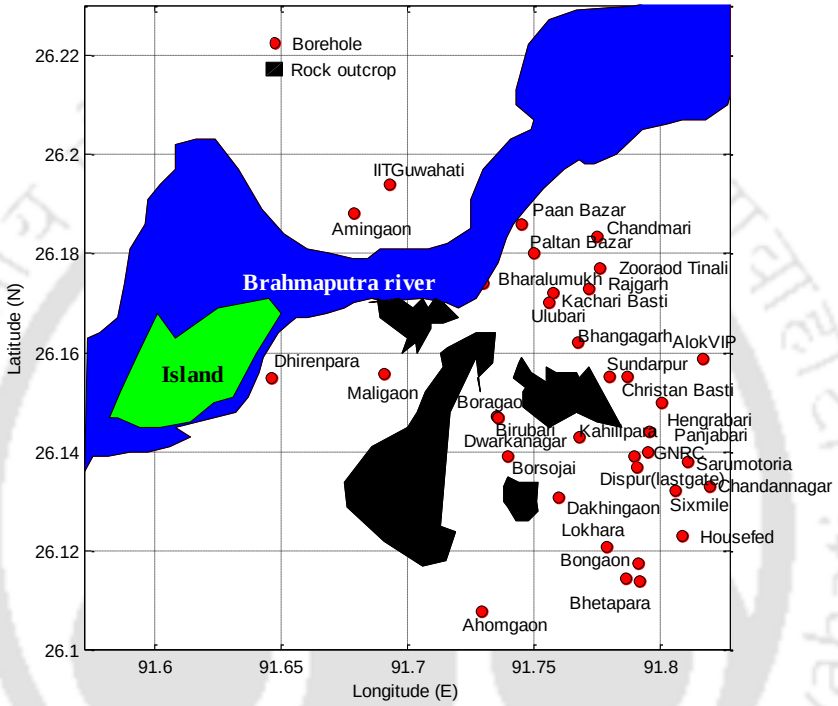

Fig. 7.2 Location of boreholes used for GRA of Guwahati city

Some typical borehole profiles at few sites, namely Boragaon (BRGN), Satgaon (STGN), Alok Sixmile (ALKSX) and Sundarpur (SUND), are presented in Fig. 7.3. As per geotechnical site investigation data, it was found that the soil deposit consists mostly of either sandy, silty and clayey soils, or their varying combinatorial mixtures. In most cases, the SPT-*N* values have been collected at an interval of 1.5 m, up to a depth of 26-30 m, or as per the premature termination depth of the boreholes. The ground water table (GWT) is located at shallow depths from the ground level (GL), mostly within 2 m from the surface. The particle size distribution of local soils were determined (as per IS: 2720, part-IV), and based on the zone of liquefiable soils as proposed by various researchers (Tsuchida, 1970; Ishihara et al., 1980; Xenaki and

Athanasopoulos, 2003), as already presented in Chapter 3, it was identified that the soils considered for the present study are susceptible to liquefaction.

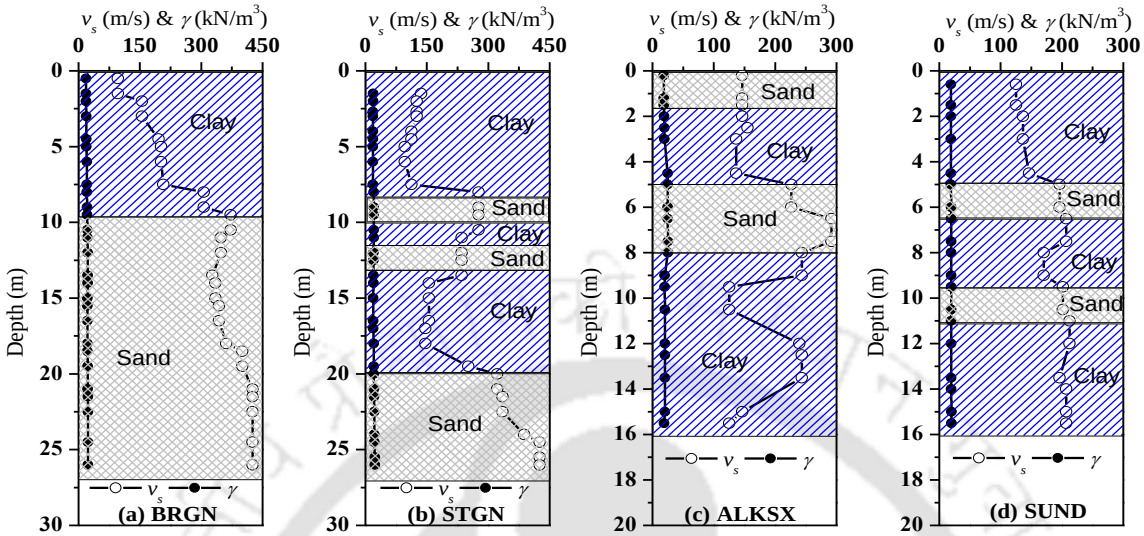

Fig. 7.3 Typical borehole profile at sites (a) BRGN (b) STGN (c) ALKSX (d) SUND

7.3.1 Dynamic properties of soils

Past earthquake events have indicated that soils may experience different extents of shear strain levels depending on their dynamic characteristics (Suetomi and Yoshida, 1998; Kiku and Yoshida, 2000; Kumar and Krishna, 2013). The response of soils at high strain levels (> 0.01%) is substantially different than that obtained at low strain levels (< 0.01%), primarily due to the nonlinear stress-strain behaviour and high damping characteristics of the soil at higher strains (Ishihara, 1996). Researchers have reported the application of different testing methodologies, e.g. resonant column tests and cyclic triaxial tests, to evaluate the dynamic properties of soil at varying range of shear strains. For the present study, cyclic triaxial shear tests were conducted to assess the liquefaction potential of cohesionless soils (over a confining pressure range of 50-150 kPa) using Bhuj, Tezpur and Kobe motions. It was revealed that the maximum value of shear strains were in the range of 0.01-0.03%, 0.06-1.8%, 5-18%, respectively. Hence, depending upon the strong motion characteristics, the same soil exhibits different degree of nonlinearity during seismic shaking. Therefore, it is highly essential to utilize the

experimentally assessed dynamic properties of soils (modulus reduction and damping ratio curves) over a wide range of shear strain to obtain a precise outcome from a seismic GRA. Experimentally evaluated modulus reduction and damping ratio curves of both locally available cohesionless and cohesive soils, for shear strains varying between 0.0001% and 5%, is presented in Fig. 7.4, and the same has been used in the GRA for the present study.

In the absence of site-specific modulus reduction and damping ratio curves, it is a common practice to adopt standard curves (Vucetic and Dobry (1991) for clays, Seed and Idriss (1970) for sands) in the evaluation of GRA (Hashash et al., 2011). It is worth mentioning that any standard curves (as shown in Fig. 7.4) are developed on the basis of certain types of experimentations on soils of particular composition, subjected to particular strain ranges (mostly within 1%). In commercially available software, such as DEEPSOIL, as used in the present study, the range of shear strain used to represent the modulus reduction and damping ratio curves are mostly extrapolated to 1-10%, beyond the actual limits for which experimentations were conducted. Hence, the usage of the standard curves, without paying due attention to the actual composition and dynamic response of the soil (especially at higher strain ranges), may yield improper response. This study highlights the difference of the responses obtained using the standard curves in comparison to the same obtained using the experimentally obtained dynamic soil properties of the local soils. The material curves, as used in DEEPSOIL, depend on the parameters such as the effective vertical stress and plasticity index (PI) of soil (Hashash et al., 2016). In the present study, the values of the required parameters were chosen accordingly as determined from the laboratory investigation of the soil samples obtained from various depths during the borehole investigation survey.

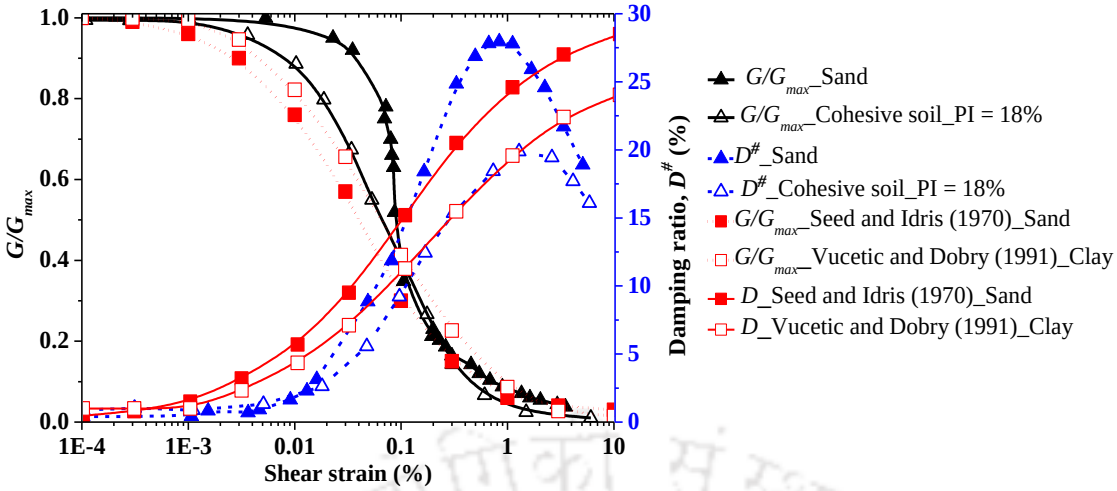

Fig. 7.4 Soil models for locally available soils used for GRA of Guwahati city

7.4 GRA METHODOLOGY

The present study utilizes the Equivalent-linear (EQL) approach to perform GRA on the basis of the following assumptions: (a) all substrata boundaries are horizontal, and the soil and bedrock layers are extended infinitely in the horizontal direction (b) the soil profile is subjected to vertically propagating shear waves. DEEPSOIL, commercial software developed by University of Illinois, Urbana Champagne (UIUC), has been used to perform the one-dimensional GRA (Hashash et al., 2016). The input parameters required to conduct the GRA are the material type with strata thickness, unit weight, shear wave velocity, material properties (modulus reduction and damping ratio curve) and the input strong motion data. Variations in shear wave velocity (V_s) and unit weight along with the depth for some typical soil profiles are presented in Fig. 7.3. In the absence of direct estimation of the shear-wave velocity (V_s) profiles, SPT-*N* values obtained from the borehole survey were used to estimate the V_s profile using the correlation (Eqn. 7.1) provided by Maheswari et al. (2010).

$$V_s = 95.64 \times N^{0.301} \tag{7.1}$$

One-dimensional seismic GRA was carried out to estimate the response of stratified soil profiles in terms of the variations in peak horizontal and peak ground acceleration (PHA and PGA),

amplification ratio (AR), response spectrum, stress ratio and strain variations with the depth of the soil profile.

7.4.1 Fundamentals of EQL method

The equivalent linear (EQL) method of GRA was developed to analyze the non-linear response of soil using frequency domain analysis with the aid of linear transfer functions. This methodology approximates the non-linear behaviour of the soil (i.e., strain dependent shear modulus and damping characteristics) using an adaptive iterative procedure (Kramer, 1996). The iterative procedure is governed by the target of finding a compatible shear modulus and damping ratio for a particular effective shear strain. Generally, the effective shear strain is considered to be 65% of the maximum shear strain developed in a particular layer (Kramer, 1996).

In the frequency domain analysis, the strain time histories obtained for each layer are used to identify the maximum shear strain, which is further used in the estimation of effective shear strain. The computed effective shear strain for a given soil layer is then used to estimate the corresponding strain-compatible shear modulus and damping ratio based on an iterative technique. This process is repeated until a convergent solution is obtained. The equivalent linear analysis considers the soil layer to be represented as a linear visco-elastic material, in which the shear modulus and damping ratio is maintained constant to the corresponding strain-compatible values during each of the iteration cycles of the analysis.

One-dimensional GRA is associated with the vertical propagation of shear waves through a linear viscoelastic system. For the purpose of viscoelastic wave propagation, soil behaviour is approximated as a Kelvin-Voigt solid (i.e., a material whose resistance to shearing deformation is the sum of elastic and viscous resistance) governed by the linear elastic shear modulus and viscous damping (Kramer, 1996). The stress-strain relationship for a Kelvin-Voigt

solid subjected to shear is presented in Eqn. 7.2.

$$\tau = G\gamma + \eta \frac{\partial \gamma}{\partial t} \tag{7.2}$$

where, τ is the shear stress, G is the shear modulus, $\gamma = \partial u / \partial z$ is the shear strain and η is the coefficient of viscous damping. One-dimensional equation of motion for vertically propagating shear waves (in z direction) is presented in Eqn. 7.3.

$$\rho \frac{\partial^2 u}{\partial t^2} = \frac{\partial \tau}{\partial z} \tag{7.3}$$

where, ρ is the mass density of medium, and u is the displacement of the medium along lateral direction.

$$\rho \frac{\partial^2 u}{\partial t^2} = G \frac{\partial^2 u}{\partial z^2} + \eta \frac{\partial^3 u}{\partial z^2 \partial t} \tag{7.4}$$

Finally, by solving Eqn. 7.2 and Eqn. 7.3, using the adaptive iteration technique, the equation of motion presented in Eqn. 7.4 yields the one-dimensional ground response.

7.5 STRONG GROUND MOTIONS

To delineate the effects of strong motions of various intensities, and explore the dynamic response of the soil in low and high strain ranges, three different acceleration-time histories were chosen for the present GRA study, namely Bhuj (2001; PGA = 0.103g), Tezpur (2012; Scaled PGA = 0.36g) and Kobe (1995; PGA = 0.834g). Fig. 7.5 presents the acceleration time histories of these earthquake motion and the detail of which are discussed in Chapter 3. The strong motion record of Kobe earthquake was obtained from the database available in DEEPSOIL, while the data of Bhuj earthquake and Tezpur earthquake were obtained from the earthquake databases available at *www.cosmos.org* and *www.pesmos.org*, respectively. The characteristics of these ground motions like predominant period, mean period, bracketed duration and significant duration were derived by using SEISMOSIGNAL program

(*www.seismosoft.com*), and are listed in Table 7.1. The mean period of strong ground motions are found to be varying from 0.17-0.64s.

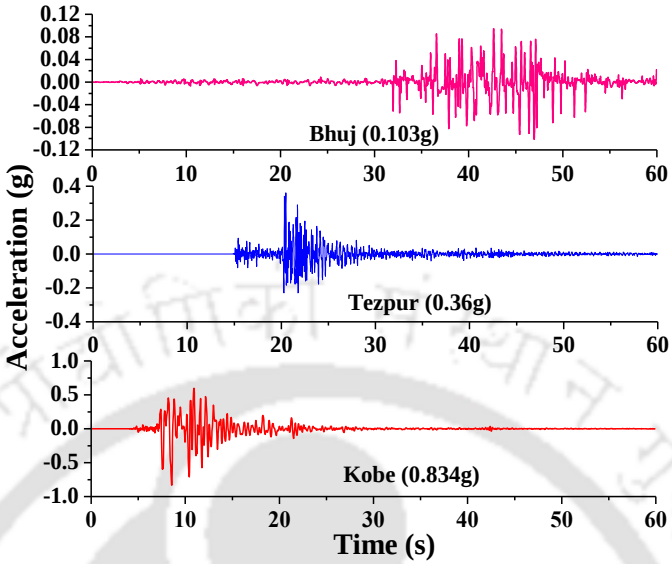

Fig. 7.5 Acceleration time histories of input motions used for GRA study

Table 7.1 Strong motion parameters for different earthquakes used for the analysis

Strong motion parameters	2001 Bhuj	2012 Tezpur (Original)	2012 Tezpur (Scaled)	1995 Kobe
Magnitude (M_w)	7.7	5.0	5.0	6.9
Station	Ahmedabad	TZP	TZP	KJMA
Site Class	B	B	B	B
Distance from source	238 km	-	-	0.6 km
Max. PGA (g)	0.103	0.027	0.36	0.834
Predominant period (s)	0.26	0.08	0.08	0.36
Mean period (s)	0.59	0.167	0.167	0.64
Frequency (Hz)	1.69	5.99	5.99	1.56
Bracketed duration (s)	55.8	28.30	28.30	21.90
Significant duration (s)	14.84	14.38	14.38	8.38
Arias intensity (m/s)	0.268	0.003	0.556	8.38
Specific energy density (cm^2/s)	438	0.17	33	7573
Cumulative absolute velocity (cm/s)	470	47	653	2119
v_{max}/a_{max} (s)	0.136	0.021	0.021	0.103

7.6 RESULTS AND DISCUSSIONS

GRA has been carried out for eighteen borehole locations at Guwahati city, using three different seismic time histories. The typical four soil sites namely, Boragaon (BRGN), Satgaon (STGN),

Alok Sixmile (ALKSX) and Sundarpur (SUND) are presented in Fig. 7.3, highlighting the variation of shear wave velocity and unit weight along the depth. The following sections illustrate the influence of different strong motions and site conditions on the outcomes of GRA. Typical results are provided for the stated four sites in order highlight the difference arising from the adoption of standard and experimentally estimated dynamic properties of soils. The results are presented in terms of the variations in acceleration and strain along the depth, as well as the Fourier amplification ratio and peak spectral acceleration at top layer. Contour maps exhibiting the overall distribution of the various outcomes along the entire Guwahati city are also reported.

7.6.1 Influence of specific strong motion on GRA of Guwahati city

This section presents the seismic response obtained at four sites (BRGN, STGN, ALKSX and SUND) subjected to Bhuj motion. All the soil layers at both the sites were defined by the dynamic soil properties obtained experimentally (i.e. experimental soil model) as well as according to the existing standard soil models (i.e. Vucetic-Dobry, VD, and Seed-Idriss, SI, models). Fig. 7.6 illustrates the variations in peak horizontal acceleration (PHA) along the depth, obtained at four sites. In comparison to the adoption of VD-SI data, PGA (PHA at the topmost layer) at BRGN site, obtained by the use of experimental data, is approximately 35% higher. It is observed that the topmost clayey strata at stratum STGN site (2.5-7.5 m) is relatively softer than that found at BRGN site (Fig. 7.3). Thus, in this case, the influence of choosing the experimental dynamic properties is evident wherein it can be observed that the adoption of standard properties leads to the underestimation of PHA or PGA magnitudes. Similarly, at STGN and SUND sites reflect nearly 40% and 9%, respectively, higher PHA based on experimental data. However, ALKSX site shows nearly 50% lesser PHA based on experimental data. This might be attributed to the clay layer with low shear wave velocity at bottom.

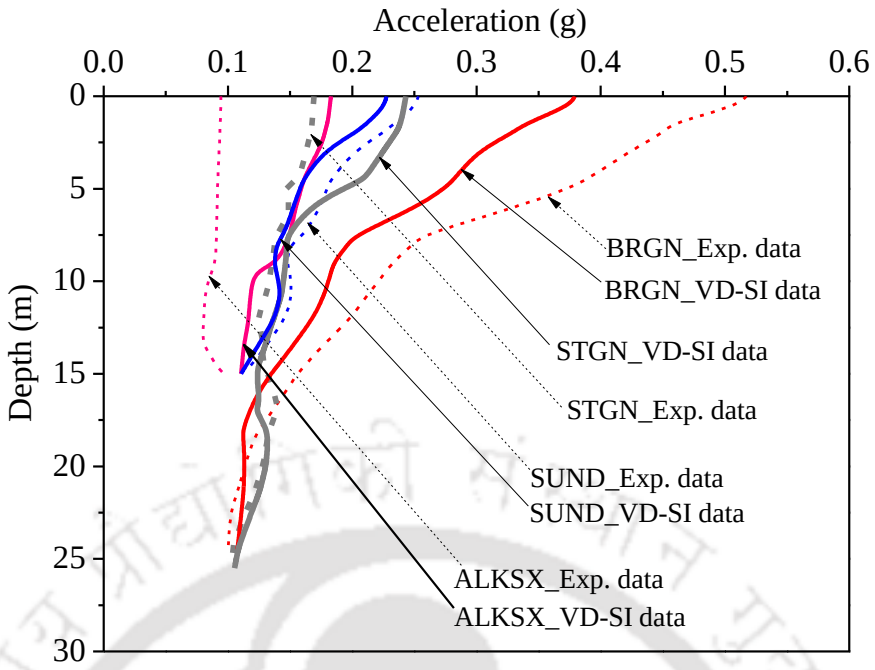

Fig. 7.6 Variation in PHA along the depth at BRGN, STGN, ALKSX and SUND sites subjected to Bhuj motion

Fig. 7.7 illustrates the variations in shear strain along with the depth obtained from GRA at aforementioned four sites subjected to Bhuj motion. The strain values at BRGN and SUND sites were observed to be less than 0.1% (Fig. 7.7a), using both experimental as well as VD-SI data. However, STGN site showed strain of nearly 2% at a depth of 7 m upon using the experimental data (Fig. 7.7b). This is attributed to the degradation of damping ratio in the soft soil layer. ALKSX site shows nearly 0.5% shear strain at approximate depth of 10 m with VD-SI data (Fig. 7.7b), which is relatively lesser than the experimental data. In comparison to the outcomes from adopting the standard damping ratio curves, the degradation of soil damping beyond 1% of shear strain, as obtained from the experimental curves, is found to significantly affect the ground response. Fig. 7.8 presents the variations in amplification ratio at the top layer, obtained at all four sites. It was seen that the amplification ratio obtained at BRGN and SUND sites, with experimentally obtained dynamic properties, is nearly 40% and 28%, respectively, higher than the same obtained from VD-SI model. However, the amplification ratio obtained from the experimental model at STGN site is nearly 20% lesser than that obtained from VD-SI

model. Similar response has been obtained at ALKSX site. This is attributed to the presence of soft soil layer represented by low shear wave velocity presented in Fig. 7.3. Therefore, from Fig. 7.8, it can be stated that the amplification or de-amplification of the strong motion depends on the variation of the damping ratio of the soil over a wide frequency range, and that the adoption of standard non-degrading damping ratio with increase in strain, will lead to imprecise results.

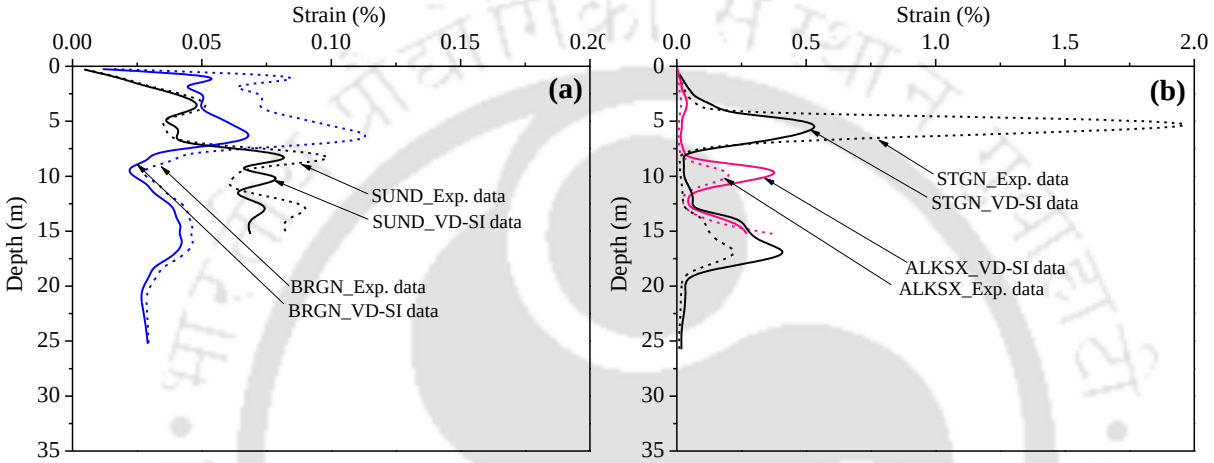

Fig. 7.7 Variations in strain at (a) BRGN and SUND (b) STGN and ALKSX sites subjected to Bhuj motion

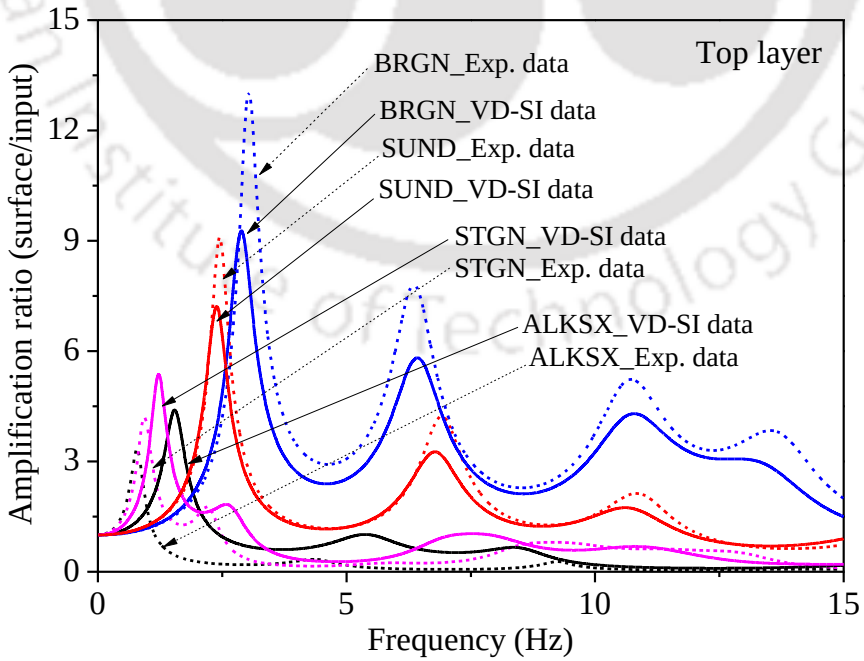

Fig. 7.8 Variations in amplification ratio at BRGN, STGN, ALKSX and SUND sites subjected to Bhuj motion

The Peak Spectral Acceleration (PSA) at ground level (considering 5% Rayleigh damping) at aforementioned four sites are presented in Fig. 7.9. In comparison to VD-SI model, higher value of PSA was observed at BRGN and SUND sites using the experimental soil model whereas, at STGN and ALKSX sites, lesser value of PSA is obtained from experimental soil model in comparison to VD-SI model. Similar outcomes have been determined for all the other test sites and the results are presented in contour plots shown in Fig. 7.10-Fig. 7.12.

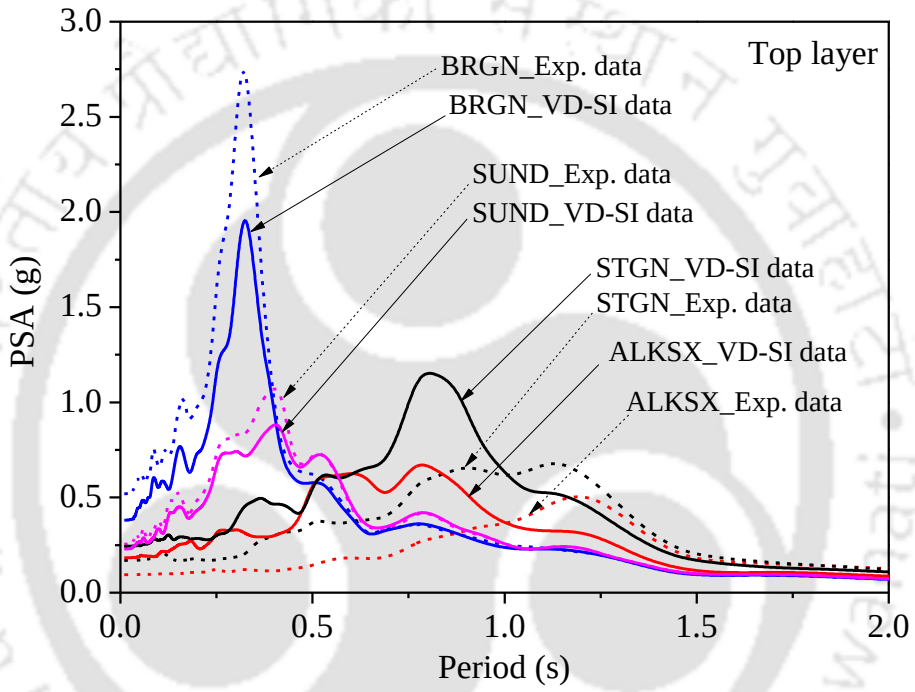

Fig. 7.9 Variations in PSA at BRGN, STGN, ALKSX and SUND sites subjected to Bhuj motion

Fig. 7.10 shows the contour map of the variations in PGA for Guwahati city using soil properties obtained from experiment and VD-SI data. On the use of experimental data (Fig. 7.10a), higher ground shaking (reflected by higher PGA) at sites Amingaon, Chandmari, Bongaon, Boragaon, Ahomgaon, GNRC were observed, in comparison to the use of VD-SI data (Fig. 7.10b).

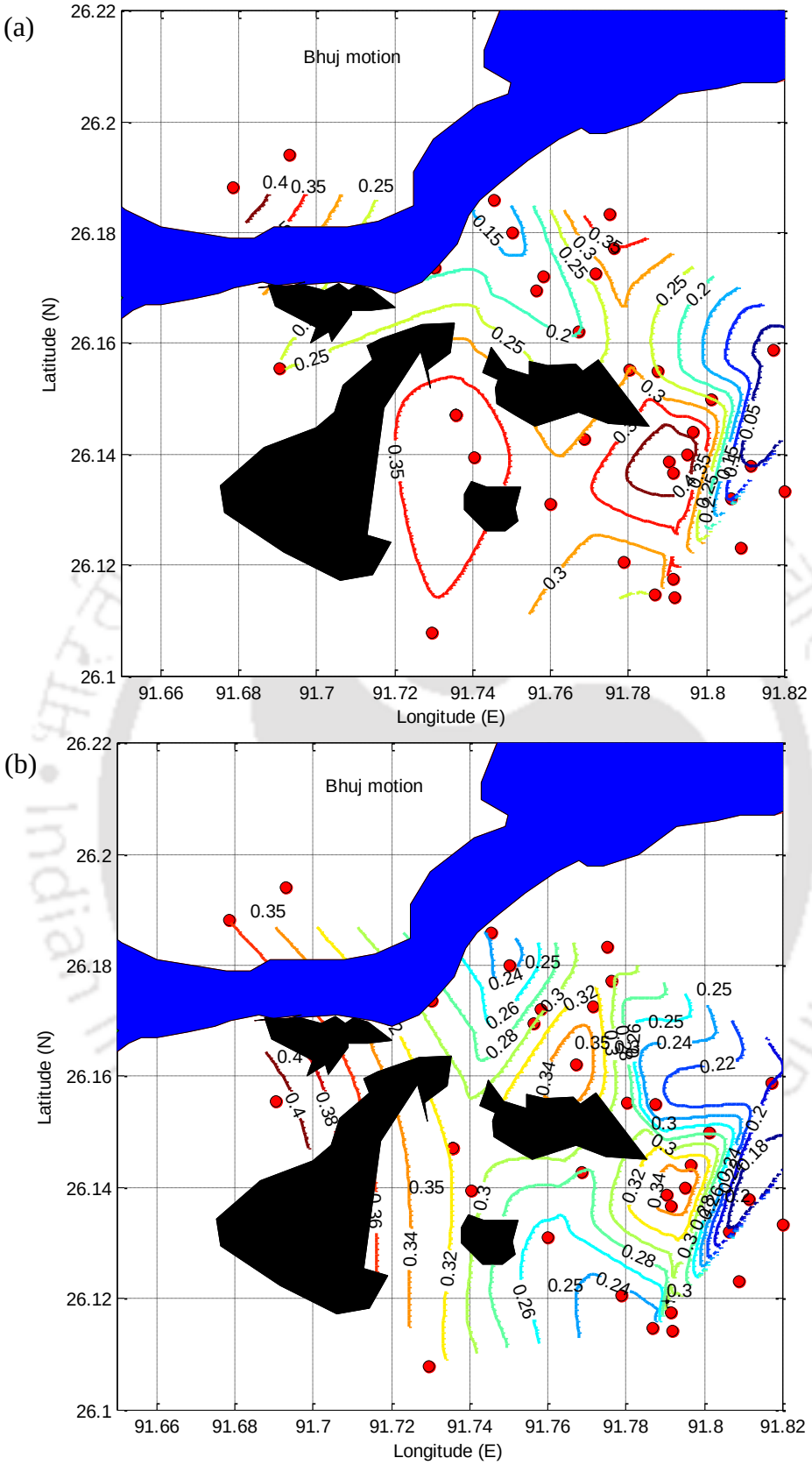

Fig. 7.10 Variations in PGA at surface level due to Bhuj motion based on (a) experimental data (b) VD-SI data

Fig. 7.11 presents the peak Fourier amplification ratio (FAR) for Guwahati city, using soil properties by experimental data and VD-SI data, on the application of Bhuj motion. Fourier amplification ratio (FAR), is the ratio of PGA at ground surface to PGA of an input motion, provides the information about amplification/deamplification of bedrock motion at ground surface. Higher values of FAR was obtained on the use of experimental data (Fig. 7.11a), at sites Amingaon, Chandmari, Bongaon, Boragaon, Ahomgaon, GNRC, in comparison to the use of VD-SI data (Fig. 7.11b).

Fig. 7.12 illustrates the variations in PSA at ground surface for damping ratio of 5%. PSA is significantly important in the design of earthquake resistant structure, as it provides an important descriptive representation of the influence of a given earthquake on a structure for a specified damping ratio. The spectral acceleration at different frequencies provides the response spectrum. Response spectrum describes the maximum response of a single-degree-of-freedom (SDOF) system subjected to a particular input motion, as a function of the natural frequency and damping ratio of the SDOF system (Kramer, 1996). The maximum response of a structure to a particular input motion is commonly used for the earthquake resistant design. Higher value of PSA was obtained on the use of experimental data (Fig. 7.12a), at sites Amingaon, Chandmari, Bongaon, Boragaon, Ahomgaon, GNRC, in comparison to the use of VD-SI data (Fig. 7.12b).

Table 7.2 presents the summary of the results in terms of percentage difference in average PGA, PSA and FAR for Guwahati city using Bhuj motion. It reflects that the average PGA is nearly 6% higher based on VD-SI data whereas, PSA is nearly 3% higher based on VD-SI data. However, the average FAR is nearly 3% higher based on experimental data. Therefore, based on Table 7.2, it is recommended that GRA of any region should be conducted on the basis of the regional dynamic soil properties, and in all possible cases, the adoption of standard reference curves should be avoided in order to achieve precise GRA results.

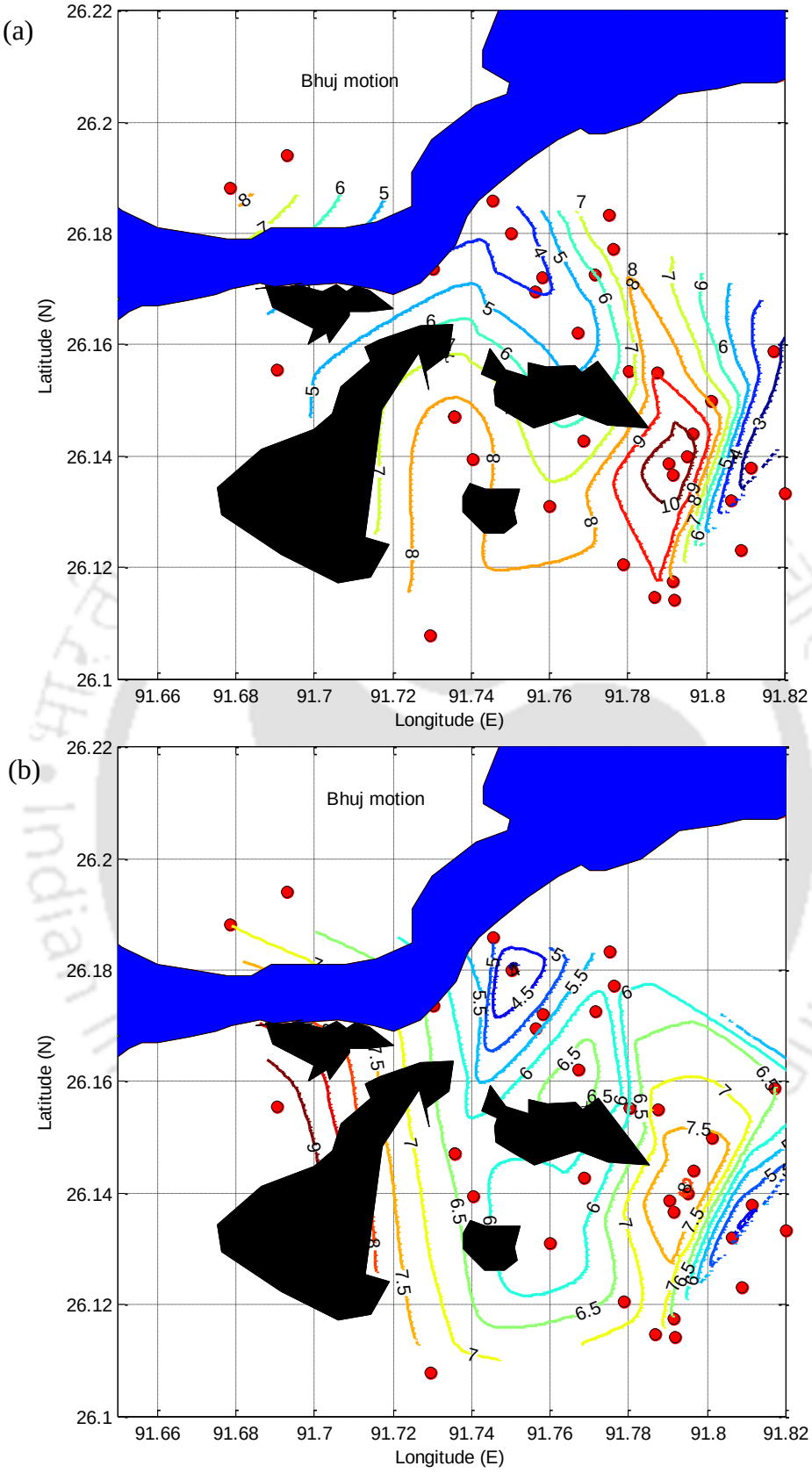

Fig. 7.11 Variations in peak FAR at surface level due to Bhuj motion based on (a) experimental data (b) VD-SI data

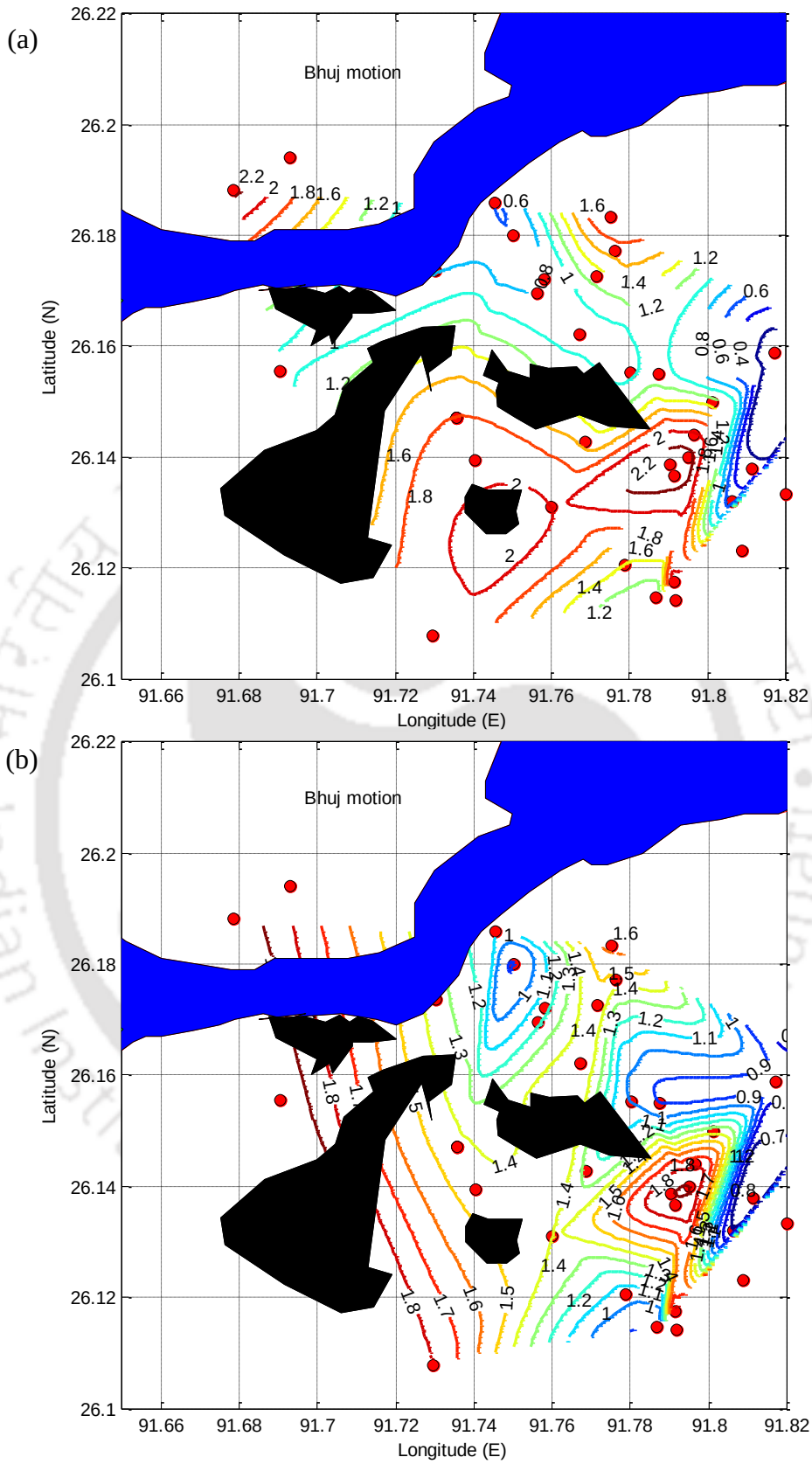

Fig. 7.12 Variations in PSA at surface level due to Bhuj motion based on (a) experimental data (b) VD-SI data

Table 7.2 Comparison of percentage difference in PGA, PSA and FAR obtained using VD-SI and Experimental data for GRA of Guwahati city using Bhuj motion

Earthquake	Average value	VD-SI data	Experimental data	Difference (%)
Bhuj	PGA (g)	0.287	0.27	6.29
	PSA (g)	1.358	1.32	2.89
	FAR	6.389	6.58	2.99

7.6.2 Influence of various strong motions on GRA of Guwahati city

Fig. 7.13 shows the variations in PHA at BRGN site along the depth using different strong motions. It illustrates that the Kobe motion get amplified at a depth of 5-7.5 m if the standard VD-SI model is used, while the usage of present experimental data illustrate the deamplification at the stated depths; while Bhuj and Tezpur motion does not show much difference at similar locations. Thus, it can be stated that the amplification and deamplification of strong motions depends on the soil strata characteristics (stiffness of soil layer), material properties (modulus degradation and damping behaviour) and strong motion characteristics.

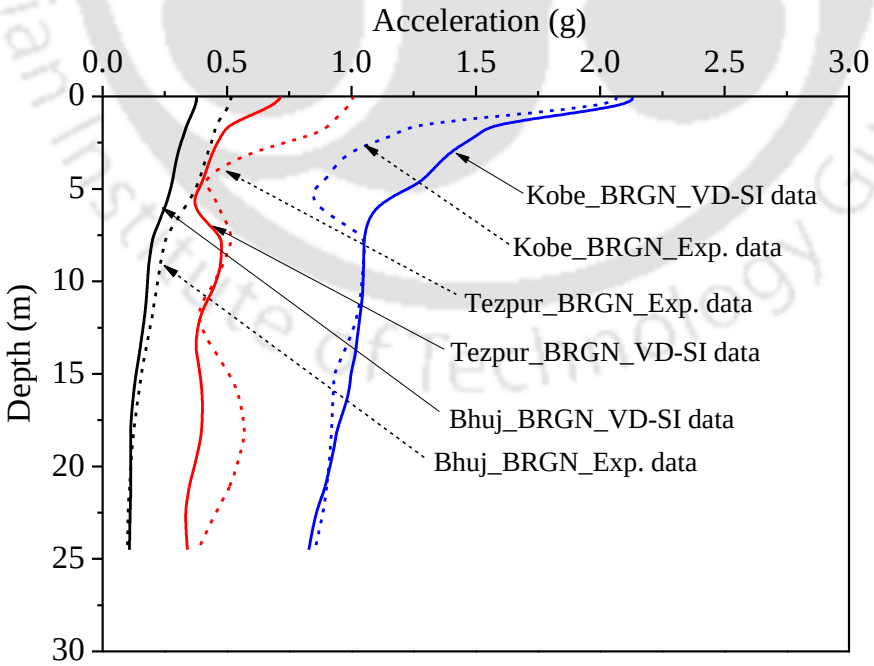

Fig. 7.13 Variations in PHA with depth at BRGN due to Bhuj, Tezpur and Kobe motions

Fig. 7.14 presents the variations in strain along the depth obtained from Bhuj, Tezpur and Kobe motion. Fig. 7.14a shows the variations in strain along the depth due to Bhuj and Tezpur motions, whereas Fig. 7.14b presents the same for Kobe motion. It can be seen that the layer with low shear wave velocity, i.e. low shear stiffness, shows significantly higher value of strains corresponding to the experimentally obtained dynamic properties for the soil model subjected to strong motion with high PBRA (Peak Bedrock Input Motion). Such high value of strain (>15%) will lead to catastrophic damage.

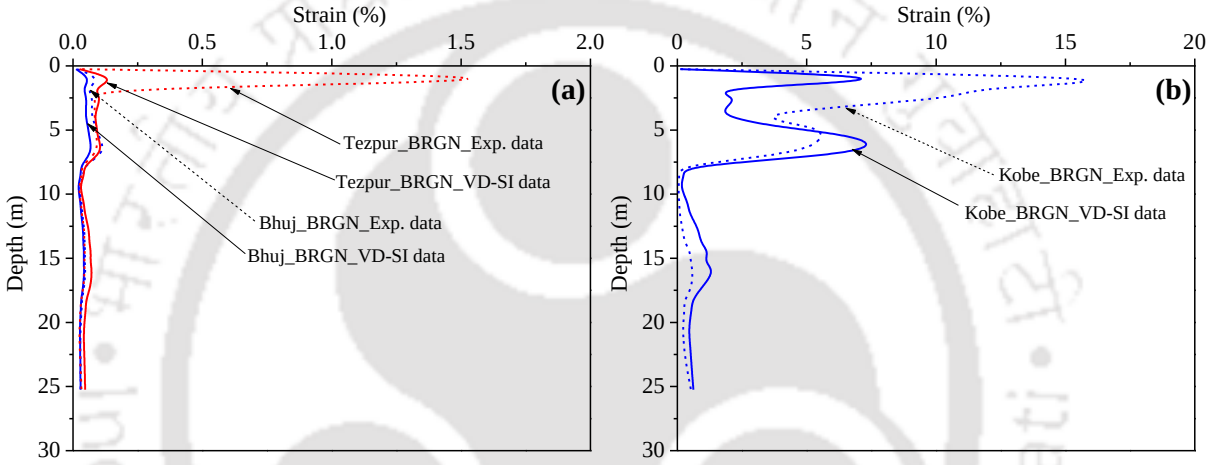

Fig. 7.14 Variations in strain with depth at BRGN using (a) Bhuj and Tezpur motions (b) Kobe motion

The variations in amplification ratio at surface layer, obtained with all three strong motions are presented in Fig. 7.15. It is seen from Fig. 7.15 that the amplification ratio obtained at BRGN site using Bhuj, Tezpur and Kobe motion, with experimental soil model, is nearly 10–40% higher than the same obtained from VD-SI model. However, the amplification ratio obtained from Kobe motion with experimental soil model shows lower magnitude of FAR with frequency shift towards the lower values by nearly 2 Hz. This is due to the availability of soft soil layer, represented by low shear wave velocity, as shown in Fig. 7.3(a), and degradation of damping ratio. The lower value of FAR indicates that the higher peak bedrock acceleration (PBRA) motion amplify less than the lower PBRA motion.

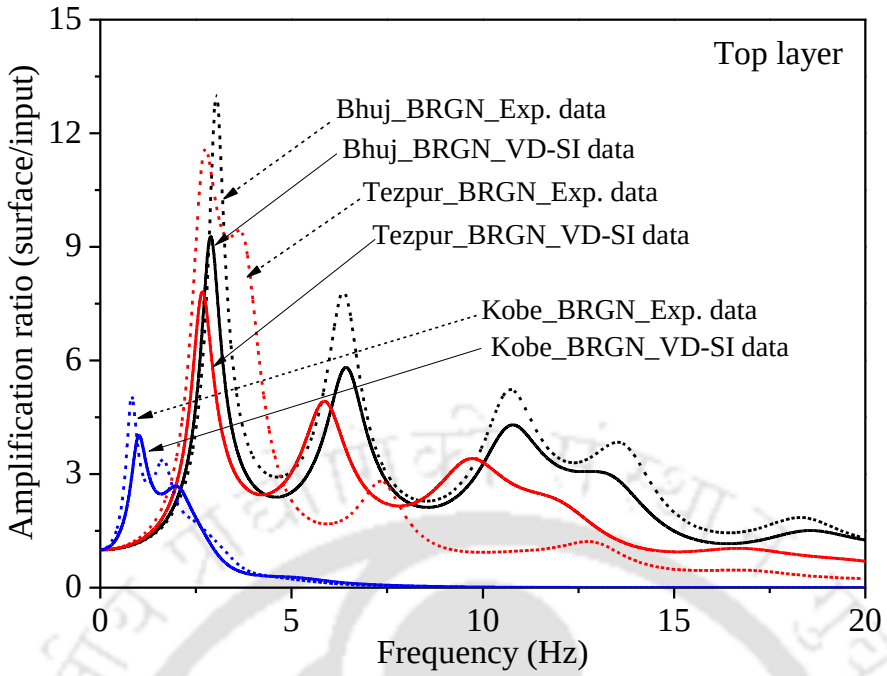

Fig. 7.15 Variations in amplification ratio at surface level for BRGN due to Bhuj, Tezpur and Kobe motions

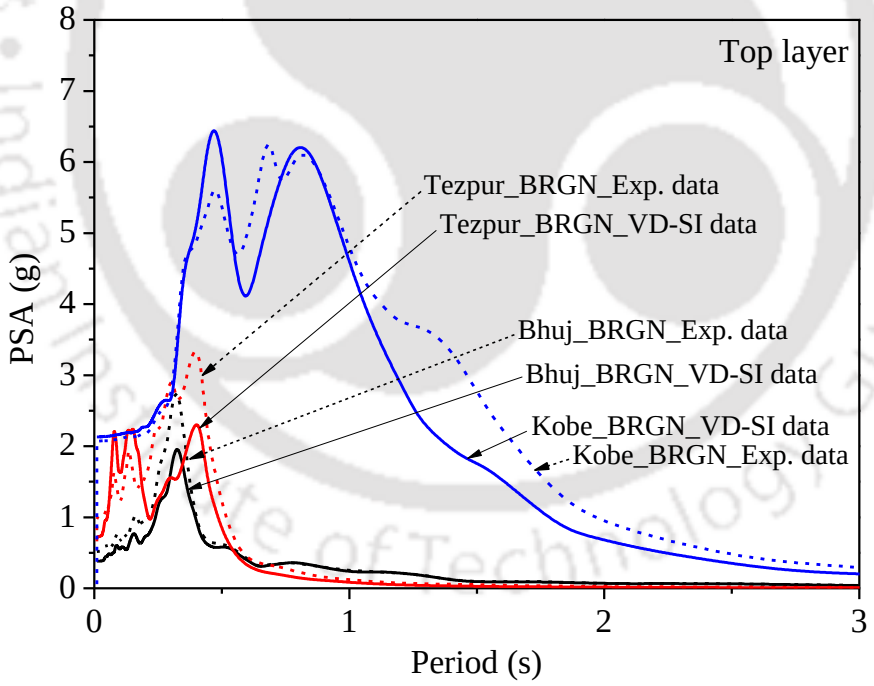

Fig. 7.16 Variations in SA at surface level for BRGN due to Bhuj, Tezpur and Kobe motions

The Peak Spectral Acceleration (PSA) at ground level for 5% damping at BRGN site are presented in Fig. 7.16. The PSA at BRGN site was observed to be significantly higher with Kobe motion than the Bhuj and Tezpur motion. The PSA obtained from Kobe motion shows

nearly similar value from both experimental as well as VD–SI model whereas, PSA obtained from Bhuj and Tezpur motion is nearly 40% higher with experimental soil model.

The PGA results obtained for all eighteen boreholes subjected to Bhuj motion are presented in contour plot as shown in Fig. 7.17. Fig. 7.17a presents the variations in PGA for Guwahati city based on the experimental soil properties data, whereas Fig. 7.17(b) presents the same obtained from VD-SI soil properties data. It is seen that, in comparison to the experimental data, VD-SI data provide approximately 6% higher PGA (average PGA). Fig. 7.18 presents the variations in PGA at all boreholes subjected to Tezpur motion. The average PGA from experimental data was found to be 0.45g (Fig. 7.18a), whereas the same with VD-SI data is 0.437g (Fig. 7.18b). Therefore, it can be stated that, in comparison to the VD-SI data, the average PGA obtained from experimental data is approximately 3% higher. Similar response of PGA was observed with Kobe motion shown in Fig. 7.19. It is seen that the average PGA with VD-SI data is 1.039g (Fig. 7.19a), whereas the same with experimental data is 0.75g (Fig. 7.19b), which is nearly 39% lesser than that obtained from the use of VD-SI data. It can also be observed that with the increase in PGA of input motion at the bottom of the soil profiles, the ground shaking also increased (reflected by PGA at ground surface).

Fig. 7.20 to Fig. 7.22 shows the variations in FAR, presented in contour plot, for Guwahati city, obtained from both experimental soil model as well as VD-SI soil model. On the use of experimental data, the average FAR was 6.58, 6.85 and 4.16 when soil profiles were subjected to Bhuj, Tezpur and Kobe motion, respectively and the same presented in Fig. 7.20a, Fig. 7.21a and Fig. 7.22a, sequentially. With VD-SI data, the average value of FAR for Guwahati city was found to be 6.389, 6.336 and 3.202 when subjected to Bhuj, Tezpur and Kobe motion, respectively and, sequentially presented in Fig. 7.20b, Fig. 7.21b and Fig. 7.22b.

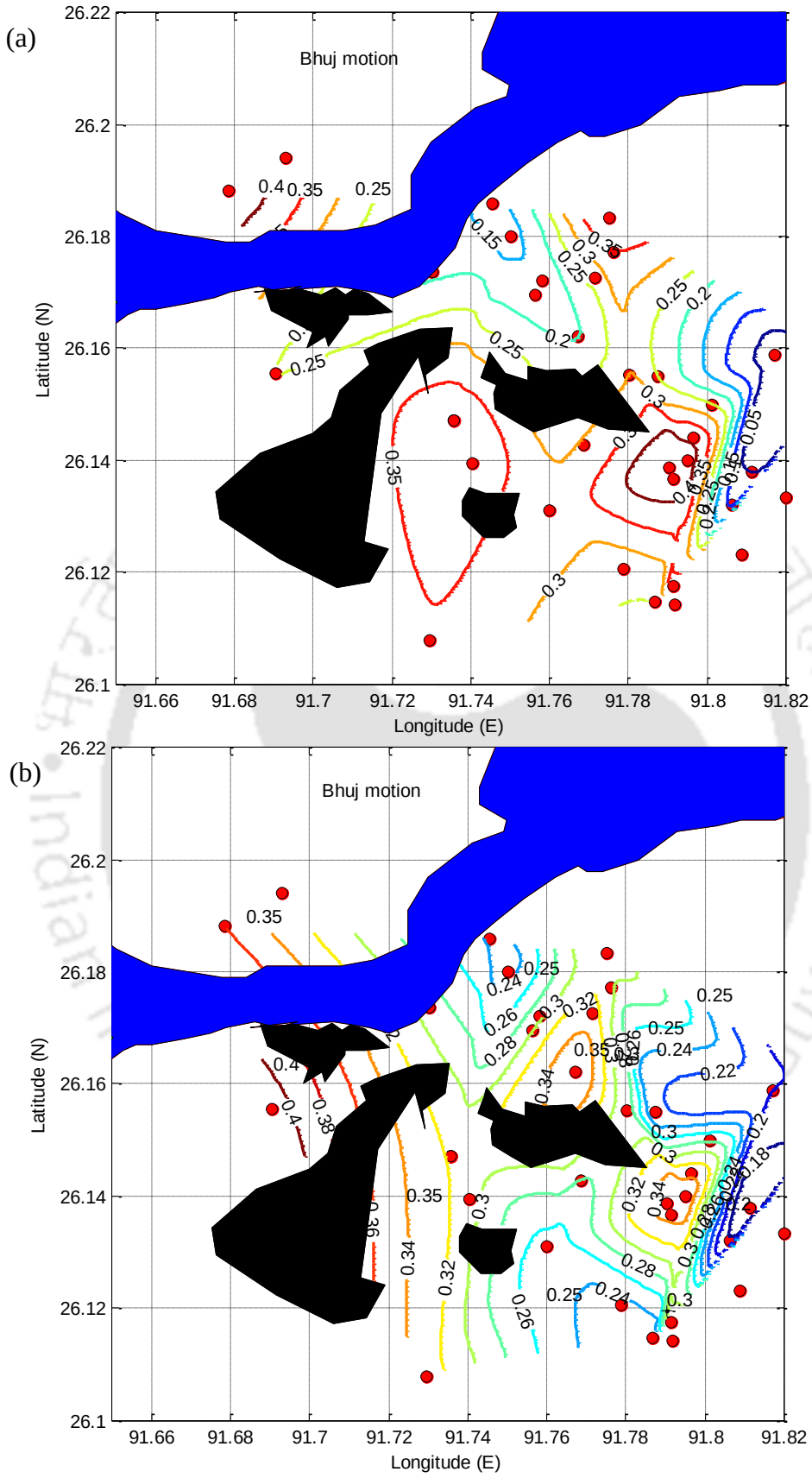

Fig. 7.17 PGA based on Bhuj motion using (a) experimental data (b) VD-SI data

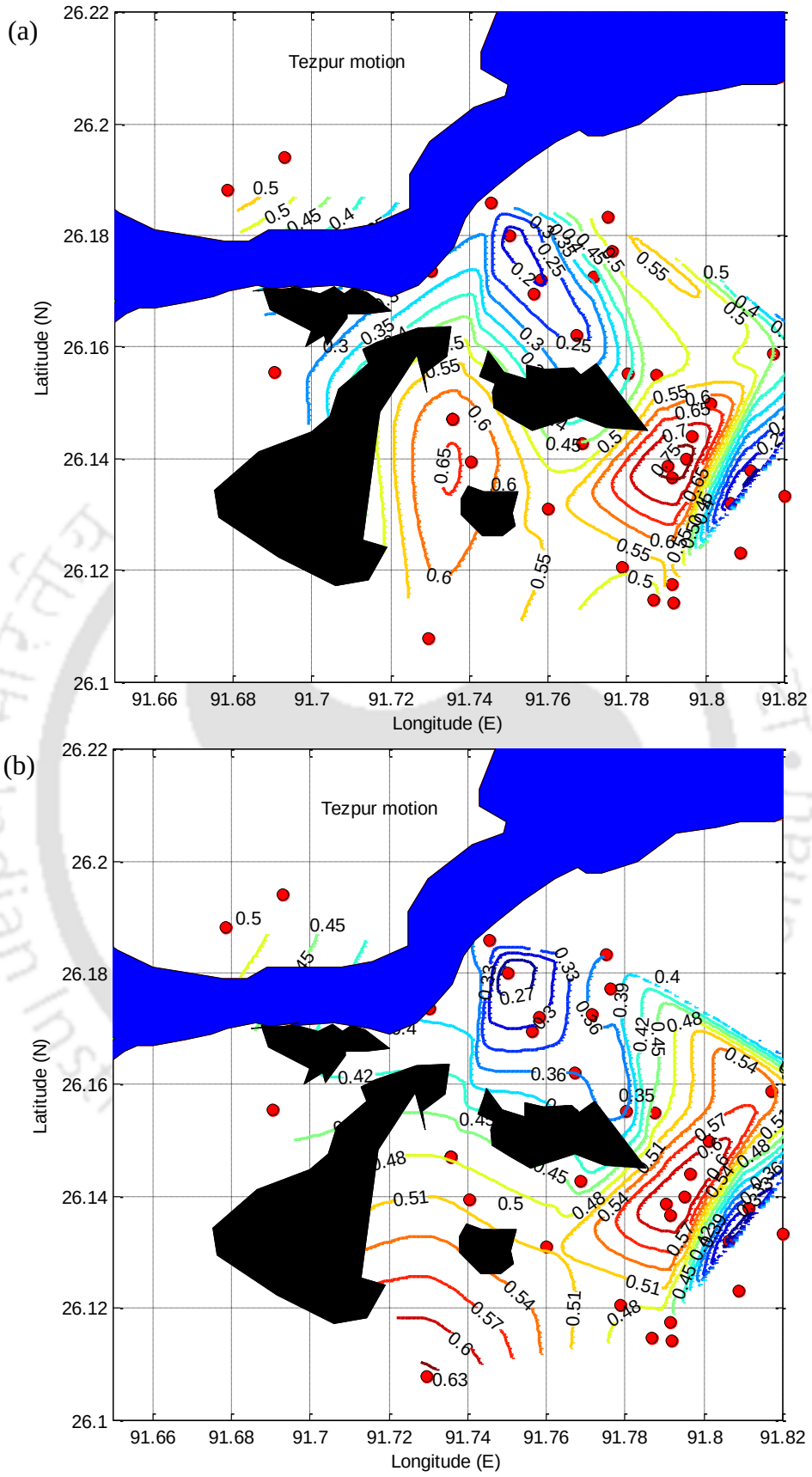

Fig. 7.18 PGA based on Tezpur motion using (a) experimental data (b) VD-SI data

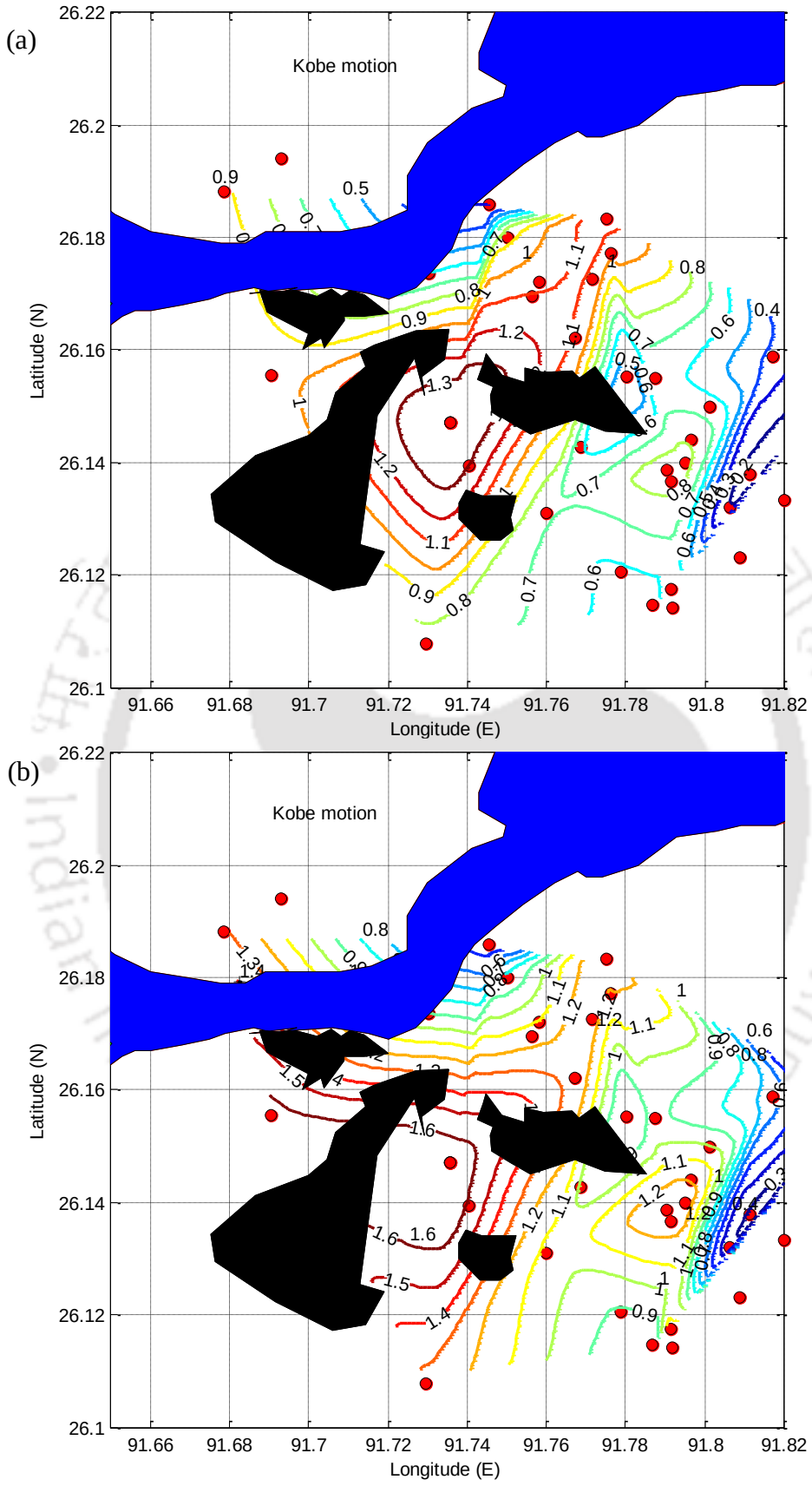

Fig. 7.19 PGA based on Kobe motion using (a) experimental data (b) VD-SI data

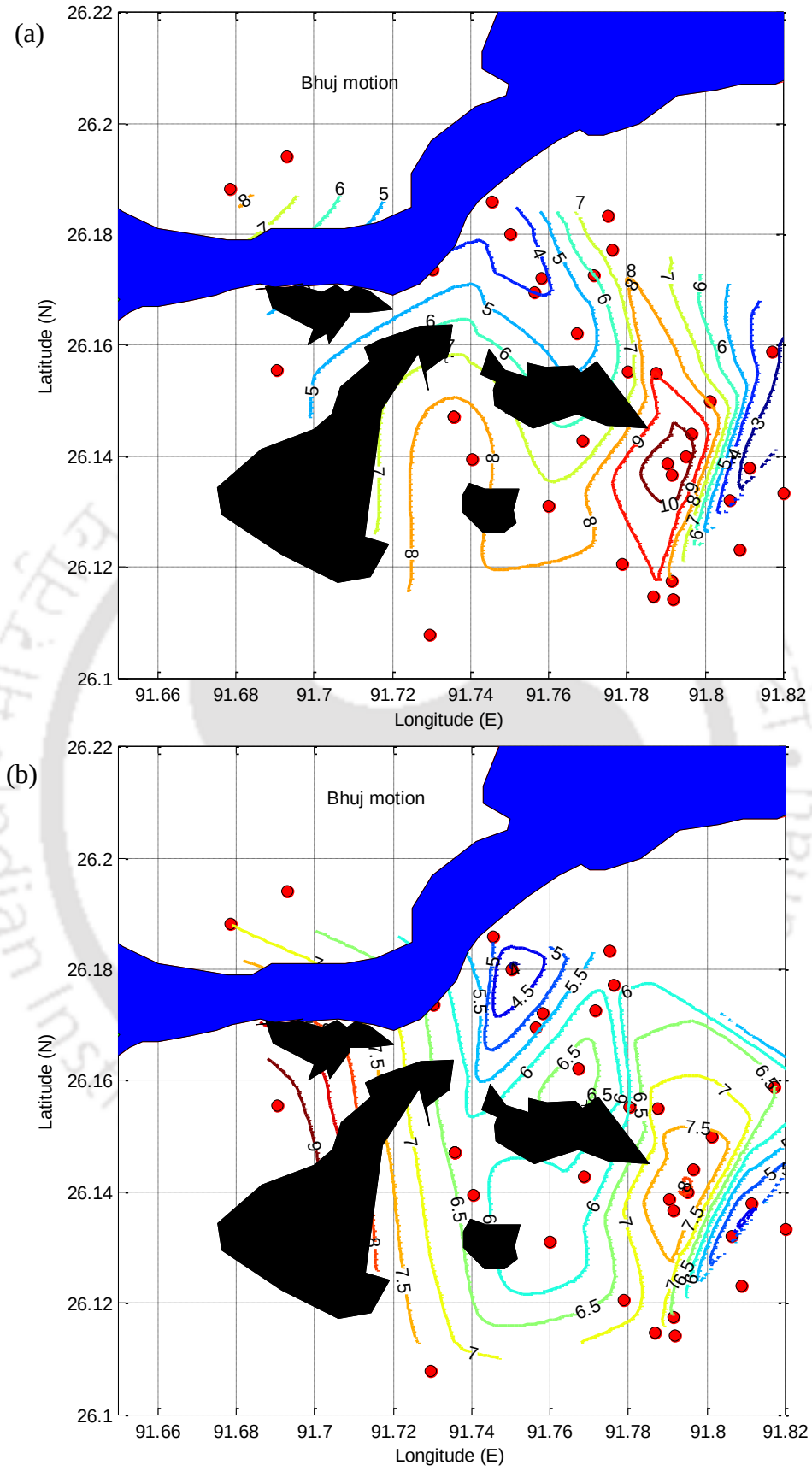

Fig. 7.20 FAR based on Bhuj motion using (a) experimental soil data (b) VD-SI data

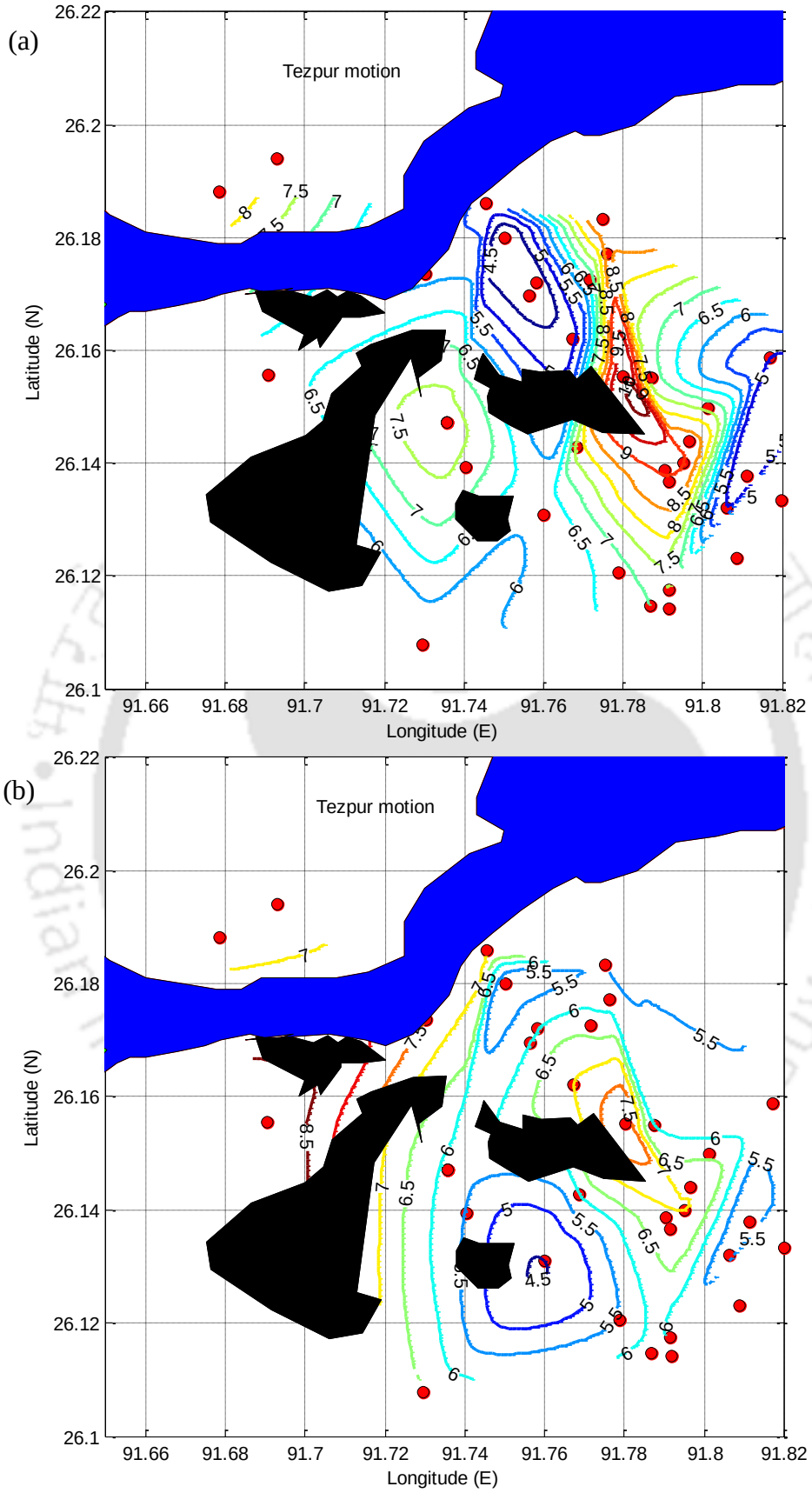

Fig. 7.21 FAR based on Tezpur motion using (a) experimental soil data (b) VD-SI data

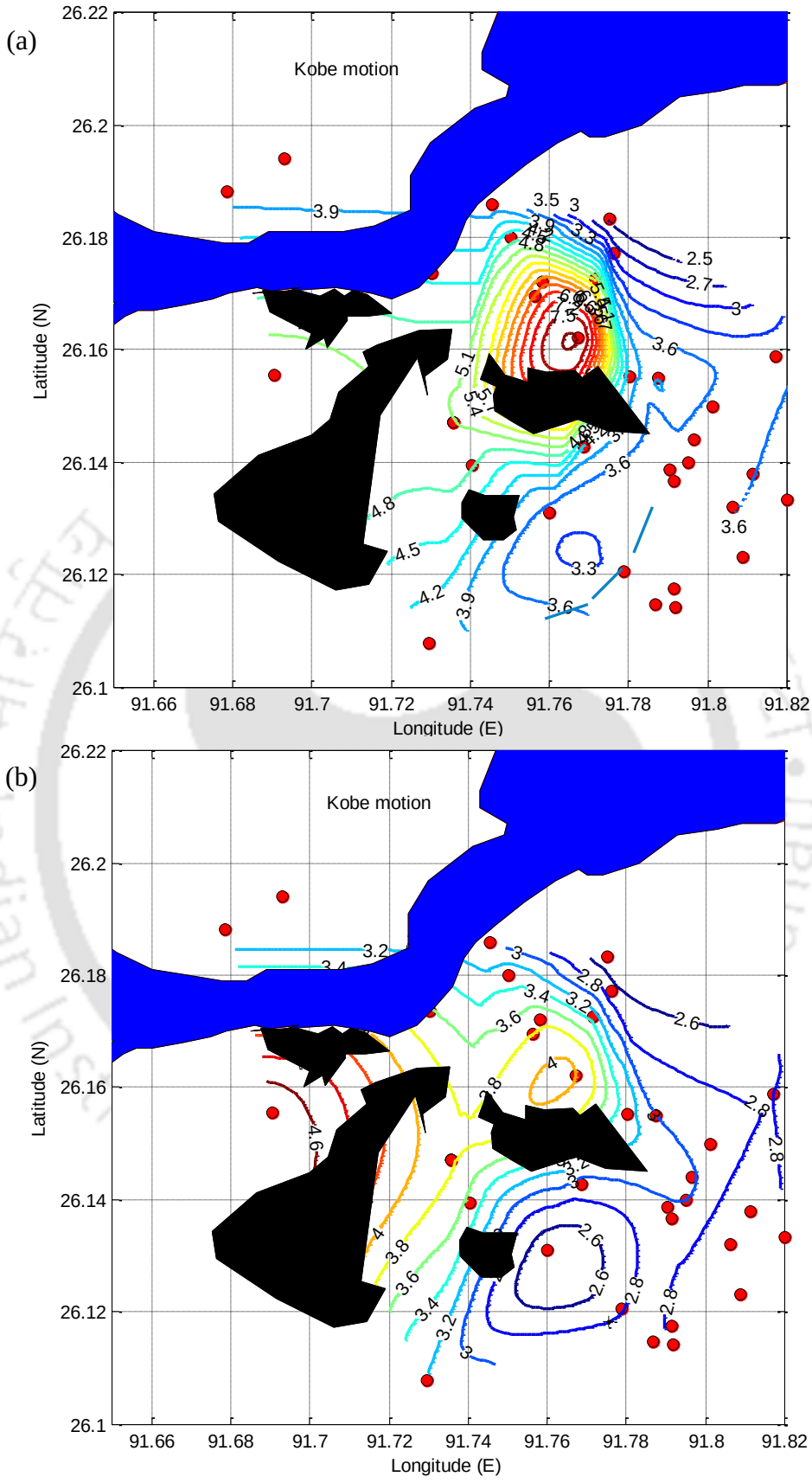

Fig. 7.22 FAR based on Kobe motion using (a) experimental data (b) VD-SI data

It was seen that, FAR obtained from experimental soil model is higher with Bhuj and Tezpur motion, than that obtained from Kobe motion. Similar observations were reported from VD-SI soil model. It was also seen that FAR obtained from experimental soil model is higher than that obtained from VD-SI soil model.

Fig. 7.23 to Fig. 7.25 shows the variations in PSA, presented in contour plot, for Guwahati city obtained from both experimental soil model as well as VD-SI soil model. It is seen that the average PSA with experimental data was 1.32, 1.79 and 2.60, when soil profiles were subjected to Bhuj, Tezpur and Kobe motion, respectively and, the same presented in Fig. 7.23a, Fig. 7.24a and Fig. 7.25a, sequentially. However, the average value of FAR with VD-SI data was found to be 1.358, 1.763 and 3.228, when subjected to Bhuj, Tezpur and Kobe motion, respectively and, sequentially presented in Fig. 7.23b, Fig. 7.24b and Fig. 7.25b. Thus, it can be stated that with the increase in PGA of input motion, PSA at ground level also increases. It can also be stated that the PGA, FAR and PSA at surface obtained from any input motion, is significantly affected by dynamic soil properties. The higher PGA of input motion shows the significantly higher values of strains at soft soil layers when analysed with experimental soil properties in comparison to the VD-SI soil properties.

From the aforementioned results and discussions on GRA, it can be stated that the depending on the strong motion and the subsurface stratigraphy, GRA can be used to find out the PGA, FAR and PSA at any required depth. The effect of strong motion propagation is predominantly visible at the ground surface or on the supported structures. However, the damages within the soil layer can also be identified by identifying the weak soil layer or liquefiable soil layer based on the outcomes of GRA.

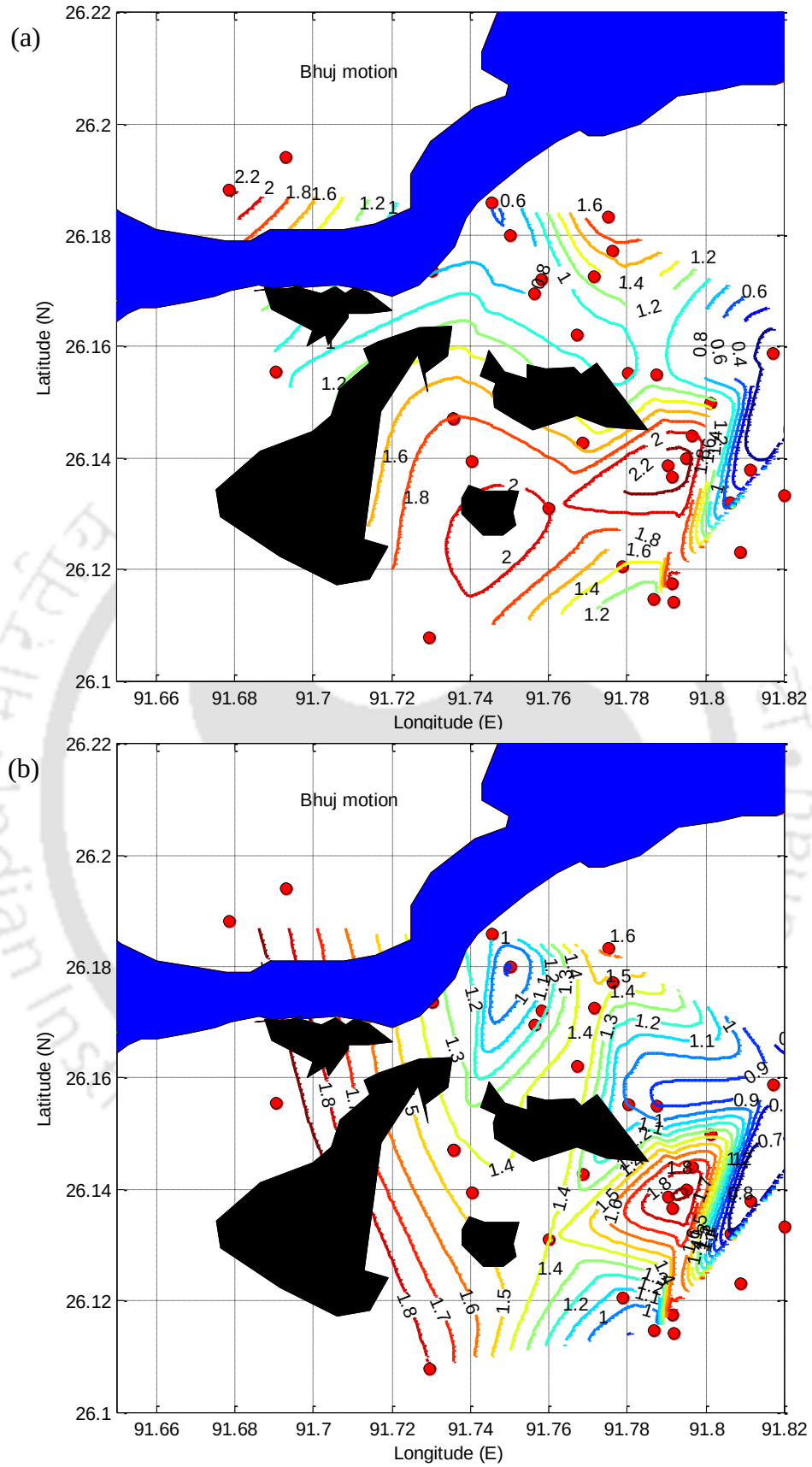

Fig. 7.23 PSA based on Bhuj motion using (a) experimental data (b) VD-SI data

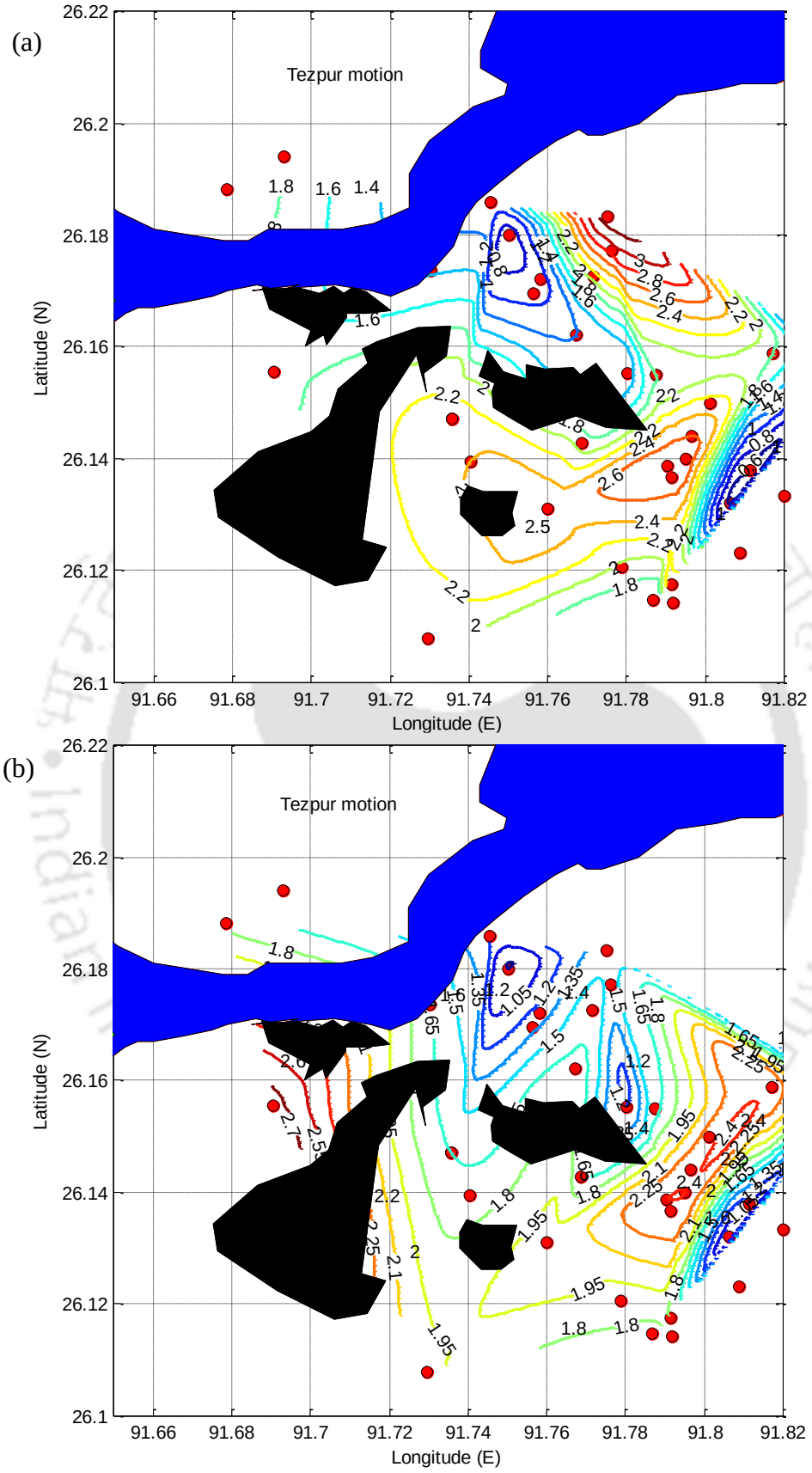

Fig. 7.24 PSA based on Tezpur motion using (a) experimental data (b) VD-SI data

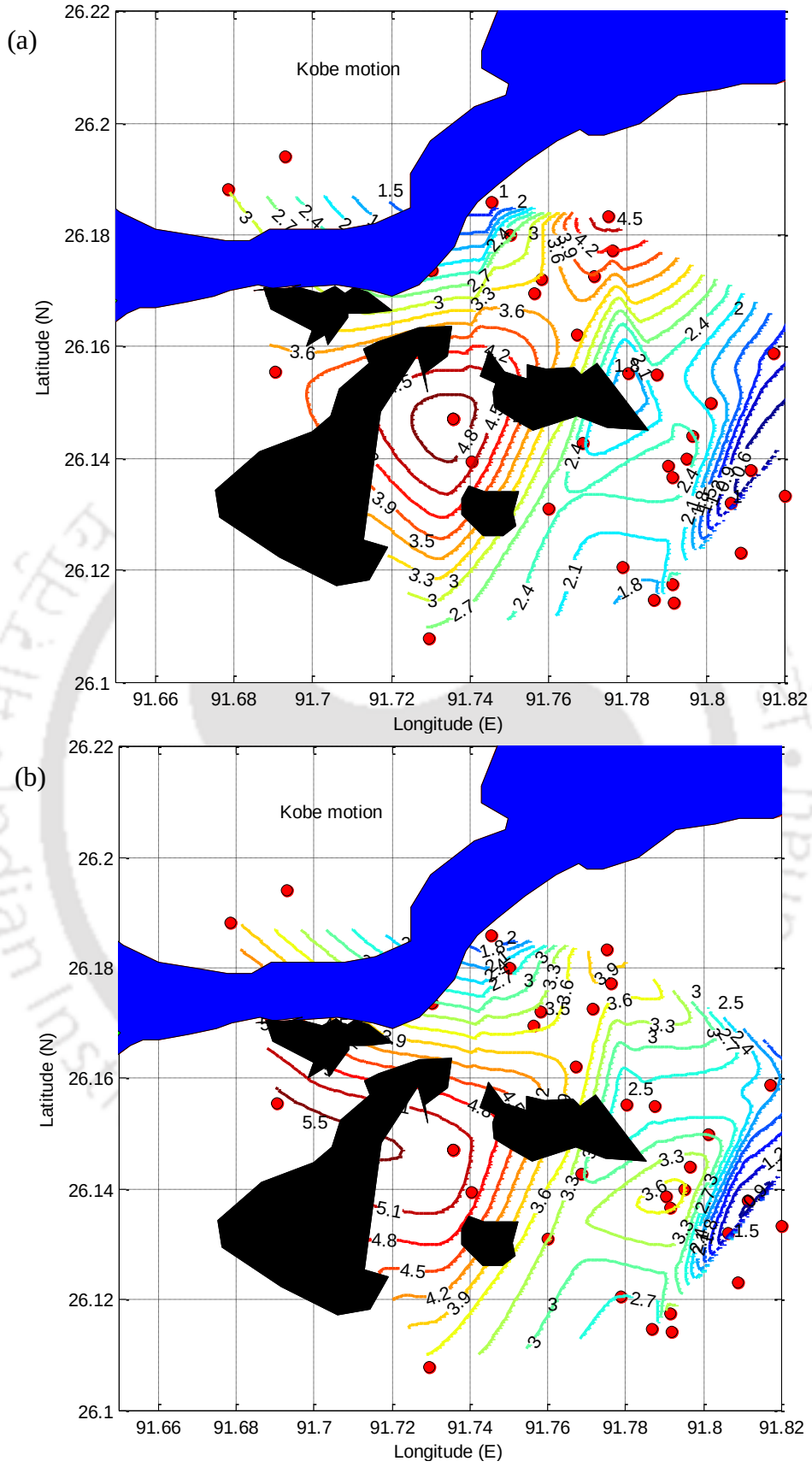

Fig. 7.25 PSA based on Kobe motion using (a) experimental data (b) VD-SI data

Table 7.3 presents the summary of the results in terms of percentage difference in PGA, PSA and FAR for Guwahati city. It reflects that the average PGA and PSA at surface level obtained using experimental data was significantly lesser (Table 7.3) than that obtained from VD-SI data, whereas, FAR was higher with experimental data. It was also found that the difference in the PGA, PSA and FAR obtained by Kobe motion is significantly higher than that obtained from Bhuj and Tezpur motion. This is attributed to the high magnitude of shear strains (greater than 1%) generated by Kobe motion, in comparison to that obtained from Bhuj and Tezpur motion, which is sufficient enough to reach the strain levels to account the variation of damping ratio at high strains. At shear strains greater than 1%, the present study indicates the reduction in damping ratio, while such reduction is not considered in the standard VD-SI models. Hence, choosing Kobe motion as a generator of higher magnitude strains helped in deciphering the influence of the mentioned difference of the strain-dependent damping characteristics on the ground response. Bhuj and Tezpur motionshaving lower magnitudes, and did not generate enough strains in the soil medium, so that the mentioned difference can be manifested. Therefore, it can be stated and also recommended that the actual dynamic soil properties would be good option for more precise GRA results.

Table 7.3 Comparison of percentage difference in PGA, PSA and FAR obtained using VD-SI and Experimental data for GRA Guwahati city using Bhuj, Tezpur and Kobe motions

Earthquake	Average value	Experimental data	VD-SI data	Difference (%)
Bhuj	PGA (g)	0.27	0.287	6.29
Tezpur		0.45	0.437	2.97
Kobe		0.75	1.039	38.53
Bhuj	FAR	6.58	6.389	2.99
Tezpur		6.85	6.336	8.11
Kobe		4.16	3.202	29.92
Bhuj	PSA (g)	1.32	1.358	2.88
Tezpur		1.79	1.673	6.99
Kobe		2.60	3.228	24.15

7.7 SUMMARY

This chapter presents the application of strain dependent dynamic properties of soils in GRA. One-dimensional GRA were performed using experimentally evaluated soil properties and compared with the VD-SI soil model. Based on GRA results obtained from both experimental and VD-SI soil model, it can be concluded that the outcomes are noticeably different. High magnitude of input PGA, such as Kobe motion, shows significant difference in the results of surface PGA, PSA and FAR, in comparison to that obtained using the input of Bhuj and Tezpur motion. This is attributed to the high magnitude of shear strains (greater than 1%) generated by Kobe motion, in comparison to that obtained from Bhuj and Tezpur motion. For the precise measurement of design ground motion parameters, the use of regional dynamic soil properties is recommended.

Chapter 8 CONCLUDING REMARKS

8.1 SUMMARY OF THE THESIS

The main objective of the present thesis was to investigate about the static and dynamic behaviour of locally available two soils present in Assam region, North-eastern part of India. In this regard, cyclic triaxial tests were conducted to evaluate the static and dynamic response (i.e. dynamic properties and liquefaction potential) of the soils. Dynamic properties of soils were evaluated using strain-controlled and stress-controlled approach using regular excitations, whereas the liquefaction potential was estimated using real-time and scaled earthquake motions (irregular excitations) as well as regular (sinusoidal) excitations. For irregular excitations, stress-controlled methodology was adopted, whereas, for regular excitations, both strain-controlled as well as stress-controlled approaches were utilized. With the aid of on-sample transducers, the local strains were measured during monotonic and cyclic shear tests on the soil specimen, and the same was compared with applied (i.e. global) strains. The evaluated dynamic properties of the locally available soils were further used to conduct the site-specific one-dimensional equivalent GRA studies of Guwahati city.

8.2 CONCLUSIONS

The experimental study indicated that dynamic behaviour and properties of cohesionless and cohesive soils are significantly affected by relative density, effective confining stress, cyclic shear strain amplitudes. The conclusions drawn from this entire study are presented as follows:

Monotonic Shear Tests

- The friction angle of SBS, obtained from consolidated undrained triaxial tests, is approximately 2˚-3˚ lesser than that of DBS.
- Based on the use of on-sample LVDTs on SBS specimens, it can be stated that on-sample

LVDTs effectively measure the local strains in triaxial testing. The shear stiffness obtained from local strain measurements are higher than that obtained using the globally strains measurements.

- The stress-strain response, pore-water pressure variation and stress path of both BS and RS are significantly affected by relative density (D_r), effective confining pressure (σ'_c) and applied displacement rate.

Cyclic Shear Tests: Dynamic Properties

- Hysteresis loops obtained at high cyclic strains exhibit noticeable asymmetric behaviour, which is not accommodated by conventional approaches of estimating the dynamic properties. Therefore, a modified methodology, duly accounting the asymmetric hysteresis loops, has been proposed for the evaluation of dynamic properties.
- Shear modulus of BS soil is observed to be significantly affected by the variations in σ'_c and D_r. G (based on the symmetrical hysteresis loop, SHL) and G_a (based on asymmetrical hysteresis loop, ASHL), respectively, are nearly same for N = 1, at different shear strain amplitudes (γ).
- Damping ratio, $D^{\#}$ (based on ASHL) for SBS exceeds D (based on SHL) by 40-70% within a shear strain range 0.015-4.5%. D increases up to $\gamma \approx 0.5\%$, followed by a decreasing trend, while $D^{\#}$ exhibits a decreasing trend beyond $\gamma \approx 1\%$. For DBS, $D^{\#}$ exceeds D by 5-70% within a shear strain range of 0.045-7%.
- Measurements from on-sample LVDTs are effective in determining the maximum shear modulus to provide the modulus reduction curve of SBS over a wide range of strains, (approximately 3×10^{-3} % to 5%) incorporating small strains as well as high strains.
- During stress-controlled stage loading on RS, the pore water pressure increases with shear strain, although the time gap occurring between consecutive incremental loadings leads to a

temporary dissipation. However, a reduction in the pore water pressure is noticed at the time gap between staged loadings. The compaction state of RS does not have significant effect on its dynamic properties.

Cyclic Shear Tests: Liquefaction Evaluation

- As obvious, both strain-controlled and stress-controlled tests with regular excitations exhibit the increase in liquefaction resistance with the increase in relative density.
- Based on strain-controlled approach, SBS specimens prepared at D_r = 30% liquefies in the 1st cycle when the shear strain and corresponding CSR exceeds 0.75% and 0.5, respectively However, for samples prepared at D_r = 90%, the CSR increases in the range of 0.6-0.85. In a nutshell, based on strain-controlled regular excitations, SBS (prepared at of D_r = 30-90% and subjected to σ'_c = 50-150 kPa) exhibits initiation of liquefaction at shear strain range 0.75%-1.0%, while from the stress-controlled regular excitation tests, the same phenomenon is observed to occur in the shear strain range of 0.5%-0.75%.
- Testing methodology significantly affects the liquefaction resistance of SBS. For strain-controlled tests, liquefaction resistance increases with the increase in confining pressure, while for stress-controlled tests, the same decreases with the increase in the confining pressure. The continuous accumulation of shear strains during cyclic loading, in stress-controlled approach, is a major contributory parameter to decrease of liquefaction resistance. Hence, stress-controlled approach should be preferred for evaluating liquefaction potential of saturated sands.
- From stress-controlled tests, all the three chosen strong motions scaled to 0.36g exhibit initiation of liquefaction in SBS specimens. The generated maximum shear followed the relative order of the arias intensity and specific energy density of the earthquake motions i.e. Bhuj (0.36g) > Kobe (0.36g) > Tezpur (0.36g). Strong motions scaled to lower PGA did not

exhibit initiation of liquefaction in the sample.

- The outcomes of the strain-controlled and stress-controlled cyclic triaxial tests, using regular and irregular excitations, indicate that SBS specimens will liquefy under the following optimum conditions: PGA ≥ 0.36g, CSR ≥ 0.3 and γ > 0.5% for D_r = 30-90% and σ'_c = 50-150 kPa. Hence, for GRA studies, γ = 0.5% should be considered as the limiting strain amplitude for initiation of liquefaction in loose cohesionless soils, whereas, γ = 1.0% should be considered as the limiting strain amplitude for initiation of liquefaction in dense cohesionless soils.

Ground Response Analysis

- The outcome of GRA studies of Guwahati city based on the experimentally evaluated dynamic properties is noticeably different from that obtained using existing standard models for strain-dependent dynamic properties (e.g. Seed and Idriss model for sand, Vucetic and Dobry model for clay). It is recommend that for more precise GRA studies, the proper/actual site-specific dynamic soil properties should be used.

8.3 LIMITATIONS OF THE STUDY

Since there are several parameters involved in the testing and investigation of the dynamic properties of locally available soils, the outcomes of the thesis are to be judiciously used considering the following limitations of the study.

- The tests conducted on only one variant of cohesionless soil (Brahmaputra sand) and cohesive (Red soil) soil.
- The results of tests on cohesive soil (RS) are restricted only to stress-controlled loading.
- To identify the effect of irregular excitations, only three strong motions were selected. The effect of various strong motion parameters on the response of soils have not been attempted

in this study.

- Only one-dimensional equivalent linear GRA was carried out for the present study.

8.4 SCOPE OF THE FUTURE RESEARCH

Any research is not complete and always has avenues for future developments. In this regard, the following are some of the future scope in the line of present research work.

- In most of the practical cases, the soils would be anisotropically consolidated. Therefore, tests can be conducted on anisotropically consolidated specimens and with drained/undrained shearing using regular and irregular excitations.
- To emphasize the importance of irregular excitations on the dynamic properties and liquefaction of soils, different strong motions with varying strong motion parameters can be further studied.
- Dynamic soil properties for different range of soils or soil mixes with varying fine contents and plasticity index can be further investigated by performing cyclic triaxial tests at different testing conditions.
- Site-specific material models for different soils of Assam region should be developed for their robust applications in detailed nonlinear GRA.
- Nonlinear GRA studies can be attempted to understand the nonlinear response of the region subjected to varied strong motions.

REFERENCES

1. Alarcon-Guzman, A., Leonards, G.A. and Chameau, J.L. (1988). Undrained monotonic and cyclic strength of sands, *Journal of Geotechnical Engineering Division*, ASCE, 114, 1089–1109.

2. Amini, F. and Chakravrty, A. (2003). Liquefaction testing of layered sand-gravel composites. *Geotechnical Testing Journal*, ASTM, 27(1), 1-11.

3. Amini, F. and Qi, G.Z. (2000). Liquefaction Testing of Stratified Silty Sands. *Journal of Geotechnical and Geoenvironmental Engineering*, ASCE, 126(3), 208–217.

4. Anbazhagan, P., Thingbaijam, K.K.S., Nath, S.K., Narendara Kumar, J.N. and Sitharam, T.G. (2010). Multi-criteria seismic hazard evaluation for Bangalore city, India. *Journal of Asian Earth Science*, 38, 186–98.

5. Andersen, K.H. and Lauritzsen, R. (1988). Bearing capacity for foundations with cyclic loads. *Journal of Geotechnical Engineering Division*, ASCE, 114, 540–55.

6. Ansal, A.M. and Erken, A. (1989). Undrained behavior of clay under cyclic shear stresses. *Journal of Geotechnical Engineering Division*, ASCE, 115(7), 968-983.

7. Arab, A., Belkhatir, M. and Sadek, M. (2016). Saturation effect on behaviour of sandy soil under monotonic and cyclic loading: A laboratory investigation. *Geotechnical and Geological Engineering*, 34(1), 347-358.

8. ASTM D2487 (2011). Standard practice for classification of soils for engineering purposes (Unified Soil Classification System). *ASTM International*, West Conshohocken, PA, https://doi.org/10.1520/D2487-11.

9. ASTM D3999/D3999M (2011). Standard test methods for the determination of the modulus and damping properties of soils using the cyclic triaxial apparatus. *ASTM International*, West Conshohocken, PA, https://doi.org/10.1520/D3999_D3999M.

10. ASTM D4253 (2016). Standard test methods for maximum index density and unit weight of soils using a vibratory table. *ASTM International*, West Conshohocken, PA, https://doi.org/10.1520/D4253-16.

11. ASTM D4254 (2016). Standard test methods for minimum index density and unit weight of soils and calculation of relative density. *ASTM International*, West Conshohocken, PA, https://doi.org/10.1520/D4254-16.

12. ASTM D4318 (2017). Standard test methods for liquid limit, plastic limit, and plasticity index of soils, *ASTM International*, West Conshohocken, PA, https://doi.org/10.1520/D4318-17.

13. ASTM D5311/D5311M (2013). Standard test method for load controlled cyclic triaxial strength of soil, *ASTM International*, West Conshohocken, PA, https://doi.org/10.1520/D5311_D5311M.

14. ASTM D6913/D6913M (2017). Standard test methods for particle-size distribution (gradation) of soils using sieve analysis. *ASTM International*, West Conshohocken, PA, https://doi.org/10.1520/D6913_D6913M-17.

15. ASTM D698 (2012). Standard test methods for laboratory compaction characteristics of soil using standard effort (12400 ft-lbf/ft^3 (600 kN-m/m^3)). *ASTM International*, West Conshohocken, PA, https://doi.org/10.1520/D0698-12E02.

16. ASTM D7928 (2017). Standard test method for particle-size distribution (gradation) of fine-grained soils using the sedimentation (hydrometer) analysis, *ASTM International*, West Conshohocken, PA, https://doi.org/10.1520/D7928-17.

17. ASTM D854 (2014). Standard test methods for specific gravity of soil solids by water pycnometer. *ASTM International*, West Conshohocken, PA, https://doi.org/10.1520/D0854-14.

18. Azzouz, A.S., Malek, A.M. and Baligh, M.M. (1989). Cyclic behavior of clays in undrained simple shear. *Journal of Geotechnical Engineering*, ASCE, 115(5), 637-657.

19. Basu, D., Dey, A. and Kumar, S.S. (2017). One-dimensional effective stress non-masing nonlinear ground response analysis of IIT Guwahati. *International Journal of Geotechnical Earthquake Engineering*, 8(1), 1-27.

20. Bésuelle, P. and Desrues, J. (2001). An internal instrumentation for axial and radial strain measurements in triaxial tests. *Geotechnical Testing Journal*, ASTM, 24(2), 193-199.

21. Bhattacharya, S. (2007). Design and foundations in seismic areas: principles and applications. *National information centre of earthquake engineering*, IIT Kanpur, India, pp. 477.

22. Boominathan, A., Dodagoudar, G.R., Suganthi, A. and Maheswari, R.U. (2008). Seismic hazard assessment of Chennai city considering local site effects. *Journal of Earth System and Science*, 117, S2, 853–863.

23. Bouferra, R., Benseddiq, N. and Shahrour, I. (2007). Saturation preloading effects on the cyclic behaviour of sand. *International Journal of Geomechanics*, 7(5), 396–401.

24. Boulanger, R.W. and Idriss, I.M. (2006). Liquefaction susceptibility criteria for silts and clays. *Journal of Geotechnical and Geoenvironmental Engineering*, ASCE, 132(11), 1413-1426.

25. Boulanger, R.W. and Idriss, I.M. (2007). Evaluation of cyclic softening in silts and clays. *Journal of Geotechnical and Geoenvironmental Engineering*, ASCE, 133(6), 641-652.

26. Bragg, R.A. and Andersland, O.B. (1982). Strain dependence of poisson's ratio for frozen sand. *In Proceeding of 4th Canadian permafrost conference*, pp. 365-373.

27. Brennan, A.J., Thusyanthan, N.I. and Madabhushi, S.P.G. (2005). Evaluation of shear modulus and damping in dynamic centrifuge tests. *Journal of Geotechnical and Geoenvironmental Engineering*, ASCE, 131, 1488–1497.

28. Brown, S.F. and Snaith, M.S. (1974). The measurement of recoverable and irrecoverable deformations in the repeated load triaxial test. *Geotechnique*, 24(2), 255-259.

29. Brown, S.F., Austin, G. and Overy, R.F. (1980). An instrumented triaxial cell for cyclic loading of clays. *Geotechnical Testing Journal*, ASTM, 3(4), 45-152.

30. Budhu, M. (2008). Soil mechanics and foundations. Wiley India Pvt. Ltd.

31. Burland, J.B. and Symes, M. (1982). A simple axial displacement gauge for use in the triaxial apparatus. *Geotechnique*, 32, 62-65.

32. Byrne, P.M., Park, S.S., Beaty, M., Sharp, M., Gonzalez, L. and Abdoun, T. (2004). Numerical modeling of liquefaction and comparison with centrifuge tests. *Canadian Geotechnical Journal*, 41, 193–211.

33. Carraro, J.A.H., Bandini, P. and Salgado, R. (2003). Liquefaction resistance of clean and nonplastic silty sands based on cone penetration resistance. *Journal of Geotechnical and Geoenvironmental Engineering*, ASCE, 129(11), 965-976.

34. Casagrande, A. and Shannon, W.L. (1948). Stress-deformation and strength characteristics of soils under dynamic loads. *In: Proceedings of the Second International Conference on Soil Mechanics and Foundation Engineering*, Rotterdam, 29-34.

35. Castro, G. (1975). Liquefaction and cyclic mobility of saturated sands. *Journal of the Geotechnical Engineering Division*, ASCE, 101(6), 551-569.

36. Cetin, K.O. and Bilge, H.T. (2011). Cyclic large strain and induced pore pressure models for saturated clean sands. *Journal of Geotechnical and Geoenvironmental Engineering*, ASCE, 138(3), 309-323.

37. Chaney, R. (2013). Dynamic properties of some eastern Mediterranean marine sediments. *Geotechnical Testing Journal*, ASTM, 36(4), 1–9.

38. Chaney, R. and Mulilis, J.P. (1978). Suggested method for soil specimen remolding by wet-raining. *Geotechnical Testing Journal* ASTM, 1(2), 107-108.

39. Chang, C.Y., Power, M.S., Tang, Y.K. and Mok, C.M. (1989). Evidence of nonlinear soil response during a moderate earthquake. *Proceeding of the 12th International Conference on Soil Mechanics and Foundation Engineering*. Rio de Janeiro, 3, 1–4.

40. Chattaraj, R. and Sengupta, A. (2016a). Liquefaction potential and strain dependent dynamic properties of Kasai river sand. *Soil Dynamics and Earthquake Engineering*, 90, 467-475.

41. Chattaraj, R. and Sengupta, A. (2016b). Dynamic properties of fly ash. *Journal of Materials in Civil Engineering*, ASCE, DOI: 10.1061/(ASCE)MT.1943-5533.0001712.

42. Choudhary, S.S., Maheshwari, B.K. and Kaynia, A.M. (2010). Liquefaction resistance of Solani sands under cyclic loads. *Indian Geotechnical Conference*, GEOtrendz, 115 – 118.

43. Chung, R.M., Yokel, F.Y. and Drnevich, V.P. (1984). Evaluation of dynamic properties of sands by resonant column testing. *Geotechnical Testing Journal*, ASTM, 7, 60-69.

44. Clayton, C.R.I. and Khatrush, S.A. (1986). A new device for measuring local axial strains on triaxial specimens. *Géotechnique*, 36(4), 593-597.

45. Clayton, C.R.I., Khatrush, S.A., Bica, A.V.D. and Siddique, A. (1989). The use of Hall effect semiconductors in geotechnical instrumentation. *Geotechnical Testing Journal*, ASTM, 12(1), 69-76.

46. Clough, G.W., Iwabuchi, J., Rad, N.S. and Kuppusamy, T. (1989). Influence of cementation on liquefaction of sands. *Journal of Geotechnical Engineering*, ASCE, 115(8), 1102-1117.

47. Cole, D. M. (1978). A technique for measuring radial deformation during repeated load triaxial testing. *Canadian Geotechnical Journal*, 15, 426-429.

48. Cooke, R.W. and Price, G. (1974). Horizontal inclinometers for the measurement of vertical displacement in the soil around experimental foundations. *Field Instrumentation in Geotechnical Engineering*, Butterworth's, London, pp. 112-125.

49. Cuccovillo, T. and Coop, M.R. (1997). The measurement of local axial strains in triaxial tests using LVDTs. *Geotechnique*, 47, 167-171.

50. Darendeli, M.B. (2001). Development of a new family of normalized modulus reduction and material damping curves. *PhD dissertation*, University of Texas, Austin.

51. Dasari, G.R., Bolton, M.D. and Ng, C.W.W. (1995). Small strain measurement using modified LDTs. *Technical Report*, University of Cambridge, Department of Engineering.

52. Dash, H.K. and Sitharam, T.G. (2009). Undrained cyclic pore pressure response of sand–silt mixtures: effect of non-plastic fines and other parameters. *Journal of Geotechnical Geological Engineering*, 27, 501–517.

53. Dash, H.K. and Sitharam, T.G. (2011). Undrained cyclic and monotonic strength of sand-silt mixtures, *Journal of Geotechnical Geological Engineering*, 29, 555–570.

54. Dash, H.K. and Sitharam, T.G. (2016). Effect of frequency of cyclic loading on liquefaction and dynamic properties of saturated sand. *International Journal of Geotechnical Engineering*, 10(5), 487-492.

55. De, S. and Basudhar, P.K. (2008). Steady state strength behavior of Yamuna sand. *Geotechnical and Geological Engineering*, 26(3), 237–250.

56. Della, N., Arab, A. and Belkhatir, M., (2011). Static liquefaction of sandy soil: an experimental investigation into the effects of saturation and initial state. *Acta Mechanica*, 218 (1-2), 175-186.

57. Dobry, R. and Abdoun, T. (2015). Cyclic shear strain needed for liquefaction triggering and assessment of overburden pressure factor K_σ. *Journal of Geotechnical and Geoenvironmental Engineering*, ASCE, 141, 04015047.

58. Dobry, R., Ladd, R.S., Yokell, F.Y., Chung, R.M. and Powell, D. (1982). Prediction of pore water pressure buildup and liquefaction of sands during earthquakes by the cyclic strain method, Vol. 138. US Department of Commerce, National Bureau of Standards.

59. Dupas, J.M., Pecker, A., Bozetto, P. and Fry, J.J. (1988). A 300 mm diameter triaxial cell with a double measuring device. *Advanced Triaxial Testing of Soil and Rock* ASTM, 977, 132-142.

60. EI-Hosri, M. S., Biarez, J. and Hicher, P.Y. (1981). Dynamic triaxial and vibratory in-situ behavior of cohesive soil. *International Conferences on Recent Advances in Geotechnical Earthquake Engineering and Soil Dynamics,* University of Missouri-Rolla.

61. Elgamal, A.W., Zeghal, M., Taboada, V. and Dobry, R. (1996). Analysis of site liquefaction and lateral spreading using centrifuge testing records. *Soils and Foundations*, 36(2), 111–121.

62. Erten, D. and Maher, M.H. (1994). Cyclic undrained behaviour of silty sand. *Soil Dynamics and Earthquake Engineering*, 14, 115–123.

63. Feng, Z.Y. and Sutter, K.G. (2000). Dynamic properties of granulated rubber/sand mixtures. *Geotechnical Testing Journal*, ASTM, 23(3), 338–344.

64. Fratta, D., Aguettant, J. and Roussel-Smith, L. (2007). Introduction to soil mechanics laboratory testing. *CRC press,* New York.

65. Fredlund, D.G. and Rahardjo, H. (1993). Soil mechanics for unsaturated soils. John Wiley & Sons.

66. Garga, V.K. and McKay, L.D. (1984). Cyclic triaxial strength of mine tailings. *Journal of Geotechnical Engineering*, ASCE, 110(8), 1091-1105.

67. Gasparre, A. and Coop, M. (2006). Techniques for performing small-strain probes in the triaxial apparatus. *Geotechnique*, 56(7), 491-495.

68. Ghionna, V.N. and Porcino, D. (2006). Liquefaction resistance of undisturbed and reconstituted samples of a natural coarse sand from undrained cyclic triaxial tests. *Journal of Geotechnical and Geoenvironmental Engineering*, ASCE, 132(2), 194-202.

69. Gookin, W., Riemer, M., Boulanger, R. and Bray, J. (1996). Development of cyclic triaxial apparatus with broad frequency and strain ranges. *Transportation Research Record: Journal of the Transportation Research Board*, 1548, 1-8.

70. Goto, S., Tatsuoka, F., Shibuya, S., Kim, Y.S. and Sato, T. (1991). A simple gauge for local small strain measurements in the laboratory. *Soils and Foundations*, 31, 169-180.

71. Govindaraju, L. (2005). Liquefaction and dynamic properties of sandy soils, *Doctoral dissertation*, Indian Institute of Science Bangalore, India.

72. Govindaraju, L. and Bhattacharya, S. (2011). Site-specific earthquake response study for hazard assessment in Kolkata city, India. *Natural Hazards*, 61(3), 943-965.

73. Grozic, J.L., Robertson, P.K. and Morgenstern, N.R. (1999). The behavior of loose gassy sand. *Canadian Geotechnical Journal*, 36(3), 482-492.

74. Guha, S., Drnevich, V.R. and Bray, J.D. (1997). Dynamic characteristics of old Bay clay. *Geotechnical Testing Journal*, ASTM, 20 (4), 383-393.

75. Hanumantharao, C. and Ramana, G.V. (2008). Dynamic soil properties for microzonation of Delhi, India. *Journal of Earth System and Science*, 117(2), 719–730.

76. Hanumantharao, H.C. and Ramana, G.V. (2010). Characterization of cyclic strength of Yamuna sand. *International Journal of Earth Sciences and Engineering*, 3(2), 234-242.

77. Hardin, B.O. and Drnevich, V.P. (1972). Shear modulus and damping in soils: measurement and parameters effects. *Journal of Soil Mechanics and Foundations Division*, ASCE, 98, 603-624.

78. Hashash, Y.M.A., Musgrove, M.I., Harmon, J.A., Groholski, D.R., Phillips, C.A. and Park, D. (2016). DEEPSOIL 6.1, User Manual. Urbana, IL, Board of Trustees of University of Illinois at Urbana-Champaign.

79. Hazirbaba, K. and Rathje, E.M. (2009). Pore pressure generation of silty sands due to induced cyclic shear strains. *Journal of Geotechnical and Geoenvironmental Engineering*, ASCE, 135(12), 1892-1905.

80. Head, K.H. (1992). Manual of soil laboratory testing, Vol. 3, Effective stress tests. *John Willy & Sons*, Ins. New York.

81. Hird, C.C. and Yung, P.C.Y. (1989). The use of proximity transducer for local strain measurements in triaxial tests. *Geotechnical Testing Journal*, ASTM, 12, 292-296.

82. Hoque, E., Sato, T. and Tatsuoka, E. (1997). Performance evaluation of ldts for use in triaxial tests. *Geotechnical Testing Journal*, ASTM, 20(2), 149-167.

83. Hosri, M.S.E., Biarez, J. and Hicher, P.Y. (1984). Liquefaction characteristic of silty clay. *Proceedings of the 8th World Conference on Earthquake Engineering*, Prentice-Hall, Inc., Englewood Cliffs, New Jersey, 3, 277–284.

84. Hsu, C.C. and Vucetic, M. (2004). Volumetric threshold shear strain for cyclic settlement. *Journal of Geotechnical and Geoenvironmental Engineering*, ASCE, 130(1), 58–70.

85. Hsu, C.C. and Vucetic, M. (2006). Threshold shear strain for cyclic pore water pressure in cohesive soils. *Journal of Geotechnical and Geoenvironmental Engineering*, ASCE, 132(10), 1325–1335.

86. http://pesmos.in/2011/ (Last accessed: 07-07-2017).

87. http://www.census2011.co.in/census/city/191-guwahati.html (Last accessed: 21-10-2017).

88. http://www.controls-group.com/eng/scheda-print.php?id_cat=soil-mechanics&id_prod=mini-on_sample-transducers-for-local-strain-measurement-in-triaxial-testing (Last accessed: 21-10-2017).

89. http://www.gdsinstruments.com/__assets__/pagepdf/0000-1/Introduction%20to%20triaxial%20testing%20-%20Part%203.pdf (Last accessed: 21-10-2017).

90. http://www.strongmotioncenter.org/vdc/scripts/default.plx (Last accessed: 21-10-2017).

91. https://www.google.co.in/search?q=ground+failure+during+earthquake&source=lnms&tbm=isch&sa=X&ved=0ahUKEwie7M_T0v_WAhUFqo8KHRdQD2cQ_AUICigB&biw=1138&bih=530 (Last accessed: 21-10-2017).

92. Idriss, I.M. and Boulanger, R.W. (2006). Semi-empirical procedures for evaluating liquefaction potential during earthquakes. *Soil Dynamics and Earthquake Engineering*, 26(2), 115-130.

93. Inci, G., Yesiller, N. and Kagawa, T. (2003). Experimental investigation of dynamic response of compacted clayey soils. *Geotechnical Testing Journal*, ASTM, 26(2), 1-17.

94. IS: 1893 (Part-1) (2002). Criteria for earthquake resistant design of structures–general provisions and buildings. *Bureau of Indian Standard*, New Delhi.

95. IS: 2720 (Part-III) (1981). Determination of Specific Gravity-fine, medium and coarse grained soils. *Bureau of Indian standard*, New Delhi.

96. IS: 2720 (Part-IV) (1975). Grain size analysis. *Bureau of Indian standard*, New Delhi.

97. IS: 2720 (Part-XIV) (1983). Determination of density index of cohesionless soils. *Bureau of Indian standard*, New Delhi

98. Ishibashi, I. and Zhang, X. (1993). Unified dynamic shear moduli and damping ratios of sand and clay. *Soils and Foundations*, 33, 182-191.

99. Ishibashi, I., Kawamura, M. and Bhatia, S.K. (1985). Effect of initial shear on cyclic behavior of sand. *Journal of Geotechnical Engineering*, 111(12), pp.1395-1410.

100. Ishihara, K. (1993). Liquefaction and flow failure during earthquakes. *Geotechnique*, 43(3), 351–415.

101. Ishihara, K. (1996). Soil behaviour in earthquake geotechnics. *Oxford: Oxford Science Publications, Clarendon Press*.

102. Ishihara, K. and Koseki, J. (1989). Cyclic shear strength of fines containing sands. *Journal of Earthquake and Geotechnical Engineering*, JSSME, Tokyo, 101–106.

103. Ishihara, K. and Yasuda, S. (1972). Soil liquefaction due to irregular excitation. *Soils and Foundations*, 12(4), 65-77.

104. Ishihara, K. and Yasuda, S. (1973). Soil liquefaction under random earthquake loading condition. *Proceeding 5th world conference on earthquake engineering*, Rome, pp. 329-338.

105. Ishihara, K. and Yasuda, S. (1975). Sand liquefaction in hollow cylinder torsion under irregular excitation. Soils *and Foundations*, 15(1), 45-59.

106. Ishihara, K., Silver, L. M. and Kitagawa, H. (1978a). Cyclic strength of unsaturated sands obtained by large diameter sampling. *Soils and Foundations*, JSSME, 18(4), 61–76.

107. Ishihara, K., Sodekawa, M. and Tanaka, Y. (1978b). Effects of over consolidation on liquefaction characteristics of sands containing fines. *Dynamic Geotechnical Testing* ASTM, 654, 246–264.

108. Ishihara, K., Tatsuoka, F. and Yasuda, S. (1975). Undrained deformation and liquefaction of sand under cyclic stresses. *Soils and Foundations*, 15(1), 29-44.

109. Ishihara, K., Troncoso, J., Kawase, Y. and Takahashi, Y. (1980). Cyclic strength characteristics of tailings materials. *Soils and Foundations*, 20, 127-142.

110. Ito, T. and Fujimoto, K. (1981). Strain rate effects on stress–strain relationships of sand. *Journal of Theoretical and Applied Mechanics Japan*, 30, 17–24.

111. Iwasaki, T. and Tatsuoka, F. (1977). Effects of grain size and grading on dynamic shear moduli of sands. *Soils and Foundations*, 17(3), 19–35.

112. Iwasaki, T., Tatsuoka, F. and Takagi, Y. (1978). Shear modulus of sands under torsional shear loading. *Soils and Foundations*, 18(1), 39–56.

113. Jafarzadeh, F. and Sadeghi, H. (2012). Experimental study on dynamic properties of sand with emphasis on the degree of saturation. *Soil Dynamics and Earthquake Engineering*, 32(1), 26-41.

114. Jakka, R.S., Datta, M. and Ramana, G.V. (2010). Liquefaction behaviour of loose and compacted pond ash. *Soil Dynamics and Earthquake Engineering*, 30(7), 580–590.

115. Jardine, R.J., Fourie, A., Maswoswe, J. and Burland, J.B. (1985). Field and laboratory measurements of soil stiffness. *Proc. of 11th International Conference on Soil Mechanics and Foundation Engineering*, San Francisco, August 12-16, pp. 511-514.

116. Jardine, R.J., Symes, M.J. and Burland, J.B. (1984). The measurement of soil stiffness in the triaxial apparatus. *Geotechnique*, 34, 323-340.

117. Jastrzębska, M. and Kowalska, M. (2016). Triaxial tests on weak cohesive soils–some practical remarks (part 2). *Architecture Civil Engineering Environment*, 9(3), 81-94.

118. Juneja, A. and Raghunandan, M.E. (2010). Effect of sample preparation on strength of sands. In *Indian Geotechnical Conference, Bombay, 16–18 December 2010*.

119. Kagawa, T. (1992). Moduli and damping factors of soft marine clays. *Journal of Geotechnical Engineering*, ASCE, 118(9), 1360-1375.

120. Karg, C. and Haegeman, W. (2009). Elasto-plastic long-term behavior of granular soils: Experimental investigation. *Soil Dynamics and Earthquake Engineering*, 29, 155–172.

121. Katayama, I., Fukui, F., Satoh, M., Makihara, Y. and Tokimatsu, K. (1986). Comparison of dynamic soil properties between undisturbed and disturbed dense sand samples, *Proc. 21st Annual Conference of JSSMFE*, 583–584.

122. Khan, M. H. and Hoag, D. L. (1979). A noncontacting transducer for measurement of lateral strains. *Canadian Geotechnical Journal*, 16(2), 409-411.

123. Khosla, V.K. and Singh, R.D. (1978). Influence of number of cycles on strain. *Canadian Geotechnical Journal*, 15(4), 584-592.

124. Kiku, H. and Yoshida, N. (2000). Dynamic deformation property tests at large strains. *12th World Conference on Earthquake Engineering*, New Zealand. Paper no. 1748.

125. Kirar, B. and Maheshwari, B.K. (2013). Effects of silt content on dynamic properties of Solani sand. *Seven International Conference on case Histories in Geotechnical Engineering*, Cichago – 2013.

126. Kirar, B., Maheshwari, B.K. and Jakka, R.S. (2012). Dynamic properties of Solani sand reinforced with coir fibres. *15th World Conference on Earthquake Engineering*, Lisboa – 2012.

127. Kokusho, T. (1980). Cyclic triaxial test of dynamic soil properties for wide strain range. *Soils and Foundations*, 20, 45-60.

128. Kokusho, T. Yoshida, Y. and Esashi, Y. (1982). Dynamic properties of soft clay for wide strain range. *Soils and Foundations*, 22, 1–18.

129. Kramer, S.L. (1996). Geotechnical earthquake engineering. *Prentice Hall*. New York.

130. Kramer, S.L. and Seed, H.B. (1988). Initiation of soil liquefaction under static loading conditions. *Journal of Geotechnical Engineering*, ASCE, 114(4), 412-430.

131. Kreyszig, E. (2010). Advanced engineering mathematics. *John Wiley & Sons*, US.

132. Kumar, S.S. (2012). Site-specific seismic ground response analysis of Guwahati city, *M. Tech. Thesis*, Submitted to Indian Institute of Technology Guwahati, Assam.

133. Kumar, S.S. and Krishna, A.M. (2012). Site-specific seismic ground response to different earthquake motions. *In proceedings of Indian Geotechnical Conference*, Delhi.

134. Kumar, S.S. and Krishna, A.M. (2013). Seismic ground response analysis of some typical sites of Guwahati city. *International Journal of Geotechnical Earthquake Engineering*, 4, 83-101.

135. Kumar, S.S., Dey, A. and Krishna, A.M. (2014). Equivalent linear and nonlinear ground response analysis of two typical sites at Guwahati city. *Proceedings of the Indian Geotechnical Conference, Kakinada, India*, pp. 603–612.

136. Kumar, S.S., Dey, A. and Krishna, A.M. (2015). Dynamic response of river bed sands using cyclic triaxial tests. *5th Young Indian Geotechnical Engineers Conference*, Vadodara, India.

137. Kumar, S.S., Krishna, A.M. and Dey, A. (2014). Nonlinear site-specific ground response analysis: case study of Amingaon, Guwahati. *Proceeding of the 15th Symposium on Earthquake Engineering*, IIT Roorkee, India, 308-318.

138. Kumar, S.S., Krishna, A.M. and Dey, A. (2016). Local strain measurements in triaxial tests using on-sample transducers. *Proceeding in the Indian Geotechnical Conference*, IIT Madras, Chennai, India.

139. Kumar, S.S., Krishna, A.M. and Dey, A. (2017). Evaluation of dynamic properties of sandy soil at high cyclic strains. *Soil Dynamics and Earthquake Engineering*, 99, 157-167.

140. Ladd, R.S. (1978). Preparing test specimens using undercompaction. *Geotechnical Testing Journal*, ASTM, 1(1), 16-23.

141. Ladd, R.S., Dobry, R., Dutko, P., Yokel, F.Y. and Chung, R.M., 1989. Pore-water pressure buildup in clean sands because of cyclic straining. *Geotechnical Testing Journal*, ASTM, 12(1), 77-86.

142. Lambe, T.W. and Whitman, R.V. (1969). Soil mechanics. John Willy and sons, New York.

143. Lanzo, G., Vucetic, M. and Doroudian M. (1997). Reduction of shear modulus at small strains in simple shear. *Journal of Geotechnical and Environmental Engineering*, ASCE, 123, 1035–1042.

144. Lee, K. and Albaisa, A. (1974). Earthquake induced settlements in saturated sands. *Journal of Geotechnical Engineering Division*, ASCE, 100(4), 387–405.

145. Lee, K.L. (1979). Cyclic strength of a sensitive clay of eastern Canada. *Canadian Geotechnical Journal*, 16(1), 163-176.

146. Lee, K.L. and Fitton, J.A (1969). Factors affecting the cyclic loading strength of soil. *In the proceeding of vibration Effects of Earthquakes on Soils and Foundations*, ASTM, 450, 71-95.

147. Lee, K.L. and Seed, H.B. (1967). Cyclic stress conditions causing liquefaction of sand. *Journal of Soil Mechanics and Foundations Division*, ASCE, 93(1), 47-70.

148. Lee, K.L., Seed, H.B. and Dunlop, P. (1969). Effect of transient loading on the strength of sand. *In Proceedings of the Seventh International Conference on Soil Mechanics and Foundation Engineering*, Mexico, 239-247.

149. Li, L. L., Dan, H.B. and Wang, L.Z. (2011). Undrained behavior of natural marine clay under cyclic loading. *Ocean Engineering*, 38(16), 1792-1805.

150. Lin, M.L., Huang, T.H. and You, J.C. (1996). The effects of frequency on damping properties of sand. *Soil Dynamics and Earthquake Engineering*, 15(4), 269-278.

151. Lin, M.L., Ni, S.H., Wright, S.G. and Stokoe II, K.H. (1988). Characterization of material damping in soil. *In Proceeding of the 9th World Conference on Earthquake Engineering*, 3, 5-10.

152. Lin, S.Y., Lin, P.S., Luo, H.S. and Juang, C.H. (2000). Shear modulus and damping ratio characteristics of gravelly deposits. *Canadian Geotechnical Journal*, 37(3), 638-651.

153. Lombardi, D., Bhattacharya, S., Hyodo, M. and Kaneko, T. (2014). Undrained behaviour of two silica sands and practical implications for modelling SSI in liquefiable soils. *Soil Dynamics and Earthquake Engineering*, 66, 293–304.

154. Maheshwari, B.K., Kale, S.S. and Kaynia, A.M. (2012a). Dynamic properties of solani sand at large strains: A parametric study. *International Journal of Geotechnical Engineering*, 6, 353–358.

155. Maheshwari, B.K., Singh, H.P. and Saran, S. (2012b). Effects of reinforcement on liquefaction resistance of Solani sand. *Journal of Geotechnical and Geoenvironmental Engineering*, ASCE, 138(7), 831–840.

156. Maheswari, R.U., Boominathan, A. and Dodagoudar, G.R. (2010). Use of surface waves in statistical correlations of shear wave velocity and penetration resistance of Chennai soils. *Journal of Geotechnical and Geological Engineering*, 28, 119–137.

157. Martin, G.R., Finn, W.D.L. and Seed, H.D. (1978). Effects of system compliance on liquefaction tests. *Journal of the Geotechnical Engineering Division*, ASCE, 104(4), 463–479.

158. Mashiri, M.S. (2014). Monotonic and cyclic behaviour of sand-tyre chip (STCh) mixtures. *PhD thesis*. School of Civil, Mining and Environmental Engineering. University of Wallongong, Australia, p 290.

159. Matasovic, N. and Vucetic, M. (1993). Cyclic characterization of liquefiable sands. *Journal of Geotechnical and Geoenvironmental Engineering*, ASCE, 119, 1805–1822.

160. Miura, S. and Toki, S. (1982). A sample preparation method and its effect on static and cyclic deformation-strength properties of sand. *Soils and Foundations*, 22(1), 61-77.

161. Mohanty, S. and Patra, N.R. (2016). Dynamic response analysis of Talcher pond ash embankment in India. *Soil Dynamics and Earthquake Engineering*, 84, 238-250.

162. Mohtar, C.S.E., Denevich, V.P. Santagata, M. and Bobet, A. (2013). Combined resonant column and cyclic triaxial tests for measuring undrained shear modulus reduction of sand with plastic fines. *Geotechnical Testing Journal*, ASTM, 36(4), 1–9.

163. Muley, P., Maheshwari, B.K. and Paul, D.K. (2012). Effect of fines on liquefaction resistance of Solani sand. *Proceeding in the 15th World Conference on Earthquake Engineering*, Lisboa – 2012.

164. Mulilis, J.P. (1975). The Effects of Method of Sample Preparation on the Cyclic Stress Strain behaviour of Sands. *EERC Report 75-18*, College of Engineering, University of California, Berkeley.

165. Mulilis, J.P., Seed, H.B., Chan, C.K., Mitchell, J.K. and Arulanandan, K., (1977). Effects of sample preparation on sand liquefaction. *Journal of Geotechnical Engineering*, ASCE, 103(2), 91–108.

166. Mulilis, J.P., Townsend, F.C. and Horz, R.C. (1978). Triaxial testing techniques and sand liquefaction. *Dynamic Geotechnical testing*, ASTM, 654, 265–279.

167. Naik, N. and Choudhury, D. (2013). Site specific ground response analysis for typical sites in Panjim city, Goa. *In the proceedings of Indian Geotechnical Conference*, Roorkee, India.

168. Nandy, D.R. (2007). Need for seismic microzonation of Kolkata megacity. *In Proceedings of workshop on microzonation*, Indian Institute of science, Bangalore, India, Vol. 2627.

169. Nath, S.K., Thingbaijam, K.K.S. and Raj, A. (2008). Earthquake hazard in Northeast India–A seismic microzonation approach with typical case studies from Sikkim Himalaya and Guwahati city. *Journal of Earth System and Science*, 117, 809–831.

170. O'Kelly, B.C. and Naughton, P.J. (2008). Use of proximity transducers or local radial strain measurements in a hollow cylinder apparatus. *Proceedings of the Fourth International Symposium on Deformation Characteristics of Geomaterials (IS-Atlanta 2008)*, Atlanta, Georgia, USA, Published by IOS Press/Millpress.

171. Okur, D.V. and Ansal, A. (2007). Stiffness degradation of natural fine grained soils during cyclic loading. *Soil Dynamics and Earthquake Engineering*, 27, 843–854.

172. Omidvar, M., Iskander, M. and Bless, S. (2012). Stress-strain behaviour of sand at high strain rates. *International journal of impact engineering*, 49, 192-213.

173. Ordonez, G.A. (2000). SHAKE2000: A computer program for the 1D analysis of geotechnical earthquake engineering problems.

174. Palito, C.P. and Martin, J.R. (2001). Effects of non-plastic fines on the liquefaction resistance of sands. *Journal of Geotechnical and Geo-environmental Engineering*, 127(5), 408–415.

175. Park, S.S. and Kim, Y.S. (2012). Liquefaction resistance of sands containing plastic fines with different plasticity. *Journal of Geotechnical and Geoenvironmental Engineering*, ASCE, 139(5), 825-830.

176. Peacock, W.H. and Seed, H.B. (1968). Sand liquefaction under cyclic loading simple shear conditions. *Journal of the Soil Mechanics and Foundations Division*, ASCE, 94(3), 689-708.

177. Phanikanth, V.S., Choudhury, D. and Reddy, G.R. (2011). Equivalent-linear seismic ground response analysis of some typical sites in Mumbai. *Journal of Geotechnical and Geological Engineering*, 29, 1109, doi: 10.1007/s10706–011–9443–8.

178. Pitilakis, K.D., Anastasiadis, A. and Raptakis, D. (1992). Field and laboratory determination of dynamic properties of natural soil deposits. In *Proceeding of 10th World Conference on Earthquake Engineering*, 3, 1275-1280.

179. Poddar, S.M.C. (1953). A short note on the Assam earthquake of August 15, 1950. A compilation of papers on the Assam earthquake of August 15, 1950, Government of India.

180. Polito, C.P. and Martin II, J.R. (2001). Effects of nonplastic fines on the liquefaction resistance of sands. *Journal of Geotechnical and Geoenvironmental Engineering*, ASCE, 127(5), 408-415.

181. Polito, C.P., Green, R.A. and Lee, J. (2008). Pore pressure generation models for sands and silty soils subjected to cyclic loading. *Journal of Geotechnical Geoenvironmental Engineering*, ASCE, 134(10), 1490–1500.

182. Prakash, S. and Puri, V.K. (1982). Liquefaction of loessial Soils. *3rd International Earthquake Microzontation Conference*, Seattle.

183. Prakash, S. and Sandoval, J.A. (1992). Liquefaction of low plasticity Silts. *Soil Dynamics and Earthquake Engineering*, 71 (7), 373-397.

184. Puri, V.K. (1984). Liquefaction behaviour and dynamic properties of loessial (silty) soils, *Ph.D. Thesis*, University of Missouri-Rolla, Missouri.

185. Qian, X., Gray, D.H. and Woods, R.D. (1991). Resonant column tests on partially saturated sands. *Geotechnical Testing Journal*, ASTM, 14(3), 266-275.

186. Qu, M., Xie, Q., Cao, X., Zhao, W., He, J. and Jin, J. (2016). Model test of stone columns as liquefaction countermeasure in sandy soils. *Frontiers of Structural and Civil Engineering*, 10(4), 481-487.

187. Raghukanth, S.T.G. (2008). Simulation of strong ground motion during the 1950 great Assam earthquake. *Pure and applied geophysics*, 165:1761-1787.

188. Raghukanth, S.T.G. and Dash, S.K. 2010. Evaluation of seismic soil-liquefaction at Guwahati city. *Environmental Earth Science*, 61: 355–368.

189. Raghukanth, S.T.G., Sreelatha, S. and Dash, S.K. (2008). Ground motion estimation at Guwahati city for an Mw 8.1 earthquake in the Shillong Plateau. *Tectonophysics*, 448(1), 98-114.

190. Raghunandan, M.E. and Juneja, A. (2010). Behaviour of soil under cyclic loading. *In proceeding of Indian Geotechnical Conference Bombay*, 195-198.

191. Ranjan, G. and Rao, A.S.R. (2007). Basic and applied soil mechanics. New Age International.

192. Ranjan, R. (2005). Seismic Response Analysis of Dehradun City, India. *M.Sc Thesis*, International Institute for Geo-Information Science and Earth Observations–Enschede, Netherlands, p. 92.

193. Ravishankar, B.V. Sitharam, T.G. and Govindaraju, L. (2005). Dynamic properties of Ahmedabad sands at large strains. *Proceeding of the Indian Geotechnical Conference*. Ahmedabad, India, 1, 369–372.

194. Rollins, K.M., Evans, M.D., Diehl, N.B. and Daily, W.D. (1998). Shear modulus and damping ratio for gravels. *Journal of Geotechnical and Geoenvironmental Engineering*, ASCE, 124, 396-405.

195. Safaqah, O.A. and Riemer, M.F. (2007). The Elastomer gage for local strain measurement in monotonic and cyclic soil testing. *Geotechnical Testing Journal*, ASTM, 30, 164-172.

196. Sandoval, J.A. (1989). Liquefaction and settlement characteristics of silt soils, *PhD Thesis*, Civil Engineering Department, University of Missouri-Rolla.

197. Santagata, M., Germaine, J.T. and Ladd. C.C. (2005). Factors affecting the initial stiffness of cohesive soils. *Journal of Geotechnical and Geoenvironmental Engineering*, ASCE, 131, 430-441.

198. Sarma, C.P., Krishna, A.M. and Dey, A. (2016). Geotechnical characterization of hill slope soils of Guwahati region. *In Proceeding of Indian Geotechnical Conference, Chennai*.

199. Sassa, S. and Yamazaki, H. (2017). Simplified liquefaction prediction and assessment method considering waveforms and durations of earthquakes. *Journal of Geotechnical and Geoenvironmental Engineering*, ASCE, 143, 2,

200. Sawada, S. Tsukamoto, Y. and Ishihara, K. (2006). Residual deformation characteristics of partially saturated sandy soils subjected to seismic excitation. *Soil Dynamics and Earthquake Engineering*, 26, 175-182.

201. Saxena, S.K., Avramidis, A.S. and Reddy, K.R. (1988). Dynamic moduli and damping ratios for cemented sands at low strains. *Canadian Geotechnical Journal*, 25(2), 353-368.

202. Scholey, G.K., Frost, J.D., Lo Presti, D.C.F. and Jamiolkowski, M. (1995). A review of instrumentation for measuring small strains during triaxial testing of soil specimens. *Geotechnical Testing Journal*, ASTM, 18, 137-156.

203. Seed, H.B. and Chan, C.K. (1964). Pulsating load tests on samples of clay and silt from anchorage, Alaska. *Report on Anchorage Area Soil Studies to U.S. Army Engineer District*, Anchorage, Alaska, Shannon & Wilson, Inc., Seattle, Wash.

204. Seed, H.B. and Idriss, I.M. (1970). Soil moduli and damping factors for dynamic response analysis. *Report No EERC 70-10*, Earthquake Engineering Research Center, University of California, Berkeley.

205. Seed, H.B. and Idriss, I.M. (1971). Simplified procedure for evaluating soil liquefaction potential. *Journal of the Soil Mechanics and Foundations Division*, ASCE, 97(9), 1249–1273.

206. Seed, H.B. and Lee, K.L. (1966). Liquefaction of Saturated Sands during Cyclic Loading. *Journal of Soil Mechanics and Foundation Division*, ASCE, 92(6), 105-134.

207. Seed, H.B., Martin, P.P. and Lysmer, J. (1975). The generation and dissipation of pore-water pressures during soil liquefaction. *Geotechnical Report*, No. EERC 75-26, Univ. of California, Berkeley, CA.

208. Seed, H.B., Wong, R.T., Idriss, I.M. and Tokimatsu, K. (1986). Moduli and damping factors for dynamic analysis of cohesionless soils. *Journal of Geotechnical Engineering*, ASCE, 112(11), 1016–1032.

209. Seismosoft (2012). Seismosignal, version 5.00. *www.seismosoft.com*.

210. Shukla, J. and Choudhury, D. (2012). Seismic hazard and site-specific ground motion for typical ports of Gujarat. *Natural Hazards*, 60, 541-565.

211. Silver, M.L. and Ishihara, K. (1977). Comparison between the strength of undisturbed and reconstituted sands from Niigata, Japan, *Contract Report, U.S. Army Engineer waterways experiment station*, Corps of Engineers, Vicksburg, Miss.

212. Silver, M.L., Tatsuoka, F., Phukunhaphan, A. and Avramidis, A.S. (1980). Cyclic undrained strength of sand by triaxial test and simple shear test. *Proceedings of 7th World Conference on Earthquake Engineering*, Istanbul, 3, 281–288.

213. Simatupang, M. and Okamura, M. (2017). Liquefaction resistance of sand remediated with carbonate precipitation at different degrees of saturation during curing. *Soils and Foundation*, 57(4), 619-631.

214. Sitharam, T.G. and Govindaraju, L. (2003). Evaluation of dynamic properties of sandy soils at large strain levels. *Proceedings of the work shop on Current Practices and Future trends in Earthquake Geotechnical Engineering*. Bangalore, India, pp. 53–60.

215. Sitharam, T.G., Govinda Raju, L. and Srinivasa Murthy, B.R. (2004a). Cyclic and monotonic undrained shear response of silty sand from Bhuj region in India. *ISET Journal of earthquake technology*, 41(2-4), 249-260.

216. Sitharam, T.G., GovindaRaju, L. and Murthy, B.R.S. (2004b). Evaluation of liquefaction potential and dynamic properties of silty sand using cyclic triaxial testing. *Geotechnical Testing Journal*, ASTM, 27(5), 423–429.

217. Sitharam, T.G., Ravishankar, B.V. and Patil, S.M. (2012). Liquefaction and pore water pressure generation in sand: Cyclic strain controlled triaxial tests. *International Journal of Geotechnical Earthquake Engineering*, 3(1), 57-85.

218. Sitharam, T.G., Ravishankar, B.V. and Vinod, J.S. (2011). Dynamic properties of sandy soils at large shear strains with special reference to the influence of non-plastic fines. *International Journal of Geotechnical Earthquake Engineering*, 2, 16–28.

219. Skempton, A.W. (1954). The pore-pressure coefficients A and B. *Geotechnique*, 4, 143–147.

220. Sreng, S., Okochi, Y., Kobayashi, K., Tanaka, H., Sugiyama, H., Kusala, T., Miki, H. and Makino, M. (2015). Centrifuge model tests of embankment with a new liquefaction countermeasure by ground improvement considering constraint effect. *6th International Conference on Earthquake Geotechnical Engineering*, Christchurch, New Zealand.

221. Stamatopoulos, C.A. (2010). An experimental study of the liquefaction strength of silty sands in terms of the state parameter. *Soil Dynamics and Earthquake Engineering*, 30(8), 662-678.

222. Stokoe, K.H., Hwang, S.H., Lee, J.N.K. and Andrus, R.D. (1995). Effects of various parameters on the stiffness and damping of soils at small to medium strains. *Proceedings of the International Symposium on Pre-failure Deformation of Geomaterials*, Sapporo, Japan, 2, 785–816.

223. Suetomi, I. and Yoshida, N. (1998). Nonlinear behavior of surface deposit during the 1995 Hyogoken-Nambu earthquake. *Soils and Foundations*, 38, 11–22.

224. Suwal, L.P. and Kuwano, R. (2012). Poisson's ratio evaluation on silty and clayey sands on laboratory specimens by flat disk shaped piezo-ceramic transducer. *Bulletin of ERS*, 45, 141-158.

225. Svoboda, J. (2013). Impact of strain rate on the shear strength and pore water pressure generation of clays and sands. *M. Sc. Thesis*, Department of Civil, Environmental, and Architectural Engineering, Oregon State University.

226. Symes, M. and Burland, J. (1984). Determination of local displacements on soil samples. *Geotechnical Testing Journal*, ASTM, 7(2), 49-59.

227. Talaganov, K.V. (1996). Stress-strain transformations and liquefaction of sands. *Soil Dynamics and Earthquake Engineering*, 15(7), 411-418.

228. Tang, Y.Q., Zhou, J. and Liu, S. (2011). Test on cyclic creep behavior of mucky clay in shangay under step cyclic loading. *Environmental Earth Sciences*, 63, 321-327.

229. Tatsuoka, F., Benedetto, H.D., Enomoto, T., Kawabe, S. and Kongkitkul, W. (2008). Various viscous types of geomaterials in shear and their mathematical expression. *Soils and Foundations*, 48(1), 41–60.

230. Tatsuoka, F., Iwasaki, T. and Takagi, Y. (1978). Hysteretic damping of sands under cyclic loading and its relation to shear modulus. *Soils and Foundations*, 18(2), 25–30.

231. Tatsuoka, F., Iwasaki, T., Tokida, K.I. and Kon-No, M. (1981). Cyclic undrained triaxial strength of sampled sand affected by confining pressure. *Soils and Foundations*, 21(2), 115-120.

232. Tatsuoka, F., Muramatsu, M. and Sakaki, T. (1982). Cyclic undrained stress-strain behaviour of dense sand by torsional simple shear tests. *Soils and Foundations*, JSSMFE, 22(2), 55–70.

233. Tatsuoka, F., Shibuya, S., Goto, S., Sato, T. and Kong, X.J. (1990). Discussion on the use of Hall Effect semiconductorsin geotechnical instrumentation. *Geotechnical Testing Journal*, ASTM, 13(1), 63-67.

234. Teachavorasinskun, S. Thongchim, P. and Lukkunaprasit, P. (2002). Shear modulus and damping of soft Bangkok clays. *Canadian Geotechnical Journal*, 39, 1201–1208.

235. Thiers, G.R. (1965). The behaviour of saturated clay under seismic loading conditions. *Ph.D. Thesis*, Department of Civil Engineers, University of California, Berkeley.

236. Townsend, F.C. (1978). A review of factors affecting cyclic triaxial tests. *Dynamic Geotechnical Testing*, ASTM, TP654, 356-383.

237. Troncoso, J.H. (1990). Failure risks of abandoned tailings dams, *Proceeding of International Symposium on Safety and Rehabilitation of Tailings Dams*, International Commission on Large Dams, Paris, 82-89.

238. Tsuchida, H. (1970). Prediction and counter measure against the liquefaction in sand deposits. *Seminar in the Port and Harbour Research Institute*, Ministry of Transport, pp.1-33.

239. Tsukamoto, Y. Ishihara, K. and Sawada, S. (2004). Settlement of silty sand deposits following liquefaction during earthquakes. *Soils and Foundations*, 44(5), 135–148.

240. Tumi, H.O.Z. (1983). Effect of confining pressure and particle angularity on resistance to liquefaction. *M. Sc. Thesis*, University of British Columbia, DOI: 10.14288/1.0062968.

241. Unnikrishnan, N., Rajagopal, K. and Krishnaswamy, N.R. (2002). Behaviour of reinforced clay under monotonic and cyclic loading. *Geotextile and Geomembranes*, 20, 117–133.

242. Vaid, Y. and Negussey, D. (1988). Preparation of reconstituted sand specimens. *Advanced Triaxial Testing of Soil and Rock*, STP29090S, R. Donaghe, R. Chaney, and M. Silver, Ed., ASTM International, West Conshohocken, PA, 405-417.

243. Vaid, Y.P. and Chern, J.C. (1983). Effect of static shear on resistance to liquefaction. *Soils and foundations*, 23(1), 47-60.

244. Vaid, Y.P. and Finn, W.D.L. (1979). Static shear and liquefaction potential. *Journal of Geotechnical and Geoenvironmental Engineering*, ASCE, 105(10), 1233-1246.

245. Vaid, Y.P. and Sivathayalan, S. (2000). Fundamental factors affecting liquefaction susceptibility of sands. *Canadian Geotechnical Journal*, 37(3), 592-606.

246. Vucetic, M. and Dobry, R. (1991). Effect of soil plasticity on cyclic response. *Journal of Geotechnical Engineering*, ASCE, 117(1), 89–107.

247. Vucetic, M., Lanzo, G. and Doroudian, M. (1998). Damping at small strains in cyclic simple shear test. *Journal of Geotechnical and Geoenvironmental Engineering*, ASCE, 124(7), 585-594.

248. Walberg, F.C. (1977). Soils-investigation of effects of freezing sand samples. *Presentation 12, Division Laboratory Conference, Corps of Engineers*, Dallas, April 1977.

249. Wang, J.N. and Kavazanjian Jr, E. (1989). Pore pressure development during non-uniform cyclic loading. *Soils and Foundations*, 29(2), 1-14.

250. Wang, M.S. (1972). Liquefaction of triaxial sand samples under different frequencies of cyclic loading. *ME Thesis*, University of Western Ontario.

251. Wang, Y., Gao, Y., Guo, L., Cai, Y., Li, B., Qiu, Y. and Mahfouz, A.H. (2017). Cyclic response of natural soft marine clay under principal stress rotation as induced by wave loads. *Ocean Engineering*, 129, 191–202.

252. Watanabe, K. and Kusakabe, O. (2013). Reappraisal of loading rate effects on sand behavior in view of seismic design for pile foundation. *Soils and Foundations*, 53(2), 215–231.

253. Whitman, R.V. and Healy, K.A. (1962). Shearing resistance of sands during rapid loadings (No. 9). Massachusetts Institute of Technology Cambridge.

254. Wong, R.T., Seed, H.B. and Chan, C.K. (1975). Cyclic loading liquefaction of gravelly soils. *Journal of Geotechnical Engineering*, ASCE, 101(6), 571–583.

255. Woods, R.D. (1991). Field and laboratory determination of soil properties at low and high strains. *In 2nd International Conference on Recent Advances in Geotechnical Earthquake Engineering and Soil Dynamics*. University of Missouri-Rolla, 1727–41.

256. Xenaki V.C. and Athanasopoulos G.A. (2003). Liquefaction resistance of sand-mixtures: an experimental investigation of the effect of fines. *Soil Dynamics and Earthquake Engineering*, 23, 183–194.

257. Xu, D.S. (2017). A new measurement approach for small deformations of soil specimens using fiber Bragg grating sensors. *Sensors*, 17(5), 1016.

258. Yamamuro, J.A. and Lade, P.V. (1993). Effects of strain rate on instability of granular soils. *Geotechnical Testing Journal*, ASTM, 16(3), 304–313.

259. Yamamuro, J.A., Abrantes, A.E. and Lade, P.V. (2011). Effect of strain rate on the stress-strain behavior of sand. *Journal of Geotechnical and Geoenvironmental Engineering*, ASCE, 137(12), 1169-1178.

260. Yang, J., Savidis, S. and Roemer, M. (2004). Evaluating liquefaction strength of partially saturated sand. *Journal of Geotechnical and Geoenvironmental Engineering*, ASCE, 130(9), 975-979.

261. Yang, Z. and Elgamal, A. (2002). Influence of permeability on liquefaction-induced shear deformation. *Journal of Engineering Mechanics*, 128(7), 720-729.

262. Yasuhara, K., Hirao, K. and Hyde, A.F.L. (1992). Effects of cyclic loading on undrained strength and compressibility of clay. *Soils and Foundations*, 32(1), 100-116.

263. Yasuhara, K., Murakami, S., Song, B.W., Yokokawa, S. and Hyde, A.F. (2003). Postcyclic degradation of strength and stiffness for low plasticity silt. *Journal of Geotechnical and Geoenvironmental Engineering*, ASCE, 129(8), 756-769.

264. Yildirim, H. and Ersan, H. (2007). Settlements under consecutive series of cyclic loading. *Soil Dynamics and Earthquake Engineering*, 27, 577-585.

265. Yilmaz, M.T., Pekcan, O. and Bakir, B.S. (2004). Undrained cyclic shear and deformation behaviour of silt-clay mixtures of Adapazari, Turkey. *Soil Dynamics and Earthquake Engineering*, 24, 497–507.

266. Yimsiri, S. and Soga, K. (2002). A review of local strain measurement systems for triaxial testing of soils. *Journal of the Southeast Asian Geotechnical Society*, 41-52.

267. Yimsiri, S., Soga, K. and Chandler, S.G. (2005). Cantilever-type local deformation transducer for local axial strain measurement in triaxial test. *Geotechnical Testing Journal*, ASTM, 28(5), 445-451.

268. Yoshida, N. (2015). Seismic Ground Response Analysis. Springer.

269. Yoshimi, Y., Tanaka, K. and Tokimatsu, K. (1989). Liquefaction resistance of a partially saturated sand. *Soils and foundations*, 29(3), 157-162.

270. Youd, T.L., Idriss, I.M., Andrus, R.D., Arango, I., Castro, G., Christian, J.T., Dobry, R., Finn, W.D.L., Harder Jr, L.F., Hynes, M.E., Ishihara, K., Koester, J.P., Liao, S.S.C., Marcuson III, W.F., Martin, G.R., Mitchell, J.K., Moriwaki, Y., Power, M.S., Robertson, P.K., Seed, R.B. and Stokoe II, K.H. (2001). Liquefaction resistance of soils: Summary report from the 1996 NCEER and1998 NCEER/NSF workshops on evaluation of liquefaction resistance of soils, *Journal of Geotechnical and Geoenvironmental Engineering*, ASCE, 127(10), 817–833.

271. Zavoral, D.Z. and Campanella, R.G. (1994). Frequency effects on damping/modulus of cohesive soil. In *Dynamic Geotechnical Testing II*, ASTM STP 1213, Ronald J. Ebelhar, Vincent P. Drnevich, and Bruce L. Kutter, Eds., American Society for Testing and Materials, Philadelphia, 1994.

272. Zhou, Y.G. and Chen, Y.M. (2007). Laboratory investigation on assessing liquefaction resistance of sandy soils by shear wave velocity. *Journal of Geotechnical and Geoenvironmental Engineering*, ASCE, 133(8), 959-972.

PUBLICATIONS

Journal Paper(s)

1. **Kumar, S.S.**, Dey, A. and Krishna, A.M. (2018) "Importance of Site-specific Dynamic Soil Properties for Seismic Ground Response Studies" *International Journal of Geotechnical Earthquake Engineering*, Vol. 9, No. 1, pp. 78-98.
2. **Kumar, S.S.**, Krishna, A.M. and Dey, A. (2017) "Evaluation of Dynamic Properties of Sandy Soil at High Cyclic Strains" *Soil Dynamics and Earthquake Engineering*, Vol. 97, pp. 157-167.
3. **Kumar, S.S.**, Krishna, A.M. and Dey, A. (2017) "High Strain Dynamic Properties of Perfectly Dry and Saturated Cohesionless Soil" *Indian Geotechnical Journal*, DOI: 10.1007/s40098-017-0255-5.
4. Basu, D., Dey, A. and **Kumar, S.S.** (2017) "One-dimensional Effective Stress Non-Masing Nonlinear Ground Response Analysis of IIT Guwahati" *International Journal of Geotechnical Earthquake Engineering*, Vol. 8, No. 1, pp. 1-27.
5. Dammala, P.K, Bhattacharya, S., Krishna, A.M., **Kumar, S.S.** and Dasgupta, K. (2017) "Scenario based Seismic Re-qualification of Caisson Supported major Bridges – A Case Study of Saraighat Bridge" *Soil Dynamics and Earthquake Engineering*, Vol. 100, pp. 270-275.
6. **Kumar, S.S.** and Krishna, A.M. (2013) "Seismic Ground Response Analysis of some Typical Sites of Guwahati City" *International Journal of Geotechnical Earthquake Engineering*, Vol. 4, No. 1, pp. 83-101.
7. **Kumar, S.S.**, Krishna, A.M. and Dey, A. (2018) "Dynamic Properties and Liquefaction Behaviour of Cohesive Soil of Northeast India under Staged Cyclic Loading" *Journal of Rock Mechanics and Geotechnical Engineering* (**Under review**)
8. **Kumar, S.S.**, Krishna, A.M. and Dey, A. "Response of Saturated Cohesionless Soil Subjected to Seismic Excitations" *Natural Hazards* (**Under review**)
9. **Kumar, S.S.**, Krishna, A.M. and Dey, A. "Application of On-sample Strain Measurements in Triaxial Testing of Cohesionless Soil" *Measurement*, (**Under review**)
10. **Kumar, S.S.**, Krishna, A.M. and Dey, A. "Cyclic Shear Strain for Liquefaction Evaluation of Sandy Soil based on Irregular and Regular Excitations" (**Under review**)
11. **Kumar, S.S.**, Krishna, A.M., and Dey, A. "Dynamic Response of Soil under Strain-controlled and Stress-controlled Cyclic Loading for Seismic Engineering Applications" (**Under review**)

Special Publication:

1. **Kumar, S.S.**, Krishna, A.M. and Dey, A. (2014) "Parameters Influencing Dynamic Soil Properties: A Review Treatise" *International Journal of Innovative Research in Science, Engineering and Technology*, Special Issue on National Conference on Recent Advances in Civil Engineering, NCRACE-2013, Vol. 3, No. 4, pp. 47-60.

Conference Paper(s):

1. **Kumar, S.S**., Krishna, A.M. and Dey, A. (2017) "Effect of strong motion parameters on the response of soil using cyclic triaxial tests" 13th *International conference on vibration problems* (ICOVP-2017), IIT Guwahati, Assam, Paper No. 179.

2. **Kumar, S.S**., Krishna, A.M. and Dey, A. (2017) "Evaluation of hysteretic damping of sand at large shear strains using cyclic triaxial tests" *Indian Geotechnical Conference-2017*, IIT Guwahati, Assam, Paper No. 462.

3. **Kumar, S.S**., Krishna, A.M. and Dey, A. (2016) "Local strain measurements in triaxial tests using on-sample transducers" *Indian Geotechnical Conference-2016*, IIT Madras, Chennai, India, Paper No: 462.

4. Singhai, A., **Kumar, S.S**. and Dey, A. (2016) "Site-Specific 1-D nonlinear effective stress GRA with pore water pressure dissipation" *Sixth International Conference on Recent Advances in Geotechnical Earthquake Engineering and Soil Dynamics* (*6ICRAGEE)*, August 1-6, 2016, IIT Roorkee Extension Centre, 20 Knowledge Park II, Greater Noida, India Delhi.

5. **Kumar, S.S**., Dey, A. and Krishna, A.M. (2015) "Cyclic response of sand using stress controlled cyclic triaxial tests"*Indian Geotechnical Conference-2015*, Pune, India, Paper No: 242.

6. **Kumar, S.S**., Dey, A. and Krishna, A.M. (2015) "Dynamic response of river bed sands using cyclic triaxial tests" *Proc. of 5th Indian Young Geotechnical Engineers Conference-2015*, Vadodara, pp. 175-176. (**Best paper award**)

7. **Kumar, S.S**., Dey, A. and Krishna, A.M. (2014) "Equivalent linear and nonlinear ground response analysis of sites at Guwahati city" *Indian Geotechnical Conference-2014*, Kakinada, India, pp. 603-612.

8. **Kumar, S.S**., Krishna, A.M. and Dey, A. (2014) "Nonlinear site-specific ground response analysis: Case study of Amingaon, Guwahati" *15th Symposium of Earthquake Engineering (15SEE-2014)*, Roorkee, India, pp. 308-318.

9. **Kumar, S.S**., Krishna, A.M. and Dey, A. (2014) "Dynamic soil properties of Brahmaputra sand using Cyclic Triaxial tests" *North-East Students Geo-Congress on Advances in Geotechnical Engineering (NESGC-2014)*, Guwahati, India, 18 Oct 2014.